Cooperative Strategies for Inter-cell Interference Management in Dense Cellular Networks

Rodolfo TORREA DURÁN

Examination committee:
Prof. dr. Adhemar Bultheel, chair
Prof. dr. ir. Marc Moonen, supervisor
dr. ir. Paschalis Tsiaflakis, supervisor
(Nokia Bell Labs)
Prof. dr. ir. Luc Vandendorpe, supervisor
Prof. dr. ir. Sofie Pollin
Prof. dr. ir. Jérôme Louveaux
Prof. dr. ir. Ana Isabel Pérez-Neira
Prof. dr. ir. Bart Nauwelaers

(Leuven, Belgium)

Dissertation presented in partial fulfillment of the requirements for the degree of Doctor in Engineering Science (PhD): Electrical Engineering

November 2017

© 2017 KU Leuven – Faculty of Engineering
Uitgegeven in eigen beheer, Rodolfo Torrea Durán, Kasteelpark Arenberg 10, B-3001 Leuven (Belgium)

Alle rechten voorbehouden. Niets uit deze uitgave mag worden vermenigvuldigd en/of openbaar gemaakt worden door middel van druk, fotokopie, microfilm, elektronisch of op welke andere wijze ook zonder voorafgaande schriftelijke toestemming van de uitgever.

All rights reserved. No part of the publication may be reproduced in any form by print, photoprint, microfilm, electronic or any other means without written permission from the publisher.

Acknowledgements

I would like to express my gratitude to all the people that have given me their friendship, support, advice, and hope during this journey.

First of all my admiration and gratitude to my supervisors prof. Marc Moonen, prof. Luc Vandendorpe, and Paschalis Tsiaflakis, for guiding me through all this work and for encouraging me with their knowledge and experience. Thanks also to the members of my supervisory and examination committee: prof. Sofie Pollin, prof. Jérôme Louveaux, prof. Bart Nauwelaers, prof. Ana Isabel Pérez-Neira, and prof. Adhemar Bultheel for their feedback and advice.

To my friends and colleagues in ESAT, Imec, and UCL with who I have shared so many fruitful discussions and meetings.

To my Belgian family in law, the Vanhoeyvelt-Craessaerts family, for all their advice and help in any aspect of life. Special thanks to Sander for all the hours of games, demos, videos, and interesting scientific discussions in so many fields of human knowledge.

To my family in Mexico, my parents and my sister in particular, who have provided unconditional love and support during all my life. I cannot imagine having arrived at this point without them.

Finally to Nele, Elías, and Demi for being part of this adventure and a huge motivation to never give up.

Abstract

The number of mobile devices and the amount of traffic generated by them has grown at a tremendous pace in the last years and it is expected to continue growing. This growth contrasts with the limited bandwidth that needs to be shared among users.

Network densification [14, 51] has been proposed as a promising technique to satisfy the previous demands over a shared bandwidth. This is realized by increasing the density of base stations deployed. Although network densification can improve the signal-to-interference-plus-noise ratio (SINR) of the users located close to the serving base station, it can also increase the inter-cell interference received by other users.

In current cellular networks, base stations deal with inter-cell interference by splitting the bandwidth in two parts. The first one is assigned to users with low interference (typically in the cell center) and it is reused in each cell. The second one is assigned to users with high interference (typically in the cell edge) and it is orthogonalized between users connected to different base stations. This cooperative allocation of bandwidth resources requires sharing channel state information (CSI) through a backhaul link. However, when orthogonalizing resources, the amount of resources that each user receives decreases with the number of users. Furthermore, the operating costs of maintaining a backhaul link for CSI sharing and the amount of CSI that needs to be exchanged between base stations and users makes such interference management techniques infeasible to be implemented in dense networks. These constraints urgently call for cooperative techniques that can reuse resources, while keeping the exchange of CSI between base stations to a minimum, which is the goal of the strategies presented in this thesis.

The common denominator of the strategies presented in this thesis is the overhearing capabilities of the network. In dense networks, the proximity of base stations and users results in finding strong links between nodes that have

no intentional communication. This could be between users and interfering base stations (first case) or between different base stations (second case).

As for the first case, base stations can use CSI transmitted by users from other base stations to allocate resources efficiently. To this end, we propose a neighbor-friendly power control strategy that allows neighboring base stations to reuse resources while minimizing inter-cell interference. The proposed power control strategy avoids any CSI exchange between base stations and can be tuned to increase the data rate of users served by the base station performing the power control strategy, while protecting the data rate of users from a neighboring cell. In high interference conditions, the proposed approach can achieve a data rate increase of the cell edge users by a factor of 3.5 compared to IWF, 15 compared to soft frequency reuse (SFR) and 60 compared to equal power allocation (EPA).

Also, users in dense networks constantly receive transmitted data from other base stations intended to users in their proximity. To this end, we develop a transmission strategy based on aligned frequency reuse (AFR) that allows cell edge users to relay overheard signals to the intended users through D2D communication during the time-slots in which users are not receiving their intended signal. We show that our approach increases the diversity and spectral efficiency of all the users in the network without decreasing the achievable degrees of freedom (DoF). Furthermore, we develop it for two cellular array configurations and we extend it to the case with multiple cell edge users.

As for the second case, base stations in dense networks can act as relays by transmitting overheard data to users from other base stations, introducing spatial diversity. For this purpose, we propose a multiple-relay communication protocol (MRCP) for achieving fairness in dense networks. MRCP is applicable to an arbitrary number of base stations and users, while keeping a small transmission time compared to traditional space-time network coding (STNC) techniques. We show that our approach achieves the highest max-min fairness among users and almost full diversity when compared to other communication schemes.

MRCP requires all the base stations and users in the network (or in a cluster of base stations) to overhear each other, while typically base stations can only overhear the closest neighboring base stations. For this purpose, we exploit a basic knowledge of the network topology using the Wyner cellular model. This is done by allowing simultaneous transmissions of those BSs that do not overhear each other during the transmission phase and the relaying phase. We then reduce the number of time-slots by allowing simultaneous transmissions of all the BSs during the relaying phase. Our result shows that our scheme is able to improve the spectral efficiency and bit error rate with unequal transmit power and unequal average channel gains.

In order to implement the previous approaches, base stations must devote some of their resources to relay the overheard signals. Evidently, this has a cost on the consumed power and on the amount of resources that could be otherwise used for their own users. For this purpose, we analyse two approaches that exploit the overhearing capabilities of the system in terms of spectral efficiency, energy efficiency, and success rate and compare them with non-overhearing approaches. We show that when at least one indirect link is stronger than the direct links, exploiting the overhearing capabilities of the transmitting nodes provides the highest performance. Finally, we propose a sub-optimal power control strategy for the two overhearing approaches that with a simple comparison and closed-form formulas can achieve an energy efficiency close to the optimal.

Beknopte samenvatting

Het aantal mobiele apparaten is de afgelopen jaren met een enorm tempo gegroeid, evenals de hoeveelheid verkeer die ze genereren, en zal naar alle waarschijnlijkheid blijven groeien. Deze groei staat in schril contrast met de beperkte bandbreedte die gedeeld moet worden door alle gebruikers.

Netwerkverdichting werd voorgesteld als een veelbelovende techniek om aan deze vereisten te voldoen over een gedeelde bandbreedte, en werd gerealiseerd door de dichtheid van de opgestelde Basisstations (base stations, BS's) te verhogen. Hoewel netwerkverdichting de signaal-tot-interferentie-plus-ruisverhouding (signal-to-interference-plus-noise ratio, SINR) kan verbeteren voor gebruikers die zich dicht bij het BS bevinden, kan het ook de door andere gebruikers ontvangen intercel-interferentie verhogen.

In de huidige mobiele netwerken gaan BS's om met intercel-interferentie door de bandbreedte in twee delen te splitsen. Eén deel van de bandbreedte wordt toegewezen aan gebruikers die weinig interferentie ervaren (meestal in het celcentrum) en wordt in iedere cel hergebruikt. Het andere deel wordt toegewezen aan gebruikers die veel interferentie ervaren (meestal aan de celrand). De overeenkomstige middelen worden georthogonaliseerd tussen gebruikers die verbonden zijn met verschillende BS's. Deze coöperatieve toewijzing van middelen vereist het delen van kanaalstatus-informatie (channel state information, CSI) via een backhaulverbinding. Door de middelen van de verschillende gebruikers te orthogonaliseren, neemt de hoeveelheid middelen die elke gebruiker ontvangt echter af met het aantal gebruikers. Voorts maken de exploitatiekosten van de backhaulverbinding, alsook de hoeveelheid CSI die moet worden uitgewisseld tussen BS's en gebruikers, dergelijke interferentiebeheersingstechnieken onimplementeerbaar in dichte netwerken. Deze restricties vragen duidelijk om coöperatieve technieken die middelen kunnen hergebruiken en die de uitwisseling van CSI tussen BS's tot een minimum beperken, wat het doel is van de strategieën die in dit proefschrift worden gepresenteerd.

De gemene deler van de strategieën die in dit proefschrift worden gepresenteerd, is het veronderstelde afluistervermogen van het netwerk. In dichte netwerken resulteert de korte afstand tussen BS's en gebruikers in sterke verbindingen tussen knooppunten die niet moedwillig met elkaar communiceren. Deze sterke verbindingen kunnen voorkomen tussen gebruikers en interfererende BS's (eerste geval), alsook tussen verschillende BS's (tweede geval).

Wat het eerste geval betreft, kunnen BS's gebruik maken van CSI die verzonden werd door gebruikers van andere BS's om de beschikbare middelen efficiënt te verdelen. Hiertoe stellen we een buurvriendelijke vermogenregelstrategie voor die het mogelijk maakt om in naburige BS's middelen te hergebruiken, en die de intercel-interferentie beperkt. De voorgestelde vermogenregelstrategie vermijdt elke CSI-uitwisseling tussen BS's, kan worden gefinetuned om de gegevenssnelheid van gebruikers die worden bediend door het basisstation dat de vermogenregelstrategie uitvoert te verhogen, en beschermt de gegevenssnelheid van de gebruikers in naburige cellen. In geval van sterke interferentie kan de voorgestelde aanpak voor gebruikers aan de celrand een stijging van de gegevenssnelheid teweegbrengen met een factor 3.5, 15 en 60 wanneer respectievelijk vergeleken wordt met IWF, zacht frequentiehergebruik (soft frequency reuse, SFR) en gelijke vermogen verdeling (equal power allocation, EPA). Daarenboven ontvangen gebruikers in dichte netwerken voortdurend verzonden data van andere BS's die bestemd is voor gebruikers in hun nabijheid. Dit leidde ons tot het ontwikkelen van een transmissiestrategie die gebaseerd is op gealigneerd frequentiehergebruik (aligned frequencey reuse, AFR), waarin gebruikers aan de celrand, wanneer zij zelf geen signaal ontvangen, afgeluisterde signalen via D2D-communicatie relayeren naar de correcte bestemming. We tonen aan dat onze aanpak de diversiteit en spectrale efficiëntie voor alle gebruikers van het netwerk verhoogt zonder de haalbare vrijheidsgraden (degrees of freedom, DoF) te verminderen. We werkten deze strategie uit voor twee cellulaire antenneconfiguraties, en breidden ze vervolgens uit naar scenario's met meerdere gebruikers aan de celrand.

Wat het tweede geval betreft, kunnen BS's in dichte netwerken fungeren als relayerende transmitter door afgeluisterde data door te sturen naar gebruikers van andere BS's, waardoor ruimtelijke diversiteit wordt geïntroduceerd. Om dit te bewerkstelligen, stellen we een meermaals relayerend communicatieprotocol (multiple-relay communication protocol, MRCP) voor om rechtvaardigheid te bereiken in dichte netwerken. MRCP kan worden toegepast onafhankelijk van het aantal BS's en gebruikers, en vereist slechts een kleine transmissietijd in vergelijking met de traditionele technieken voor ruimte-tijdnetwerkcodering (space-time network coding, STNC). We tonen bovendien aan dat onze aanpak, in vergelijking met andere communicatiestrategieën, de hoogste max-min rechtvaardigheid behaalt tussen gebruikers evenals bijna volledige diversiteit.

MRCP vereist dat alle BS's en gebruikers in het netwerk (of in een cluster van BS's) elkaar afluisteren, terwijl de BS's typisch enkel naburige BS's kunnen horen. Om hier mee om te gaan, exploiteren we een basiskennis van de netwerktopologie in de vorm van het Wyner cellulair model. Dit wordt gedaan door tijdens de transmissiefase en de relayeerfase gelijktijdige transmissie toe te staan voor die BS's die elkaar niet kunnen afluisteren. Vervolgens verminderen we het aantal tijdsleuven door gelijktijdige transmissie van alle BS's toe te laten tijdens de relayeerfase. Ons resultaat toont aan dat onze strategie de spectrale efficiëntie en bitfoutkans kan verbeteren met ongelijke transmissievermogens en ongelijke gemiddelde kanaalversterkingen.

Om de voorgaande strategieën te implementeren moeten BS's een deel van hun middelen besteden om de afgeluisterde signalen te relayeren. Dit brengt uiteraard een kost met zich mee in termen van het verbruikte vermogen en de hoeveelheid middelen die anders voor hun eigen gebruikers beschikbaar zouden zijn. Daarom analyseren we twee strategieën die het afluistervermogen van het systeem uitbuiten in termen van spectrale efficiëntie, energie-efficiëntie en succesfrequentie, en vergelijken we deze met een strategieën die het afluistervermogen van het systeem niet uitbuiten. We tonen aan dat, wanneer tenminste één indirecte verbinding sterker is dan de directe verbindingen, strategieën die het afluistervermogen van het systeem uitbuiten de beste prestatie bieden. Tot slot stellen we voor beide strategieën die het afluistervermogen van het systeem uitbuiten een suboptimale vermogenregelstrategie voor die, aan de hand van een eenvoudige vergelijkingsstap en het evalueren van een uitdrukking in gesloten vorm, een energie-efficiëntie bereikt die dicht bij de optimale ligt.

Abbreviations

AFR	Aligned Frequency Reuse
BER	Bit Error Rate
BS	Base Station
CDF	Cumulative Distribution Function
CSI	Channel State Information
D2D	Device-to-device
DoF	Degrees of freedom
DRCP	Double Relay Communication Protocol
EPA	Equal Power Allocation
FDMA	Frequency Division Multiple Access
HetNet	Heterogeneous Network
IWF	Iterative Water Filling
JFI	Jain's Fairness Index
KKT	Karush-Kuhn-Tucker
LOS	Line-of-Sight
LTE	Long Term Evolution
MIMO	Multiple-Input Multiple-Output
MMSE	Minimum Mean-Square Error
MRCP	Multiple Relay Communication Protocol
NF-IWF	Neighbor-friendly Iterative Water Filling
OFDM	Orthogonal Frequency Division Multiplexing
PDF	Probability Density Function
PNC	Physical-layer Network Coding
RX	Receiving node
SFR	Soft Frequency Reuse
STNC	Space-Time Network Coding
TAS	Topology-aware STNC
TDMA	Time Division Multiple Access
TWRC	Two-Way Relay Channel
TX	Transmitting node

Contents

Abstract iii

Contents xiii

List of Figures xix

List of Tables xxv

1 General Introduction 1

1.1 Network Densification 1

1.2 Inter-cell Interference in Dense Networks 2

1.3 Cooperative Strategies 3

1.4 Overview of this Thesis 5

2 Neighbor-Friendly Autonomous Power Control 9

2.1 Introduction 10

2.2 IWF-Based Power Control 12

2.3 Neighbor-Friendly Autonomous Power Control 14

2.3.1 Victim Users Protection with NF-IWF 14

2.3.2 Estimation of the victim users channel 18

2.3.3 Complexity reduction of NF-IWF 20

2.4 Performance Evaluation 22
2.4.1 Macro-Macro Interference 23
2.4.2 Femto-Macro Interference 24
2.4.3 Multi-user Multi-cell Interference 25
2.5 Sensitivity Analysis 29
2.6 Computational Complexity for Convergence 31
2.7 Conclusions 32

3 Exploiting the Overhearing Capabilities of Relaying D2D Users 35
3.1 Introduction 36
3.2 System Model 38
3.3 Resource Orthogonalization Approach: TDMA 39
3.4 AFR with D2D Communication 40
3.4.1 Square Array 40
3.4.2 Hexagonal Array 46
3.5 Multiple Cell Edge Users 52
3.6 Performance Analysis 57
3.6.1 Square Array (M=1) 57
3.6.2 Hexagonal Array (M=1) 59
3.6.3 Multiple Cell Edge Users 60
3.6.4 Spectral Efficiency and BER 61
3.7 Performance Evaluation 62
3.7.1 Varying the D2D users transmit power with fixed BS transmit power 62
3.7.2 Varying equally the D2D users transmit power and the BS transmit power 65
3.8 Conclusions 67

4 Exploiting the Overhearing Capabilities of Base Stations in Dense Networks 69

4.1 Introduction 70

4.2 System Model 73

4.2.1 Baseline Approaches 74

4.2.2 Proposed Approach with Two Base Stations: MRCP-2 . 78

4.3 Extension to an Arbitrary Number of Base Stations and Users 82

4.3.1 Extended Baseline Approaches 82

4.3.2 Proposed Approach with L Base Stations: MRCP-L . . 87

4.4 Performance Evaluation 91

4.4.1 JFI Evaluation 91

4.4.2 Spectral Efficiency Evaluation 91

4.4.3 BER Evaluation 94

4.4.4 Final remarks 95

4.5 Conclusions 96

5 Topology-Aware Space-Time Network Coding 97

5.1 Introduction 98

5.2 System Model 100

5.3 Baseline Schemes 101

5.3.1 Simultaneous Transmissions Scheme (INTF) 101

5.3.2 Orthogonal Transmissions Scheme (TDMA) 102

5.3.3 Modified STNC (mSTNC) 103

5.4 Topology-Aware STNC (TAS) 105

5.4.1 Simple Case with $K = 1$ 105

5.4.2 General Case with $K \geq 1$ 109

5.4.3 Performance Analysis 115

5.5 Performance Evaluation 120

5.5.1 Evaluation with Equal Transmit Power and Channel Conditions . . . 120
5.5.2 Evaluation with Unequal Transmit Power and Channel Conditions . . . 124
5.6 Conclusions . . . 125

6 Are Overhearing Strategies Energy Efficient? 129

6.1 Introduction . . . 130
6.2 System Model . . . 133
6.3 Baseline Approaches That Do Not Exploit the Overhearing Capabilities of TXs . . . 135
6.3.1 TDMA . . . 135
6.3.2 INTF . . . 136
6.4 Approaches That Exploit the Overhearing Capabilities of TXs 137
6.4.1 DIV . . . 138
6.4.2 MRCP . . . 141
6.5 Complexity Analysis . . . 149
6.6 Performance Evaluation . . . 150
6.7 Conclusions . . . 154

7 General Conclusions and Future Work 159

7.1 Chapter 2 . . . 160
7.2 Chapter 3 . . . 160
7.3 Chapter 4 . . . 161
7.4 Chapter 5 . . . 161
7.5 Chapter 6 . . . 161
7.6 Future Work . . . 162

A Appendix 165

A.1 165
A.2 167
A.3 168
A.4 170
A.5 171

Bibliography **175**

List of Publications **185**

List of Figures

1.1 Graphical overview of the thesis chapters. 7

2.1 Soft frequency reuse. 11

2.2 Data rate difference between IWF and EPA for a network with 5 macrocells evenly distributed over a 30x30 km area. 14

2.3 Network with 5 macrocells, 20 femtocells, and 500 users. 15

2.4 Data rate difference between IWF and EPA for a network with 5 macrocells evenly distributed and 20 femtocells randomly distributed over a 30x30 km area. 15

2.5 Transmit power allocation from 2 neighboring base stations to 2 cell-edge users over 200 subcarriers. Each base station is transmitting to a cell-edge user and interfering with the other base station. One base station uses NF-IWF and the other uses IWF. 18

2.6 Case 1: high interference. The victim user is located within the coverage of the neighboring cell, resulting in high interference. . 20

2.7 Case 2: low interference. The victim user is located between two cells, resulting in low interference. 20

2.8 Normalized data rates for different values of distance d when applying NF-IWF. 21

2.9 Rate region of the primary and victim users of the macro-macro high interference case. 24

2.10 Rate region of the primary and victim users of the macro-macro low interference case. 25

2.11 Case 1: high interference. The victim user attached to the macrocell is located within the coverage of the neighboring femtocell, resulting in high interference. 26

2.12 Case 2: low interference. The victim user attached to the macrocell is far from the femtocell, resulting in low interference. 26

2.13 Rate region of the primary and victim users of the macro-femto high interference case. 27

2.14 Rate region of the primary and victim users of the macro-femto low interference case. 27

2.15 CDF of victim and primary users of the multi-user scenario. . . 28

2.16 Channel transfer function with an estimation error of zero mean and *std* standard deviation. 29

2.17 Sensitivity analysis on the channel estimation. 30

2.18 Number of iterations per subcarrier per base station to reach convergence in the proposed algorithms. 32

2.19 Complexity analysis for different values of windows. 32

3.1 Square array with TDMA transmission. The white cells have BSs transmitting to one of their cell edge users, while the shaded cells have inactive BSs (not transmitting to any cell edge user). 40

3.2 Hexagonal array with TDMA transmission. The white cells have BSs transmitting to one of their cell edge users, while the shaded cells have inactive BSs (not transmitting to any cell edge user). Cell edge users are represented by the black dots (only the cell edge users in the numbered cells are shown). 41

3.3 Square array. The red thin arrows point out the isotropic transmission from a BS intended for a particular user. The magenta arrows represent the D2D transmissions. The shaded cells represent the inactive cells. The basic tile of this transmission scheme has diagonal stripes as background. 43

3.4 Hexagonal array. The red thin arrows point out the isotropic transmission from a BS intended for a particular user. The magenta thick arrows represent the D2D transmissions. The shaded cells represent the inactive cells (not transmitting to any cell edge user). The basic tile of this transmission scheme has diagonal stripes as background. Cell edge users are represented by the dots and numbered clockwise from 1 to 6 starting with the white dot (only the cell edge users from BS_1 are shown). . 47

3.5 Square array with multiple cell edge users for TS1 in the first transmission round. The red thin arrows point out the isotropic transmission from a BS intended for a particular user. The magenta thick arrows represent the D2D transmissions to the user inside the blue circle. 53

3.6 Square array with multiple cell edge users per cell edge for TS1 in the second transmission round. The red thin arrows point out the isotropic transmission from a BS intended for a particular user. The magenta thick arrows represent the D2D transmissions to the user inside the blue circle. 54

3.7 Spectral efficiency per time-slot of the studied approaches with $P_l = 5\text{dB}\ \forall l$ for the square array. 63

3.8 Spectral efficiency per time-slot of the studied approaches with $P_l = 5\text{dB}\ \forall l$ for the hexagonal array. 63

3.9 BER of the proposed approach with $P_l = 5\text{dB}\ \forall l$ for the square array. 64

3.10 BER of the proposed approach with $P_l = 5\text{dB}\ \forall l$ for the hexagonal array. 64

3.11 Spectral efficiency per time-slot of the studied approaches with equal transmit power for the square array. 65

3.12 Spectral efficiency per time-slot of the studied approaches with equal transmit power for the hexagonal array. 66

3.13 BER of the proposed approach with $P_T = P_l = p_{m,l}\ \forall m, l$ for the square array. 66

3.14 BER of the proposed approach with $P_T = P_l = p_{m,l}\ \forall m, l$ for the hexagonal array. 67

4.1 System model for the case of two base stations and two users. The parameter h_{ml} defines the channel gain of Ul from BSm and g_{mn} defines the channel gain of BSn from BSm. TSt defines the t-th time-slot. 79

4.2 JFI for $L = 2$ and $L = 10$. We consider the same η_m from all but one base station, i.e. $\eta_1 = \eta_3 = \cdots = \eta_L = \bar{\eta}$ and $\eta_2 = 0$dB. 92

4.3 Minimum spectral efficiency per time-slot for $\eta_2 = 0$dB. 92

4.4 Minimum spectral efficiency per time-slot for $\eta_2 = 10$dB. . . . 93

4.5 Minimum spectral efficiency per time-slot for L = 10. We consider the same η_m from all but one base station, i.e. $\eta_1 = \eta_3 = \cdots = \eta_L = \bar{\eta}$ and $\eta_2 = 0$dB. 93

4.6 Minimum spectral efficiency of the studied approaches. We consider the same η_m from all but one base station, i.e. $\eta_1 = \eta_3 = \cdots = \eta_L = \bar{\eta}$ and $\eta_2 = 0$dB. 94

4.7 BER for BPSK for $L = 2, 5, 10, 20$ (small numbers). For simplicity we consider the same η_m from all the base stations $\eta_1 = \eta_2 = \cdots = \eta_L = \bar{\eta}$. 95

4.8 BER for BPSK for $L = 2$ and $\eta_2 = 0$dB, 10dB. 96

5.1 Wyner model for a cellular network. The cluster considers the $2K$ closest BSs, i.e. $\mathcal{C}_l = \text{BS}\{l-1, l, l+1\}$ for $K = 1$, with a distance d between BSs. 100

5.2 Transmission phase TAS1 and TAS2. BS$(l-1) \rightarrow s_{l-1}$ and BS$(l+1) \rightarrow s_{l+1}$. 106

5.3 Transmission phase TAS1 and TAS2. BS$l \rightarrow s_l$. 106

5.4 Relaying phase TAS1. BS$(l-1) \rightarrow s_{l-2} + s_l$ and BS$(l+1) \rightarrow s_l + s_{l+2}$. 106

5.5 Relaying phase TAS1. BS$l \rightarrow s_{l-1} + s_{l+1}$. 107

5.6 Relaying phase TAS2. BS$(l-1) \rightarrow s_{l-2} + s_l$, BS$l \rightarrow s_{l-1} + s_{l+1}$, and BS$(l+1) \rightarrow s_l + s_{l+2}$. 107

5.7 Spectral efficiency per time-slot of the different schemes with $K = 1$ and equal transmit power and channel conditions. 121

5.8 Spectral efficiency per time-slot of the different schemes with $K = 2$ and equal transmit power and channel conditions. 121

5.9 Spectral efficiency per time-slot of the different schemes with $K = 4$ and equal transmit power and channel conditions. . . . 122

5.10 BER of the different schemes with equal transmit power and channel conditions.. 123

5.11 Spectral efficiency per time-slot of TAS1. 123

5.12 Spectral efficiency per time-slot of the different schemes for $K = 2$ with unequal transmit power and equal average channel gains, i.e. $\mathbb{E}\{|h_{m,l}|^2\} = \mathbb{E}\{|g_{m,n}|^2\} = 1\ \forall m, l, n.$ 125

5.13 BER of the different schemes for $K = 2$ with unequal transmit power and equal average channel gains, i.e. $\mathbb{E}\{|h_{m,l}|^2\} = \mathbb{E}\{|g_{m,n}|^2\} = 1\ \forall m, l, n.$ 126

5.14 Spectral efficiency per time-slot of the different schemes for $K = 2$ with equal transmit power and unequal channel conditions, i.e. $\mathbb{E}\{|h_{l,l}|^2\}$ is 10dB lower than the average channel gain of the rest of the links. 126

5.15 BER of the different schemes for $K = 2$ with equal transmit power and unequal channel conditions, i.e. $\mathbb{E}\{|h_{l,l}|^2\}$ is 10dB lower than the average channel gain of the rest of the links. . . 127

5.16 Spectral efficiency per time-slot of the different schemes for $K = 2$ with equal transmit power and unequal channel conditions, i.e. $\mathbb{E}\{|h_{l,l}|^2\}$ and $\mathbb{E}\{|g_{m,n}|^2\}$ $\forall m, n$ are 10dB lower than the average channel gain of the rest of the links 127

5.17 BER of the different schemes for $K = 2$ with equal transmit power and unequal channel conditions, i.e. $\mathbb{E}\{|h_{l,l}|^2\}$ and $\mathbb{E}\{|g_{m,n}|^2\}$ $\forall m, n$ are 10dB lower than the average channel gain of the rest of the links 128

6.1 Exploiting the strong overhearing link in dense networks for downlink and uplink communication. 131

6.2 Energy efficiency of the studied approaches in the transmit power dominated regime with $S_1^{\min} = S_1^{\min} = 0.3$bits/Hz. 152

6.3 Success rate of the studied approaches in the transmit power dominated regime with $S_1^{\min} = S_1^{\min} = 0.3$bits/Hz. 153

6.4 Energy efficiency of the studied approaches in the transmit power dominated regime with $S_1^{\min} = S_1^{\min} = 0.3$bits/Hz. 153

6.5 Success rate of the studied approaches in the transmit power dominated regime with $S_1^{\min} = S_1^{\min} = 0.3$bits/Hz. 154

6.6 Energy efficiency of the studied approaches in the circuit power dominated regime with $S_1^{\min} = S_1^{\min} = 0.3$bits/Hz. 154

6.7 Spectral efficiency of the studied approaches in the circuit power dominated regime with $S_1^{\min} = S_1^{\min} = 0.3$bits/Hz. 155

6.8 Success rate of the studied approaches in the circuit power dominated regime with $S_1^{\min} = S_1^{\min} = 0.3$bits/Hz. 155

6.9 Energy efficiency of the studied approaches in the transmit power dominated regime with equal average links. 156

6.10 Success rate of the studied approaches in the transmit power dominated regime with equal average links. 156

6.11 Energy efficiency of the studied approaches in the circuit power dominated regime with equal average links. 157

6.12 Success rate of the studied approaches in the circuit power dominated regime with equal average links. 157

List of Tables

2.1 Simulation Parameters. 23

5.1 TDMA transmission strategy 103
5.2 mSTNC transmission strategy ($K = 1$) 104
5.3 TAS1 transmission strategy ($K = 1$) 108
5.4 TAS2 transmission strategy ($K = 1$) 108

Chapter 1

General Introduction

1.1 Network Densification

Cellular networks are ubiquitous. There are few places on Earth where some type of wireless access is not deployed. Just in 2016, almost half a billion mobile devices and connections were added, most of which were smartphones. It is expected that this number will grow by 50% within the next 5 years, up to 1.5 devices per capita. Not only are the number of mobile devices increasing with the years, but also the amount of traffic generated by each of them. Mobile data traffic has grown 18-fold over the past 5 years, with a 63% growth just in the last year, reaching 7.2 exabytes per month at the end of 2016. By 2021, this is expected to increase to 49 exabytes per month, the strongest growth coming from Middle East, Africa, and China [22].

This growth contrasts with the limited bandwidth that needs to be shared among an increasing number of users, turning bandwidth into a scarce and valuable resource that requires careful management. This tendency is motivating research institutions, service providers, and chip vendors to develop more efficient solutions to manage the bandwidth in multi-user communication systems [15].

Improvements from a physical layer perspective have shown low potential to deal with these demands. Coopers Law, proposed by the celebrated pioneer of cellular communications Martin Cooper, states that the wireless system capacity has grown a million times since 1957 [24]. But what are the main factors driving these improvements? According to Cooper this growth can be attributed to 3 main factors. From the million times increase, 5 times can be attributed to the ability of dividing the spectrum in narrower slices to transmit

independently in each of them: frequency division. Another 5 times can be attributed to different modulation techniques and spread spectrum and link adaptation approaches. Then, 25 times can be attributed to the use of more spectrum. Finally, an amazing 1600 times can be attributed to the spectrum reuse through the increase in the number of wireless infrastructure nodes, or network densification, which reduces the cell size and the transmission distance.

It might seem that adding more base stations has a marginal effect on the network capacity since both the received signal power and the interference power increase similarly. As long as we assume that the network is interference-limited (noise is negligible vs interference), that mobile users connect to the strongest base station (open access), and Rayleigh fading, the signal-to-interference-plus-noise ratio (SINR) distribution is independent from the density of BSs, from the number of tiers, and from their relative power levels [38]. This results in the aereal capacity of the network (capacity per unit of area) increasing linearly with the number of base stations deployed [30]. In practice, factors such as the minimum distance between BS and user, the path loss decay, and the line of sight decay reduce this gain [53]. Furthermore, many base stations are closed access and it might be suboptimal for users to connect to the strongest base stations if they are heavily loaded. In any case, a careful network planning, interference management schemes, and users' resource allocation can mitigate these losses. Still, the intuition behind these theoretical results strongly supports increasing the density of base stations deployed as shown in different papers [38, 53, 43, 27]. No wonder why network densification has become one of the main strategies to cope with the capacity demands of 5G networks [14, 51].

1.2 Inter-cell Interference in Dense Networks

Femtocells offer the easiest and most cost-effective way to increase the current deployment of base stations [21]. Femtocells are low-power base stations mainly for indoor usage with a coverage of tens of meters, compared to the coverage of a few kilometers of high-power base stations (macrocells). Femtocells are typically deployed within the coverage of macrocells in order to improve the data rates at given hotspots like restaurants, airports, schools, and office buildings. However they are not the only small base stations that are deployed. Microcells, picocells as well as distributed antenna systems (remote radio heads) all have similar goals with a few differences in their transmit powers, coverage areas, physical size, backhaul connection, and propagation characteristics [38, 63]. In literature they are all mostly referred to as small cells. The coexistence of different types of cells in the same area is referred to as a heterogeneous network (HetNet) [27].

For users located close to their serving base station, the signal of the serving base station is stronger than the signal from neighboring base stations. We refer to these users as cell center users. In this case, each base station only needs to divide the bandwidth among its center users to avoid generating interference among them, or intra-cell interference. Simple orthogonal approaches that assign disjoint time or frequency resources to users, such as time division multiple access (TDMA) or frequency division multiple access (FDMA), have been proven to deal with intra-cell interference efficiently [86]. Since inter-cell interference is not an issue for these users, reusing the bandwidth in each cell represents the best option.

The largest negative impact of network densification is for users located between neighboring cells, referred to as cell edge users. It is at the cell edge where the signal strength coming from neighboring base stations equals or even exceeds that from the serving base station, generating inter-cell interference.

Most urban areas are already fully-covered by macrocells. Hence, the addition of more small cells in these areas creates serious inter-cell interference problems. Since femtocells are likely to be deployed in an unplanned manner by end-users and not by network operators, this problem is only going to grow in the coming years [7, 79]. This situation becomes worse if we consider closed-access base stations. Closed-access base stations are meant to serve only some specific users and might thus be a source of a very large inter-cell interference for users close to them that have no access. The practical challenges of HetNets have been widely identified by academia and organizations such as 3GPP [7] and the Small Cell Forum [79].

1.3 Cooperative Strategies

The goal of traditional approaches in wireless networks is to cancel inter-cell interference in order to improve the system performance. However, this often leads to suboptimal and counter-productive solutions. Instead, by exploiting cooperation among nodes from different cells, the overall system performance can be increased by allowing nodes to help each other at the cost of dedicating some of their resources for other nodes. Furthermore, in dense cellular networks, the probability of finding strong links between different nodes makes it a suitable use case for cooperation. In this context, inter-cell interference can be considered an opportunity instead of an obstacle.

Base stations play a crucial role in dealing with inter-cell interference. Cooperation between base stations is key in this respect since it results in a more efficient allocation of bandwidth resources. Proof of this is the

implementation of inter-cell interference coordination (ICIC) techniques in cellular networks [54, 89, 63, 55, 16, 69].

Most cooperative strategies between base stations assume some sort of communication between base stations, typically realized through a backhaul link. The availability of a backhaul link between base stations allows them to exchange detailed channel state information (CSI). This information helps each base station to select a given resource allocation and to inform of this allocation to other base stations. This is typically done per user for different time-slots and for different subcarriers (in OFDM networks).

However, there are a few problems with this type of cooperation in dense networks. First, the operating costs of maintaining a backhaul link between all the small cells are substantial [20]. Second, given the large number of base stations and users in dense networks and the large variability in time and frequency of the wireless channel, obtaining reliable and global CSI remains an expensive overhead [67].

These constraints urgently call for cooperative strategies that can reuse resources, while keeping the exchange of CSI between base stations to a minimum. One way consists in exploiting the broadcast nature of the wireless channel to overhear transmitted data or CSI. This is especially favorable in dense networks, where the proximity between the nodes results in a high probability of finding strong links between transmitting nodes that have no intentional communication. This could be between users and interfering base stations (first case) or between different base stations (second case).

In the first case, base stations can use CSI transmitted by users from other base stations to allocate resources efficiently, for instance to select a given subcarrier and a given transmit power (Chapter 2). Also, users can relay data from interfering base stations to the (closest) intended users (Chapter 3). Different from most cooperative relay strategies that require dedicated resources (time-slots) for the transmission phase and the relaying phase, we focus on the case where the time-slots are reused, i.e. shared by other users.

In the second case, base stations can act as relays to retransmit data to users from different base stations in order to improve their spectral efficiency and spatial diversity (Chapters 4, 5). We focus on the case where the resources (time-slots) are shared by the relaying base stations. However, these strategies still require some of the wireless resources to be split for serving the intended user and other users. This has an impact not only in the number of additional resources, but also on the extra energy consumption (Chapter 6). However, as we will see later, the gains in spectral efficiency and energy efficiency are worth their implementation.

As seen from the previous cases, the strategies presented in this thesis aim to exploit the overhearing capabilities of the network instead of cancelling inter-cell interference while reducing the CSI exchange and reusing resources. As we will see in the following chapters, the performance gains that can be achieved by using the overheard information in an altruistic way can serve as incentive to promote the use of the proposed cooperative strategies.

1.4 Overview of this Thesis

This thesis is divided in 7 chapters. Chapters 2-6 correspond to published or submitted journal papers, while Chapter 7 presents the general conclusions and future work. In the following we give a brief overview of Chapters 2-6.

Chapter 2 presents a power control algorithm for wireless OFDM networks. Power control allows base stations to reuse the bandwidth by regulating the transmit power to serve a given user, while reducing the inter-cell interference of users served by neighboring cells. However, most power control strategies in current cellular networks require a backhaul link between base stations that allows them to cooperate to allocate resources for their users. The X2 interface in the Long Term Evolution (LTE) standard is such an example [23, 33, 62, 71, 74].

In dense networks, the proximity between base stations allows them to overhear the CSI transmitted by users to their serving base stations. This information can be used by the base station to adopt an autonomous power control strategy that, without any CSI exchange between base stations, can increase the data rate of the users served by the base station performing the power control strategy, while protecting the data rate of users from neighboring cells. This is more thoroughly explained in Chapter 2.

Users can also exploit overheard data from base stations. Cell edge users in dense network constantly receive (interfering) signals from other base stations intended to users located in the proximity. Due to this proximity, these cell edge users can relay the overheard signals to the intended users *without traversing the base station*, introducing spatial diversity. This is called device-to-device (D2D) communication. The key of this strategy is to realize this communication during the time-slots in which users are not receiving their intended signal in order to avoid creating additional inter-cell interference. This is explained in Chapter 3.

Base stations in dense networks can also act as relays by transmitting overheard data to users from other base stations. In this way, data arrives to each user from different signal paths, introducing spatial diversity. As we will see in

Chapter 4, this cooperative strategy not only increases the spatial diversity for all the users, but it also serves as a means to improve fairness.

The previous strategy considers that all the base stations and users can overhear the transmissions from all the other base stations in the network (or in a cluster of base stations). However, base stations and users typically overhear only a set of the closest neighboring BSs and this set can be partially overlapping with other sets. A widely-used cellular model to represent this interaction is the Wyner model [92].

In Chapter 5 we present a strategy that exploits the network topology represented by the Wyner model. This is done by allowing base stations that *do not overhear each other* to transmit simultaneously the data to their intended users in a first (transmission) phase, hence reusing the bandwidth in these base stations. Then, in a second (relaying phase), these base stations relay again simultaneously the overheard signals in order to increase the spatial diversity and spectral efficiency.

As mentioned before, base stations must split their resources to serve intended users and other users. This of course has a cost on energy consumption and amount of resources that could be otherwise used for the intended users. This is analyzed in Chapter 6 for two overhearing strategies. Moreover, the best strategy might not always be to transmit with full power, but to transmit with power according to the channel conditions. However, knowing the transmit power of each base station that maximizes the overall energy efficiency often requires an exhaustive search, even for a small network. Therefore, we also propose a sub-optimal power control strategy that achieves a performance close to the optimal. This is done by dividing the problem into two power regimes (circuit power and transmit power dominated regimes) and then performing a simple comparison and a closed-form formula.

A graphical overview of the chapters of this thesis can be seen in Fig. 1.1.

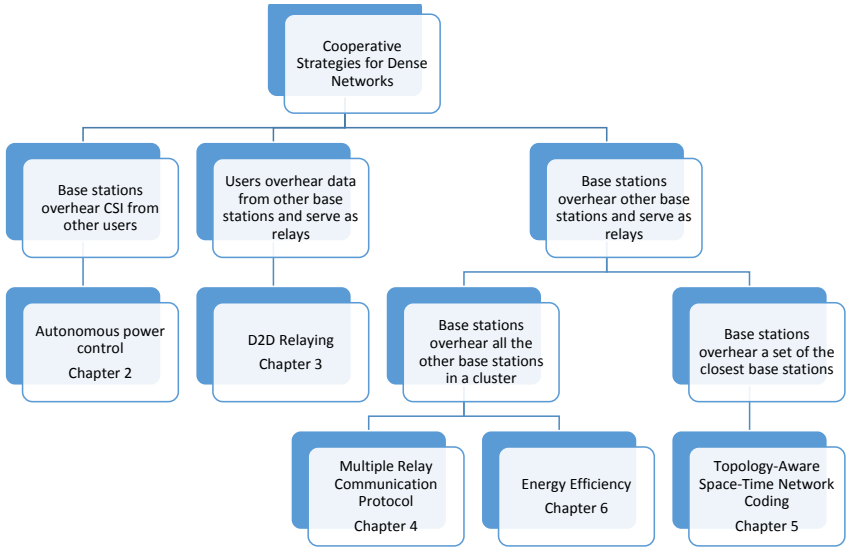

Figure 1.1: Graphical overview of the thesis chapters.

Chapter 2

Neighbor-Friendly Autonomous Power Control

Abstract

The widespread deployment of base stations constitutes a promising solution to cope with the ever-increasing wireless data rate demands. However, it also increases the interference levels, especially at the cell-edge. Most interference management techniques assume coordination between base stations, which involves undesired overhead and delays. To solve this problem, we propose a neighbor-friendly autonomous algorithm for power control in wireless heterogeneous networks that protects victim users from neighboring cells through a penalty factor in the power allocation level. We refer to this algorithm as neighbor-friendly iterative waterfilling (NF-IWF). In addition, we propose a low-complexity closed-form version that fixes the penalty factor by assuming a linear approximation of the victim users data rate. In high interference conditions, it can achieve a victim users data rate increase by a factor of 3.5 compared to IWF, 15 compared to soft frequency reuse (SFR) and 60 compared to equal power allocation (EPA) with a marginal decrease of the primary users data rate.[1]

[1]This chapter is cited from Torrea-Duran, R., Tsiaflakis, P., Vandendorpe, L., Moonen, M., "Neighbor-Friendly Autonomous Power Control in Wireless Heterogeneous Networks", EURASIP Journal on Wireless Communications and Networking, vol. 175, 2014, pp. 1–17, doi:10.1186/1687-1499-2014-175.

2.1 Introduction

Varying the transmission power levels according to the channel conditions has shown important gains in orthogonal frequency division multiplexing (OFDM) networks [16, 54, 55, 63]. The basic idea of OFDM is to exploit the frequency variability of the wireless channel by dividing the total bandwidth in several subcarriers, each with a flat channel. Then, by controlling the power allocated in each subcarrier a given base station can reduce inter-cell interference and as a result neighboring base stations can reuse those same subcarriers. However, most of the power control schemes implemented in current networks allow only a few discrete power values spanning over large frequency bands, lacking adaptivity to the channel conditions.

A typical example is soft frequency reuse (SFR) [1], in which the total bandwidth of each cell is divided in two non-overlapping frequency bands, one for center users (primary users in our case) and one for cell-edge users (victim users in our case). The center users band can be reused in all the cells, while the cell-edge users band is non-overlapping between neighboring cells, as can be seen in Fig. 2.1. The transmit power level is constant in each band, but larger for the cell-edge users' band to compensate for the performance degradation. This approach offers a simple way to deal with frequency and power allocation jointly without interference, but with the disadvantage of a fixed allocation of frequency bands and transmit powers. The optimization of SFR is usually done by adapting the parameters α and β, which represent the total power fraction and total bandwidth fraction of the center users band, respectively [35]. However, this can only be achieved through network coordination.

To support coordination between base stations, a dedicated backhaul link is required. In LTE, the X2 interface between macrocells helps to configure dynamically the frequency bands and power levels [23, 33, 62, 71, 74]. However, this interface is not yet standardized between macro and femtocells in early versions of LTE release 11 [5, 6]. Even with an interface available, the dynamics of the wireless channel and the variability in the number of users attached to a cell, users' location, and interference conditions, this coordination constitutes a significant information overhead resulting in large delays.

An alternative approach is that each base station optimizes its own resource allocation without any information exchange. We refer to it as an autonomous algorithm. Two well-known autonomous power control algorithms for OFDM networks are equal power allocation (EPA) and iterative waterfilling (IWF) [95]. In EPA, the total transmit power is allocated equally in all available subcarriers. In IWF, each base station maximizes its own data rate in a greedy way by allocating more power to those subcarriers with the best channel to interference

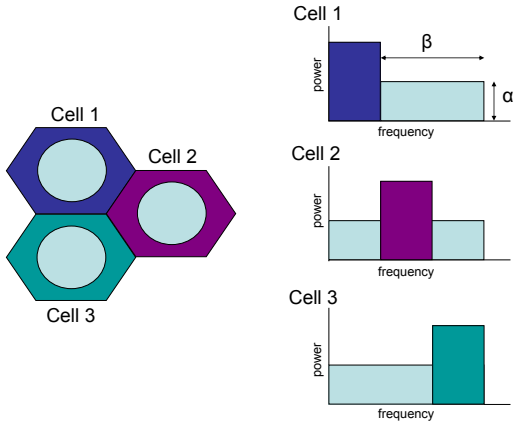

Figure 2.1: Soft frequency reuse.

and noise ratio (CINR), without considering the interference caused to victim users from neighboring cells.

Non-greedy autonomous power control algorithms have been studied in the context of digital subscriber line (DSL) networks. In [19] and [87] low-complexity autonomous power control algorithms for DSL, called ASB and ASB-2 are presented, which allow a non-orthogonalized share of resources. The concept of a protected reference line (or reference user) is introduced in these papers as a statistical average of all victim lines suffering interference. However, the implementation of these algorithms in practical wireless networks imposes a challenge given the multi-user scheduling and non-stationarity of the wireless channel.

A first attempt was made in [81] to apply the previous concept to a wireless network where the user suffering the strongest interference from the neighboring cells is selected as the reference user. However, this scheme is not autonomous since it needs periodical information exchange between base stations to adapt to the time-varying reference user channel characteristics.

To tackle the mentioned problems, we propose in this chapter a neighbor-friendly autonomous algorithm for power control in wireless heterogeneous networks. It protects victim users within a certain distance from the base station through a frequency-dependent penalty factor in the power allocation level. The level of protection can be tuned to provide individualized quality of service (QoS). We refer to this algorithm as neighbor-friendly iterative waterfilling (NF-IWF). Additionally, we propose a low-complexity closed-form version that fixes the

penalty factor by assuming a linear approximation of the data rate of the victim users.

We can summarize the main contributions of this chapter as follows:

1. A power control algorithm that protects victim users from neighboring cells located a a distance from the base station without any coordination between base stations.
2. A practical way to tune the protection to victim users from neighboring cells.
3. A practical way to obtain the channel information of victim users attached to neighboring cells without communication between base stations.
4. A low complexity closed-form version of the previous algorithm by assuming a linear approximation of the data rate of the victim users.
5. The exploitation of frequency and time correlation of the wireless channel to further reduce the complexity of the algorithm.

2.2 IWF-Based Power Control

Autonomous algorithms do not rely on information between base stations, they only exploit locally-available (and a-priori known) information about the environment such as direct channel gains, received interference, and noise. IWF exploits this information to maximize the data rate in each cell:

$$\begin{aligned} \underset{s_k^c\ \forall k}{\text{maximize}} \quad & R^c \\ \text{s.t.} \quad & \sum_{k\in\mathcal{K}} s_k^c \le P^{c,\text{tot}} \\ & 0 \le s_k^c \le s_k^{c,\text{mask}}\ \forall k \in \mathcal{K} \end{aligned} \tag{2.1}$$

with

$$R^c = f_s \sum_{k\in\mathcal{K}} b_k^c = f_s \sum_{k\in\mathcal{K}} \log_2 \left(1 + \frac{1}{\Gamma} \frac{|h_k^c|^2 s_k^c}{\sum\limits_{\substack{\bar{c}\neq c \\ \bar{c}\in\mathcal{C}}} |h_k^{\bar{c}}|^2 s_k^{\bar{c}} + \sigma_k^c} \right) \tag{2.2}$$

where R^c is the data rate of all users in cell c, f_s is the symbol rate, b_k^c, h_k^c, σ_k^c, s_k^c, and $s_k^{c,mask}$ are the bit loading for a standard interference channel model, the channel transfer function, the noise power, the base station transmit power,

and the spectral emission mask constraints on subcarrier k in cell c, respectively; $h_k^{\bar{c}}$ and $s_k^{\bar{c}}$ are the channel transfer function and transmit power on subcarrier k from the interfering cell $\bar{c}$, which are both assumed to be known as they affect users in cell c. We call h_k^c the direct channel and $h_k^{\bar{c}}$ the interfering channel of the users attached to cell c. The parameters $\mathcal{C}$ and $\mathcal{K}$ are the set of available cells and subcarriers, respectively, and $P^{c,\text{tot}}$ is the total power budget in cell c. A given subcarrier can only be allocated to one user in cell c, but it can also be allocated to a user from a neighboring cell resulting in inter-cell interference. The allocation of subcarriers to users in cell c can be done prior to the described power allocation strategies (based, for example, on instantaneous channel conditions or iteratively with the power allocation). However, our focus is only on the power allocation. A joint autonomous power and subcarrier allocation algorithm is nevertheless an interesting scenario that we will study for future work. The parameter Γ denotes the signal-to-noise ratio (SNR) gap to capacity, which depends on the desired bit error rate (BER), the coding gain, and the noise margin. We will assume it to be equal to 1 without loss of generality.

It can be shown, using the corresponding Karush-Kuhn-Tucker (KKT) conditions, that the transmit powers have a closed-form solution as follows

$$s_k^c = \left[\frac{f_s}{\log(2)\lambda_c} - \frac{\sum_{\bar{c}\neq c} \Gamma |h_k^{\bar{c}}|^2 s_k^{\bar{c}} + \Gamma \sigma_k^c}{|h_k^c|^2} \right]_0^{s_k^{c,\text{mask}}} \tag{2.3}$$

where $[x]_a^b = \max(a, \min(x, b))$ and λ_c is the Lagrange multiplier that should be updated (e.g. with bisection) to satisfy the corresponding total power constraint $P^{c,\text{tot}}$.

To analyze the benefit of exploiting locally-available information, we consider a network with 5 macrocells evenly distributed over a 30x30km area, each with a 43dBm total transmit power and 5MHz bandwidth. As channel model we use the 3GPP spatial channel model (SCM [8]) with suburban macro environment and a distance(d)-dependent path loss of $31.5 + 35 \log_{10}(d[m])$. This model was chosen due to its general use in environments with a combination of macro and femtocells. We show in Fig. 2.2 the difference between the data rates obtained using IWF and EPA of a user moving along every possible location on this area. The results can be seen in a tri-dimensional plot where the x and y axis correspond to the area, and the z axis corresponds to the data rate difference between IWF and EPA. A maximum difference of 400 Mbps can be observed, interestingly, at the cell-edge of neighboring cells.

This scenario becomes more critical when femtocells are deployed. We now introduce into the previous network topology 20 femtocells randomly distributed (i.e. deployed in an unplanned manner), each with a 15dBm total transmit power. The exact location of each base station can be seen in Fig. 2.3. We assume that some of the base stations are closed-access, hence the users can be within the range of a neighboring cell without connecting to it. We compute again the difference between the data rates obtained using IWF and EPA of a user moving along every possible location. The results are shown in Fig. 2.4. The femtocells deployment results in more severe interference problems, especially at the cell-edges. Remarkably, a maximum difference of 1250 Mbps can be observed at the cell-edge of multiple interfering cells (macro and femtocells). This again shows the potential gains exploiting locally-available information.

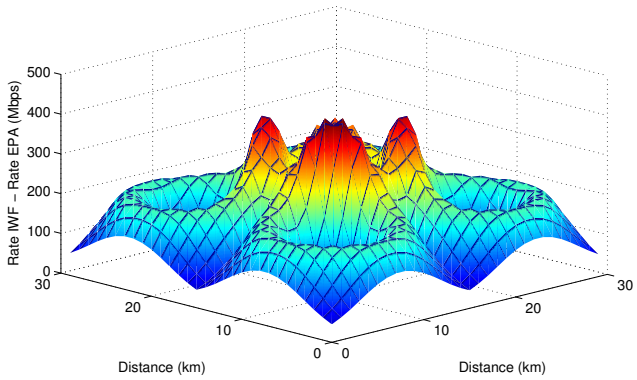

Figure 2.2: Data rate difference between IWF and EPA for a network with 5 macrocells evenly distributed over a 30x30 km area.

The advantage of IWF is its simplicity, its closed-form solution, and the fact that it does not need any information exchange between base stations. However, each cell maximizes its own data rate in a greedy fashion by allocating power especially to those subcarriers with the best CINR, without considering the interference caused to victim users from neighboring cells.

2.3 Neighbor-Friendly Autonomous Power Control

2.3.1 Victim Users Protection with NF-IWF

Our aim is therefore to design a neighbor-friendly approach that, without any information exchange in the network, limits this damage. Using the concept

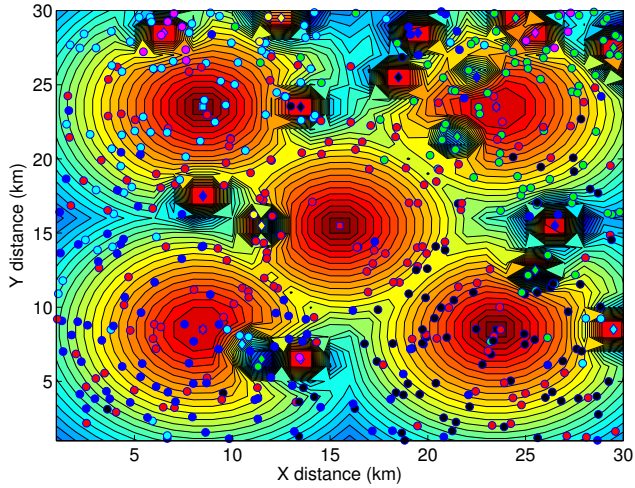

Figure 2.3: Network with 5 macrocells, 20 femtocells, and 500 users.

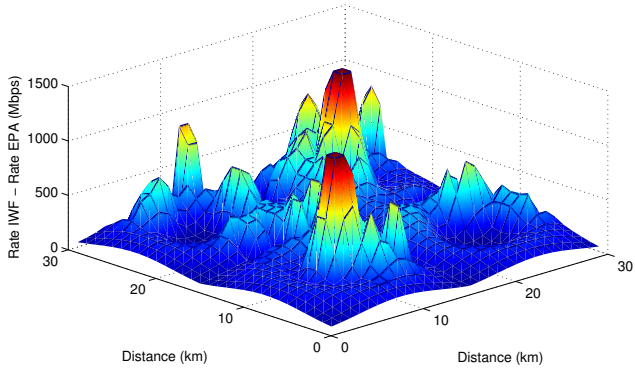

Figure 2.4: Data rate difference between IWF and EPA for a network with 5 macrocells evenly distributed and 20 femtocells randomly distributed over a 30x30 km area.

of a protected reference user, we formulate optimization problem (2.1) as the weighted sum of the data rate of users attached to cell c, or primary users, denoted as R^c and the data rate of victim users attached to one neighboring cell, denoted as R^{vc}. Both cells share the set of subcarriers $\mathcal{K}$. Adding extra optimization terms for other neighboring cells only brings minimal performance at a high complexity cost since most of the per-subcarrier interference comes from one base station [81]. However, other neighboring cells can be considered

if they share a different set of subcarriers with cell c. Again, the subcarrier allocation to users is assumed to be done prior to the power allocation.

$$\begin{aligned} \underset{s_k^c\ \forall k}{\text{maximize}} \quad & w^c R^c + w^{vc} R^{vc} \\ \text{s.t.} \quad & \sum_k s_k^c \leq P^{c,\text{tot}} \\ & 0 \leq s_k^c \leq s_k^{c,\text{mask}}\ \forall k \in \mathcal{K} \end{aligned} \tag{2.4}$$

with

$$R^{vc} = f_s \sum_{k\in\mathcal{K}} b_k^{vc} = f_s \sum_{k\in\mathcal{K}} \log_2\left(1 + \frac{1}{\Gamma}\frac{|h_k^{vc}|^2 s_k^{vc}}{|h_k^{vc,c}|^2 s_k^c + \sigma_k^{vc}}\right) \tag{2.5}$$

where b_k^{vc}, h_k^{vc}, s_k^{vc}, and σ_k^{vc} are the bit loading, the direct channel, the transmit power, and the noise power on subcarrier k of the victim user, respectively, and $h_k^{vc,c}$ is interfering channel on subcarrier k from cell c to a victim user. w^c and w^{vc} are the weights of the primary users and the victim users, repectively. We assume w^c equal for all primary users and w^{vc} equal for all victim users. We consider that $w^c = 1 - w^{vc}$, which represents a tradeoff between protecting victim users of a neighboring cell at the cost of degrading the data rate of primary users. In practice, these weights can be chosen based on upper layer information such as queue length or quality of service requirements. Setting $w^{vc} = 0$ shifts to a greedy algorithm like IWF, which can be useful when interference between neighboring cells is negligible.

Applying the KKT stationarity condition to problem (2.4) leads to

$$\begin{aligned} \forall k: \frac{w^c f_s |h_k^c|^2}{\log(2)\left(|h_k^c|^2 s_k^c + \sum_{\bar{c}\neq c}\Gamma|h_k^{\bar{c}}|^2 s_k^{\bar{c}} + \Gamma\sigma_k^c\right)} \\ - \frac{w^{vc} f_s |h_k^{vc}|^2 s_k^{vc} |h_k^{vc,c}|^2}{\log(2)\left(\Gamma|h_k^{vc,c}|^2 s_k^c + \Gamma\sigma_k^{vc}\right)\left(|h_k^{vc}|^2 s_k^{vc} + \Gamma|h_k^{vc,c}|^2 s_k^c + \Gamma\sigma_k^{vc}\right)} \\ -\lambda_c = 0. \end{aligned} \tag{2.6}$$

By taking into account the KKT complementarity conditions of (2.4), s_k^c from the first term of equation (2.6) can be isolated to obtain:

$$s_k^c = \left[\frac{\frac{w^c f_s}{\log(2)}}{\lambda_c + P_k^{NF,c}} - \frac{\sum_{\bar{c}\neq c}\Gamma|h_k^{\bar{c}}|^2 s_k^{\bar{c}} + \Gamma\sigma_k^c}{|h_k^c|^2}\right]_0^{s_k^{c,\text{mask}}} \tag{2.7}$$

where $P_k^{NF,c}$ is referred to as the penalty factor, defined as

$$P_k^{NF,c} = \frac{w^{vc} f_s |h_k^{vc}|^2 s_k^{vc} \Gamma |h_k^{vc,c}|^2}{\log(2)\left(\Gamma|h_k^{vc,c}|^2 s_k^c + \Gamma\sigma_k^{vc}\right)\left(|h_k^{vc}|^2 s_k^{vc} + \Gamma|h_k^{vc,c}|^2 s_k^c + \Gamma\sigma_k^{vc}\right)}. \tag{2.8}$$

Note the similarity with the IWF solution. The first term in equation (2.7) corresponds to a power level with per-subcarrier penalty factor $P_k^{NF,c}$ that reduces the interference to victim users from a neighboring cell. Setting $P_k^{NF,c}$ to zero will reduce to the IWF algorithm. However, in contrast to equation (2.3), this is a fixed-point equation as $P_k^{NF,c}$ depends on s_k^c.

Problem (2.4) is a nonconvex function for which a duality gap exists to the optimal solution. However, as the number of subcarriers increase, this duality gap becomes zero and it can be solved via bisection [73]. By adding to equation (2.7) a bisection search on the Lagrange multiplier to satisfy the total cell power constraint, we obtain Algorithm (1), which we refer to as the neighbor-friendly IWF (NF-IWF). The parameter δ indicates the accuracy of the total power constraint, γ indicates the stopping criterion of the bisection search on λ_c in the case of an inactive total power constraint, and $\Lambda^{\max}$ is the maximum value for λ_c. The transmit powers of the neighboring cells s_k^{vc} are assumed as an equal power allocation (EPA) without performance degradation as observed in later sections.

Algorithm 1 NF-IWF

For each cell c:
Initialize w^c and w^{vc} according to the protection level assigned to each user
Initialize h^{vc} according to the victim user path loss
Initialize $s_k^c = 0$ and s_k^{vc} =EPA
repeat
  $\lambda_c^{\min} = 0; \lambda_c^{\max} = \Lambda^{\max}$
  $\lambda_c = (\lambda_c^{\max} + \lambda_c^{\min})/2$
  while $|\sum_k s_k^c - P^{c,\text{tot}}| > \delta$ and $\lambda_c > \gamma$ **do**
    $\lambda_c = (\lambda_c^{\max} + \lambda_c^{\min})/2$
    for $k = 1 : \mathcal{K}$ **do**
      repeat
        Update s_k^c in (2.7)
      until convergence
    end for
    if $\sum_k s_k^c > P^{c,\text{tot}}$ **then**
      $\lambda_c^{\min} = \lambda_c$
    else
      $\lambda_c^{\max} = \lambda_c$
    end if
  end while
until network convergence

Contrary to most ICIC techniques that orthogonalize resources, an advantage of NF-IWF is that it allows subcarriers to be shared between users as long as adequate power levels are used. This can be seen in Fig. 2.5. Interestingly, NF-IWF allocates more power to those subcarrier less used for transmission by the interfering base station, which uses IWF. Still, some subcarriers are shared by both base stations.

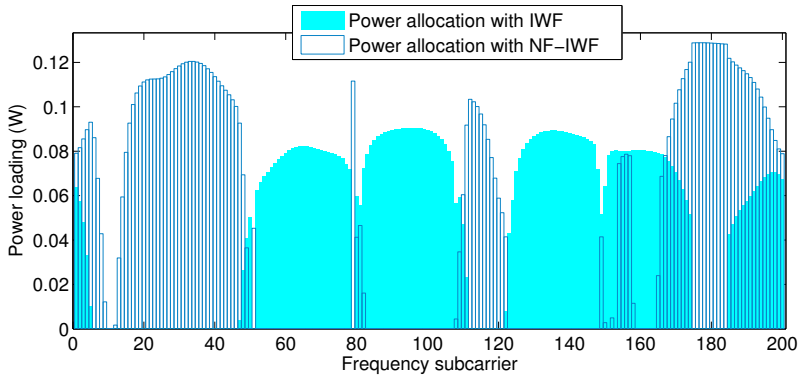

Figure 2.5: Transmit power allocation from 2 neighboring base stations to 2 cell-edge users over 200 subcarriers. Each base station is transmitting to a cell-edge user and interfering with the other base station. One base station uses NF-IWF and the other uses IWF.

The challenge of implementing NF-IWF in a wireless network resides on obtaining the parameters in equation (2.8) in an autonomous way. For example, $h_k^{vc,c}$ can be obtained from the channel feedback of victim users when scanning pilot signals of a neighboring cell for a potential handover [3, 4]. However, the direct channel h_k^{vc} can only be known from the information received from other base stations. Therefore we propose in section 2.3.2 a novel approach to estimate h_k^{vc} based on the distance from the base station to the cell-edge.

2.3.2 Estimation of the victim users channel

Full knowledge of h_k^{vc} is unfeasible in an autonomous fashion. Nevertheless, the path loss, i.e. the average channel gain over all the allocated subcarriers, is easier to obtain because it mainly depends on the distance to the base station. Since the signal strength coming from 2 neighboring base stations can be considered equal at the cell-edge (this is how the cell-edge is typically defined), the path loss from each base station to the cell-edge can be known. This can be exploited to approximate the direct channel of any victim user (h_k^{vc}) by using the path

loss from the base station to the cell-edge. Therefore, $\tilde{h}^{vc}$ is assumed to be an average over all the available subcarriers such that any user located at a distance d from the base station would present the same average channel and experience the same path loss given by $31.5 + 35\log_{10}(d[m])$ [8]. This results in a constant value for h_k^{vc} along all the set of subcarriers $\mathcal{K}$, i.e. $h_k^{vc} = \tilde{h}^{vc}\ \forall k \in \mathcal{K}$ where $\tilde{h}^{vc} = \frac{1}{\mathcal{K}}\sum_{k=1}^{\mathcal{K}} h_k^c$. Even though an irregular propagation channel (i.e. with shadowing) might affect each victim user differently, we will see later that $\tilde{h}^{vc}$ is a good approximation for the direct channel of all potential victim users if $h_k^{vc,c}$ of each user is known.

To estimate d in practice, we can use the information available at the base station on the channel estimated by new users entering the cell [93] or predefined by the manufacturer. As we will see later, an exact definition of d is not necessary for improved performance. Furthermore, this information does not need to be updated regularly (since the cell-edge will only be modified when a new base station is deployed in the neighborhood).

Despite its simplicity, this model provides an accurate estimation of the victim users channel characteristics. To analyze the sensitivity of this model, we consider two users in a high interference case 1 (where the victim user is severely interfered by cell c) and a low interference case 2 (where the victim user is at the cell-edge) as reconstructed in Fig. 2.6 and Fig. 2.7, respectively. MBS stands for macro base station and FBS stands for femto base station. The color regions indicate the signal strength in the direct channel to the closest base station and the user color indicates the base station to which the user is attached. We assume that there is no handover, like in a closed-access base station.

Fig. 2.8 computes the normalized data rate of both users for cases 1 and 2 by evaluating $\tilde{h}^{vc}$ at different values of d, but keeping the users' positions as in Fig. 2.6 and Fig. 2.7. The distance d is then varied between 0 and the actual distance between base stations and it is normalized such that $d_{norm} = 0$ means a radius of zero and $d_{norm} = 1$ means a radius equal to the distance between both base stations (d_{BS}). The smaller the path loss distance, the more protection to the victim user at the cost of the primary user data rate. At $d_{norm} = 0.5$, i.e. between the two base stations, we have the highest normalized data rate of the victim user for a primary user data rate of 20% in case 1 and 50% in case 2. This is because in case 1 the base station needs to significantly reduce the transmit power to the primary user when protecting a more vulnerable victim user located within its coverage. Fig. 2.8 also shows that the accuracy to define $\tilde{h}^{vc}$ is not so critical when d_{norm} ranges between 0.5 and 0.75, decreasing at most 20% the data rate of the victim cell-edge user. To achieve the maximum performance for the victim user, from here on we assume a victim user path loss at a distance $d_{norm} = 0.5$.

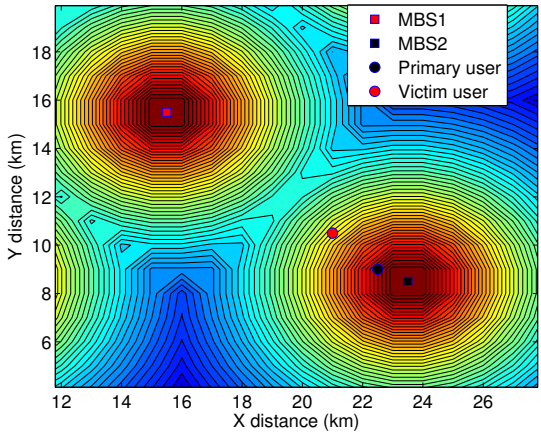

Figure 2.6: Case 1: high interference. The victim user is located within the coverage of the neighboring cell, resulting in high interference.

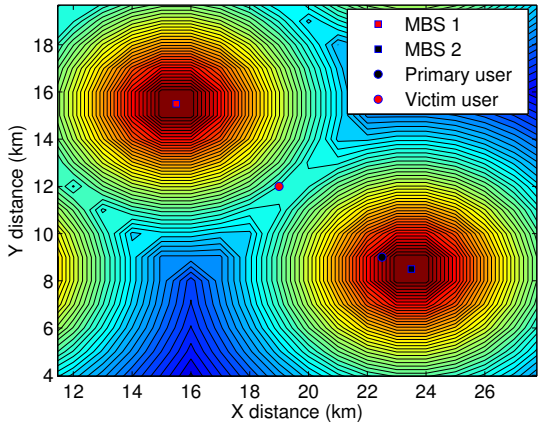

Figure 2.7: Case 2: low interference. The victim user is located between two cells, resulting in low interference.

2.3.3 Complexity reduction of NF-IWF

Since the channel conditions can change rapidly in a wireless environment, it is crucial from a practical point of view that the power allocation computation be performed with a small number of iterations. However equation (2.7) does not have a closed-form since $P_k^{NF,c}$ depends on s_k^c. Therefore, we propose an

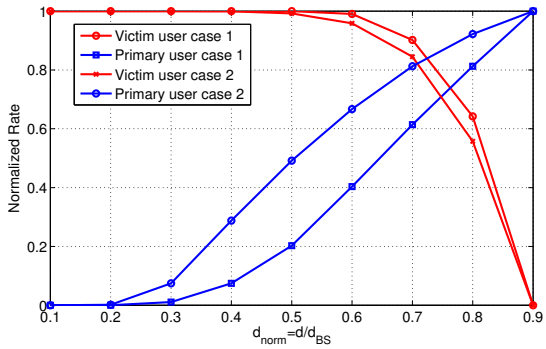

Figure 2.8: Normalized data rates for different values of distance d when applying NF-IWF.

approximation of the penalty factor that reduces the complexity of Algorithm (1) by eliminating the loop of line 11.

Let us first expand expression (2.4) into

$$\begin{aligned} \underset{s_k^c\ \forall k}{\text{maximize}} \quad & w^c f_s \sum_k \log_2 \left(1 + \frac{1}{\Gamma} \frac{|h_k^c|^2 s_k^c}{\sum_{\substack{\bar{c}\neq c \\ \bar{c}\in\mathcal{C}}} |h_k^{\bar{c}}|^2 s_k^{\bar{c}} + \sigma_k^c}\right) + \\ & w^{vc} f_s \sum_k \log_2 \left(1 + \frac{1}{\Gamma} \frac{|h_k^{vc}|^2 s_k^{vc}}{|h_k^{vc,c}|^2 s_k^c + \sigma_k^{vc}}\right) \\ \text{s.t.} \quad & \sum_k s_k^c \leq P^{c,\text{tot}} \\ & 0 \leq s_k^c \leq s_k^{c,\text{mask}}\ \forall k \in \mathcal{K} \end{aligned} \tag{2.9}$$

We approximate (2.9) by linearizing the second term in the objective function such that the maximization problem becomes

$$\begin{aligned} \underset{s_k^c\ \forall k}{\text{maximize}} \quad & w^c f_s \sum_k \log_2 \left(1 + \frac{1}{\Gamma} \frac{|h_k^c|^2 s_k^c}{\sum_{\substack{\bar{c}\neq c \\ \bar{c}\in\mathcal{C}}} |h_k^{\bar{c}}|^2 s_k^{\bar{c}} + \sigma_k^c}\right) - \\ & w^{vc} f_s \sum_k |h_k^{vc,c}|^2 s_k^c \\ \text{s.t.} \quad & \sum_k s_k^c \leq P^{c,\text{tot}} \\ & 0 \leq s_k^c \leq s_k^{c,\text{mask}}\ \forall k \in \mathcal{K} \end{aligned} \tag{2.10}$$

For a linear equation of type $ax + b$, b is disregarded when applying the KKT conditions, while the slope a is included in w^{vc} when tuning a particular

operating point. The KKT stationarity condition of (2.10) leads to

$$\forall k : \frac{w^{n,c} f_s |h_k^c|^2}{\log(2)\left(|h_k^c|^2 s_k^c + \sum_{\bar{c}\neq c} \Gamma |h_k^{\bar{c}}|^2 s_k^{\bar{c}} + \Gamma \sigma_k^c\right)} - w^{vc} f_s (|h_k^{vc,c}|^2) - \lambda_c = 0 \tag{2.11}$$

resulting in

$$s_k^c = \left[\frac{\frac{w^c f_s}{\log(2)}}{\lambda_c + \tilde{P}_k^{NF,c}} - \frac{\sum_{\bar{c}\neq c} \Gamma |h_k^{\bar{c}}|^2 s_k^{\bar{c}} + \Gamma \sigma_k^c}{|h_k^c|^2} \right]_0^{s_k^{c,\mathrm{mask}}} \tag{2.12}$$

where the penalty factor is approximated by

$$\tilde{P}_k^{NF,c} = w^{vc} f_s |h_k^{vc,c}|^2. \tag{2.13}$$

This corresponds to a linear penalty on the power level determined by the interfering channel of the victim users. In other words, the power allocation is proportionally penalized in those subcarriers with a strong interfering channel because this can easily damage the victim users data rate. This approximation results in a closed-form formula with complexity similar to IWF (and lower than NF-IWF), but improved performance as we will see later. We refer to it as NF-IWF-approx.

2.4 Performance Evaluation

We consider a wireless OFDM network with the parameters shown in Table 2.1. In order to evaluate the performance of our approaches, we first focus on two users (one primary and one victim user) connected to neighboring cells. We consider 2 scenarios, one with interference between macrocells, and one with interference between a femtocell and a macrocell. For each scenario, we analyze 2 cases, one with high and another with low interference.

We compare our proposed approaches against EPA and IWF by generating the achievable rate region, which shows the trade-off between the two users data rates. In the case of NF-IWF and NF-IWF-approx, changing the weights w^c and w^{vc} allows us to reach different full-power operating points to form the achievable rate region. This is not possible with IWF, for which the total power budget has to be tuned between 0 and $P^{c,\mathrm{tot}}$ to obtain different operating points. This controllable tunability can be seen as an important advantage of NF-IWF.

Table 2.1: Simulation Parameters.

Parameter	Value
System Bandwidth	5 MHz
Number of subcarriers	200
Γ	1
δ	10^{-6}
γ	10^{-6}
Λ^{max}	10^{8}
f_s	2.8 Gsymbols/s
Channel profile	3GPP SCM suburban macro
Macrocell total transmit power	43 dBm
Femtocell total transmit power	15 dBm

We also compare our proposed approaches with a practical scheme like SFR, in which we divide the total bandwidth in two non-overlapping frequency bands. In order to achieve different operating points, we need to vary parameters α and β from Fig. 2.1. In the case of a multi-user scenario, each band is assigned to either primary or victim users and has a constant power level. However, in the case of two users connected to neighboring cells, the optimal approach consists in transmitting with full power to each user in one non-overlapping band, i.e. in each cell $\alpha = 1$ and β varies from 0 to 1 to achieve different operating points (discontiguous bands are not considered). In the multi-user case, this results in starvation of resources for some users.

As an upper bound, we consider the case in which the base station has full knowledge of the interfering and direct channels and of the power allocation of the neighboring base station. We call this approach NF-full, which is equivalent to the distributed algorithm (DSB) of [87]. Evidently, this is not an autonomous approach, since it requires coordination between base stations.

For all the evaluated approaches, the transmit powers are updated alternately between base stations until network convergence is reached. In the following simulations, only 3 to 5 iterations are necessary for convergence.

2.4.1 Macro-Macro Interference

The 2 cases to be analyzed for the macro-macro scenario are shown in Fig. 2.6 and 2.7. In case 1, the victim user is located within the coverage of the neighboring cell, resulting in high interference. In case 2, the interference to the victim user is low as it is located between the coverage of the two cells.

Fig. 2.9 shows the gains in the rate region that can be achieved with NF-IWF in the case of high interference. For example, with a primary user data rate of 600 Mbps, NF-IWF can achieve 6 Mbps for the victim user instead of 1.7 Mbps for IWF, 0.4 Mbps for SFR, and 0.1 Mbps for EPA, i.e. an increase by a factor of 3.5 compared to IWF, a factor of 15 compared to SFR, and a factor of 60 compared to EPA. Furthermore, the difference between the approach with full knowledge and NF-IWF proves to be marginal. NF-IWF-approx can achieve similar gains with reduced complexity when the data rate of the primary user is lower than 500 Mbps. Needless to say, the underperformance and lack of tunability of EPA is evident. SFR is able to improve the performance for both primary and victim users compared to EPA, but not compared to IWF. This is because SFR partitions the available bandwidth in non-overlapping bands, avoiding interference in this way. However, SFR does not exploit a variable per-subcarrier power allocation, which results in a large degradation.

Fig. 2.10 shows the rate region for the low interference case. Except for EPA and SFR, the performance of all algorithms is similar. This is because the direct channels are stronger compared to the interfering channels, hence even a greedy algorithm like IWF has improved performance.

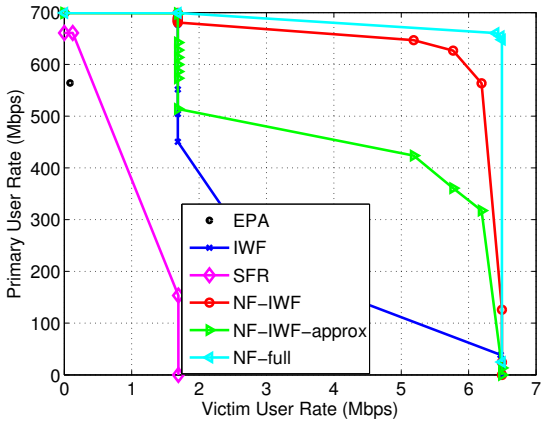

Figure 2.9: Rate region of the primary and victim users of the macro-macro high interference case.

2.4.2 Femto-Macro Interference

The 2 cases to be analyzed for the scenario with femto-macro interference are shown in Fig. 2.11 and 2.12. In case 1, the victim user of the macrocell is

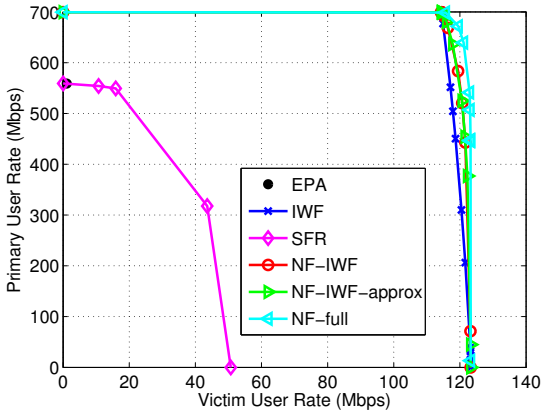

Figure 2.10: Rate region of the primary and victim users of the macro-macro low interference case.

located within the coverage of the neighboring femtocell, resulting in a high interference. In case 2, the interference to the victim user is low as it is located far from the femtocell coverage.

Fig. 2.13 shows that with a primary user data rate of 80 Mbps, NF-IWF can achieve 1.45 Mbps for the victim user instead of 0.5 Mbps for IWF, 0.7 for SFR, and 0.02 Mbps for EPA, i.e. an increase by a factor of 2.9 compared to IWF, a factor of 2 compared to SFR, and a factor of 73 compared to EPA. For this primary user data rate, NF-IWF-approx achieves the same gains. In the low interference case, all the algorithms perform similar except for EPA and SFR as seen in Fig. 2.14.

It is interesting to note that with high interference, NF-IWF-approx provided more than 50% increase in the victim user data rate compared to IWF with less complexity than NF-IWF. This result indicates that the linear approximation of the penalty factor indeed provides most of the useful information to achieve significant gains.

2.4.3 Multi-user Multi-cell Interference

The achievable rate regions presented so far show the advantages of our proposed approaches in a two user evaluation. However, a multi-user multi-cell evaluation is needed to assess the total network gains.

We consider a wireless heterogeneous network consisting of 5 macrocells (evenly

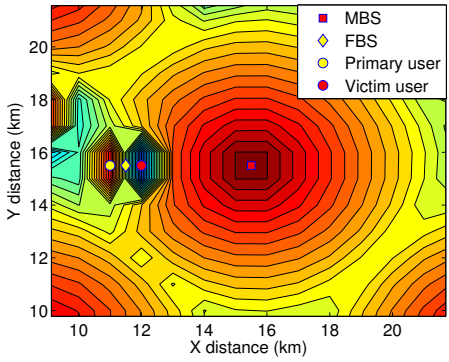

Figure 2.11: Case 1: high interference. The victim user attached to the macrocell is located within the coverage of the neighboring femtocell, resulting in high interference.

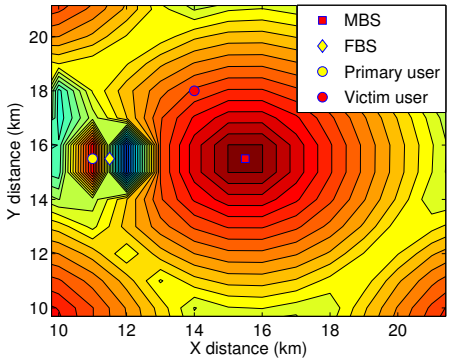

Figure 2.12: Case 2: low interference. The victim user attached to the macrocell is far from the femtocell, resulting in low interference.

distributed), 20 femtocells (randomly distributed), and 500 users (randomly distributed). Any two neighboring cells share a set of subcarriers and each user is randomly allocated the same number of consecutive subcarriers within a cell. This topology is shown in Fig. 2.3 and the performance results are shown in Fig. 2.15. The user color indicates the base station to which the users are attached. Users located within the coverage of their macrocell are classified as macro primary users, while users located farther than the coverage of their macrocell (i.e. closer to a neighboring cell than to the cell they are attached to) are classified as macro victim users and are those to be protected. Users attached to femtocells are classified as femto users.

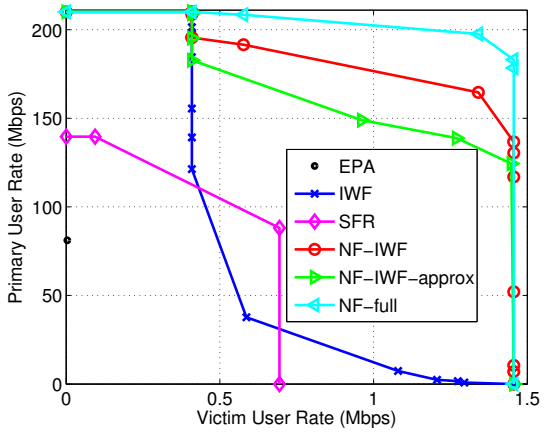

Figure 2.13: Rate region of the primary and victim users of the macro-femto high interference case.

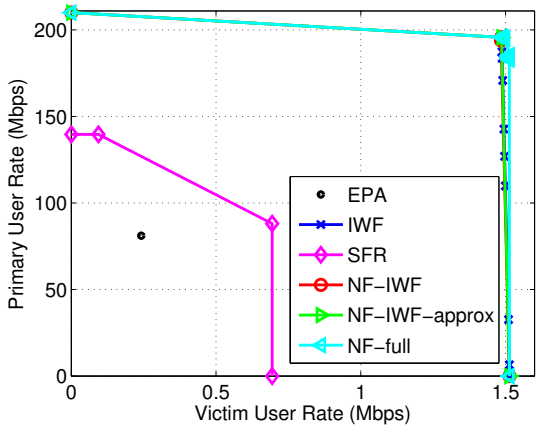

Figure 2.14: Rate region of the primary and victim users of the macro-femto low interference case.

For a fair comparison, all base stations use the same algorithm with the best rate region operating point for any two neighboring cells. For IWF, the best operating point corresponds to a full-power scheme, while for SFR, NF-IWF, NF-IWF-approx, and NF-full we consider a point on the rate region boundary with a tangent with slope equal to -1.

From the cumulative distribution function (CDF) of Fig. 2.15 we can observe

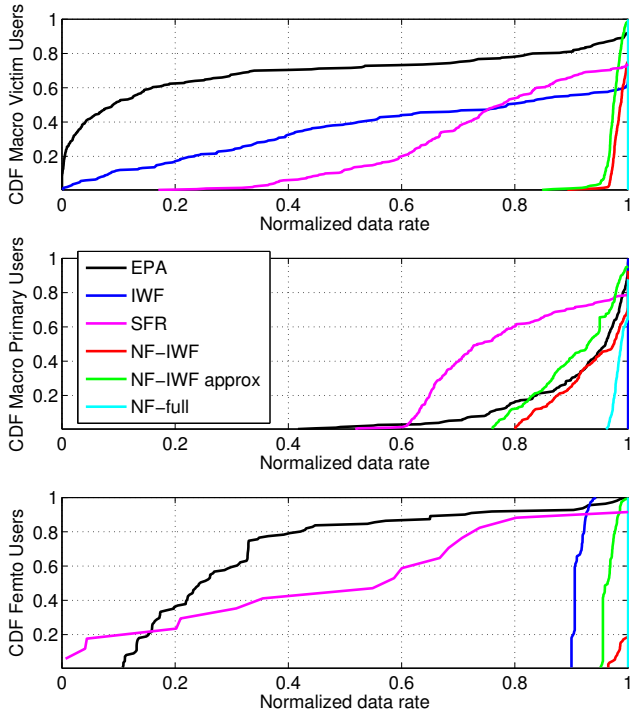

Figure 2.15: CDF of victim and primary users of the multi-user scenario.

the gains achieved by our proposed approaches. As expected, NF-full achieves the best data rate performance for the macro victim users, followed closely by NF-IWF and NF-IWF-approx. IWF and EPA present a clear underperformance due to their greediness towards victim users, while the SFR suffers from the band partitioning and lack of power control within each band. For example, with the NF algorithms, macro victim users have a very large probability of obtaining a normalized data rate higher than 95%; while with SFR, IWF, and EPA they have 40% probability of a normalized data rate lower than 70%, 50%, and 5%, respectively. Femto users achieve similar gains.

Additionally, the gains come with a marginal degradation in the macro primary users data rates. Since we consider the full-power operating point for IWF, it achieves the highest data rate for the macro primary users, followed closely by NF-full, NF-IWF, NF-IWF-approx, and SFR. EPA can sometimes present a higher primary user data rate compared to SFR and the NF algorithms. This is because, depending on the channel conditions, the EPA operating point can have a higher primary user data rate than the operating point of SFR and NF

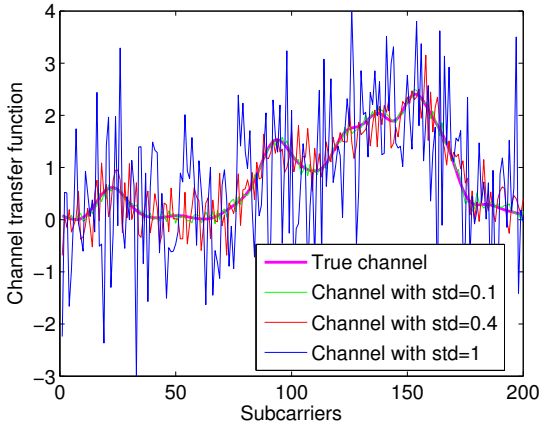

Figure 2.16: Channel transfer function with an estimation error of zero mean and *std* standard deviation.

algorithms. However, the NF algorithms never achieve a normalized data rate lower than 75%.

2.5 Sensitivity Analysis

In this section we evaluate the data rate performance of our approaches for a given channel estimation error in all the channels with some frequency variation, i.e. h_k^c, $h_k^{\bar{c}}$, and $h_k^{vc,c}$. We model the channel estimation error Δ as a Gaussian random variable with zero mean and different values of standard deviation (*std*). A visual representation of the channel estimation error is shown in Fig. 2.16. The value of *std* represents a fraction of the average channel value.

The power allocation is then computed as

$$\hat{s}_k^c = \left[\frac{\frac{w^c f_s}{\log(2)}}{\lambda_c + \hat{P}_k^{NF,c}} - \frac{\sum_{\bar{c} \neq c} \Gamma |\hat{h}_k^{\bar{c}}|^2 s_k^{\bar{c}} + \Gamma \sigma_k^c}{|\hat{h}_k^c|^2} \right]_0^{s_k^{c,\mathrm{mask}}} \tag{2.14}$$

with the penalty factor of NF-IWF modeled as

$$\hat{P}_k^{NF,c} = \frac{w^{vc} f_s |\tilde{h}^{vc}|^2 s_k^{vc} \Gamma |\hat{h}_k^{vc,c}|^2}{\log(2) \left(\Gamma |\hat{h}_k^{vc,c}|^2 s_k^c + \Gamma \sigma_k^{vc} \right) \left(|\tilde{h}^{vc}|^2 s_k^{vc} + \Gamma |\hat{h}_k^{vc,c}|^2 s_k^c + \Gamma \sigma_k^{vc} \right)} \tag{2.15}$$

and the penalty factor of NF-IWF-approx modeled as

$$\hat{\hat{P}}_k^{NF,c} = w^{vc} f_s |\hat{h}_k^{vc,c}|^2 \tag{2.16}$$

where $\hat{h} = h + \Delta$ for all channels, with h being the true channel (subscripts and superscripts omitted).

With the obtained power allocation values, we compute the achievable data rate for each cell as

$$R^c = f_s \sum_{k \in \mathcal{K}} \log_2 \left(1 + \frac{1}{\Gamma} \frac{|h_k^c|^2 \hat{s}_k^c}{\sum\limits_{\substack{\bar{c} \neq c \\ \bar{c} \in \mathcal{C}}} |h_k^{\bar{c}}|^2 \hat{s}_k^{\bar{c}} + \sigma_k^c} \right). \tag{2.17}$$

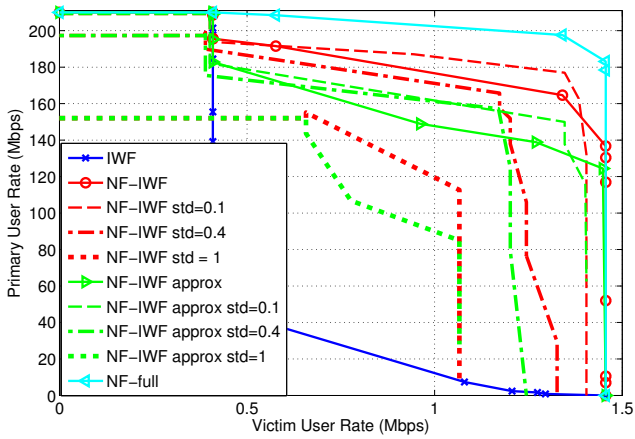

Figure 2.17: Sensitivity analysis on the channel estimation.

Fig. 2.17 shows that our approaches are robust to very high channel estimation errors and can still present significant gains compared to IWF even with $std = 1$. It is also interesting to note that for small values of *std* the primary user data rate can improve compared to the case without errors. This is because the primary user is less vulnerable to channel estimation errors and can profit from the power level decrease of the victim user.

2.6 Computational Complexity for Convergence

In this section we quantify the computational complexity needed for each algorithm to converge to transmit powers satisfying the total power constraints. EPA and SFR do not need to update the transmit powers. All the NF algorithms have two or three levels of iterations as shown in Algorithm (1). First, there is an outer level that iterates over the base stations until network convergence in the power allocation is achieved. The number of iterations at this level is denoted with N_o. A second level of iterations is used for the bisection search of λ_c in each base station until the total power constraint is satisfied. The number of iterations at this level is denoted by N_λ. These two levels of iterations are shared by IWF, NF-IWF, and NF-IWF-approx. However, NF-IWF has an extra level of iterations on $P_k^{NF,c}$ to update s_k^c. The number of iterations at this level is denoted with N_P.

The convergence properties of the proposed algorithms can be seen in Fig. 2.18 in terms of the number of iterations per subcarrier per base station, i.e. we evaluate the product $N_\lambda N_P$. We can observe that after 10 iterations, all of the proposed algorithms reach convergence. However, NF-IWF-approx is the first one to reach convergence at 3 iterations within a 10% range of the final value, followed by NF-IWF at 4 iterations, and finally NF-full at 6 iterations. Since we consider the best operating point in the rate region of each algorithm, the different algorithms converge to a different value. Interesting to note is that both NF-IWF and NF-IWF-approx show a fluctuating behavior during the first iterations, while NF-full shows a smoother behavior. This is due to the approximations involved in NF-IWF and NF-IWF-approx that make the algorithms fluctuate before reaching convergence.

Within the different levels of iterations, the transmit power computation needs to be done on a per-subcarrier basis, i.e. we need $\mathcal{K}$ transmit power calculations. This leads to a total complexity in the number of power computations of $N_o N_\lambda N_P \mathcal{K}$ for NF-IWF and $N_o N_\lambda \mathcal{K}$ for IWF and NF-IWF-approx.

This complexity can be further reduced by exploiting the frequency correlation of the wireless channel. We analyze the impact of this complexity reduction for both NF-IWF and NF-IWF-approx. For this purpose, we define a window of wd subcarriers in which we reuse the transmit power value of one of the middle subcarriers. The data rate impact of this reduction can be seen in Fig. 2.19. We note that the degradation is marginal for a window of 2 and 4 subcarriers, and becomes more visible for a window of 8 subcarriers. A similar rationale can be used to exploit the time correlation of the channel.

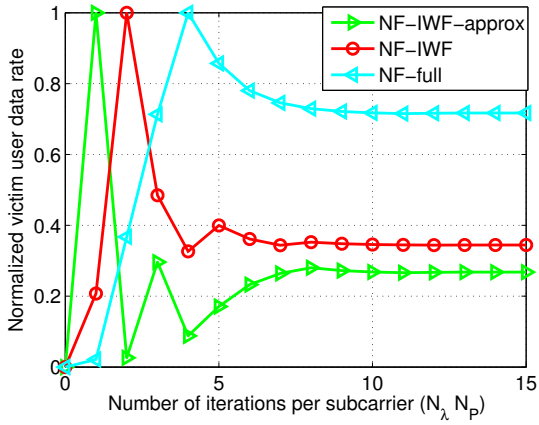

Figure 2.18: Number of iterations per subcarrier per base station to reach convergence in the proposed algorithms.

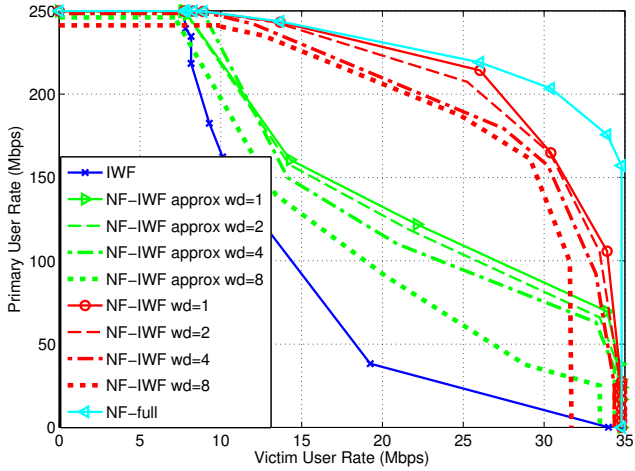

Figure 2.19: Complexity analysis for different values of windows.

2.7 Conclusions

In this chapter we have proposed NF-IWF, a neighbor-friendly autonomous algorithm for power control in wireless heterogeneous networks. In contrast to greedy algorithms like EPA and IWF, NF-IWF protects the data rate of victim users located within a certain distance from the base station. This is

done through a factor that penalizes the power allocation in those subcarriers that damage the data rate of victim users. Furthermore, we have developed a low-complexity version, NF-IWF-approx, which reduces the complexity by assuming a linear approximation of the victim user data rate, resulting in a closed-form formula. Other options have been analyzed to further reduce complexity by exploiting frequency and time correlation of the channel. We have evaluated our algorithms under high and low interference conditions in a heterogeneous network with macro and femtocells. Our approaches present higher tunability, robustness, and better data rate performance, especially in high interference conditions. We have shown an increase by a factor of 3.5 compared to IWF, 15 compared to SFR, and 60 compared to EPA in the victim users data rate with a marginal decrease of the primary users data rate. We have also shown that the rate region of our approaches lies close to the upper bound with full knowledge of the interfering channel and the power allocation of the neighboring cell.

Chapter 3

Exploiting the Overhearing Capabilities of Relaying D2D Users

Abstract

Dealing with inter-cell interference is a main challenge in wireless networks, especially for cell edge users. Resource orthogonalization approaches have been typically used to deal with this problem by assigning disjoint resources to users served by different base stations (BSs). However, these approaches can achieve at most 1/2 degrees of freedom (DoF) per cell. Blind interference alignment (BIA) has emerged as a means to achieve higher data rates by aligning all the interference in one dimension to facilitate its cancellation using reconfigurable antennas. A simple form of BIA without such antennas can be realized through aligned frequency reuse (AFR). For a cell with N neighboring cells, AFR can achieve $N/(N+1)$ DoF per cell. However, BIA-based approaches lack spatial diversity. Therefore, we propose an approach that increases the spatial diversity and the spectral efficiency by allowing device-to-device (D2D) communication among cell edge users during the time-slots in which they are not receiving their intended signal from their serving BS. We develop the proposed approach for different cellular topologies and extend it to the scenario with multiple cell edge users per cell edge. [1]

[1]This chapter is cited from Torrea-Duran, R., Morales, M., Plata-Chaves, J., Vandendorpe, L., Moonen, M., "Aligned Frequency Reuse with D2D Communication" (Submitted to IEEE Transactions on Communications, 2017).

3.1 Introduction

The increasing demand for wireless connectivity has lead to an increased number of base stations (BSs) deployed, resulting in larger areas affected by inter-cell interference [51]. Users located close to their serving BS, i.e. cell center users, rely on good channel conditions to achieve large data rates. Hence for these users the time and frequency resources can be reused in each cell. However, users located in areas with high inter-cell interference, i.e. cell edge users, typically suffer a severe degradation in the achievable data rate and the reuse of resources is not possible.

The most widely used approaches to tackle inter-cell interference are based on resource orthogonalization, which means that disjoint resources are assigned to users served by different BSs. For example, in soft frequency reuse (SFR) [2] the total bandwidth in each cell is divided in two non-overlapping frequency bands, one for the cell center users and one for the cell edge users. The first band can be reused in all the cells, while the second one is orthogonalized among neighboring cells. Optimizing SFR can be done by adapting the size of the bands and the transmit power in each band according to the number of users and their channel conditions [35]. SFR can be straightforwardly extended to the time domain by assigning different time-slots to the cell edge users of neighboring cells [94]. In this chapter we focus on the time domain scenario.

However, when orthogonalizing resources, the amount of resources that each user receives decreases with the number of users. Moreover, in order to keep up with the variable wireless channel conditions, channel state information at the transmitter (CSIT) is required to dynamically adapt the amount of resources given to each user. This constitutes an expensive overhead in terms of network resources, especially for networks with a large number of users [67].

Interference alignment (IA) [11] has emerged as an alternative to resource orthogonalization approaches aiming to achieve higher data rates by aligning all the interference in one dimension, facilitating in this way simple interference cancellation techniques. However, the main drawback is the need for perfect and global CSIT.

A form of IA that does not require CSIT is blind interference alignment (BIA) [41]. BIA employs reconfigurable antennas that can switch among a number of preset radiation patterns in order to align all the interference in the same dimension. However, aligning inter-cell interference without CSIT can also be achieved for some cellular topologies without reconfigurable antennas as in aligned frequency reuse (AFR) [47]. Other than the name suggests, AFR works also in the time domain. In a uniformly distributed array of cells where each cell has N neighboring cells and one cell edge user per cell edge, AFR has

a reuse pattern of $N+1$ cells. This means that a cell is inactive every $N+1$-th time-slot and then all the cell edge users close to the inactive cell receive their signal from their serving BS free of inter-cell interference. The transmission scheme is shifted over one cell in the following time-slots. This approach achieves $N/(N+1)$ degrees of freedom (DoF) per cell, which is optimal for one cell edge user per cell edge even with CSIT [47]. Using a resource orthogonalization approach, only cells that do not share a cell edge can be active at the same time or in the same frequency, hence achieving at most 1/2 DoF per cell.

One of the main drawbacks of all the IA-based approaches is the lack of spatial diversity. In the presented example, each user receives its signal only from the serving BS. However, due to the large number of users in today's networks, the proximity among users offers the potential of achieving a high connectivity with other users that can relay the overheard information. In particular, device-to-device (D2D) communication may be used, which allows two nearby users to communicate directly with each other without traversing any BS [84].

D2D has been widely used to enhance spectral efficiency [9]. However, when it is not carefully managed, D2D communication between neighbor users can become a source of interference for other users, and especially critical for cell edge users. For this purpose, D2D relay selection schemes have been recently studied. For instance, the authors in [29] propose a D2D relay selection and resource allocation scheme for multi-user, multi-carrier and multi-cellular networks. In [65], a cross-layer D2D relay selection scheme was proposed for LTE-A systems and in [28] the authors use a greedy algorithm for D2D relay selection that can increase the fairness and reduce the transmission power consumption.

To increase spatial diversity and spectral efficiency, in this chapter we propose the use of D2D communication among cell edge users using AFR. Specifically, we propose that cell edge users relay the overheard information during the time-slots in which they are not receiving their intended signal from their serving BS. Hence each cell edge user receives its signal from different signal paths, increasing the diversity of the system and without affecting the achievable DoF. We develop the proposed approach for different cellular topologies and extend it to the scenario with multiple cell edge users per cell edge.

The rest of the chapter is organized as follows. Section 3.2 describes the system model. Section 3.3 describes a resource orthogonalization approach typically used to cancel inter-cell interference. Section 3.4 describes the proposed approach that uses D2D communication. Section 3.5 extends the proposed approach to the scenario with multiple cell edge users. Section 3.6 provides the performance analysis. Section 3.7 provides the performance evaluation. Finally, Section 3.8 draws some conclusions.

Notation: Matrices and vectors are denoted by upper and lower case boldface letters, respectively. $\mathbf{A}^T$ and $|\mathbf{A}|$ denote the transpose and determinant of $\mathbf{A}$, respectively. $\mathbb{E}\{\}$ is the expected value operator.

3.2 System Model

We consider an infinite array of cells that are uniformly distributed with no overlap and no holes between them. We consider two cellular topologies, namely a square array (Fig. 3.1), and a hexagonal array (Fig. 3.2). Intra-cell interference is typically avoided by assigning disjoint resources to each of the cell center users in a cell. This set of resources can be a frequency band different to that used by the cell edge users. In this way cells can reuse the same frequency band for the cell center users. In this chapter, we are mainly interested in the cell edge users since these are subject to inter-cell interference. In this context, each cell edge user connected to a BS is assumed to be subject to inter-cell interference from only one neighboring cell.

It is assumed that BSs and users are half-duplex (i.e. they cannot transmit and receive simultaneously) and that they only have a single antenna. Finally, we consider downlink transmission.

Let us denote $s_{m,l}$ as the symbol to be delivered from the l-th BS (denoted as BS_l) to the m-th user served by BS_l (denoted as $\mathrm{U}_{m,l}$). Symbols are assumed to be uncorrelated. Let us also define P_l as the transmit power of BS_l, $p_{m,l}$ as the D2D transmit power of $\mathrm{U}_{m,l}$, and $\gamma_{m,l}^{l,(t)} = P_l|h_{m,l}^{l,(t)}|^2\sigma_\mathrm{s}^2$ as the signal power received by $\mathrm{U}_{m,l}$ in time-slot t and coming from BS_l and $\xi_{m,l}^{n,k,(t)} = p_{n,k}|g_{m,l}^{n,k,(t)}|^2\sigma_\mathrm{s}^2$ as the signal power received by $\mathrm{U}_{m,l}$ in time-slot t and coming from $\mathrm{U}_{n,k}$, where $h_{m,l}^{l,(t)}$ is the channel from BS_l to $\mathrm{U}_{m,l}$ in time-slot t and $g_{m,l}^{n,k,(t)}$ is the channel from $\mathrm{U}_{n,k}$ to $\mathrm{U}_{m,l}$ in time-slot t, and $\sigma_\mathrm{s}^2 = \mathbb{E}\{|s_{m,l}|^2\}\ \forall m, l$. It is assumed that the channel coherence time is one time-slot, which means that a given symbol transmitted by the same node experiences a different channel from one time-slot to the next. Finally, σ_n^2 is the received noise power, assumed to be equal for all users. It is assumed that the BSs transmit in an isotropic way so that the symbol transmitted from BS_l is received by all the users in the cell served by BS_l and by all the cell edge users in the neighboring cells and located in the cell edge closest to BS_l.

3.3 Resource Orthogonalization Approach: TDMA

Assume the square array of Fig. 3.1 where each cell has $N = 4$ neighboring cells and there is one cell edge user per cell edge in each cell. In a traditional time domain multiple access (TDMA) approach, the communication is done in turns, i.e. even time-slots are assigned to half of the cells in a checkers board pattern, i.e. to those cells that do not share a cell edge, and odd time-slots are assigned to the other half of the cells. This transmission pattern completely removes the inter-cell interference in a square array. It is easy to see then that this approach achieves 1/2 DoF per cell.

In the hexagonal array of Fig. 3.2 each cell has $N = 6$ neighboring cells and there is one cell edge user per cell edge in each cell. Cell edge users are represented by the black dots in the figure. The traditional TDMA approach in this case uses a conventional reuse pattern. The transmission is done in different time-slots to the cell edge users close to an inactive cell (i.e. with the BS not transmitting to any cell edge user). For instance, BS_1 takes 3 time-slots to transmit to each of its cell edge users close to BS_3, BS_5, and BS_7 (and so do BS_2, BS_4, and BS_6). Then the pattern of active/inactive cells is shifted over one cell to the right and BS_1 takes 3 more time-slots to transmit to each of its cell edge users close to BS_2, BS_4, and BS_6 (and so do BS_3, BS_5, and BS_7). Finally, the pattern of active/inactive cells is shifted over one more cell to the right and BS_1 remains inactive for the next 3 time-slots. In this way, 1/3 DoF per cell can be achieved [47].

The spectral efficiency per time-slot of $\mathrm{U}_{m,l}$ using this approach can be directly computed as

$$S_{m,l}^{\mathrm{TDMA}} = \frac{1}{L}\mathbb{E}\left\{\log_2\left(1+\frac{\gamma_{m,l}^{l,(t)}}{\sigma_{\mathrm{n}}^2}\right)\right\}, \tag{3.1}$$

where t is the time-slot in which $s_{m,l}$ is received by $\mathrm{U}_{m,l}$ and $L = 8$ for square array and $L = 9$ for the hexagonal array due to the reuse pattern. Assuming BPSK transmissions, a minimum mean square error (MMSE) receiver and Rayleigh fading statistics (assumptions holding throughout the chapter), the bit error rate (BER) of $\mathrm{U}_{m,l}$ is computed in terms of the Gaussian Q-function as [78]

$$\mathrm{BER}_{m,l}^{\mathrm{TDMA}} = \mathbb{E}\left\{Q\left(\sqrt{2\frac{\gamma_{m,l}^{l,(t)}}{\sigma_{\mathrm{n}}^2}}\right)\right\}. \tag{3.2}$$

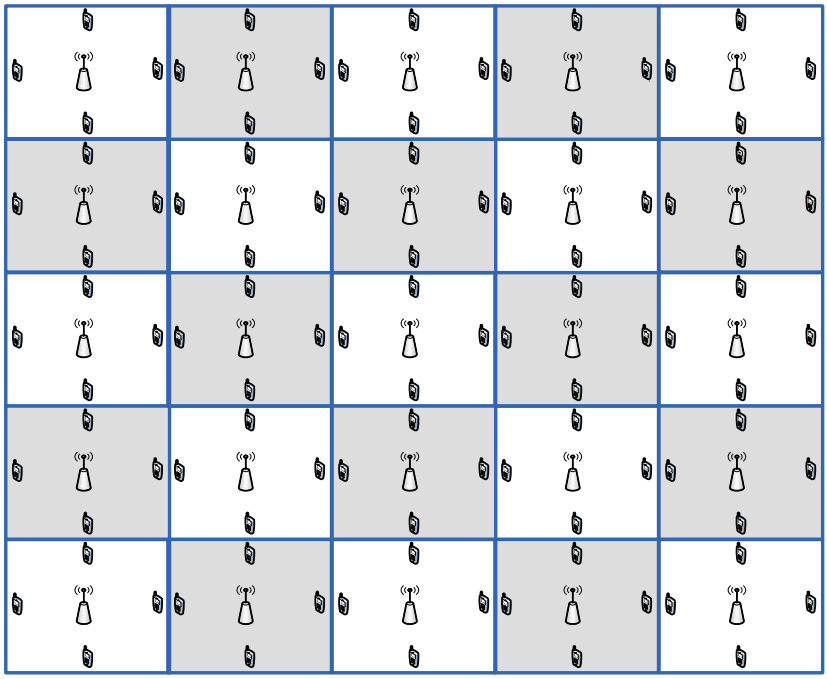

Figure 3.1: Square array with TDMA transmission. The white cells have BSs transmitting to one of their cell edge users, while the shaded cells have inactive BSs (not transmitting to any cell edge user).

3.4 AFR with D2D Communication

3.4.1 Square Array

Consider the square array depicted in Fig. 3.3 with $N = 4$ and one cell edge user per cell edge in each cell, i.e. 4 cell edge users in each cell. The thick arrows should not yet be considered as these correspond to the D2D operations that will be explained later. With the AFR approach presented in [47], each cell cycles through a sequence of $N + 1 = 5$ operations, which is referred to here as a transmission round with 5 time-slots (TS1, TS2, ..., TS5). In each transmission round, a cell is active in 4 time-slots, used to transmit a symbol from its BS to each of the 4 cell edge users, and inactive (i.e. not transmitting to any cell edge user) in one time-slot.

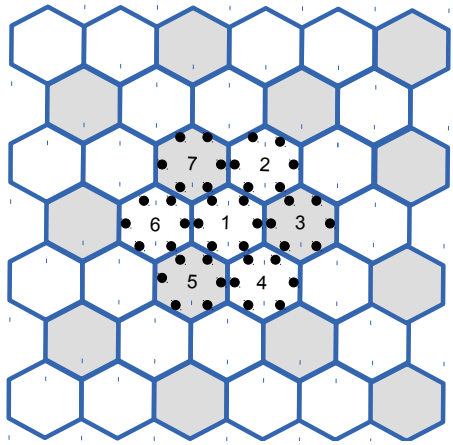

Figure 3.2: Hexagonal array with TDMA transmission. The white cells have BSs transmitting to one of their cell edge users, while the shaded cells have inactive BSs (not transmitting to any cell edge user). Cell edge users are represented by the black dots (only the cell edge users in the numbered cells are shown).

Fig. 3.3 gives the transmission pattern for TS1, where inactive cells are shaded. A tile pattern can be identified, where each tile covers one inactive cell together with its 4 neighboring cells. One such (cross-shaped) tile is highlighted by means of diagonal stripes in the figure. All tiles together cover the complete array, with no overlap and no holes between them. A tile represents a collection of transmission and reception operations, which are applied in the cells covered by the tile. A transmission round starts with the tile at a specific location (TS1) and then the tile is shifted over the array one cell to the right per time-slot. In other words, the tile of Fig. 3.3 is shifted 1, 2, 3, 4 cells to the right in TS2, TS3, TS4, and TS5, respectively. This then fully defines the sequence of operations that each cell cycles through. For instance, the transmission operations for BS_{13} are as follows: BS_{13} is inactive in TS1. In TS2 it transmits the desired symbol for $\mathrm{U}_{1,13}$. In TS3, TS4, and TS5 it transmits the desired symbol for $\mathrm{U}_{2,13}$, $\mathrm{U}_{4,13}$, and $\mathrm{U}_{3,13}$, respectively. For instance, the reception operations for $\mathrm{U}_{1,13}$ are as follows: in TS1 it receives $s_{3,14}$ from BS_{14}. In TS2 it receives its desired symbol $s_{1,13}$ from BS_{13}. In TS3, TS4, and TS5 it receives $s_{2,13}$, $s_{4,13}$, and $s_{3,13}$ from BS_{13} and $s_{1,14}$, $s_{2,14}$, and $s_{4,14}$ from BS_{14}, respectively.

Since each user receives one desired symbol in every 5 time-slots and there are 4 users per cell, it is easy to see that AFR achieves 4/5 DoF per cell.

Here we propose to add D2D communication between users located in the

same cell edge. For instance, considering $U_{1,13}$ and $U_{3,14}$, in TS1 $U_{1,13}$ and $U_{3,14}$ both receive $s_{3,14}$ (as shown in Fig.3.3) and in TS2 $U_{1,13}$ and $U_{3,14}$ both receive symbol $s_{1,13}$. Then, in TS3, TS4, and TS5, $U_{1,13}$ and $U_{3,14}$ are neither receiving their desired symbol, nor the symbol of their neighbor. Therefore, we can exploit two of these time-slots to perform a D2D transmission and a D2D reception. For instance, in TS3 of the *following transmission round* (the time-slot numbering is reset after each transmission round), $U_{1,13}$ can transmit to $U_{3,14}$ the symbol $s_{3,14}$ that was received from BS_{14} in TS1. Then in TS4 of the following round, $U_{1,13}$ can receive (together with $s_{4,13}$ from BS_{13} and $s_{2,14}$ from BS_{14}) from $U_{3,14}$ the symbol $s_{1,13}$ that was received from BS_{13} in TS2. TS5 is left without D2D transmission or reception between $U_{1,13}$ and $U_{3,14}$ to avoid an imbalance in the number of symbols transmitted and received (but $U_{1,13}$ still receives $s_{3,13}$ from BS_{13} and $s_{4,14}$ from BS_{14}). In this way each symbol is D2D transmitted once and D2D received once by each user in each transmission round, while again 4/5 DoF per cell are achieved.

Let us consider an amplify-and-forward (AF) strategy. The received signal for $U_{1,13}$ during five time-slots is given as

$$\begin{aligned}
y_{1,13}^{(1)} &= \sqrt{P_{14}} h_{1,13}^{14,(1)} s_{3,14} + n_{1,13}^{(1)} \\
y_{1,13}^{(2)} &= \sqrt{P_{13}} h_{1,13}^{13,(2)} s_{1,13} + n_{1,13}^{(2)} \\
y_{1,13}^{(4)} &= \sqrt{P_{13}} h_{1,13}^{13,(4)} s_{4,13} + \sqrt{P_{14}} h_{1,13}^{14,(4)} s_{2,14} + \\
&\quad \sqrt{p_{3,14}} g_{1,13}^{3,14,(4)} z_{1,13}^{3,14,(2)} + n_{1,13}^{(4)} \\
y_{1,13}^{(5)} &= \sqrt{P_{13}} h_{1,13}^{13,(5)} s_{3,13} + \sqrt{P_{14}} h_{1,13}^{14,(5)} s_{4,14} + n_{1,13}^{(5)}
\end{aligned} \tag{3.3}$$

where $y_{m,l}^{(t)}$ is the signal received by $U_{m,l}$ in time-slot t and $n_{m,l}^{(t)}$ is the noise received by $U_{m,l}$ in time-slot t and

$$z_{m,l}^{n,k,(t)} = s_{m,l} + \frac{n_{n,k}^{(t)}}{\sqrt{P_l} h_{n,k}^{l,(t)}}. \tag{3.4}$$

Since TS3 is used for transmission by $U_{1,13}$, it does not appear in (3.3). Note that TS4 refers to the next transmission round and that the symbol $s_{1,13}$ received by D2D communication was received by $U_{3,14}$ in TS2.

Equation (3.3) can be expressed in matrix form as equation (6.15), which is equivalent to $\mathbf{y}_{1,13} = \mathbf{a}_{1,13} s_{1,13} + \sum_{\substack{\kappa \in \mathcal{S}_{1,13} \\ \kappa \notin 1,13}} \mathbf{a}_\kappa \mathbf{s}_{1,13}(\kappa) + \mathbf{n}_{1,13} = \mathbf{a}_{1,13} s_{1,13} + \mathbf{w}_{1,13}$,

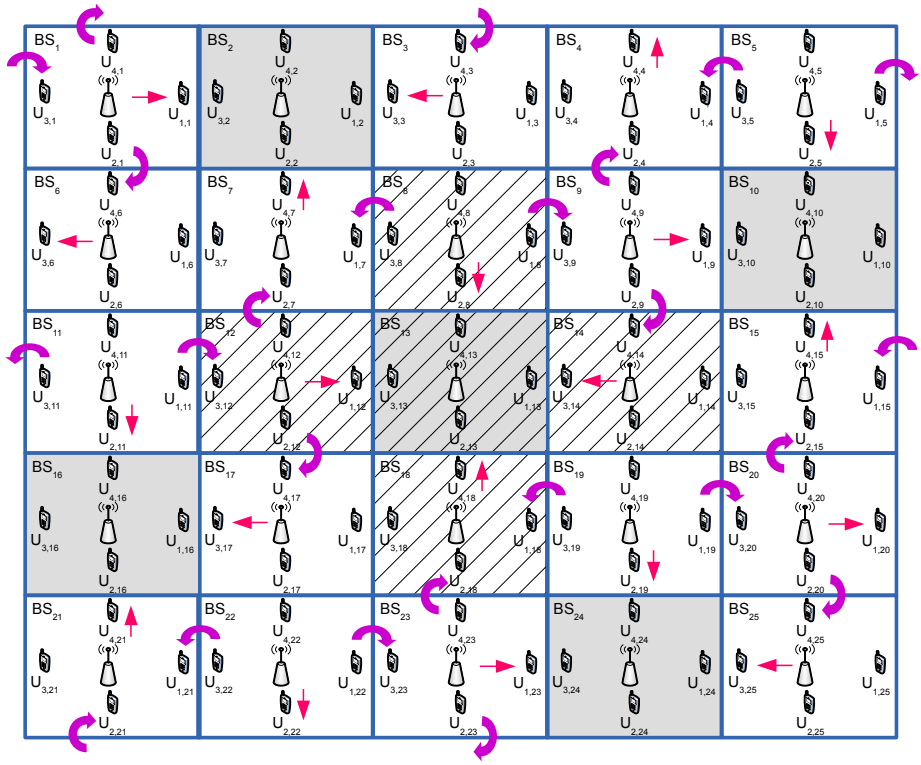

Figure 3.3: Square array. The red thin arrows point out the isotropic transmission from a BS intended for a particular user. The magenta arrows represent the D2D transmissions. The shaded cells represent the inactive cells. The basic tile of this transmission scheme has diagonal stripes as background.

where $\mathbf{a}_{m,l}$ is the column vector of matrix $\mathbf{A}_{m,l}$ corresponding to $s_{m,l}$, $\mathbf{w}_{m,l}$ is the vector of interference-plus-noise of $\mathrm{U}_{m,l}$, $\mathbf{s}_{m,l}(\kappa)$ is the element of vector

$\mathbf{s}_{m,l}$ corresponding to s_κ, and $\mathcal{S}_{m,l}$ is the set of symbols received by $\mathrm{U}_{m,l}$.

$$\underbrace{\begin{bmatrix} y_{1,13}^{(1)} \\ y_{1,13}^{(2)} \\ y_{1,13}^{(4)} \\ y_{1,13}^{(5)} \end{bmatrix}}_{\mathbf{y}_{1,13}} = \underbrace{\begin{bmatrix} n_{1,13}^{(1)} \\ n_{1,13}^{(2)} \\ n_{1,13}^{(4)} + \frac{\sqrt{p_{3,14}} g_{1,13}^{3,14,(4)} n_{3,14}^{(2)}}{\sqrt{P_{13}} h_{3,14}^{13,(2)}} \\ n_{1,13}^{(5)} \end{bmatrix}}_{\mathbf{n}_{1,13}} +$$

$$\underbrace{\begin{bmatrix} \sqrt{P_{14}} h_{1,13}^{14,(1)} & 0 & 0 & 0 & 0 & 0 \\ 0 & \sqrt{P_{13}} h_{1,13}^{13,(2)} & 0 & 0 & 0 & 0 \\ 0 & \sqrt{p_{3,14}} g_{1,13}^{3,14,(4)} & \sqrt{P_{13}} h_{1,13}^{13,(4)} & \sqrt{P_{14}} h_{1,13}^{14,(4)} & 0 & 0 \\ \underbrace{0}_{\mathbf{a}_{3,14}} & \underbrace{0}_{\mathbf{a}_{1,13}} & \underbrace{0}_{\mathbf{a}_{4,13}} & \underbrace{0}_{\mathbf{a}_{2,14}} & \underbrace{\sqrt{P_{13}} h_{1,13}^{13,(5)}}_{\mathbf{a}_{3,13}} & \underbrace{\sqrt{P_{14}} h_{1,13}^{14,(5)}}_{\mathbf{a}_{4,14}} \end{bmatrix}}_{\mathbf{A}_{1,13}} \underbrace{\begin{bmatrix} s_{3,14} \\ s_{1,13} \\ s_{4,13} \\ s_{2,14} \\ s_{3,13} \\ s_{4,14} \end{bmatrix}}_{\mathbf{s}_{1,13}} \tag{3.5}$$

A similar transmission/reception pattern can be identified for each of the users connected to BS_{13}. Consider $\mathrm{U}_{2,13}$. The received signal for $\mathrm{U}_{2,13}$ is given in equation (4.13).

$$\underbrace{\begin{bmatrix} y_{2,13}^{(1)} \\ y_{2,13}^{(3)} \\ y_{2,13}^{(4)} \\ y_{2,13}^{(5)} \end{bmatrix}}_{\mathbf{y}_{2,13}} = \underbrace{\begin{bmatrix} n_{2,13}^{(1)} \\ n_{2,13}^{(3)} \\ n_{2,13}^{(4)} + \frac{\sqrt{p_{4,18}} g_{2,13}^{4,18,(4)} n_{4,18}^{(3)}}{\sqrt{P_{13}} h_{4,18}^{13,(3)}} \\ n_{2,13}^{(5)} \end{bmatrix}}_{\mathbf{n}_{2,13}} +$$

$$\underbrace{\begin{bmatrix} \sqrt{P_{18}} h_{2,13}^{18,(1)} & 0 & 0 & 0 & 0 & 0 \\ 0 & \sqrt{P_{13}} h_{2,13}^{13,(3)} & 0 & 0 & 0 & 0 \\ 0 & \sqrt{p_{4,18}} g_{2,13}^{4,18,(4)} & \sqrt{P_{13}} h_{2,13}^{13,(4)} & \sqrt{P_{18}} h_{2,13}^{18,(4)} & 0 & 0 \\ \underbrace{0}_{\mathbf{a}_{4,18}} & \underbrace{0}_{\mathbf{a}_{2,13}} & \underbrace{0}_{\mathbf{a}_{4,13}} & \underbrace{0}_{\mathbf{a}_{1,18}} & \underbrace{\sqrt{P_{13}} h_{2,13}^{13,(5)}}_{\mathbf{a}_{3,13}} & \underbrace{\sqrt{P_{18}} h_{2,13}^{18,(5)}}_{\mathbf{a}_{2,18}} \end{bmatrix}}_{\mathbf{A}_{2,13}} \underbrace{\begin{bmatrix} s_{4,18} \\ s_{2,13} \\ s_{4,13} \\ s_{1,18} \\ s_{3,13} \\ s_{2,18} \end{bmatrix}}_{\mathbf{s}_{2,13}} \tag{3.6}$$

Since TS2 is used for transmission by $\mathrm{U}_{2,13}$, it does not appear in (4.13). Note that TS4 refers to the following round and that the symbol $s_{2,13}$ received by D2D communication was received by $\mathrm{U}_{4,18}$ in TS3.

Consider now $U_{3,13}$. The received signal for $U_{3,13}$ is given in equation (3.7).

$$\underbrace{\begin{bmatrix} y_{3,13}^{(1)} \\ y_{3,13}^{(2)} \\ y_{3,13}^{(4)} \\ y_{3,13}^{(5)} \end{bmatrix}}_{\mathbf{y}_{3,13}} = \underbrace{\begin{bmatrix} n_{3,13}^{(1)} \\ n_{3,13}^{(2)} + \frac{\sqrt{p_{1,12}} g_{3,13}^{1,12,(2)} n_{1,12}^{(5)}}{\sqrt{P_{13}} h_{1,12}^{13,(5)}} \\ n_{3,13}^{(4)} \\ n_{3,13}^{(5)} \end{bmatrix}}_{\mathbf{n}_{3,13}} +$$

$$\underbrace{\begin{bmatrix} \sqrt{P_{12}} h_{3,13}^{12,(1)} & 0 & 0 & 0 & 0 & 0 \\ 0 & \sqrt{P_{13}} h_{3,13}^{13,(2)} & \sqrt{P_{12}} h_{3,13}^{12,(2)} & \sqrt{p_{1,12}} g_{3,13}^{1,12,(2)} & 0 & 0 \\ 0 & 0 & 0 & 0 & \sqrt{P_{13}} h_{3,13}^{13,(4)} & \sqrt{P_{12}} h_{3,13}^{12,(4)} \\ \underbrace{0}_{\mathbf{a}_{1,12}} & \underbrace{0}_{\mathbf{a}_{1,13}} & \underbrace{0}_{\mathbf{a}_{2,12}} & \underbrace{\sqrt{P_{13}} h_{3,13}^{13,(5)}}_{\mathbf{a}_{3,13}} & \underbrace{0}_{\mathbf{a}_{4,13}} & \underbrace{0}_{\mathbf{a}_{3,12}} \end{bmatrix}}_{\mathbf{A}_{3,13}} \underbrace{\begin{bmatrix} s_{1,12} \\ s_{1,13} \\ s_{2,12} \\ s_{3,13} \\ s_{4,13} \\ s_{3,12} \end{bmatrix}}_{\mathbf{s}_{3,13}} \tag{3.7}$$

Since TS3 is used for transmission by $U_{3,13}$, it does not appear in (3.7). Note that TS2 refers to the following transmission round and that the symbol $s_{3,13}$ received by D2D communication was received by $U_{1,12}$ in TS5.

Consider $U_{4,13}$. The received signal for $U_{4,13}$ is given in equation (3.8).

$$\underbrace{\begin{bmatrix} y_{4,13}^{(1)} \\ y_{4,13}^{(3)} \\ y_{4,13}^{(4)} \\ y_{4,13}^{(5)} \end{bmatrix}}_{\mathbf{y}_{4,13}} = \underbrace{\begin{bmatrix} n_{4,13}^{(1)} \\ n_{4,13}^{(3)} \\ n_{4,13}^{(4)} \\ n_{4,13}^{(5)} + \frac{\sqrt{p_{2,8}} g_{4,13}^{2,8,(5)} n_{2,8}^{(4)}}{\sqrt{P_{13}} h_{2,8}^{13,(4)}} \end{bmatrix}}_{\mathbf{n}_{4,13}} + \tag{3.8}$$

$$\underbrace{\begin{bmatrix} \sqrt{P_8} h_{4,13}^{8,(1)} & 0 & 0 & 0 & 0 & 0 \\ 0 & \sqrt{P_{13}} h_{4,13}^{13,(3)} & \sqrt{P_8} h_{4,13}^{8,(3)} & 0 & 0 & 0 \\ 0 & 0 & 0 & \sqrt{P_{13}} h_{4,13}^{13,(4)} & 0 & 0 \\ \underbrace{0}_{\mathbf{a}_{2,8}} & \underbrace{0}_{\mathbf{a}_{2,13}} & \underbrace{0}_{\mathbf{a}_{3,8}} & \underbrace{\sqrt{p_{2,8}} g_{4,13}^{2,8,(5)}}_{\mathbf{a}_{4,13}} & \underbrace{\sqrt{P_{13}} h_{4,13}^{13,(5)}}_{\mathbf{a}_{3,13}} & \underbrace{\sqrt{P_8} h_{4,13}^{8,(5)}}_{\mathbf{a}_{1,8}} \end{bmatrix}}_{\mathbf{A}_{4,13}} \underbrace{\begin{bmatrix} s_{2,8} \\ s_{2,13} \\ s_{3,8} \\ s_{4,13} \\ s_{3,13} \\ s_{1,8} \end{bmatrix}}_{\mathbf{s}_{4,13}}$$

Since TS2 is used for transmission by $U_{4,13}$, it does not appear in (3.8). Note that TS5 refers to the following transmission round and that the symbol $s_{4,13}$ received by D2D communication was received by $U_{2,8}$ in TS4.

Notice also that all the users achieve the same diversity.

3.4.2 Hexagonal Array

Consider the hexagonal array depicted in Fig. 3.4 with $N = 6$ and one user per cell edge in each cell, i.e. 6 cell edge users in each cell. Again, the thick arrows should not yet be considered, as these correspond to the D2D operations that will be explained later. In the figure only the users served by BS_1 are depicted. In each cell, users are assumed to be located at each cell edge and numbered clockwise from 1 to 6 starting at the upper right cell edge (white dot). With the AFR presented in [47] each cell cycles through a sequence of $N + 1 = 7$ operations, i.e. a transmission round with 7 time-slots (TS1,TS2,..,TS7). In each transmission round, a cell is active in 6 time-slots, used to transmit a symbol from its BS to each of the 6 cell edge users, and inactive (i.e. with the BS not transmitting to any cell edge user) in one time-slot.

Fig. 3.4 gives the transmission/reception pattern for TS1, where inactive cells are shaded. A tile pattern can again be identified where each tile covers one inactive cell together with its 6 neighboring cells. One such tile is highlighted in the figure with diagonal stripes. All tiles together cover the complete array. A transmission round starts with the tile pattern at a specific location (TS1) and then the tile pattern is shifted over one cell to the right each time-slot. This then fully defines the sequence of operations that each cell cycles through. For instance, the transmission operations for BS_1 are as follows: BS_1 is inactive in TS1. In TS2 it transmits the desired symbol for $U_{2,1}$. In TS3, TS4, TS5, TS6, and TS7 it transmits the desired symbols for $U_{4,1}$, $U_{3,1}$, $U_{6,1}$, $U_{1,1}$, and $U_{5,1}$, respectively. For instance, the reception operations for $U_{1,1}$ are as follows: in TS1 it receives $s_{4,2}$ from BS_2. In TS2 it receives $s_{2,1}$ from BS_1 and $s_{3,2}$ from BS_2. In TS3, TS4 and TS5, it receives $s_{4,1}$, $s_{3,1}$, and $s_{6,1}$ from BS_1, and $s_{6,2}$, $s_{1,2}$, and $s_{5,2}$ from BS_2, respectively. In TS6, it receives the desired symbol $s_{1,1}$ from BS_1 and in TS7, it receives $s_{5,1}$ from BS_1 and $s_{2,2}$ from BS_2.

Since each user receives one desired symbol in every 7 time-slots and there are 6 users per cell, it is easy to see that AFR achieves 6/7 DoF per cell.

Here again we propose to perform D2D communication between users located in the same cell edge. For instance, considering $U_{1,1}$ and $U_{4,2}$ in TS2, TS3, TS4, TS5, and TS7, $U_{1,1}$ and $U_{4,2}$ are neither receiving their desired symbol, nor the symbol of their neighbor. Therefore, we can exploit these time-slots to perform a D2D transmission or D2D reception. For instance, in TS2 of the following round, $U_{1,1}$ can transmit to $U_{4,2}$ the symbol $s_{4,2}$ that was received from BS_2 in TS1. In TS3 of the following round, $U_{1,1}$ can transmit again to $U_{4,2}$ the symbol $s_{4,2}$ that was received from BS_2 in TS1. In TS4 of the following round, $U_{1,1}$ can

receive (together with $s_{3,1}$ from BS_1 and $s_{1,2}$ from BS_2) from $U_{4,2}$ its desired symbol $s_{1,1}$ that was received from BS_1 in TS6. In TS5 of the following round, $U_{1,1}$ can receive again (together with $s_{6,1}$ from BS_1 and $s_{5,2}$ from BS_2) from $U_{4,2}$ its desired symbol $s_{1,1}$ that was received from BS_1 in TS6. In TS6, $U_{1,1}$ receives from BS_1 its desired symbol $s_{1,1}$ without inter-cell interference. Finally, in TS7 is left without D2D transmission or reception to avoid an imbalance in the number of symbols transmitted and received (but $U_{1,1}$ still receives $s_{5,1}$ from BS_1 and $s_{2,2}$ from BS_2). In this way each symbol is D2D transmitted and D2D received twice by each user in each transmission round, while again 6/7 DoF per cell are achieved.

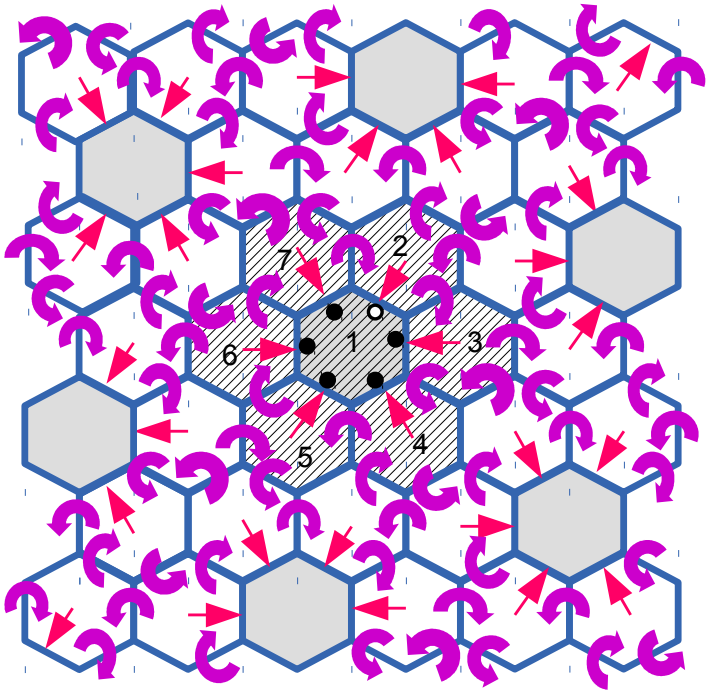

Figure 3.4: Hexagonal array. The red thin arrows point out the isotropic transmission from a BS intended for a particular user. The magenta thick arrows represent the D2D transmissions. The shaded cells represent the inactive cells (not transmitting to any cell edge user). The basic tile of this transmission scheme has diagonal stripes as background. Cell edge users are represented by the dots and numbered clockwise from 1 to 6 starting with the white dot (only the cell edge users from BS_1 are shown).

Assuming again an AF strategy, the received signal for $U_{1,1}$ during seven time-slots is given as

$$\begin{aligned}
y_{1,1}^{(1)} &= \sqrt{P_2} h_{1,1}^{2,(1)} s_{4,2} + n_{1,1}^{(1)} \\
y_{1,1}^{(4)} &= \sqrt{P_1} h_{1,1}^{1,(4)} s_{3,1} + \sqrt{P_2} h_{1,1}^{2,(4)} s_{1,2} + \\
&\quad \sqrt{p_{4,2}} g_{1,1}^{4,2,(4)} z_{1,1}^{4,2,(6)} + n_{1,1}^{(4)} \\
y_{1,1}^{(5)} &= \sqrt{P_1} h_{1,1}^{1,(5)} s_{6,1} + \sqrt{P_2} h_{1,1}^{2,(5)} s_{5,2} + \\
&\quad \sqrt{p_{4,2}} g_{1,1}^{4,2,(5)} z_{1,1}^{4,2,(6)} + n_{1,1}^{(5)} \\
y_{1,1}^{(6)} &= \sqrt{P_1} h_{1,1}^{1,(6)} s_{1,1} + n_{1,1}^{(6)} \\
y_{1,1}^{(7)} &= \sqrt{P_1} h_{1,1}^{1,(7)} s_{5,1} + \sqrt{P_2} h_{1,1}^{2,(7)} s_{2,2} + n_{1,1}^{(7)}
\end{aligned} \tag{3.9}$$

Note that TS2 and TS3 are used for transmission and hence do not appear in (3.9). Note also that TS4 and TS5 refer to the following transmission round and that the symbol $s_{1,1}$ received by D2D was received by $U_{4,2}$ in TS6.

Equation (3.9) can be expressed in matrix form as equation (3.10), which is equivalent to $\mathbf{y}_{1,1} = \mathbf{a}_{1,1} s_{1,1} + \sum_{\substack{\kappa \in \mathcal{S}_{1,1} \\ \kappa \notin 1,1}} \mathbf{a}_\kappa \mathbf{s}_{1,1}(\kappa) + \mathbf{n}_{1,1} = \mathbf{a}_{1,1} s_{1,1} + \mathbf{w}_{1,1}$.

$$\underbrace{\begin{bmatrix} y_{1,1}^{(1)} \\ y_{1,1}^{(4)} \\ y_{1,1}^{(5)} \\ y_{1,1}^{(6)} \\ y_{1,1}^{(7)} \end{bmatrix}}_{\mathbf{y}_{1,1}} = \underbrace{\begin{bmatrix} n_{1,1}^{(1)} \\ n_{1,1}^{(4)} + \frac{\sqrt{p_{4,2}} g_{1,1}^{4,2,(4)} n_{4,2}^{(6)}}{\sqrt{P_1} h_{4,2}^{1,(6)}} \\ n_{1,1}^{(5)} + \frac{\sqrt{p_{4,2}} g_{1,1}^{4,2,(5)} n_{4,2}^{(6)}}{\sqrt{P_1} h_{4,2}^{1,(6)}} \\ n_{1,1}^{(6)} \\ n_{1,1}^{(7)} \end{bmatrix}}_{\mathbf{n}_{1,1}} +$$

$$\underbrace{\begin{bmatrix} \sqrt{P_2} h_{1,1}^{2,(1)} & 0 & 0 & 0 & 0 & 0 & 0 & 0 \\ 0 & \sqrt{P_1} h_{1,1}^{1,(4)} & \sqrt{P_2} h_{1,1}^{2,(4)} & \sqrt{p_{4,2}} g_{1,1}^{4,2,(4)} & 0 & 0 & 0 & 0 \\ 0 & 0 & 0 & \sqrt{p_{4,2}} g_{1,1}^{4,2,(5)} & \sqrt{P_1} h_{1,1}^{1,(5)} & \sqrt{P_2} h_{1,1}^{2,(5)} & 0 & 0 \\ 0 & 0 & 0 & \sqrt{P_1} h_{1,1}^{1,(6)} & 0 & 0 & 0 & 0 \\ \underbrace{0}_{\mathbf{a}_{4,2}} & \underbrace{0}_{\mathbf{a}_{3,1}} & \underbrace{0}_{\mathbf{a}_{1,2}} & \underbrace{0}_{\mathbf{a}_{1,1}} & \underbrace{0}_{\mathbf{a}_{6,1}} & \underbrace{0}_{\mathbf{a}_{5,2}} & \underbrace{\sqrt{P_1} h_{1,1}^{1,(7)}}_{\mathbf{a}_{5,1}} & \underbrace{\sqrt{P_2} h_{1,1}^{2,(7)}}_{\mathbf{a}_{2,2}} \end{bmatrix}}_{\mathbf{A}_{1,1}} \underbrace{\begin{bmatrix} s_{4,2} \\ s_{3,1} \\ s_{1,2} \\ s_{1,1} \\ s_{6,1} \\ s_{5,2} \\ s_{5,1} \\ s_{2,2} \end{bmatrix}}_{\mathbf{s}_{1,1}} \tag{3.10}$$

A similar transmission/reception pattern can be identified for each of the users connected to BS_1. Consider $U_{2,1}$, the received signal is given in equation (3.11).

$$\underbrace{\begin{bmatrix} y_{2,1}^{(1)} \\ y_{2,1}^{(2)} \\ y_{2,1}^{(3)} \\ y_{2,1}^{(5)} \\ y_{2,1}^{(6)} \end{bmatrix}}_{\mathbf{y}_{2,1}} = \underbrace{\begin{bmatrix} n_{2,1}^{(1)} \\ n_{2,1}^{(2)} \\ n_{2,1}^{(3)} + \frac{\sqrt{p_{5,3}} g_{2,1}^{5,3,(3)} n_{5,3}^{(2)}}{\sqrt{P_1} h_{5,3}^{1,(2)}} \\ n_{2,1}^{(5)} \\ n_{2,1}^{(6)} + \frac{\sqrt{p_{5,3}} g_{2,1}^{5,3,(6)} n_{5,3}^{(2)}}{\sqrt{P_1} h_{5,3}^{1,(2)}} \end{bmatrix}}_{\mathbf{n}_{2,1}} +$$

$$\underbrace{\begin{bmatrix} \sqrt{P_3} h_{2,1}^{3,(1)} & 0 & 0 & 0 & 0 & 0 & 0 & 0 \\ 0 & \sqrt{P_1} h_{2,1}^{1,(2)} & 0 & 0 & 0 & 0 & 0 & 0 \\ 0 & \sqrt{p_{5,3}} g_{2,1}^{5,3,(3)} & \sqrt{P_1} h_{2,1}^{1,(3)} & \sqrt{P_3} h_{2,1}^{3,(3)} & 0 & 0 & 0 & 0 \\ 0 & 0 & 0 & 0 & \sqrt{P_1} h_{2,1}^{1,(5)} & \sqrt{P_3} h_{2,1}^{3,(5)} & 0 & 0 \\ \underbrace{0}_{\mathbf{a}_{5,3}} & \underbrace{\sqrt{p_{5,3}} g_{2,1}^{5,3,(6)}}_{\mathbf{a}_{2,1}} & \underbrace{0}_{\mathbf{a}_{4,1}} & \underbrace{0}_{\mathbf{a}_{2,3}} & \underbrace{0}_{\mathbf{a}_{6,1}} & \underbrace{0}_{\mathbf{a}_{3,3}} & \underbrace{\sqrt{P_1} h_{2,1}^{1,(6)}}_{\mathbf{a}_{1,1}} & \underbrace{\sqrt{P_3} h_{2,1}^{3,(6)}}_{\mathbf{a}_{6,3}} \end{bmatrix}}_{\mathbf{A}_{2,1}} \underbrace{\begin{bmatrix} s_{5,3} \\ s_{2,1} \\ s_{4,1} \\ s_{2,3} \\ s_{6,1} \\ s_{3,3} \\ s_{1,1} \\ s_{6,3} \end{bmatrix}}_{\mathbf{s}_{2,1}} \tag{3.11}$$

Note that TS4 and TS7 are used for transmission and hence do not appear in (3.11). Note also that TS3 and TS6 refer to the following transmission round and that the symbol $s_{2,1}$ received by D2D was received by $U_{5,3}$ in TS2.

Consider $U_{3,1}$. The received signal for $U_{3,1}$ is given in equation (3.12).

$$\underbrace{\begin{bmatrix} y_{3,1}^{(1)} \\ y_{3,1}^{(2)} \\ y_{3,1}^{(4)} \\ y_{3,1}^{(6)} \\ y_{3,1}^{(7)} \end{bmatrix}}_{\mathbf{y}_{3,1}} = \underbrace{\begin{bmatrix} n_{3,1}^{(1)} \\ n_{3,1}^{(2)} + \frac{\sqrt{p_{6,4}} g_{3,1}^{6,4,(2)} n_{6,4}^{(4)}}{\sqrt{P_1} h_{6,4}^{1,(4)}} \\ n_{3,1}^{(4)} \\ n_{3,1}^{(6)} \\ n_{3,1}^{(7)} + \frac{\sqrt{p_{6,4}} g_{3,1}^{6,4,(7)} n_{6,4}^{(4)}}{\sqrt{P_1} h_{6,4}^{1,(4)}} \end{bmatrix}}_{\mathbf{n}_{3,1}} +$$

$$\underbrace{\begin{bmatrix} \sqrt{P_4} h_{3,1}^{4,(1)} & 0 & 0 & 0 & 0 & 0 & 0 & 0 \\ 0 & \sqrt{P_1} h_{3,1}^{1,(2)} & \sqrt{P_4} h_{3,1}^{4,(2)} & \sqrt{p_{6,4}} g_{3,1}^{6,4,(2)} & 0 & 0 & 0 & 0 \\ 0 & 0 & 0 & \sqrt{P_1} h_{3,1}^{1,(4)} & 0 & 0 & 0 & 0 \\ 0 & 0 & 0 & 0 & \sqrt{P_1} h_{3,1}^{1,(6)} & \sqrt{P_4} h_{3,1}^{4,(6)} & 0 & 0 \\ \underbrace{0}_{\mathbf{a}_{6,4}} & \underbrace{0}_{\mathbf{a}_{2,1}} & \underbrace{0}_{\mathbf{a}_{1,4}} & \underbrace{\sqrt{p_{6,4}} g_{3,1}^{6,4,(7)}}_{\mathbf{a}_{3,1}} & \underbrace{0}_{\mathbf{a}_{1,1}} & \underbrace{0}_{\mathbf{a}_{4,4}} & \underbrace{\sqrt{P_1} h_{3,1}^{1,(7)}}_{\mathbf{a}_{5,1}} & \underbrace{\sqrt{P_4} h_{3,1}^{4,(7)}}_{\mathbf{a}_{3,4}} \end{bmatrix}}_{\mathbf{A}_{3,1}} \underbrace{\begin{bmatrix} s_{6,4} \\ s_{2,1} \\ s_{1,4} \\ s_{3,1} \\ s_{1,1} \\ s_{4,4} \\ s_{5,1} \\ s_{3,4} \end{bmatrix}}_{\mathbf{s}_{3,1}} \tag{3.12}$$

Note that TS3 and TS5 are used for transmission and hence do not appear in (3.12). Note also that TS2 and TS7 refer to the following transmission round and that the symbol $s_{3,1}$ received by D2D was received by $U_{6,4}$ in TS4.

Consider $U_{4,1}$, the received signal is given in equation (3.13).

$$\underbrace{\begin{bmatrix} y_{4,1}^{(1)} \\ y_{4,1}^{(2)} \\ y_{4,1}^{(3)} \\ y_{4,1}^{(4)} \\ y_{4,1}^{(5)} \end{bmatrix}}_{\mathbf{y}_{4,1}} = \underbrace{\begin{bmatrix} n_{4,1}^{(1)} \\ n_{4,1}^{(2)} \\ n_{4,1}^{(3)} \\ n_{4,1}^{(4)} + \frac{\sqrt{p_{1,5}} g_{4,1}^{1,5,(4)} n_{1,5}^{(3)}}{\sqrt{P_1} h_{1,5}^{1,(3)}} \\ n_{4,1}^{(5)} + \frac{\sqrt{p_{1,5}} g_{4,1}^{1,5,(5)} n_{1,5}^{(3)}}{\sqrt{P_1} h_{1,5}^{1,(3)}} \end{bmatrix}}_{\mathbf{n}_{4,1}} +$$

$$\underbrace{\begin{bmatrix} \sqrt{P_5} h_{4,1}^{5,(1)} & 0 & 0 & 0 & 0 & 0 & 0 & 0 \\ 0 & \sqrt{P_1} h_{4,1}^{1,(2)} & \sqrt{P_5} h_{4,1}^{5,(2)} & 0 & 0 & 0 & 0 & 0 \\ 0 & 0 & 0 & \sqrt{P_1} h_{4,1}^{1,(3)} & 0 & 0 & 0 & 0 \\ 0 & 0 & 0 & \sqrt{p_{1,5}} g_{4,1}^{1,5,(4)} & \sqrt{P_1} h_{4,1}^{1,(4)} & \sqrt{P_5} h_{4,1}^{5,(4)} & 0 & 0 \\ \underbrace{0}_{\mathbf{a}_{1,5}} & \underbrace{0}_{\mathbf{a}_{2,1}} & \underbrace{0}_{\mathbf{a}_{5,5}} & \underbrace{\sqrt{p_{1,5}} g_{4,1}^{1,5,(5)}}_{\mathbf{a}_{4,1}} & \underbrace{0}_{\mathbf{a}_{3,1}} & \underbrace{0}_{\mathbf{a}_{2,5}} & \underbrace{\sqrt{P_1} h_{4,1}^{1,(5)}}_{\mathbf{a}_{6,1}} & \underbrace{\sqrt{P_5} h_{4,1}^{5,(5)}}_{\mathbf{a}_{4,5}} \end{bmatrix}}_{\mathbf{A}_{4,1}} \underbrace{\begin{bmatrix} s_{1,5} \\ s_{2,1} \\ s_{5,5} \\ s_{4,1} \\ s_{3,1} \\ s_{2,5} \\ s_{6,1} \\ s_{4,5} \end{bmatrix}}_{\mathbf{s}_{4,1}} \tag{3.13}$$

Note that TS6 and TS7 are used for transmission and hence do not appear in (3.13). Note also that TS4 and TS5 refer to the following transmission round and that the symbol $s_{4,1}$ received by D2D was received by $U_{1,5}$ in TS3.

Consider $U_{5,1}$, the received signal is given in equation (3.14).

$$\underbrace{\begin{bmatrix} y_{5,1}^{(1)} \\ y_{5,1}^{(3)} \\ y_{5,1}^{(4)} \\ y_{5,1}^{(6)} \\ y_{5,1}^{(7)} \end{bmatrix}}_{\mathbf{y}_{5,1}} = \underbrace{\begin{bmatrix} n_{5,1}^{(1)} \\ n_{5,1}^{(3)} + \frac{\sqrt{p_{2,6}} g_{5,1}^{2,6,(3)} n_{2,6}^{(7)}}{\sqrt{P_1} h_{2,6}^{1,(7)}} \\ n_{5,1}^{(4)} \\ n_{5,1}^{(6)} + \frac{\sqrt{p_{2,6}} g_{5,1}^{2,6,(6)} n_{2,6}^{(7)}}{\sqrt{P_1} h_{2,6}^{1,(7)}} \\ n_{5,1}^{(7)} \end{bmatrix}}_{\mathbf{n}_{5,1}} +$$

$$\underbrace{\begin{bmatrix} \sqrt{P_6} h_{5,1}^{6,(1)} & 0 & 0 & 0 & 0 & 0 & 0 & 0 \\ 0 & \sqrt{P_1} h_{5,1}^{1,(3)} & \sqrt{P_6} h_{5,1}^{6,(3)} & \sqrt{p_{2,6}} g_{5,1}^{2,6,(3)} & 0 & 0 & 0 & 0 \\ 0 & 0 & 0 & 0 & \sqrt{P_1} h_{5,1}^{1,(4)} & \sqrt{P_6} h_{5,1}^{6,(4)} & 0 & 0 \\ 0 & 0 & 0 & \sqrt{p_{2,6}} g_{5,1}^{2,6,(6)} & 0 & 0 & \sqrt{P_1} h_{5,1}^{1,(6)} & \sqrt{P_6} h_{5,1}^{6,(6)} \\ \underbrace{0}_{\mathbf{a}_{2,6}} & \underbrace{0}_{\mathbf{a}_{4,1}} & \underbrace{0}_{\mathbf{a}_{3,6}} & \underbrace{\sqrt{P_1} h_{5,1}^{1,(7)}}_{\mathbf{a}_{5,1}} & \underbrace{0}_{\mathbf{a}_{3,1}} & \underbrace{0}_{\mathbf{a}_{6,6}} & \underbrace{0}_{\mathbf{a}_{1,1}} & \underbrace{0}_{\mathbf{a}_{5,6}} \end{bmatrix}}_{\mathbf{A}_{5,1}} \underbrace{\begin{bmatrix} s_{2,6} \\ s_{4,1} \\ s_{3,6} \\ s_{5,1} \\ s_{3,1} \\ s_{6,6} \\ s_{1,1} \\ s_{5,6} \end{bmatrix}}_{\mathbf{s}_{5,1}} \tag{3.14}$$

Note that TS2 and TS5 are used for transmission and hence do not appear in (3.14). Note also that TS3 and TS6 refer to the following transmission round and that the symbol $s_{5,1}$ received by D2D was received by $U_{2,6}$ in TS7.

Consider $U_{6,1}$, the received signal is given in (3.15).

$$\underbrace{\begin{bmatrix} y_{6,1}^{(1)} \\ y_{6,1}^{(2)} \\ y_{6,1}^{(3)} \\ y_{6,1}^{(5)} \\ y_{6,1}^{(7)} \end{bmatrix}}_{\mathbf{y}_{6,1}} = \underbrace{\begin{bmatrix} n_{6,1}^{(1)} \\ n_{6,1}^{(2)} + \frac{\sqrt{p_{3,7}} g_{6,1}^{3,7,(2)} n_{3,7}^{(5)}}{\sqrt{P_1} h_{3,7}^{1,(5)}} \\ n_{6,1}^{(3)} \\ n_{6,1}^{(5)} \\ n_{6,1}^{(7)} + \frac{\sqrt{p_{3,7}} g_{6,1}^{3,7,(7)} n_{3,7}^{(5)}}{\sqrt{P_1} h_{3,7}^{1,(5)}} \end{bmatrix}}_{\mathbf{n}_{6,1}} +$$

$$\underbrace{\begin{bmatrix} \sqrt{P_7} h_{6,1}^{7,(1)} & 0 & 0 & 0 & 0 & 0 & 0 & 0 \\ 0 & \sqrt{P_1} h_{6,1}^{1,(2)} & \sqrt{P_7} h_{6,1}^{7,(2)} & \sqrt{p_{3,7}} g_{6,1}^{3,7,(2)} & 0 & 0 & 0 & 0 \\ 0 & 0 & 0 & 0 & \sqrt{P_1} h_{6,1}^{1,(3)} & \sqrt{P_7} h_{6,1}^{7,(3)} & 0 & 0 \\ 0 & 0 & 0 & \sqrt{P_1} h_{6,1}^{1,(5)} & 0 & 0 & 0 & 0 \\ \underbrace{0}_{\mathbf{a}_{3,7}} & \underbrace{0}_{\mathbf{a}_{2,1}} & \underbrace{0}_{\mathbf{a}_{6,7}} & \underbrace{\sqrt{p_{3,7}} g_{6,1}^{3,7,(7)}}_{\mathbf{a}_{6,1}} & \underbrace{0}_{\mathbf{a}_{4,1}} & \underbrace{0}_{\mathbf{a}_{1,7}} & \underbrace{\sqrt{P_1} h_{6,1}^{1,(7)}}_{\mathbf{a}_{5,1}} & \underbrace{\sqrt{P_7} h_{6,1}^{7,(7)}}_{\mathbf{a}_{4,7}} \end{bmatrix}}_{\mathbf{A}_{6,1}} \underbrace{\begin{bmatrix} s_{3,7} \\ s_{2,1} \\ s_{6,7} \\ s_{6,1} \\ s_{4,1} \\ s_{1,7} \\ s_{5,1} \\ s_{4,7} \end{bmatrix}}_{\mathbf{s}_{6,1}} \tag{3.15}$$

Note that TS4 and TS6 are used for transmission and hence do not appear in (3.15). Note also that TS2 and TS7 refer to the following transmission round and that the symbol $s_{6,1}$ received by D2D was received by $U_{3,7}$ in TS5.

In this way all the users achieve the same diversity.

3.5 Multiple Cell Edge Users

We now extend the previous approach to the scenario with an arbitrary M cell edge users per cell edge in each cell. In this way, exploiting D2D communication will further increase the spatial diversity for all the users. While the number of time-slots required in the transmission scheme grows with M, so does the number of cell edge users. Hence the DoFs per cell achieved with each cellular topology are the same as in the scenario with a single cell edge user per cell edge in each cell.

As an extension of the scenario with a single cell edge user per cell edge we consider a transmission scheme performed in M transmission rounds with $N+1$ time-slots each. In this section we assume a square cellular array as in Fig. 3.3, but a similar rationale can be used for the hexagonal array.

We first assume that there are $M = 2$ users per cell edge in each cell (a total of $NM = 8$ cell edge users in each cell for the square array and $NM = 12$ for the hexagonal array). The basic tile for the first transmission round is shown in Fig. 3.5, defining the AFR transmission pattern (not considering the thick arrows) of the covered cells in TS1. In subsequent time-slots (TS2, TS3, TS4, and TS5 of round 1) this tile is shifted over one cell to the right. The basic tile for the second transmission round is shown in Fig. 3.6, defining the AFR transmission pattern of the covered cells in TS1. In subsequent time-slots (TS2, TS3, TS4, and TS5 of round 2) this tile is shifted over one cell to the right. For instance, the transmission operations for BS_{13} in the first transmission round are as follows: BS_{13} is inactive in TS1. In TS2, TS3, TS4, and TS5 it transmits the desired symbols for $U_{1,13}$, $U_{3,13}$, $U_{7,13}$, and $U_{5,13}$, respectively. In the second transmission round, BS_{13} is inactive in TS1. In TS2, TS3, TS4, and TS5 it transmits the desired symbols for $U_{2,13}$, $U_{4,13}$, $U_{8,13}$, and $U_{6,13}$, respectively. For instance, the reception operations for $U_{1,13}$ in the first transmission round are as follows: in TS1 it receives $s_{5,14}$ from BS_{14}. In TS2 it receives its desired symbol $s_{1,13}$ from BS_{13}. In TS3, TS4, and TS5 it receives $s_{3,13}$, $s_{7,13}$, and $s_{5,13}$ from BS_{13} and $s_{1,14}$, $s_{3,14}$, and $s_{7,14}$ from BS_{14}, respectively. In the second transmission round: $U_{1,13}$ receives $s_{6,14}$ from BS_{14} in TS1. In TS2 it receives $s_{2,13}$ from BS_{13}. In TS3, TS4, and TS5 it receives $s_{4,13}$, $s_{8,13}$, and $s_{6,13}$ from BS_{13} and $s_{2,14}$, $s_{4,14}$, and $s_{8,14}$ from BS_{14}, respectively.

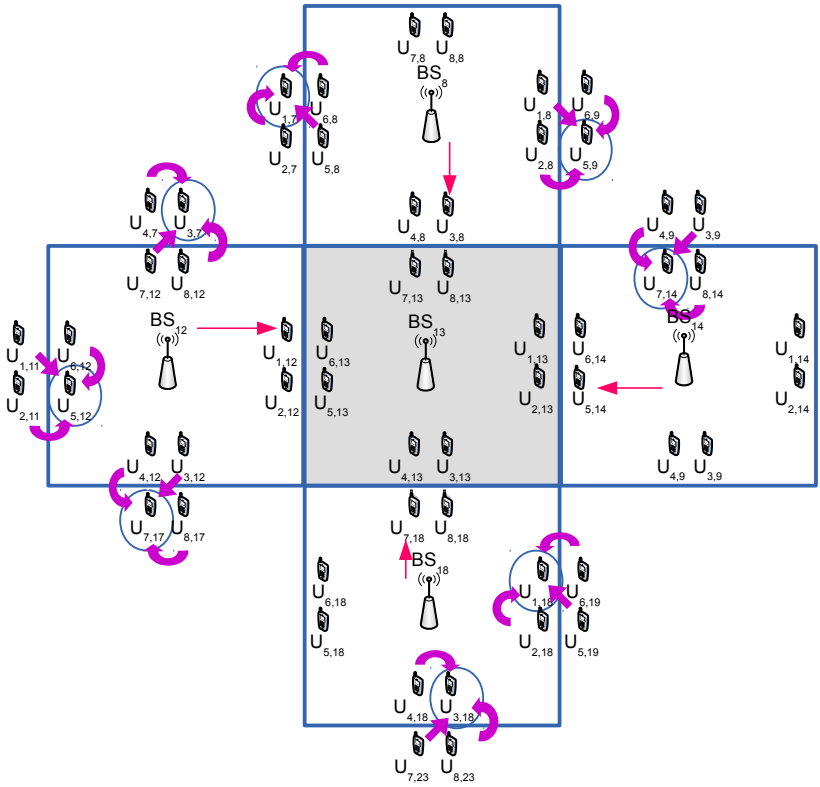

Figure 3.5: Square array with multiple cell edge users for TS1 in the first transmission round. The red thin arrows point out the isotropic transmission from a BS intended for a particular user. The magenta thick arrows represent the D2D transmissions to the user inside the blue circle.

There are now $2M-1$ cell edge users that can transmit through D2D communication a desired symbol to a given user. Consider $\mathrm{U}_{1,13}$. In TS3 of the $M+1=$ 3rd transmission round, $\mathrm{U}_{1,13}$, $\mathrm{U}_{2,13}$, and $\mathrm{U}_{6,14}$ transmit simultaneously to $\mathrm{U}_{5,14}$ the symbol $s_{5,14}$ that was received from BS_{14} in TS1 of round 1. Then in TS4 of round 3, $\mathrm{U}_{1,13}$ receives (together with $s_{7,13}$ from BS_{13} and $s_{3,14}$ from BS_{14}) from $\mathrm{U}_{2,13}$, $\mathrm{U}_{5,14}$, and $\mathrm{U}_{6,14}$ its desired symbol $s_{1,13}$ that was received from BS_{13} in TS2 of round 1. TS5 is left without D2D transmissions or receptions (but $\mathrm{U}_{1,13}$ still receives $s_{5,13}$ from BS_{13} and $s_{7,14}$ from BS_{14}). In TS3 of the $M+2=$ 4th transmission round, $\mathrm{U}_{1,13}$, $\mathrm{U}_{2,13}$, and $\mathrm{U}_{5,14}$ transmit simultaneously to $\mathrm{U}_{6,14}$ the symbol $s_{6,14}$ that was received from BS_{14} in TS1 of round 2. Then in TS4 of round 4, $\mathrm{U}_{2,13}$ receives (together with $s_{8,13}$ from

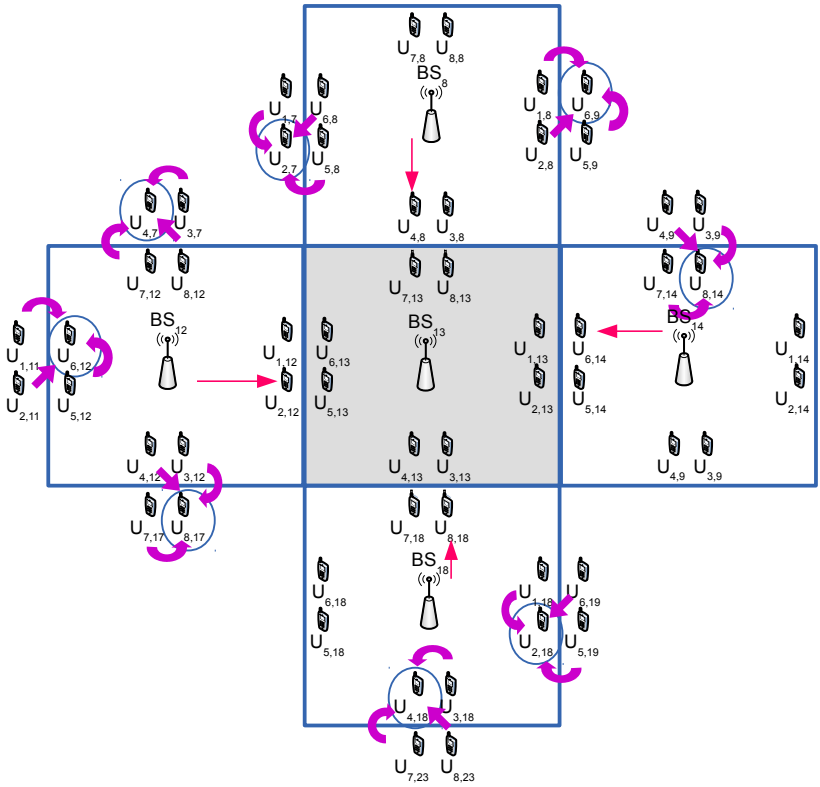

Figure 3.6: Square array with multiple cell edge users per cell edge for TS1 in the second transmission round. The red thin arrows point out the isotropic transmission from a BS intended for a particular user. The magenta thick arrows represent the D2D transmissions to the user inside the blue circle.

BS_{13} and $s_{4,14}$ from BS_{14}) from $U_{1,13}$, $U_{5,14}$, and $U_{6,14}$ its desired symbol $s_{2,13}$ that was received from BS_{13} in TS2 of round 2. TS5 is left without D2D transmissions or receptions (but $U_{2,13}$ still receives $s_{6,13}$ from BS_{13} and $s_{8,14}$ from BS_{14}). In this way each symbol is D2D transmitted once by each user in M transmission rounds.

Assuming an AF strategy, the received signal for $\mathrm{U}_{1,13}$ during $M(N+1)=10$ time-slots is given as

$$
\begin{aligned}
y_{1,13}^{(1)} &= \sqrt{P_{14}} h_{1,13}^{14,(1)} s_{5,14} + n_{1,13}^{(1)} \\
y_{1,13}^{(2)} &= \sqrt{P_{13}} h_{1,13}^{13,(2)} s_{1,13} + n_{1,13}^{(2)} \\
y_{1,13}^{(4)} &= \sqrt{P_{13}} h_{1,13}^{13,(4)} s_{7,13} + \sqrt{P_{14}} h_{1,13}^{14,(4)} s_{3,14} + n_{1,13}^{(4)} + \\
&\quad \sqrt{p_{2,13}} g_{1,13}^{2,13,(4)} z_{1,13}^{2,13,(2)} + \sqrt{p_{5,14}} g_{1,13}^{5,14,(4)} z_{1,13}^{5,14,(2)} + \\
&\quad \sqrt{p_{6,14}} g_{1,13}^{6,14,(4)} z_{1,13}^{6,14,(2)} \\
y_{1,13}^{(5)} &= \sqrt{P_{13}} h_{1,13}^{13,(5)} s_{5,13} + \sqrt{P_{14}} h_{1,13}^{14,(5)} s_{7,14} + n_{1,13}^{(5)} \\
y_{1,13}^{(6)} &= \sqrt{P_{14}} h_{1,13}^{14,(6)} s_{6,14} + n_{1,13}^{(6)} \\
y_{1,13}^{(7)} &= \sqrt{P_{13}} h_{1,13}^{13,(7)} s_{2,13} + n_{1,13}^{(7)} \\
y_{1,13}^{(10)} &= \sqrt{P_{13}} h_{1,13}^{13,(10)} s_{6,13} + \sqrt{P_{14}} h_{1,13}^{14,(10)} s_{8,14} + n_{1,13}^{(10)}
\end{aligned}
\tag{3.16}
$$

where superscripts (6), (7), (8), (9), and (10) refer to a following transmission round, i.e. the time-slot numbering is now reset only after M transmission rounds.

Note that TS3, TS8, and TS9 are used for transmission by $\mathrm{U}_{1,13}$ so they do not appear in (3.16). Furthermore, each symbol is received free of inter-cell interference once every 10 time-slots and it is relayed simultaneously by all the D2D users in the same cell edge once every 10 time-slots. A similar transmission/reception pattern can be identified for all other users.

Equation (3.16) can be expressed in matrix form as equation (3.18) with

$$
\lambda_{1,13}^{(4)} = \sqrt{p_{2,13}} g_{1,13}^{2,13,(4)} + \sqrt{p_{5,14}} g_{1,13}^{5,14,(4)} + \sqrt{p_{6,14}} g_{1,13}^{6,14,(4)}, \tag{3.17}
$$

which is equivalent to $\mathbf{y}_{1,13} = \mathbf{a}_{1,13} s_{1,13} + \sum_{\substack{\kappa \in \mathcal{S}_{1,13} \\ \kappa \notin 1,13}} \mathbf{a}_{\kappa} \mathbf{s}_{1,13}(\kappa) + \mathbf{n}_{1,13} = \mathbf{a}_{1,13} s_{1,13} + \mathbf{w}_{1,13}$.

$$
\underbrace{\begin{bmatrix} y_{1,13}^{(1)} \\ y_{1,13}^{(2)} \\ y_{1,13}^{(4)} \\ y_{1,13}^{(5)} \\ y_{1,13}^{(6)} \\ y_{1,13}^{(7)} \\ y_{1,13}^{(10)} \end{bmatrix}}_{\mathbf{y}_{1,13}}
=
\underbrace{\begin{bmatrix} n_{1,13}^{(1)} \\ n_{1,13}^{(2)} \\ n_{1,13}^{(4)} + \frac{\sqrt{P_{2,13}}^{2,13,(4)} n_{2,13}^{(2)}}{\sqrt{P_{13}} h_{2,13}^{13,(2)}} + \frac{\sqrt{P_{5,14}}^{5,14,(4)} n_{5,14}^{(2)}}{\sqrt{P_{13}} h_{5,14}^{13,(2)}} + \frac{\sqrt{P_{6,14}}^{6,14,(4)} n_{6,14}^{(2)}}{\sqrt{P_{13}} h_{6,14}^{13,(2)}} \\ n_{1,13}^{(5)} \\ n_{1,13}^{(6)} \\ n_{1,13}^{(7)} \\ n_{1,13}^{(10)} \end{bmatrix}}_{\mathbf{n}_{1,13}}
+
\underbrace{\begin{bmatrix} \sqrt{P_{14}} h_{1,13}^{14,(1)} & 0 & 0 & 0 & 0 & 0 & 0 & 0 & 0 & 0 \\ 0 & \sqrt{P_{13}} h_{1,13}^{13,(2)} & 0 & 0 & 0 & 0 & 0 & 0 & 0 & 0 \\ 0 & \lambda_{1,13}^{(4)} & \sqrt{P_{13}} h_{1,13}^{13,(4)} & \sqrt{P_{14}} h_{1,13}^{14,(4)} & 0 & 0 & 0 & 0 & 0 & 0 \\ 0 & 0 & 0 & 0 & \sqrt{P_{13}} h_{1,13}^{13,(5)} & \sqrt{P_{14}} h_{1,13}^{14,(5)} & 0 & 0 & 0 & 0 \\ 0 & 0 & 0 & 0 & 0 & 0 & \sqrt{P_{14}} h_{1,13}^{14,(6)} & 0 & 0 & 0 \\ 0 & 0 & 0 & 0 & 0 & 0 & 0 & \sqrt{P_{13}} h_{1,13}^{13,(7)} & 0 & 0 \\ 0 & 0 & 0 & 0 & 0 & 0 & 0 & 0 & \sqrt{P_{13}} h_{1,13}^{13,(10)} & \sqrt{P_{14}} h_{1,13}^{14,(10)} \\ \underbrace{0}_{\mathbf{a}_{5,14}} & \underbrace{0}_{\mathbf{a}_{1,13}} & \underbrace{0}_{\mathbf{a}_{7,13}} & \underbrace{0}_{\mathbf{a}_{3,14}} & \underbrace{0}_{\mathbf{a}_{5,13}} & \underbrace{0}_{\mathbf{a}_{7,14}} & \underbrace{0}_{\mathbf{a}_{6,14}} & \underbrace{0}_{\mathbf{a}_{2,13}} & \underbrace{\sqrt{P_{13}} h_{1,13}^{13,(10)} \sqrt{P_{14}} h_{1,13}^{14,(10)}}_{\mathbf{a}_{6,13}} & \underbrace{\mathbf{a}_{8,14}} \end{bmatrix}}_{\mathbf{A}_{1,13}}
\underbrace{\begin{bmatrix} s_{5,14} \\ s_{1,13} \\ s_{7,13} \\ s_{3,14} \\ s_{5,13} \\ s_{7,14} \\ s_{6,14} \\ s_{2,13} \\ s_{6,13} \\ s_{8,14} \end{bmatrix}}_{\mathbf{s}_{1,13}}
\tag{3.18}
$$

3.6 Performance Analysis

Using the well-known expression for the entropy of a multivariate complex Gaussian distribution [25] the capacity achieved by $\mathrm{U}_{m,l}$ is computed as

$$\begin{aligned}\log_2 \frac{|\mathbf{R}_{y_{m,l}}|}{|\mathbf{R}_{w_{m,l}}|} &= \log_2 \left(1 + \mathbf{a}_{m,l}^H \mathbf{R}_{w_{m,l}}^{-1} \mathbf{a}_{m,l} \sigma_{\mathrm{s}}^2\right) \\ &= \log_2 \left(1 + \mathrm{SNR}_{m,l}\right),\end{aligned} \tag{3.19}$$

where $\mathrm{SNR}_{m,l}$ is the signal-to-noise ratio of $\mathrm{U}_{m,l}$, $|x|$ is the determinant of x, $\mathbf{a}_{m,l}$ is the column vector of matrix $\mathbf{A}_{m,l}$ corresponding to symbol $s_{m,l}$. The covariance matrix of the received signal $\mathbf{R}_{y_{m,l}}$ is given as

$$\mathbf{R}_{y_{m,l}} = \mathbf{a}_{m,l} \mathbf{a}_{m,l}^H \sigma_{\mathrm{s}}^2 + \mathbf{R}_{w_{m,l}} \tag{3.20}$$

and the covariance matrix of the interference-plus-noise $\mathbf{R}_{w_{m,l}}$ is given as

$$\begin{aligned}\mathbf{R}_{w_{m,l}} &= \mathbb{E}\left\{ \left(\sum_{\substack{\kappa \in \mathcal{S}_{m,l} \\ \kappa \notin m,l}} \mathbf{a}_\kappa \mathbf{s}_{m,l}(\kappa) + \mathbf{n}_{m,l} \right) \left(\sum_{\substack{\kappa \in \mathcal{S}_{m,l} \\ \kappa \notin m,l}} \mathbf{a}_\kappa \mathbf{s}_{m,l}(\kappa) + \mathbf{n}_{m,l} \right)^H \right\} \\ &= \sum_{\substack{\kappa \in \mathcal{S}_{m,l} \\ \kappa \notin m,l}} \mathbf{a}_\kappa \mathbf{a}_\kappa^H \sigma_{\mathrm{s}}^2 + \mathbf{N}_{m,l},\end{aligned} \tag{3.21}$$

where $\mathbf{N}_{m,l} = \mathbb{E}\left\{ \mathbf{n}_{m,l} \mathbf{n}_{m,l}^H \right\}$.

3.6.1 Square Array (M=1)

From the structure of matrix $\mathbf{A}_{1,13}$ in equation (6.15), it can be seen that TS1 and TS5 do not bring any performance improvement for $\mathrm{U}_{1,13}$ since the received interference is uncorrelated with the interference in other time-slots. The received signals in TS1 and TS5 are only included for the sake of completeness.

For this reason, $|\mathbf{R}_{y_{1,13}}|/|\mathbf{R}_{w_{1,13}}|$ can be defined as

$$\frac{|\mathbf{R}_{y_{1,13}}|}{|\mathbf{R}_{w_{1,13}}|} = \frac{\begin{vmatrix} |\mathbf{a}_{1,13}(2)|^2\sigma_s^2 + N^{(2)} & \mathbf{a}_{1,13}(2)\mathbf{a}_{1,13}(4)\sigma_s^2 \\ \mathbf{a}_{1,13}(2)\mathbf{a}_{1,13}(4)\sigma_s^2 & (|\mathbf{a}_{1,13}(4)|^2 + |\mathbf{a}_{4,13}(4)|^2 + \\ & |\mathbf{a}_{2,14}(4)|^2)\sigma_s^2 + N^{(4)} \end{vmatrix}}{\begin{vmatrix} N^{(2)} & 0 \\ 0 & (|\mathbf{a}_{4,13}(4)|^2 + |\mathbf{a}_{2,14}(4)|^2)\sigma_s^2 + N^{(4)} \end{vmatrix}} \tag{3.22}$$

where $\mathbf{a}_{m,l}(t)$ is the element of vector $\mathbf{a}_{m,l}$ corresponding to time-slot t and $N^{(t)}$ is the element corresponding to time-slot t in the main diagonal of matrix $\mathbf{N}_{m,l} = \text{diag}\left[\sigma_{\text{n}}^2, \sigma_{\text{n}}^2, \left(\rho_{1,13,(2)}^{3,14,(4)}\right)^2, \sigma_{\text{n}}^2\right]$, where

$$\left(\rho_{m,l,(t)}^{n,k,(\tau)}\right)^2 = \sigma_{\text{n}}^2 + \frac{p_{n,k}\mathbb{E}\left\{|g_{m,l}^{n,k,(\tau)}|^2\right\}\sigma_{\text{n}}^2}{P_l\mathbb{E}\left\{|h_{n,k}^{l,(t)}|^2\right\}} \tag{3.23}$$

is the forwarded noise power in time-slot τ of the following round that was received in time-slot t.

Expanding equation (3.22) and generalizing for $\text{U}_{m,l}$ results in the SNR of $\text{U}_{m,l}$ as

$$\text{SNR}_{m,l} = \frac{\gamma_{m,l}^{l,(t)}}{N^{(t)}} + D \tag{3.24}$$

with

$$D = \frac{\xi_{m,l}^{n,k,(\tau)}}{\gamma_{m,l}^{l,(\tau)} + \gamma_{m,l}^{k,(\tau)} + N^{(\tau)}}. \tag{3.25}$$

Note that t is the time-slot where $s_{m,l}$ is received by $\text{U}_{m,l}$ from BS_l and τ is the time-slot of the next transmission round in which $s_{m,l}$ is received through D2D communication. For $\text{U}_{1,13}$, $t = 2$ and $\tau = 4$. Note also that BS_l is the serving BS of $\text{U}_{m,l}$, BS_k is the neighboring BS (the interfering BS closest to $\text{U}_{m,l}$), and $\text{U}_{n,k}$ is the D2D user connected to BS_k.

The first term of equation (6.25) corresponds to the SNR from the transmission of the serving BS. The second term corresponds to the contribution from the D2D communication. Specifically, the numerator represents the signal power from the D2D communication and the denominator includes the (interference) signal power from BS_l and BS_k during the D2D communication plus the noise power.

3.6.2 Hexagonal Array (M=1)

From the structure of matrix $\mathbf{A}_{1,1}$ in equation (3.10), it can be seen that TS1 and TS7 do not bring any performance improvement for $\mathrm{U}_{1,1}$ since the received interference is uncorrelated with the interference in other time-slots. The received signals in TS1 and TS7 are only included for the sake of completeness. For this reason, $|\mathbf{R}_{y_{1,1}}|/|\mathbf{R}_{w_{1,1}}|$ can be defined as

$$\frac{|\mathbf{R}_{y_{1,1}}|}{|\mathbf{R}_{w_{1,1}}|} = \frac{\begin{vmatrix} (|\mathbf{a}_{3,1}(4)|^2 + |\mathbf{a}_{1,2}(4)|^2 + |\mathbf{a}_{1,1}(4)|^2)\sigma_s^2 + N^{(4)} & \mathbf{a}_{1,1}(4)\mathbf{a}_{1,1}(5)\sigma_s^2 & \mathbf{a}_{1,1}(4)\mathbf{a}_{1,1}(6)\sigma_s^2 \\ \mathbf{a}_{1,1}(4)\mathbf{a}_{1,1}(5)\sigma_s^2 & (|\mathbf{a}_{1,1}(5)|^2 + |\mathbf{a}_{6,1}(5)|^2 + |\mathbf{a}_{5,2}(5)|^2)\sigma_s^2 + N^{(5)} & \mathbf{a}_{1,1}(5)\mathbf{a}_{1,1}(6)\sigma_s^2 \\ \mathbf{a}_{1,1}(4)\mathbf{a}_{1,1}(6)\sigma_s^2 & \mathbf{a}_{1,1}(5)\mathbf{a}_{1,1}(6)\sigma_s^2 & |\mathbf{a}_{1,1}(6)|^2\sigma_s^2 + N^{(6)} \end{vmatrix}}{\begin{vmatrix} (|\mathbf{a}_{3,1}(4)|^2 + |\mathbf{a}_{1,2}(4)|^2)\sigma_s^2 + N^{(4)} & 0 & 0 \\ 0 & (|\mathbf{a}_{6,1}(5)|^2 + |\mathbf{a}_{5,2}(5)|^2)\sigma_s^2 + N^{(5)} & 0 \\ 0 & 0 & N^{(6)} \end{vmatrix}} \tag{3.26}$$

where $\mathbf{N}_{m,l} = \mathrm{diag}\left[\sigma_{\mathrm{n}}^2, \left(\rho_{1,1,(6)}^{4,2,(4)}\right)^2, \left(\rho_{1,1,(6)}^{4,2,(5)}\right)^2, \sigma_{\mathrm{n}}^2, \sigma_{\mathrm{n}}^2\right]$.

Expanding equation (3.26) and generalizing for $\mathrm{U}_{m,l}$ results in the SNR of $\mathrm{U}_{m,l}$ as

$$\mathrm{SNR}_{m,l} = \frac{\gamma_{m,l}^{l,(t)}}{N^{(t)}} + D \tag{3.27}$$

with

$$D = \frac{\xi_{m,l}^{n,k,(\tau_1)}}{\gamma_{m,l}^{l,(\tau_1)} + \gamma_{m,l}^{k,(\tau_1)} + N^{(\tau_1)}} + \frac{\xi_{m,l}^{n,k,(\tau_2)}}{\gamma_{m,l}^{(\tau_2)} + \gamma_{m,l}^{(\tau_2)} + N^{(\tau_2)}}. \tag{3.28}$$

Note that t is the time-slot where $s_{m,l}$ is received by $\mathrm{U}_{m,l}$ from BS_l and τ_1 and τ_2 are the time-slots of the next transmission round in which $s_{m,l}$ is received through D2D communication. For $\mathrm{U}_{1,1}$, $t = 6$, $\tau_1 = 4$ and $\tau_2 = 5$.

The first term of equation (3.27) corresponds to the SNR from the transmission of the serving BS. The second and third terms correspond to the contribution from the D2D communication of each of the two D2D transmissions. Specifically, the numerators represent the signal power from the D2D communication and the denominators include the (interference) signal power from BS_l and BS_k during the D2D communication plus the noise power.

3.6.3 Multiple Cell Edge Users

From the structure of matrix $\mathbf{A}_{1,13}$ in equation (3.18), it can be seen that only TS2 and TS4 bring any performance improvement for $\mathrm{U}_{1,13}$. All the received signals are only included for the sake of completeness. For this reason, $|\mathbf{R}_{y_{1,13}}|/|\mathbf{R}_{w_{1,13}}|$ can be defined as

$$\frac{|\mathbf{R}_{y_{1,13}}|}{|\mathbf{R}_{w_{1,13}}|} = \frac{\begin{vmatrix} |\mathbf{a}_{1,13}(2)|^2\sigma_s^2 + N^{(2)} & \mathbf{a}_{1,13}(2)\mathbf{a}_{1,13}(4)\sigma_s^2 \\ \mathbf{a}_{1,13}(2)\mathbf{a}_{1,13}(4)\sigma_s^2 & (|\mathbf{a}_{1,13}(4)|^2 + |\mathbf{a}_{7,13}(4)|^2 + |\mathbf{a}_{3,14}(4)|^2)\sigma_s^2 + N^{(4)} \end{vmatrix}}{\begin{vmatrix} N^{(2)} & 0 \\ 0 & (|\mathbf{a}_{7,13}(4)|^2 + |\mathbf{a}_{3,14}(4)|^2)\sigma_s^2 + N^{(4)} \end{vmatrix}} \tag{3.29}$$

where $\mathbf{N}_{m,l} = \mathrm{diag}\left[\sigma_{\mathrm{n}}^2, \sigma_{\mathrm{n}}^2, \left(\rho_{1,13,(2)}^{(4)}\right)^2, \sigma_{\mathrm{n}}^2, \cdots, \sigma_{\mathrm{n}}^2\right]$, and where

$$\begin{aligned} \left(\rho_{1,13,(2)}^{(4)}\right)^2 = \sigma_{\mathrm{n}}^2 + \frac{p_{2,13}\mathbb{E}\left\{|g_{1,13}^{2,13,(4)}|^2\right\}\sigma_{\mathrm{n}}^2}{P_{13}\mathbb{E}\left\{|h_{2,13}^{13,(2)}|^2\right\}} + \\ \frac{p_{5,14}\mathbb{E}\left\{|g_{1,13}^{5,14,(4)}|^2\right\}\sigma_{\mathrm{n}}^2}{P_{13}\mathbb{E}\left\{|h_{5,14}^{13,(2)}|^2\right\}} + \frac{p_{6,14}\mathbb{E}\left\{|g_{1,13}^{6,14,(4)}|^2\right\}\sigma_{\mathrm{n}}^2}{P_{13}\mathbb{E}\left\{|h_{6,14}^{13,(2)}|^2\right\}}. \end{aligned} \tag{3.30}$$

Generalizing for multiple cell edge users

$$\left(\rho_{m,l,(t)}^{(\tau)}\right)^2 = \sigma_{\mathrm{n}}^2 + \sigma_{\mathrm{n}}^2 \sum_{\substack{\kappa \in \mathcal{R}_{m,l} \\ \kappa \notin m,l}} \frac{p_\kappa \mathbb{E}\left\{|g_{m,l}^{\kappa,(\tau)}|^2\right\}}{P_l \mathbb{E}\left\{|h_\kappa^{l,(t)}|^2\right\}}, \tag{3.31}$$

where $\mathcal{R}_{m,l}$ is the set of D2D users communicating with $\mathrm{U}_{m,l}$.

Expanding equation (3.29) and generalizing for $\mathrm{U}_{m,l}$ for the square array results in the SNR of $\mathrm{U}_{m,l}$ as

$$\mathrm{SNR}_{m,l} = \frac{\gamma_{m,l}^{l,(t)}}{N^{(t)}} + D \tag{3.32}$$

with

$$D = \frac{|\lambda_{m,l}^{(\tau)}|^2}{\gamma_{m,l}^{l,(\tau)} + \gamma_{m,l}^{k,(\tau)} + N^{(\tau)}}, \tag{3.33}$$

where

$$\lambda_{m,l}^{(\tau)} = \sum_{\substack{\kappa \in \mathcal{R}_{m,l} \\ \kappa \notin m,l}} \sqrt{p_\kappa} g_{m,l}^{\kappa,(\tau)}. \tag{3.34}$$

Notice the contribution to the SNR of each D2D communication.

And in the case of the hexagonal array, the SNR of $\mathrm{U}_{m,l}$ is

$$\mathrm{SNR}_{m,l} = \frac{\gamma_{m,l}^{l,(t)}}{N^{(t)}} + D \tag{3.35}$$

with

$$D = \frac{|\lambda_{m,l}^{(\tau_1)}|^2}{\gamma_{m,l}^{l,(\tau_1)} + \gamma_{m,l}^{k,(\tau_1)} + N^{(\tau_1)}} + \frac{|\lambda_{m,l}^{(\tau_2)}|^2}{\gamma_{m,l}^{(\tau_2)} + \gamma_{m,l}^{k,(\tau_2)} + N^{(\tau_2)}}. \tag{3.36}$$

3.6.4 Spectral Efficiency and BER

In the square and hexagonal array, M transmission rounds are needed to serve all the users, with a total of $M(N+1)$ times-lots. Therefore, the spectral efficiency per time-slot in these cases is given as

$$S_{m,l}^{\mathrm{D2D}} = \frac{1}{M(N+1)} \mathbb{E}\left\{\log_2\left(1 + \mathrm{SNR}_{m,l}\right)\right\}, \tag{3.37}$$

Note that equation (3.37) corresponds to the spectral efficiency achieved by each user.

In both cases assuming a MMSE receiver with BPSK transmissions and Rayleigh fading statistics, the BER of $\mathrm{U}_{m,l}$ is given in terms of the Q-function as [78]

$$\mathrm{BER}_{m,l}^{\mathrm{D2D}} = \mathbb{E}\left\{Q(\sqrt{2\mathrm{SNR}_{m,l}})\right\}. \tag{3.38}$$

3.7 Performance Evaluation

In this section we compare the approaches presented and analyzed in previous sections in terms of spectral efficiency per time-slot and BER. Our evaluations consider a Rayleigh fading channel model with $\mathbb{E}\{|h_{m,l}^{l,(t)}|^2\} = \mathbb{E}\{|g_{m,l}^{n,k,(t)}|^2\} = 1$ $\forall m, l, n, k, t$ and $\sigma_s^2 = \sigma_{\mathrm{n}}^2 = 1$.

3.7.1 Varying the D2D users transmit power with fixed BS transmit power

In this section we assume a transmit power of 5dB from all the BSs, i.e. $P_l = 5\text{dB}$ $\forall l$ and $p_{m,l}$ increases equally for all the D2D users. Figs. 3.7 and 3.8 show the spectral efficiency per time-slot of the presented approaches for the square and hexagonal array, respectively. The performance of the proposed D2D approach is compared to the performance of TDMA and to the approach presented in [47], referred to as AFR, which does not use D2D communication.

We can observe that the performance gain achieved by adding D2D increases with $p_{m,l}$. In both cellular topologies, the D2D approach exceeds the performance of AFR and TDMA for any value of M.

It is worth to note that the difference between the proposed D2D approach and the other approaches increases with the number of cell edge users. For instance, using D2D at 20dB in the square cellular array, the spectral efficiency is 1.4 times higher than AFR and 2.4 times higher than TDMA with $M = 1$, while with $M = 10$, the spectral efficiency of D2D is 3.7 times higher than AFR and 5.5 times higher than TDMA. In the hexagonal array at 20dB, the spectral efficiency is 1.7 times higher than AFR and 2.1 times higher than TDMA with $M = 1$, while with $M = 10$, the spectral efficiency of D2D is 3.8 times higher than AFR and 4.8 times higher than TDMA. This highlights the potential of exploiting D2D communication in a multiuser scenario.

In Figs. 3.9 and 3.10 we can see the BER performance of the presented approaches for the square and hexagonal array, respectively. TDMA and AFR provide no diversity gain and no BER improvement by increasing $p_{m,l}$. As expected using D2D communication results in achieving a higher spatial diversity, which increases with the number of D2D users. Due to the effect of the cumulative forwarded noise, the BER of D2D tends to floor at high values of $p_{m,l}$. Comparing the different cellular topologies, the hexagonal array presents the lowest BER for larger values of M because it exploits the D2D communication between users twice in every transmission round.

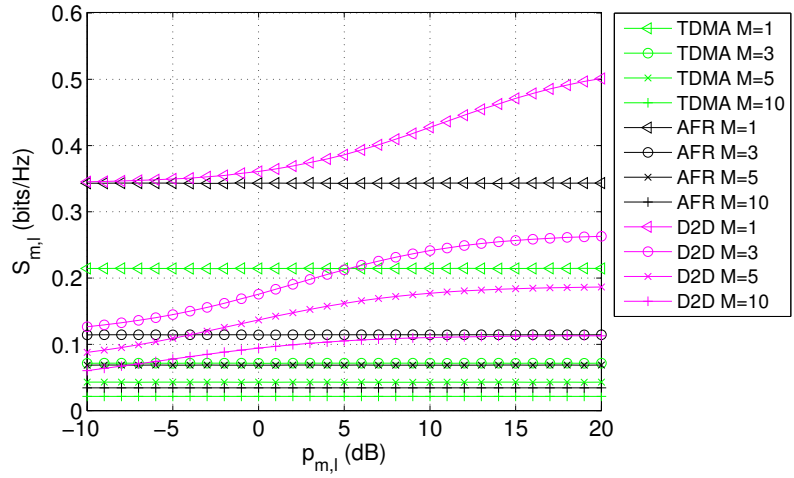

Figure 3.7: Spectral efficiency per time-slot of the studied approaches with $P_l = 5\text{dB}\ \forall l$ for the square array.

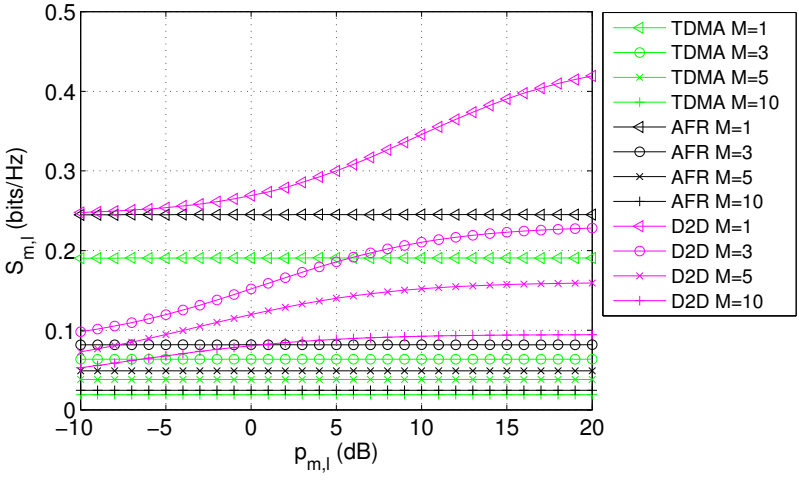

Figure 3.8: Spectral efficiency per time-slot of the studied approaches with $P_l = 5\text{dB}\ \forall l$ for the hexagonal array.

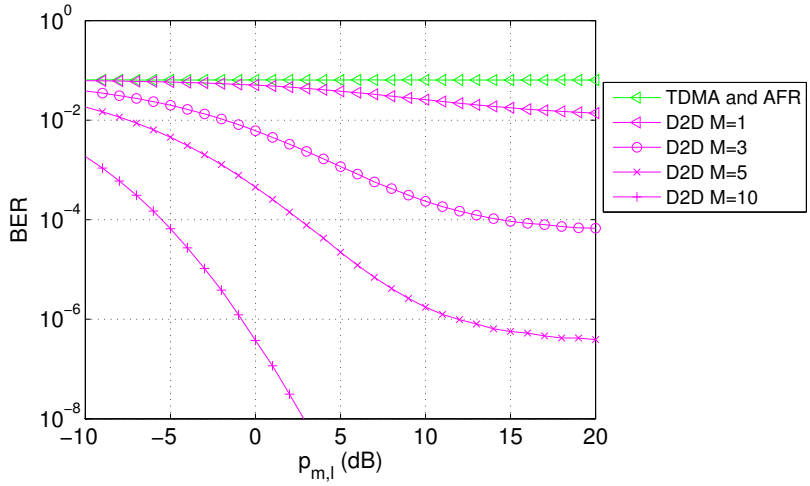

Figure 3.9: BER of the proposed approach with $P_l = 5\text{dB}\ \forall l$ for the square array.

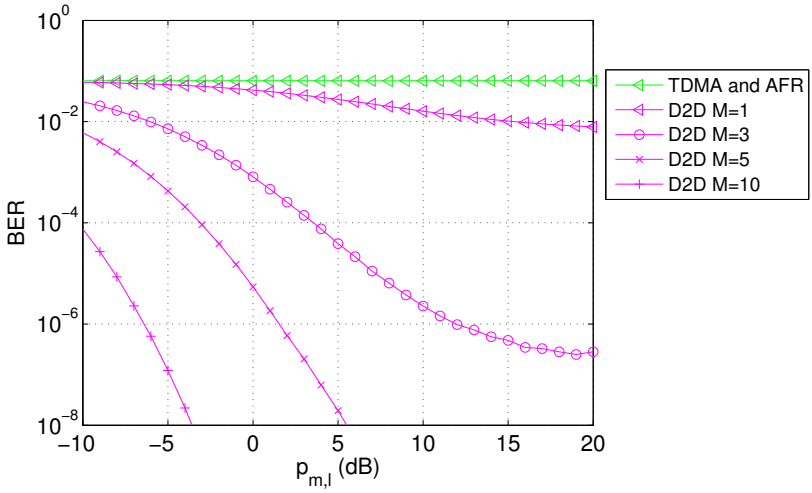

Figure 3.10: BER of the proposed approach with $P_l = 5\text{dB}\ \forall l$ for the hexagonal array.

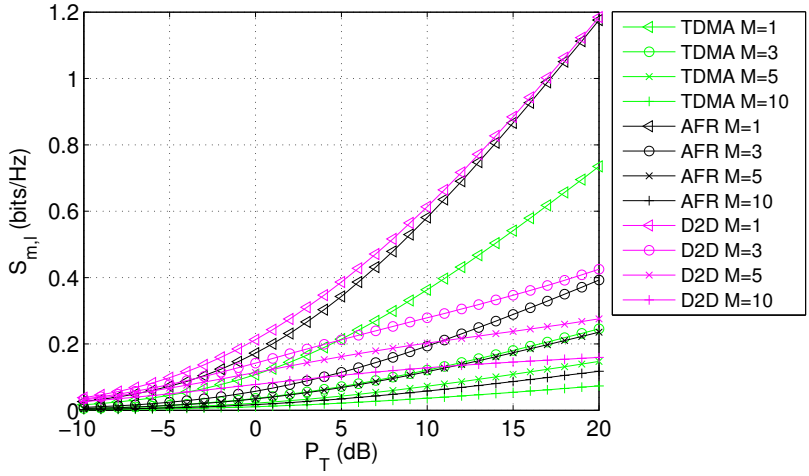

Figure 3.11: Spectral efficiency per time-slot of the studied approaches with equal transmit power for the square array.

3.7.2 Varying equally the D2D users transmit power and the BS transmit power

In this section we assume that the transmit power of all the D2D users and all the BSs in the network increases equally, i.e. $P_T = P_l = p_{m,l}\ \forall m, l$. Figs. 3.11 and 3.12 show the spectral efficiency per time-slot of the studied approaches for the square and hexagonal array, respectively.

Similarly to the results shown in section 3.7.1, the D2D approach always exceed the performance of AFR and TDMA.

The BER is shown in Figs. 3.13 and 3.14 for the square and hexagonal array, respectively. Again, TDMA and AFR provide no diversity gain, while the D2D approach is able to increase drastically the spatial diversity.

Comparing the different cellular topologies, it is clear that the hexagonal array achieves a lower BER for large values of M because it is able to exploit D2D communication twice in every transmission round.

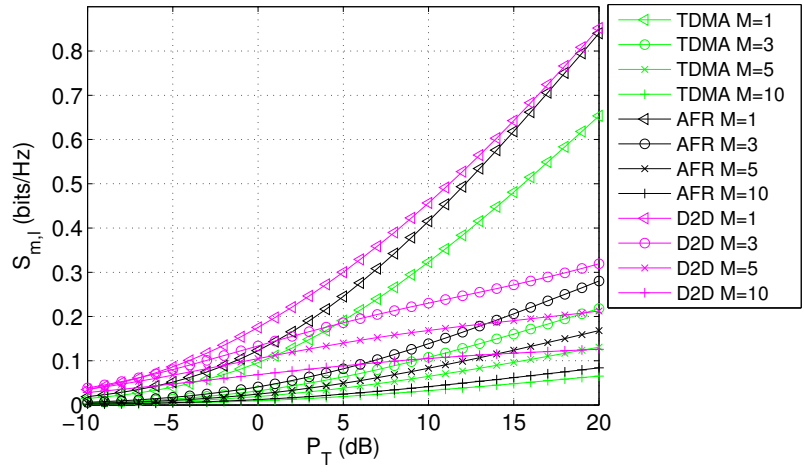

Figure 3.12: Spectral efficiency per time-slot of the studied approaches with equal transmit power for the hexagonal array.

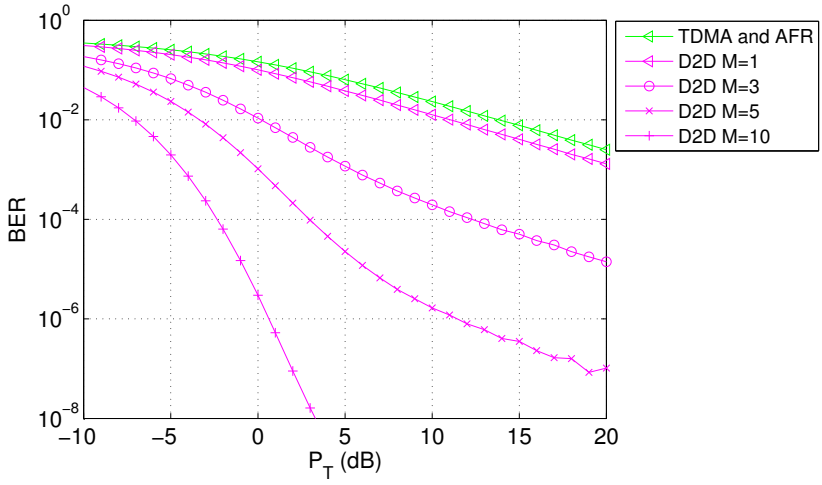

Figure 3.13: BER of the proposed approach with $P_T = P_l = p_{m,l}\ \forall m, l$ for the square array.

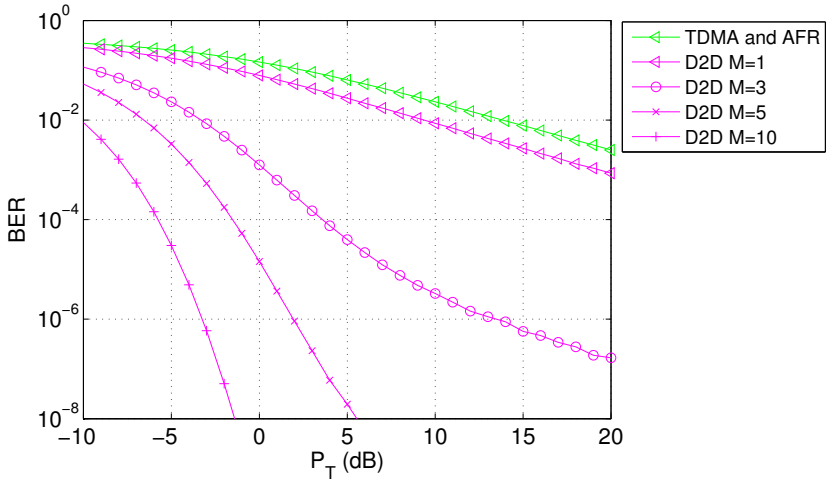

Figure 3.14: BER of the proposed approach with $P_T = P_l = p_{m,l}\ \forall m, l$ for the hexagonal array.

3.8 Conclusions

In this chapter we have proposed an approach based on AFR that exploits the connectivity of cell edge users in a wireless network. It allows D2D communication among cell edge users during the time-slots in which they are not receiving their desired symbol from their serving BS. The proposed approach is developed for two cellular topologies: square and hexagonal array, and extended to multiple cell edge users. Our results show that the proposed approach increases the spatial diversity and the spectral efficiency per time-slot without decreasing the achievable DoF. The gain compared to other approaches is independent of the cellular topology and it grows with the number of cell edge users per cell edge.

Chapter 4

Exploiting the Overhearing Capabilities of Base Stations in Dense Networks

Abstract

Increasing the density of base stations deployment is regarded as a means to satisfy the growing demand of wireless connectivity over a shared bandwidth, however increasing the disparity in the service received by each user. Fairness can be realized by dynamically allocating resources to users using detailed channel state information at the transmitter (CSIT), which constitutes an expensive overhead, especially for dense networks. One solution to improve the fairness without CSIT is to introduce spatial diversity through the use of relays in combination with physical-layer network coding (PNC). Most relaying-PNC solutions focus on the particular case of the two-way relay channel or they require additional relays and a large transmission time. In this chapter we propose a multiple-relay communication protocol (MRCP) for achieving fairness in dense networks. It exploits spatial diversity without requiring additional relays since it uses the base stations as relays. Furthermore, MRCP is applicable to an arbitrary number of base stations and users, while keeping a small transmission time. We show that our approach achieves the highest max-min fairness among users and almost full diversity with asymmetric transmissions.[1]

[1]This chapter is cited from Torrea-Duran, R., Rosas, F., Pollin, S., Vandendorpe, L., Moonen, M., "Multiple-Relay Communication Protocol for Achieving Fairness in Cellular Systems". Submitted to IEEE Access, 2017.

4.1 Introduction

It is expected that by 2021 there will be globally 11.6 billion mobile devices with an average mobile connection speed three times larger than that of 2016 [22]. This growth contrasts with the limited bandwidth that needs to be shared among an increasing number of users.

Network densification [14, 51] has been proposed as a promising technique to satisfy the previous demands over a shared bandwidth. This is realized by increasing the density of base stations deployed, resulting in dense clusters of base stations severely affected by inter-cell interference.

The most widely used approach to tackle inter-cell interference consists in orthogonalizing resources for users with high interference (typically in the cell edge), which means to assign disjoint resources (time or frequency) to users connected to different base stations, while reusing resources for users with low interference (typically in the cell center). However, when orthogonalizing resources, the amount of resources that each user receives decreases with the number of users. Furthermore, since additional base stations (such as femtocells) are usually deployed in an unplanned way and with restricted access, the inter-cell interference becomes extremely high for some users and extremely low for others. Therefore, providing a fair resource allocation for all the users while efficiently managing a shared bandwidth is of key importance in dense networks [77].

Traditionally, fairness in cellular networks is realized by dynamically allocating time, frequency [54, 55], or power [39, 50] to users according to strategies such as max-min or proportional fairness [34, 46, 61]. However, such a dynamic allocation can only be achieved with detailed channel state information at the transmitter (CSIT) from the whole network. Furthermore, given the large number of base stations and users in dense networks and the large variability of the wireless channel, obtaining reliable CSIT for a fair resource assignment remains an expensive overhead [67]. Moreover, sharing all this information through a backhaul link might be costly or even prohibitive for base stations in dense networks [36, 51].

One solution to improve fairness over a shared bandwidth without CSIT is to introduce spatial diversity through multiple-input multiple-output (MIMO) systems. which can average out the channel variability over different signal paths. However, physical constraints such as the number of radio frequency chains necessary at each device to support MIMO and the required separation between antennas of at least half of a wavelength, make this technology unsuitable for the widespread small-size and energy-limited devices found in dense networks.

In order to maintain the benefits of MIMO systems without the previous limitations, cooperative communication can be exploited with the aid of relays. Relays can achieve spatial diversity by forwarding received signals in dedicated time-slots without the need for a backhaul connection [57, 75]. However, relays require certain coordination with the base stations in order to use the bandwidth efficiently. For this purpose, relays have been used in combination with physical-layer network coding (PNC), first proposed in [98]. PNC exploits the linear superposition of wireless signals by combining transmissions overheard from different sources, hence providing a balance between orthogonalization and reuse of resources.

Much of the available literature on relaying-PNC focuses on the particular case of the two-way relay channel (TWRC) [64, 72]. In fact, most contributions deal with ways to combine the signals to achieve higher rates in a TWRC. For example, in [45] base stations and users transmit the symbols multiplied by the inverse of the channel so that the relay can receive the coherently added symbols. In [44] this scheme is extended to support multiple users simultaneously. In [13], a modulo operation is performed at the relay instead of transmitting a simple superposition of signals, and in [18, 68, 80], relays use a lattice-based approach to combine signals with a compress-and-forward strategy in [80] and with a compute-and-forward strategy in [18, 68].

However, the spatial diversity achieved by these systems is limited since the users can only receive signals from the relay and not from the base station. Hence, a more general relaying-PNC configuration has been proposed in [52], where two users can achieve spatial diversity by receiving signals from a base station and a relay node. Yet, all of the previous approaches require additional infrastructure (i.e. relay nodes), with the operational and economical costs that their deployment implies. Furthermore, they all consider only a limited number of nodes, leaving the extension to an arbitrary number of base stations and users an open issue.

A different way of exploiting spatial diversity in a larger network using PNC principles is through space-time network coding (STNC) [56]. With STNC, each of the L base stations of a cluster broadcasts its own signal in dedicated time-slots during the transmission phase, and during the relaying phase M relays broadcast a combination of the received symbols in dedicated time-slots, hence achieving diversity order of $M+1$. This allows to achieve spatial diversity from different transmissions. A step to increase the diversity of the previous system was taken in [91] and in [99], where the authors propose that each relay decodes the transmission not only from the base stations but from the previous relays. However, a main disadvantage of these type of schemes is that, apart from requiring additional relays, the price to achieve such diversity is the use of $L + M$ time-slots. This makes the previous approaches unsuitable for dense

networks.

To tackle these problems, in this chapter we present a multiple-relay communication protocol (MRCP) for achieving fairness in dense networks. Different from the approaches in [56, 91, 99], our approach exploits spatial diversity from a cluster of L base stations with only $L + 1$ time-slots, while it avoids the need for a backhaul connection and additional relays by using currently-deployed base stations as relays. With MRCP, all the base stations transmit in dedicated time-slots during the first L time-slots, and in the $L + 1$-th time-slot they all transmit a combination of the overheard symbols. The last time-slot comes with an imperfect synchronization due to the multiple simultaneous transmissions. However, recent advances in delay-tolerant codes [26] or joint frequency and timing synchronization [97] show that this issue can be mitigated.

We then analyze the capabilities of the proposed system in terms not only of spectral efficiency and diversity, but also in terms of fairness, a critical metric for dense networks which has been mostly overlooked in relaying-PNC schemes. When compared to other communication schemes, we show that MRCP achieves the highest max-min fairness among users and a bit error rate (BER) that achieves almost full diversity.

The main contributions of this chapter can be summarized as follows:

1. A new communication protocol for dense networks that achieves fairness by exploiting spatial diversity with a reduced number of time-slots compared to state-of-the-art. This is achieved without the need of backhaul connection nor additional relays.

2. The computation of closed-form expressions of the spectral efficiency and BER for any number of base stations and users using the proposed approach. This allows to analyze and predict the achievable gains for any network size and to compare it to other approaches.

3. The analysis of the studied approaches in terms of fairness. To our best knowledge, all the relaying-PNC schemes have overlooked the potential of achieving fairness from the combination of transmissions from different sources. Here we analyze the fairness based on a number of metrics for an integrated view of the system performance.

The rest of this chapter is organized as follows. First, Section 4.2 describes the system model with the baseline and proposed approaches. Then, Section 4.3 describes the extension to a larger system size. Next, Section 4.4 shows the performance evaluation of the proposed approach and its benchmarking

against other communication schemes. Finally, Section 4.5 presents the main conclusions.

Notation: Matrices and vectors are denoted by upper and lower case boldface letters, respectively; $\mathbf{A}^T$ means transpose of $\mathbf{A}$; $\mathbf{A}^H$ means Hermitian of $\mathbf{A}$; $|\mathbf{A}|$ means determinant of $\mathbf{A}$; $\mathbb{E}\{\}$ is the expected value operator.

4.2 System Model

Consider a dense cluster composed by L base stations, each of which has data to be delivered to a specific user over a shared bandwidth.[2] We denote as s_l the symbol from the l-th base station (BSl) intended to the l-th user (Ul). It is assumed that symbols for different users are uncorrelated. The short distance between base stations allows all base stations and users to overhear all the transmitted symbols. Our goal is to find an efficient way to perform these transmissions.

It is assumed that all the base stations and users are half-duplex (i.e. they cannot transmit and receive simultaneously) and, if available, the backhaul link is only used for control information, not for data sharing. This last condition excludes the use of communication schemes that require coordinated base stations, e.g. space-time block codes like Alamouti codes.

For the following sections, let us define P_m as the transmit power of BSm and introduce the variable $\eta_m = \frac{\sigma_{\mathrm{s}}^2}{\sigma_{\mathrm{n}}^2} P_m$, where $\sigma_{\mathrm{s}}^2 = \mathbb{E}\{|s_1|^2\} = \mathbb{E}\{|s_2|^2\} = \cdots = \mathbb{E}\{|s_L|^2\}$ and σ_{n}^2 is the received noise power, which is assumed to be equal for all the users. We define the signal-to-noise ratio (SNR) from BSm at Ul as $\gamma_{ml} = \eta_m |h_{ml}|^2$, where h_{ml} is the channel gain from BSm to Ul and we define the SNR from BSm at BSn as $\xi_{mn} = \eta_m |g_{mn}|^2$, where g_{mn} is the channel gain from BSm to BSn.

Since fairness is a key parameter in this chapter, different metrics are necessary to provide an integrated view of the system performance. Therefore, we propose to use the following:

1. Jain's Fairness Index (JFI), which is one of the most widely used quantitative fairness measures [77], first proposed in [49]. It has the advantages of being independent of the population size and the scale,

[2] The shared bandwidth can represent a (set of) subcarrier(s) in an OFDM system.

continuous, and bounded between 0 and 1. It is defined as

$$\text{JFI} = \frac{\left(\sum_{l=1}^{L} x_l\right)^2}{L\sum_{l=1}^{L} x_l^2}. \tag{4.1}$$

In this chapter x_l represents spectral efficiency per time-slot of Ul. A large JFI value represents a fairer system. However, the JFI does not help in identifying unfairly treated users.

2. The *minimum spectral efficiency*, defined here as the spectral efficiency of the user with the lowest signal-to-interference-plus-noise ratio (SINR), provides an indication of the max-min fairness of the system. Although this metric does not reflect the overall system performance, it can pinpoint the performance of those unfairly treated users.

3. Finally, we use the bit error rate (BER) with BPSK modulation as a measure of the diversity of the system.

For the sake of clarity, in this section we focus on the case where there are only two base stations and two users (i.e. $L = 2$), leaving the extension to larger systems for Section 4.3. In the following, Section 4.2.1 presents the analysis of the spectral efficiency and BER of three baseline approaches. Then, Sections 4.2.2 and 4.2.2 present the analysis of the proposed transmission and reception strategies.

4.2.1 Baseline Approaches

This section presents the analysis of three baseline approaches, which will be used to benchmark the performance of the proposed approach.

TDMA-2

In a basic time division multiple access (TDMA) approach, the communication is done in turns, i.e. first BS1 transmits s_1 to U1 while BS2 is inactive, and then BS2 transmits s_2 to U2 while BS1 is inactive, hence requiring 2 time-slots. We refer to this approach as TDMA-2, where the 2 refers to $L = 2$. The weakness of this approach is the absence of spatial diversity and of fairness: if

the channel between a user and its base station is in a deep fading, the transfer of information will be limited.

The spectral efficiency per time-slot of Ul using TDMA-2 is given as

$$C_{\mathrm{U}l}^{\mathrm{TDMA-2}} = \frac{1}{2}\mathbb{E}\{\log_2(1+\gamma_{ll})\} \tag{4.2}$$

where the expected value is calculated over the distribution of the channel coefficients. Note that the $\frac{1}{2}$ scaling factor is due to the number of required time-slots for each transmission round. It can be seen that the spectral efficiency in equation (4.2) can be quite different for different users, which shows that this is not a fair approach.

Assuming BPSK transmissions and Rayleigh fading statistics (assumptions holding throughout the whole chapter), the BER of Ul is computed in terms of the Gaussian Q-function using the results of appendix A.1 as

$$\begin{aligned}\mathrm{BER}_{\mathrm{U}l}^{\mathrm{TDMA-2}} &= \mathbb{E}\left\{Q(\sqrt{2\gamma_{ll}})\right\} \\ &= \frac{1}{\pi}\int_0^{\pi/2}\left(\frac{1}{1+\frac{\bar{\gamma_{ll}}}{\sin^2\phi}}\right)d\phi \approx \frac{1}{\bar{\gamma_{ll}}},\end{aligned} \tag{4.3}$$

where $\bar{\gamma_{ml}} = \mathbb{E}\{\gamma_{ml}\} = \eta_m\mathbb{E}\{|h_{ml}|^2\}$ and the approximation only holds in the high SNR regime [40]. Equation (4.3) shows the lack of diversity of this approach since the BER decays as $1/\bar{\gamma_{ll}}$.

DIV-2

One way of increasing the spatial diversity, and hence the fairness, is to exploit the overhearing capabilities of the system in order to share the transmitted symbols between the base stations. In this way, each symbol can reach its destination following more than one signal path. For instance, BS1 transmits s_1 to both U1 and BS2 in time-slot 1, then BS2 transmits s_2 to both U2 and BS1 in time-slot 2. Finally, BS1 relays s_2 in time-slot 3 and BS2 relays s_1 in time-slot 4. We refer to this approach as *Diversity*-2 (DIV-2). The relayed symbols are assumed to be the noisy versions of the original symbols.

Assuming a channel coherence time larger than four time-slots, the received signals for Ul in the four time-slots are given as:

$$\begin{aligned} y_{\mathrm{U}l}^{(1)} &= \sqrt{P_1} h_{1l} s_1 + n_{\mathrm{U}l}^{(1)} \\ y_{\mathrm{U}l}^{(2)} &= \sqrt{P_2} h_{2l} s_2 + n_{\mathrm{U}l}^{(2)} \\ y_{\mathrm{U}l}^{(3)} &= \sqrt{P_1} h_{1l} z_{21} + n_{\mathrm{U}l}^{(3)} \\ y_{\mathrm{U}l}^{(4)} &= \sqrt{P_2} h_{2l} z_{12} + n_{\mathrm{U}l}^{(4)} \end{aligned} \tag{4.4}$$

with

$$\begin{aligned} z_{12} &= s_1 + \frac{n_{\mathrm{BS2}}^{(1)}}{\sqrt{P_1} g_{12}} \\ z_{21} &= s_2 + \frac{n_{\mathrm{BS1}}^{(2)}}{\sqrt{P_2} g_{21}}, \end{aligned} \tag{4.5}$$

where $y_{\mathrm{U}l}^{(t)}$ is the received signal of Ul in time-slot t, and $n_{\mathrm{U}l}^{(t)}$ and $n_{\mathrm{BS}m}^{(t)}$ are the AWGN noise of Ul and of BSm, respectively, in time-slot t.

The received signal $\mathbf{y}_l = \begin{bmatrix} y_{\mathrm{U}l}^{(1)} & y_{\mathrm{U}l}^{(2)} & y_{\mathrm{U}l}^{(3)} & y_{\mathrm{U}l}^{(4)} \end{bmatrix}^T$, can be expressed in matrix form as

$$\begin{bmatrix} y_{\mathrm{U}l}^{(1)} \\ y_{\mathrm{U}l}^{(2)} \\ y_{\mathrm{U}l}^{(3)} \\ y_{\mathrm{U}l}^{(4)} \end{bmatrix} = \begin{bmatrix} \sqrt{P_1} h_{1l} & 0 \\ 0 & \sqrt{P_2} h_{2l} \\ 0 & \sqrt{P_1} h_{1l} \\ \sqrt{P_2} h_{2l} & 0 \end{bmatrix} \begin{bmatrix} s_1 \\ s_2 \end{bmatrix} + \begin{bmatrix} n_{\mathrm{U}l}^{(1)} \\ n_{\mathrm{U}l}^{(2)} \\ n_{\mathrm{U}l}^{(3)} + \frac{\sqrt{P_1} h_{1l}}{\sqrt{P_2} g_{21}} n_{\mathrm{BS1}}^{(2)} \\ n_{\mathrm{U}l}^{(4)} + \frac{\sqrt{P_2} h_{2l}}{\sqrt{P_1} g_{12}} n_{\mathrm{BS2}}^{(1)} \end{bmatrix}. \tag{4.6}$$

Using a minimum mean-square error (MMSE) receiver (as described in section 4.2.2), the spectral efficiency per time-slot of Ul using DIV-2 is computed as

$$C_{\mathrm{U}l}^{\mathrm{DIV-2}} = \frac{1}{4} \mathbb{E} \left\{ \log_2 \left(1 + \gamma_{ll} + \frac{\gamma_{ml}}{\frac{\gamma_{ml}}{\xi_{lm}} + 1} \right) \right\}, \tag{4.7}$$

for $m \neq l$ (i.e. $m = 1$ if $l = 2$ and $m = 2$ if $l = 1$), which shows the SNR gain of Ul from the transmission of both base stations. From equation (4.7), it is observed that when the channel gain between BSl and BSm is strong compared

to the channel gain between BSm and Ul[3], i.e. $\xi_{lm} \gg \gamma_{ml}$, DIV-2 achieves high fairness from the transmission of both base stations.

Using this assumption and the results of appendix A.1 and assuming independent and identically distributed Rayleigh fading paths as well as equally-likely transmitted symbols, the BER for Ul is computed as

$$\begin{aligned} \mathrm{BER}_{\mathrm{U}l}^{\mathrm{DIV}-2} &= \mathbb{E}\left\{ Q\left(\sqrt{2\left(\gamma_{ll} + \frac{\gamma_{ml}}{\frac{\gamma_{ml}}{\xi_{lm}} + 1} \right)} \right) \right\} \\ &= \frac{1}{\pi} \int_0^{\pi/2} \left(\frac{1}{1 + \frac{\bar{\gamma_{1l}}}{\sin^2 \phi}} \right) \left(\frac{1}{1 + \frac{\bar{\gamma_{2l}}}{\sin^2 \phi}} \right) d\phi \approx \frac{1}{\bar{\gamma_{1l}} \bar{\gamma_{2l}}}, \end{aligned} \tag{4.8}$$

Again, the approximation holds in the high SNR regime. Equation (4.8) shows that DIV-2 achieves full diversity, i.e. a diversity gain of order L, at the cost of doubling the number of time-slots compared to TDMA-2.

INTF-2

A last baseline approach consists in both base stations transmitting simultaneously regardless of the resulting interference. We refer to this approach as *Interference*-2 (INTF-2). The spectral efficiency per time-slot of Ul using INTF-2 is computed as

$$C_{\mathrm{U}l}^{\mathrm{INTF}-2} = \mathbb{E}\left\{ \log_2\left(1 + \frac{\gamma_{ll}}{1 + \gamma_{ml}} \right) \right\} \tag{4.9}$$

for $m \neq l$. Although it uses each time-slot for transmission, equation (6.8) shows that this approach is not fair as it only benefits the user with the smallest interference.

To compute the BER of Ul with INTF-2, we use equation (A.1) from appendix A.1 and integrate over the joint PDF of γ_{1l} and γ_{2l}, i.e. $p(\gamma_{1l}, \gamma_{2l})$. Since γ_{1l} and γ_{2l} are statistically independent, $p(\gamma_{1l}, \gamma_{2l}) = p(\gamma_{1l})p(\gamma_{2l})$, which

[3]This is a reasonable assumption since base stations are usually equipped with more powerful receivers (i.e. with greater sensitivity and smaller noise figure) and they often count with line-of-sight (LOS) between them.

for Rayleigh fading statistics results in

$$\begin{aligned}\mathrm{BER}_{\mathrm{U}l}^{\mathrm{INTF-2}} &= \mathbb{E}\left\{Q\left(\sqrt{2\left[\frac{\gamma_{ll}}{1+\gamma_{ml}}\right]}\right)\right\} \\ &= \frac{1}{\bar{\gamma_{1l}}\bar{\gamma_{2l}}}\int_0^\infty\int_0^\infty Q\left(\sqrt{2\left[\frac{\gamma_{ll}}{1+\gamma_{ml}}\right]}\right)\exp\left(-\left[\frac{\gamma_{1l}}{\bar{\gamma_{1l}}}+\frac{\gamma_{2l}}{\bar{\gamma_{2l}}}\right]\right)d\gamma_{1l}d\gamma_{2l}.\end{aligned} \tag{4.10}$$

Equation (4.10) shows that the diversity gain of this approach is lower than the diversity gain achieved by TDMA-2, especially when $\gamma_{ml} > \gamma_{ll}$.

4.2.2 Proposed Approach with Two Base Stations: MRCP-2

This section presents the proposed approach with $L = 2$, which combines a three-time-slot transmission strategy and an MMSE reception strategy. We refer to this approach as multiple-relay communication protocol-2 (MRCP-2).

Three-Time-Slot Transmission Strategy

The proposed approach exploits spatial diversity while using only three time-slots. In the first time-slot, BS1 transmits s_1 to U1, U2, and BS2. Then, in the second time-slot, BS2 transmits s_2 to U1, U2, and BS1. Finally, in the third time-slot, each base station relays the received symbols (s_2 for BS1 and s_1 for BS2) to U1 and U2. The relayed symbols are assumed to be the noisy versions of the original symbols. This is shown in Fig. 4.1.

Assuming a channel coherence time larger than three time-slots, the received signals for Ul in the three time-slots are given as:

$$\begin{aligned} y_{\mathrm{U}l}^{(1)} &= \sqrt{P_1}h_{1l}s_1 + n_{\mathrm{U}l}^{(1)} \\ y_{\mathrm{U}l}^{(2)} &= \sqrt{P_2}h_{2l}s_2 + n_{\mathrm{U}l}^{(2)} \\ y_{\mathrm{U}l}^{(3)} &= \sqrt{P_1}h_{1l}z_{21} + \sqrt{P_2}h_{2l}z_{12} + n_{\mathrm{U}l}^{(3)}, \end{aligned} \tag{4.11}$$

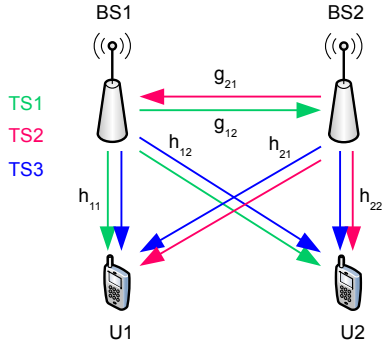

Figure 4.1: System model for the case of two base stations and two users. The parameter h_{ml} defines the channel gain of Ul from BSm and g_{mn} defines the channel gain of BSn from BSm. TSt defines the t-th time-slot.

with

$$z_{12} = s_1 + \frac{n^{(1)}_{\mathrm{BS2}}}{\sqrt{P_1} g_{12}}$$
$$z_{21} = s_2 + \frac{n^{(2)}_{\mathrm{BS1}}}{\sqrt{P_2} g_{21}}, \tag{4.12}$$

where $y^{(t)}_{\mathrm{U}l}$ is the received signal of Ul in time-slot t, and $n^{(t)}_{\mathrm{U}l}$ and $n^{(t)}_{\mathrm{BS}m}$ are the AWGN noise of Ul and of BSm, respectively, in time-slot t.

This approach is intermediate between TDMA-2 and INTF-2, as it exploits the transmissions of both base stations without requiring too many additional time-slots.

The received signal $\mathbf{y}_l = \begin{bmatrix} y^{(1)}_{\mathrm{U}l} & y^{(2)}_{\mathrm{U}l} & y^{(3)}_{\mathrm{U}l} \end{bmatrix}^T$, can be expressed in matrix form as

$$\begin{bmatrix} y^{(1)}_{\mathrm{U}l} \\ y^{(2)}_{\mathrm{U}l} \\ y^{(3)}_{\mathrm{U}l} \end{bmatrix} = \begin{bmatrix} \sqrt{P_1} h_{1l} & 0 \\ 0 & \sqrt{P_2} h_{2l} \\ \sqrt{P_2} h_{2l} & \sqrt{P_1} h_{1l} \end{bmatrix} \begin{bmatrix} s_1 \\ s_2 \end{bmatrix} + \begin{bmatrix} n^{(1)}_{\mathrm{U}l} \\ n^{(2)}_{\mathrm{U}l} \\ n^{(3)}_{\mathrm{U}l} + \frac{\sqrt{P_1} h_{1l}}{\sqrt{P_2} g_{21}} n^{(2)}_{\mathrm{BS1}} + \frac{\sqrt{P_2} h_{2l}}{\sqrt{P_1} g_{12}} n^{(1)}_{\mathrm{BS2}} \end{bmatrix}. \tag{4.13}$$

Considering U1, equation (4.13) can be expressed in vector form as

$$\mathbf{y}_1 = \mathbf{a}_1 s_1 + \mathbf{a}_2 s_2 + \mathbf{n}_1 = \mathbf{a}_1 s_1 + \mathbf{w}_1, \tag{4.14}$$

where $\mathbf{a}_1 = \begin{bmatrix}\sqrt{P_1}h_{1l} & 0 & \sqrt{P_2}h_{2l}\end{bmatrix}^T$, $\mathbf{a}_2 = \begin{bmatrix}0 & \sqrt{P_2}h_{2l} & \sqrt{P_1}h_{1l}\end{bmatrix}^T$, $\mathbf{w}_1 = \mathbf{a}_2 s_2 + \mathbf{n}_1$ is defined as the interference-plus-noise vector of U1, and $\mathbf{n}_1 = \begin{bmatrix}n_{\mathrm{U1}}^{(1)} & n_{\mathrm{U1}}^{(2)} & n_{\mathrm{U1}}^{(3)} + \frac{\sqrt{P_1}h_{11}}{\sqrt{P_2}g_{21}} n_{\mathrm{BS1}}^{(2)} + \frac{\sqrt{P_2}h_{21}}{\sqrt{P_1}g_{12}} n_{\mathrm{BS2}}^{(1)}\end{bmatrix}^T$.

MMSE Reception Strategy

The MMSE receiver is well known for being an efficient low-complexity linear receiver, which provides sufficient statistics to detect the input signal when it follows a Gaussian distribution [86]. The MMSE receiver of U1 can be derived in two steps. The first step consists in whitening the colored noise term $\mathbf{w}_1$ from equation (4.14) with its covariance matrix $\mathbf{R}_{w_1}$. This is achieved by filtering the received signal in (4.14) with the matrix $\mathbf{R}_{w_1}^{-1/2}$:

$$\mathbf{R}_{w_1}^{-1/2}\mathbf{y}_1 = \mathbf{R}_{w_1}^{-1/2}\mathbf{a}_1 s_1 + \mathbf{R}_{w_1}^{-1/2}\mathbf{w}_1. \tag{4.15}$$

The second step consists in performing maximal ratio combining (MRC) over the remaining signal, which is an optimal processing when the additive noise is white [86]. This is achieved by taking the inner product of the signal of (4.15) and the vector $\mathbf{R}_{w_1}^{-1/2}\mathbf{a}_1$:

$$\begin{aligned}\hat{z} = (\mathbf{R}_{w_1}^{-1/2}\mathbf{a}_1)^H \mathbf{R}_{w_1}^{-1/2}\mathbf{y}_1 &= \mathbf{a}_1^H \mathbf{R}_{w_1}^{-1}\mathbf{a}_1 s_1 + \mathbf{a}_1^H \mathbf{R}_{w_1}^{-1}\mathbf{w}_1 \\ &= \hat{z}_{\mathrm{sig}} + \hat{z}_{\mathrm{noise}}.\end{aligned} \tag{4.16}$$

From equation (4.16), the signal power can be calculated as

$$\begin{aligned}\mathbb{E}\{|\hat{z}_{\mathrm{sig}}|^2\} &= \mathbb{E}\{(\mathbf{a}_1^H \mathbf{R}_{w_1}^{-1}\mathbf{a}_1 s_1)(\mathbf{a}_1^H \mathbf{R}_{w_1}^{-1}\mathbf{a}_1 s_1)^H\} \\ &= (\mathbf{a}_1^H \mathbf{R}_{w_1}^{-1}\mathbf{a}_1)^2 \sigma_{\mathrm{s}}^2\end{aligned} \tag{4.17}$$

and the noise power as

$$\begin{aligned}\mathbb{E}\{|\hat{z}_{\mathrm{noise}}|^2\} &= \mathbb{E}\{(\mathbf{a}_1^H \mathbf{R}_{w_1}^{-1}\mathbf{w}_1)(\mathbf{a}_1^H \mathbf{R}_{w_1}^{-1}\mathbf{w}_1)^H\} \\ &= (\mathbf{R}_{w_1}^{-1/2}\mathbf{a}_1)^H \mathbb{E}\{\mathbf{R}_{w_1}^{-1/2}\mathbf{w}_1 (\mathbf{R}_{w_1}^{-1/2}\mathbf{w}_1)^H\}\mathbf{R}_{w_1}^{-1/2}\mathbf{a}_1 \\ &= \mathbf{a}_1^H \mathbf{R}_{w_1}^{-1}\mathbf{a}_1.\end{aligned} \tag{4.18}$$

Using equations (4.17) and (4.18), the SNR of U1 using the MMSE receiver is found to be

$$\mathrm{SNR}_{\mathrm{U1}}^{\mathrm{MRCP-2}} = \frac{\mathbb{E}\{|\hat{z}_{\mathrm{sig}}|^2\}}{\mathbb{E}\{|\hat{z}_{\mathrm{noise}}|^2\}} = \mathbf{a}_1^H \mathbf{R}_{w_1}^{-1}\mathbf{a}_1 \sigma_{\mathrm{s}}^2. \tag{4.19}$$

Performance Analysis

Let us now derive the spectral efficiency of U1 using the proposed transmission strategy. By assuming s_1 and s_2 as independent symbols with a Gaussian distribution, the spectral efficiency per time-slot of U1 is calculated as

$$C_{\mathrm{U1}}^{\mathrm{MRCP-2}} = \frac{1}{3}\left[H(\mathbf{y}_1) - H(\mathbf{w}_1)\right] = \frac{1}{3}\log_2\frac{|\mathbf{R}_{y_1}|}{|\mathbf{R}_{w_1}|}, \tag{4.20}$$

where $H(\mathbf{y}_1)$ and $H(\mathbf{w}_1)$ are the entropies of $\mathbf{y}_1$ and $\mathbf{w}_1$, and $\mathbf{R}_{y_1}$ and $\mathbf{R}_{w_1}$ are the covariance matrices of $\mathbf{y}_1$ and $\mathbf{w}_1$. The $\frac{1}{3}$ scaling factor corresponds to the number of time-slots used for each transmission round. The last equality in (4.20) is obtained by using the well-known expression for the entropy of a multivariate complex Gaussian distribution [25]. Moreover, $\mathbf{R}_{w_1}$ is given as

$$\mathbf{R}_{w_1} = \mathbb{E}\{(\mathbf{a}_2 s_2 + \mathbf{n}_1)(\mathbf{a}_2 s_2 + \mathbf{n}_1)^H\} = \mathbf{a}_2\mathbf{a}_2^H\sigma_{\mathrm{s}}^2 + \mathbf{N}_1, \tag{4.21}$$

where $\mathbf{N}_1 = \mathrm{diag}\left[\sigma_{\mathrm{n}}^2, \sigma_{\mathrm{n}}^2, \sigma_{\mathrm{n}}^2\left(1 + \frac{P_1\mathbb{E}\{|h_{11}|^2\}}{P_2\mathbb{E}\{|g_{21}|^2\}} + \frac{P_2\mathbb{E}\{|h_{21}|^2\}}{P_1\mathbb{E}\{|g_{12}|^2\}}\right)\right]$, and $\mathbf{R}_{y_1}$ is given as

$$\begin{aligned}\mathbf{R}_{y_1} &= \mathbb{E}\{(\mathbf{a}_1 s_1 + \mathbf{w}_1)(\mathbf{a}_1 s_1 + \mathbf{w}_1)^H\} \\ &= \mathbf{a}_1\mathbf{a}_1^H\sigma_{\mathrm{s}}^2 + \mathbf{a}_2\mathbf{a}_2^H\sigma_{\mathrm{s}}^2 + \mathbf{N}_1.\end{aligned} \tag{4.22}$$

Hence, equation (4.20) can be re-written as

$$\begin{aligned}C_{\mathrm{U1}}^{\mathrm{MRCP-2}} &= \frac{1}{3}\log_2|\mathbf{R}_{w_1}^{-1}(\mathbf{R}_{w_1} + \mathbf{a}_1\mathbf{a}_1^H\sigma_{\mathrm{s}}^2)| \\ &= \frac{1}{3}\log_2\left(1 + \mathbf{a}_1^H\mathbf{R}_{w_1}^{-1}\mathbf{a}_1\sigma_{\mathrm{s}}^2\right).\end{aligned} \tag{4.23}$$

Comparing equation (4.19) with equation (4.23), it is clear that the MMSE receiver is able to achieve the channel capacity. Following the same procedure, the spectral efficiency per time-slot of U2 is calculated as

$$C_{\mathrm{U2}}^{\mathrm{MRCP-2}} = \frac{1}{3}\log_2\left(1 + \mathbf{a}_2^H\mathbf{R}_{w_2}^{-1}\mathbf{a}_2\sigma_{\mathrm{s}}^2\right), \tag{4.24}$$

where in this case $\mathbf{R}_{w_2} = \mathbf{a}_1\mathbf{a}_1^H\sigma_{\mathrm{s}}^2 + \mathbf{N}_2$.

Using equations (4.21), (4.22), and (4.23), and the results presented in appendix A.2, the spectral efficiency per time-slot of Ul using MRCP-2 is computed as

$$C_{\mathrm{U}l}^{\mathrm{MRCP-2}} = \frac{1}{3}\mathbb{E}\left\{\log_2\left(1 + \gamma_{ll} + \frac{\gamma_{ml}}{\frac{\gamma_{ll}}{\gamma_{ml}+1} + \frac{\gamma_{ll}}{\xi_{ml}} + \frac{\gamma_{ml}}{\xi_{lm}} + 1}\right)\right\} \tag{4.25}$$

where $m \neq l$. Equation (4.25) indicates an SNR gain from the transmission of both base stations. When the channel gains between base stations are stronger than the channel gains between base stations and users, i.e. $\xi_{ml} \gg \gamma_{ll}$ and $\xi_{lm} \gg \gamma_{ml}$, MRCP-2 shows symmetry between γ_{ll} and γ_{ml}, which highlights the fairness of the proposed approach.

Let us now calculate the BER of Ul. By noting that γ_{1l} and γ_{2l} are statistically independent and defining $\gamma_{\mathrm{MRCP}} = \gamma_{ll} + \frac{\gamma_{ml}}{\frac{\gamma_{ll}}{\gamma_{ml}+1}+\frac{\gamma_{ll}}{\xi_{ml}}+\frac{\gamma_{ml}}{\xi_{lm}}+1}$, it is shown that

$$\begin{aligned} \mathrm{BER}_{\mathrm{U}l}^{\mathrm{MRCP-2}} &= \mathbb{E}\left\{Q\left(\sqrt{2\gamma_{\mathrm{MRCP}}}\right)\right\} \\ &= \frac{1}{\bar{\gamma_{1l}}\bar{\gamma_{2l}}}\int_0^\infty\int_0^\infty Q\left(\sqrt{2\gamma_{\mathrm{MRCP}}}\right)\exp\left(-\left[\frac{\gamma_{1l}}{\bar{\gamma_{1l}}}+\frac{\gamma_{2l}}{\bar{\gamma_{2l}}}\right]\right)d\gamma_{1l}d\gamma_{2l}. \end{aligned} \tag{4.26}$$

Note that $\gamma_{\mathrm{MRCP}} \leq \gamma_{1l} + \gamma_{2l}$, the difference being small if $\gamma_{1l} \gg \gamma_{2l}$ or if $\gamma_{2l} \gg \gamma_{1l}$. Therefore, the diversity gain provided by this approach is larger than the diversity provided by TDMA-2 but smaller than the diversity provided by DIV-2.

4.3 Extension to an Arbitrary Number of Base Stations and Users

This section extends the results of Section 4.2 to a larger system size. In the following, Section 4.3.1 presents the analysis of the extended baseline approaches, and then Section 4.3.2 presents the analysis of the extended proposed approach.

4.3.1 Extended Baseline Approaches

This section presents the analysis of the extended baseline approaches without diversity (TDMA-L), with diversity (DIV-L), and with interfering continuous transmissions (INTF-L). These will be used to benchmark the performance of the extended proposed approach.

TDMA-L

In this approach, every base station performs one transmission while the others remain inactive, taking L time-slots to transmit all L symbols. We refer to this

approach as TDMA-L. The spectral efficiency per time-slot of Ul is computed as

$$C_{\mathrm{U}l}^{\mathrm{TDMA-L}} = \frac{1}{L}\mathbb{E}\{\log_2(1+\gamma_{ll})\}. \tag{4.27}$$

Equation (4.27) shows that the spectral efficiency per time-slot of each user decreases with L. Also, each user can have a very different spectral efficiency depending on γ_{ll}, which shows that this is not a fair approach.

The BER of Ul remains the same as in the case where $L = 2$:

$$\mathrm{BER}_{\mathrm{U}l}^{\mathrm{TDMA-L}} = \frac{1}{\pi}\int_0^{\pi/2}\left(\frac{1}{1+\frac{\bar{\gamma_{ll}}}{\sin^2\phi}}\right)d\phi \approx \frac{1}{\bar{\gamma_{ll}}}, \tag{4.28}$$

From equation (5.6), it can be seen that the BER is independent of L and hence no diversity gain is achieved.

DIV-L

In this approach, each base station first transmits a symbol to its intended user and then relays each received symbol in a dedicated time-slot. Specifically, BS1 transmits s_1 to all users and base stations in the first time-slot, then BS2 transmits s_2 to all users and base stations in the second time-slot, until BSL transmits s_L to all users and base stations in time-slot L. Similarly in time-slots $L+1$ to $2L$, but this time BS1 relays s_2, BS2 relays s_3, and so on until BSL relays s_1. Finally, in time-slots $(L-1)L+1$ to L^2, BS1 relays s_L, BS2 relays s_1, and so on until BSL relays s_{L-1}. Hence, one complete round of transmission takes L^2 time-slots. We refer to this approach as DIV-L. The relayed symbols are assumed to be the noisy versions of the original symbols. In comparison to TDMA-L, DIV-L achieves fairness and diversity from all the base stations at the cost of increasing the transmission time to L^2.

Assuming a channel coherence time larger than L^2 time-slots, the received signals for Ul in the L^2 time-slots are given as:

$$\begin{aligned}
y_{\mathrm{U}l}^{(1)} &= \sqrt{P_1} h_{1l} s_1 + n_{\mathrm{U}l}^{(1)} \\
y_{\mathrm{U}l}^{(2)} &= \sqrt{P_2} h_{2l} s_2 + n_{\mathrm{U}l}^{(2)} \\
&\vdots \\
y_{\mathrm{U}l}^{(L)} &= \sqrt{P_L} h_{Ll} s_L + n_{\mathrm{U}l}^{(L)} \\
y_{\mathrm{U}l}^{(L+1)} &= \sqrt{P_1} h_{1l} z_{21} + n_{\mathrm{U}l}^{(L+1)} \\
y_{\mathrm{U}l}^{(L+2)} &= \sqrt{P_2} h_{2l} z_{32} + n_{\mathrm{U}l}^{(L+2)} \\
&\vdots \\
y_{\mathrm{U}l}^{((L-1)L)} &= \sqrt{P_L} h_{Ll} z_{(L-2)L} + n_{\mathrm{U}l}^{((L-1)L)} \\
y_{\mathrm{U}l}^{((L-1)L+1)} &= \sqrt{P_1} h_{1l} z_{L1} + n_{\mathrm{U}l}^{((L-1)L+1)} \\
y_{\mathrm{U}l}^{((L-1)L+2)} &= \sqrt{P_2} h_{2l} z_{12} + n_{\mathrm{U}l}^{((L-1)L+2)} \\
&\vdots \\
y_{\mathrm{U}l}^{(L^2)} &= \sqrt{P_L} h_{Ll} z_{(L-1)L} + n_{\mathrm{U}l}^{(L^2)}
\end{aligned} \tag{4.29}$$

with

$$z_{lm} = s_l + \frac{n_{\mathrm{BS}m}^{(l)}}{\sqrt{P_l} g_{lm}}, \tag{4.30}$$

$\forall m \neq l$.

The received signal $\mathbf{y}_l = \begin{bmatrix} y_{\mathrm{U}l}^{(1)} & y_{\mathrm{U}l}^{(2)} & \cdots & y_{\mathrm{U}l}^{(L^2)} \end{bmatrix}^T$, can be expressed in matrix form as in equation (4.31).

Using the methodology described in section 4.3.2, the spectral efficiency per time-slot of Ul using DIV-L is computed as

$$C_{\mathrm{U}l}^{\mathrm{DIV-L}} = \frac{1}{L^2} \mathbb{E} \left\{ \log_2 \left(1 + \gamma_{ll} + \sum_{\substack{m=1 \\ m \neq l}}^{L} \frac{\gamma_{ml}}{\frac{\gamma_{ml}}{\xi_{lm}} + 1} \right) \right\}, \tag{4.32}$$

$$\begin{bmatrix} y_{\mathrm{Ul}}^{(1)} \\ y_{\mathrm{Ul}}^{(2)} \\ \vdots \\ y_{\mathrm{Ul}}^{(L)} \\ y_{\mathrm{Ul}}^{(L+1)} \\ y_{\mathrm{Ul}}^{(L+2)} \\ \vdots \\ y_{\mathrm{Ul}}^{((L-1)L)} \\ y_{\mathrm{Ul}}^{((L-1)L+1)} \\ y_{\mathrm{Ul}}^{((L-1)L+2)} \\ \vdots \\ y_{\mathrm{Ul}}^{(L^2)} \end{bmatrix} = \begin{bmatrix} \sqrt{P_1}h_{1l} & 0 & 0 & \cdots & 0 & 0 \\ 0 & \sqrt{P_2}h_{2l} & 0 & \cdots & 0 & 0 \\ \vdots & \vdots & \vdots & \ddots & \vdots & \vdots \\ 0 & 0 & 0 & \cdots & 0 & \sqrt{P_L}h_{Ll} \\ 0 & \sqrt{P_1}h_{1l} & 0 & \cdots & 0 & 0 \\ 0 & 0 & \sqrt{P_2}h_{2l} & \cdots & 0 & 0 \\ \vdots & \vdots & \vdots & \ddots & \vdots & \vdots \\ 0 & 0 & 0 & \cdots & 0 & \sqrt{P_1}h_{1l} \\ \sqrt{P_2}h_{2l} & 0 & 0 & \cdots & 0 & 0 \\ \vdots & \vdots & \vdots & \ddots & \vdots & \vdots \\ 0 & 0 & 0 & \cdots & \sqrt{P_L}h_{Ll} & 0 \end{bmatrix} \begin{bmatrix} s_1 \\ s_2 \\ \vdots \\ s_L \end{bmatrix} +$$

$$\begin{bmatrix} n_{\mathrm{Ul}}^{(1)} \\ n_{\mathrm{Ul}}^{(2)} \\ \vdots \\ n_{\mathrm{Ul}}^{(L)} \\ n_{\mathrm{Ul}}^{(L+1)} + \frac{\sqrt{P_1}h_{1l}}{\sqrt{P_2}g_{21}} n_{\mathrm{BS1}}^{(2)} \\ n_{\mathrm{Ul}}^{(L+2)} + \frac{\sqrt{P_2}h_{2l}}{\sqrt{P_3}g_{32}} n_{\mathrm{BS2}}^{(3)} \\ \vdots \\ n_{\mathrm{Ul}}^{((L-1)L)} + \frac{\sqrt{P_L}h_{Ll}}{\sqrt{P_{L-2}}g_{(L-2)L}} n_{\mathrm{BS}L}^{(L-2)} \\ n_{\mathrm{Ul}}^{((L-1)L+1)} + \frac{\sqrt{P_1}h_{1l}}{\sqrt{P_L}g_{L1}} n_{\mathrm{BS1}}^{(L)} \\ n_{\mathrm{Ul}}^{((L-1)L+2)} + \frac{\sqrt{P_2}h_{2l}}{\sqrt{P_1}g_{12}} n_{\mathrm{BS2}}^{(1)} \\ \vdots \\ n_{\mathrm{Ul}}^{(L^2)} + \frac{\sqrt{P_L}h_{Ll}}{\sqrt{P_{L-1}}g_{(L-1)L}} n_{\mathrm{BS}L}^{(L-1)} \end{bmatrix}. \tag{4.31}$$

When the channel gains between base stations are strong compared to the channel gains between base stations and users, i.e. $\xi_{lm} \gg \gamma_{ml}\ \forall m \neq l$ and for the particular case in which $\gamma_{1l} = \gamma_{2l} = \cdots = \gamma_{Ll} = \bar{\gamma}$ assuming a large L, then

$$1 + \gamma_{ll} + \sum_{\substack{m=1 \\ m \neq l}}^{L} \frac{\gamma_{ml}}{\frac{\gamma_{ml}}{\xi_{lm}} + 1} \approx L\bar{\gamma}. \tag{4.33}$$

This results in

$$C_{\mathrm{U}l}^{\mathrm{DIV-L}} \approx \frac{1}{L^2} \left[\log_2(L) + \log_2(\bar{\gamma}) \right]. \tag{4.34}$$

As $\log_2(L)/L^2$ tends to zero faster than $1/L$, it is seen that $C_{\mathrm{U}l}^{\mathrm{DIV-L}}$ decreases faster with L than $C_{\mathrm{U}l}^{\mathrm{TDMA-L}}$. However, DIV-L achieves a high fairness from the transmission of multiple base stations.

Using the results from appendix A.1, the BER of Ul is computed as

$$\mathrm{BER}_{\mathrm{U}l}^{\mathrm{DIV-L}} = \frac{1}{\pi} \int_0^{\pi/2} \prod_{m=1}^{L} \left(\frac{1}{1 + \frac{\bar{\gamma_{ml}}}{\sin^2 \phi}} \right) d\phi \approx \frac{1}{\prod_{m=1}^{L} \bar{\gamma_{ml}}}, \tag{4.35}$$

where the approximation only holds in the high SNR regime. Again, equation (4.35) shows the full diversity achieved by DIV-L.

INTF-L

In this case all the base stations transmit continuously regardless of the resulting interference. Hence, a full transmission round takes only one time slot. We refer to this approach as INTF-L. The spectral efficiency per time-slot of Ul using INTF-L is computed as

$$C_{\mathrm{U}l}^{\mathrm{INTF-L}} = \mathbb{E}\left\{ \log_2 \left(1 + \frac{\gamma_{ll}}{1 + \sum_{\substack{m=1 \\ m \neq l}}^{L} \gamma_{ml}} \right) \right\}. \tag{4.36}$$

Although this approach uses all the time-slots for transmitting to each user, it is unfair since it benefits the user with the lowest interference level. For the particular case in which $\gamma_{1l} = \gamma_{2l} = \cdots = \gamma_{Ll} = \bar{\gamma}$ and for a large L, using a first order Taylor series expansion $\log(1 + x) \approx x$ shows that

$$C_{\mathrm{U}l}^{\mathrm{INTF-L}} \approx \mathbb{E}\left\{ \frac{\gamma_{ll}}{1 + L\bar{\gamma}} \right\} = \frac{1}{\bar{\gamma}^{-1} + L}. \tag{4.37}$$

This shows that the spectral efficiency decreases as $1/L$.

The BER of Ul using this approach is computed as

$$\begin{aligned}\mathrm{BER}_{\mathrm{U}l}^{\mathrm{INTF-L}} &= \mathbb{E}\left\{Q\left(\sqrt{2\gamma_{\mathrm{INTF}}}\right)\right\} \\ &= \frac{1}{\prod_{m=1}^{L}\bar{\gamma_{ml}}}\int_0^{\infty}\cdots\int_0^{\infty} Q\left(\sqrt{2\gamma_{\mathrm{INTF}}}\right)\exp\left(-\sum_{m=1}^{L}\frac{\gamma_{ml}}{\bar{\gamma_{ml}}}\right)d\gamma_{1l}d\gamma_{2l}\cdots d\gamma_{Ll},\end{aligned} \tag{4.38}$$

where $\gamma_{\mathrm{INTF}} = \gamma_{ll}/\left(1+\sum_{\substack{m=1\\m\neq l}}^{L}\gamma_{ml}\right)$. Since $\gamma_{ll} \geq \gamma_{\mathrm{INTF}}$, equation (4.38) shows that the diversity gain is lower than that of TDMA-L and it decreases with L.

4.3.2 Proposed Approach with L Base Stations: MRCP-L

This section extends the proposed approach defined in Section 4.2.2 to an arbitrary number of base stations and users. It also shows the computation of closed-form expressions of the spectral efficiency and BER of the proposed approach.

(L+1)-Time-Slot Transmission Strategy

First each base station transmits its symbol to all the users and base stations in its own dedicated time-slot. At the end of this round one extra time slot is added, where each base station relays a linear combination of all the received symbols as inspired by PNC. Specifically, in time-slot l, BSl transmits s_l to Ul and to all other base stations and users for $l = 1, 2, \cdots, L$ and in time-slot $L+1$ BSl relays $\sum_{\substack{m=1\\m\neq l}}^{L} s_m$ for $l = 1, 2, \cdots, L$. The relayed symbols are assumed to be the noisy versions of the original symbols. Hence, one complete round of transmission takes $L+1$ time-slots. We refer to this approach as MRCP-L.

Assuming that the channel coherence time is larger than $L+1$ time-slots, the received signals for Ul in $L+1$ time-slots is given as

$$\begin{aligned} y_{\mathrm{U}l}^{(1)} &= \sqrt{P_1} h_{1l} s_1 + n_{\mathrm{U}l}^{(1)} \\ y_{\mathrm{U}l}^{(2)} &= \sqrt{P_2} h_{2l} s_2 + n_{\mathrm{U}l}^{(2)} \\ &\vdots \\ y_{\mathrm{U}l}^{(L)} &= \sqrt{P_L} h_{Ll} s_L + n_{\mathrm{U}l}^{(L)} \\ y_{\mathrm{U}l}^{(L+1)} &= \sum_{m=1}^{L} \sqrt{P_m} h_{ml} \sum_{\substack{r=1 \\ r \neq m}}^{L} z_{rm} + n_{\mathrm{U}l}^{(L+1)} \end{aligned} \tag{4.39}$$

with

$$z_{lm} = s_l + \frac{n_{\mathrm{BS}m}^{(l)}}{\sqrt{P_l} g_{lm}}, \tag{4.40}$$

The received signal $\mathbf{y}_l = \begin{bmatrix} y_{\mathrm{U}l}^{(1)} & y_{\mathrm{U}l}^{(2)} & \cdots & y_{\mathrm{U}l}^{(L)} & y_{\mathrm{U}l}^{(L+1)} \end{bmatrix}^T$ can be expressed in matrix form as equation (4.41). The vector form of the received signal is then

$$\mathbf{y}_l = \sum_{m=1}^{L} \mathbf{a}_m s_m + \mathbf{n}_l = \mathbf{a}_l s_l + \mathbf{w}_l, \tag{4.42}$$

where $\mathbf{a}_l$ is the lth column of matrix $\mathbf{A}$, $\mathbf{n}_l =$

$$\begin{bmatrix} n_{\mathrm{U}l}^{(1)} & n_{\mathrm{U}l}^{(2)} & \cdots & n_{\mathrm{U}l}^{(L)} & n_{\mathrm{U}l}^{(L+1)} + \sum_{m=1}^{L} \sqrt{P_m} h_{ml} \sum_{\substack{r=1 \\ r \neq m}}^{L} \frac{n_{\mathrm{BS}m}^{(r)}}{\sqrt{P_r} g_{rm}} \end{bmatrix}^T, \tag{4.43}$$

and $\mathbf{w}_l = \sum_{\substack{m=1 \\ m \neq l}}^{L} \mathbf{a}_m s_m + \mathbf{n}_l$ is defined as the interference-plus-noise vector of Ul.

The MMSE reception strategy can be derived similarly as in equations (4.15) and (4.16). Then, the SNR of Ul results in

$$\mathrm{SNR}_{\mathrm{U}l}^{\mathrm{MRCP-L}} = \mathbf{a}_l^H \mathbf{R}_{w_l}^{-1} \mathbf{a}_l \sigma_{\mathrm{s}}^2, \tag{4.44}$$

where $\mathbf{R}_{w_l}$ is the covariance matrix of $\mathbf{w}_l$, whose explicit expression can be found in equation (A.16) for $l = 1$.

$$\begin{bmatrix} y_{\mathrm{U}l}^{(1)} \\ y_{\mathrm{U}l}^{(2)} \\ \vdots \\ y_{\mathrm{U}l}^{(L)} \\ y_{\mathrm{U}l}^{(L+1)} \end{bmatrix} = \underbrace{\begin{bmatrix} \sqrt{P_1}h_{1l} & 0 & \cdots & 0 \\ 0 & \sqrt{P_2}h_{2l} & \cdots & 0 \\ \vdots & \vdots & \ddots & \vdots \\ 0 & 0 & \cdots & \sqrt{P_L}h_{Ll} \\ \sum\limits_{\substack{m=1 \\ m\neq 1}}^{L} \sqrt{P_m}h_{ml} & \sum\limits_{\substack{m=1 \\ m\neq 2}}^{L} \sqrt{P_m}h_{ml} & \cdots & \sum\limits_{\substack{m=1 \\ m\neq L}}^{L} \sqrt{P_m}h_{ml} \end{bmatrix}}_{\mathbf{A}} \begin{bmatrix} s_1 \\ s_2 \\ \vdots \\ s_L \end{bmatrix} + \begin{bmatrix} n_{\mathrm{U}l}^{(1)} \\ n_{\mathrm{U}l}^{(2)} \\ \vdots \\ n_{\mathrm{U}l}^{(L)} \\ n_{\mathrm{U}l}^{(L+1)} + \sum\limits_{m=1}^{L} \sqrt{P_m}h_{ml} \sum\limits_{\substack{r=1 \\ r\neq m}}^{L} \frac{n_{\mathrm{BS}m}^{(r)}}{\sqrt{P_r}g_{rm}} \end{bmatrix} \tag{4.41}$$

Performance Analysis

Let us now derive the spectral efficiency per time-slot of Ul using the proposed extended approach. For statistically independent Gaussian symbols, the covariance matrix $\mathbf{R}_{w_l}$ is computed as

$$\begin{aligned} \mathbf{R}_{w_l} &= \mathbb{E}\left\{ \left(\sum_{\substack{m=1 \\ m\neq l}}^{L} \mathbf{a}_m s_m + \mathbf{n}_l \right) \left(\sum_{\substack{m=1 \\ m\neq l}}^{L} \mathbf{a}_m s_m + \mathbf{n}_l \right)^H \right\} \\ &= \sum_{\substack{m=1 \\ m\neq l}}^{L} \mathbf{a}_m \mathbf{a}_m^H \sigma_{\mathrm{s}}^2 + \mathbf{N}_l \end{aligned} \tag{4.45}$$

where $\mathbf{N}_l = \text{diag}\left[\sigma_{\text{n}}^2, \sigma_{\text{n}}^2, \cdots, \sigma_{\text{n}}^2\left(1+D_l\right)\right]$, with

$$D_l = \sum_{m=1}^{L} P_m \mathbb{E}\{|h_{ml}|^2\} \sum_{\substack{r=1 \\ r\neq m}}^{L} \frac{1}{P_r \mathbb{E}\{|g_{rm}|^2\}} \tag{4.46}$$

and the covariance matrix $\mathbf{R}_{y_l}$ is

$$\begin{aligned} \mathbf{R}_{y_l} &= \mathbb{E}\{(\mathbf{a}_l s_l + \mathbf{w}_l)(\mathbf{a}_l s_l + \mathbf{w}_l)^H\} \\ &= \sum_{m=1}^{L} \mathbf{a}_m \mathbf{a}_m^H \sigma_{\text{s}}^2 + \mathbf{N}_l. \end{aligned} \tag{4.47}$$

Hence, the spectral efficiency per time-slot achieved by Ul is written as

$$C_{\text{U}l}^{\text{MRCP-L}} = \frac{1}{L+1} \log_2 \frac{|\mathbf{R}_{y_l}|}{|\mathbf{R}_{w_l}|}. \tag{4.48}$$

Solving equation (4.48) as shown in appendix A.4, it can be shown that $C_{\text{U}l}^{\text{MRCP-L}}$ results in

$$C_{\text{U}l}^{\text{MRCP-L}} = \frac{1}{L+1} \mathbb{E}\left\{ \log_2 \left(1 + \gamma_{ll} + \frac{\overbrace{\Upsilon_l}^{\Gamma}}{\sum\limits_{\substack{m=1 \\ m\neq l}}^{L} \frac{\Upsilon_m}{1+\gamma_{ml}} + D_l + 1} \right) \right\}, \tag{4.49}$$

where

$$\Upsilon_l = \left(\sum_{\substack{r=1 \\ r\neq l}}^{L} \sqrt{\gamma_{rl}} \right)^2. \tag{4.50}$$

From equation (4.49) it is seen that Γ tends to zero as L increases. As a result, $C_{\text{U}l}^{\text{MRCP-L}}$ tends to $C_{\text{U}l}^{\text{TDMA-L}}$ as L increases.

Finally, using the results presented in appendix A.1, the BER of Ul is calculated as

$$\begin{aligned} \text{BER}_{\text{U}l}^{\text{MRCP-L}} = \frac{1}{\prod\limits_{m=1}^{L} \bar{\gamma_{ml}}} & \int_0^{\infty} \cdots \int_0^{\infty} Q\left(\sqrt{2\left(\gamma_{ll}+\Gamma\right)}\right) \\ & \exp\left(- \sum_{m=1}^{L} \frac{\gamma_{ml}}{\bar{\gamma_{ml}}} \right) d\gamma_{1l} d\gamma_{2l} \cdots d\gamma_{Ll}. \end{aligned} \tag{4.51}$$

Note that $\gamma_{ll} + \Gamma \leq \sum_{m=1}^{L} \gamma_{ml}$. Therefore, the diversity gain provided by this approach is larger than that of TDMA-L but smaller than that of DIV-L.

4.4 Performance Evaluation

In this section we compare the approaches analyzed in previous sections in terms of the JFI in Section 4.4.1, in terms of minimum spectral efficiency per time-slot in Section 4.4.2, and in terms of BER in Section 4.4.3. Throughout this section, we use the JFI as a quantitative measure of the fairness of the system and we use the minimum spectral efficiency per time-slot as a measure of the max-min fairness of the system. Finally, we also consider the BER using BPSK modulation as a measure of the diversity. Our evaluations consider BPSK modulation and a Rayleigh fading channel model with $\mathbb{E}\{|h_{ml}|^2\} = 1$ and $\mathbb{E}\{|g_{mn}|^2\} = 10\text{dB}\ \forall l, m, n$. Unless stated otherwise, we consider the same η_m from all but one base station, i.e. $\eta_1 = \eta_3 = \cdots = \eta_L = \bar{\eta}$ and $\eta_2 = 0\text{dB}$. This is done in order to evaluate the system performance with strongly asymmetric transmissions, typical of dense networks.

4.4.1 JFI Evaluation

The JFI can be interpreted as a quantitative measure of the "equality" in allocating resources to users. If all the users get the same amount of resources, then the system is 100% fair. If only a few users get most of the resources, then the JFI approaches zero. From this, it is easy to see that DIV and MRCP achieve the highest JFI since all the users benefit almost equally from the transmission of multiple base stations. In contrast, TDMA and INTF show a low fairness as they benefit only the user with the best conditions. This explains why when one user has a low SINR, the fairness of TDMA and INTF is very low for $L = 2$, while the effect of that unfairly treated user fades out with the rest of the users when L increases as seen in Fig. 4.2.

4.4.2 Spectral Efficiency Evaluation

Max-min fairness can be achieved with a high minimum spectral efficiency. In this sense, it is seen from equations (4.25) and (4.49), and confirmed from the numerical evaluations in this section that MRCP provides the highest max-min fairness. This can be seen for $L = 2$ in Figs. 4.3 and 4.4 and for different values of L in Fig. 4.6. This gain in minimum spectral efficiency increases not only with L, but also with $\bar{\eta}$ as can be seen in Fig. 4.5. Only for low values of $\bar{\eta}$, the

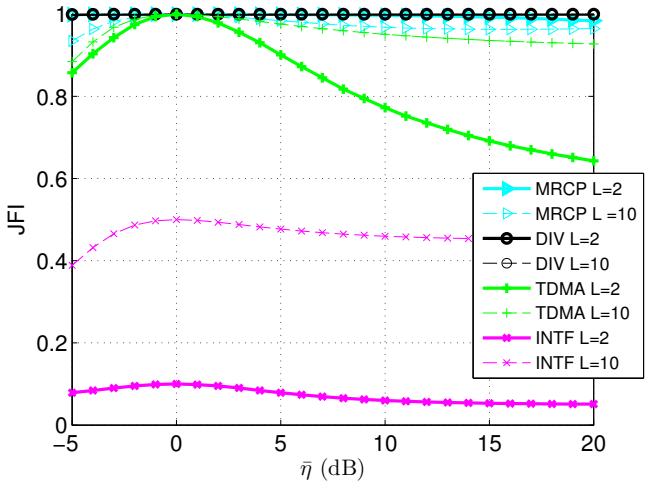

Figure 4.2: JFI for $L = 2$ and $L = 10$. We consider the same η_m from all but one base station, i.e. $\eta_1 = \eta_3 = \cdots = \eta_L = \bar{\eta}$ and $\eta_2 = 0$dB.

minimum spectral efficiency of INTF is higher due to the low interference level between users, which is not common in dense networks.

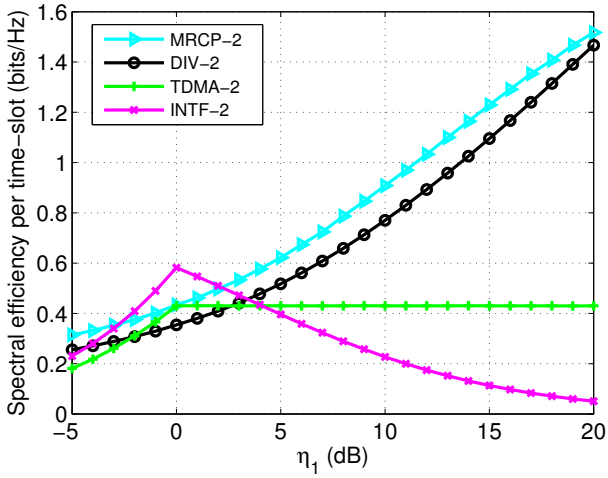

Figure 4.3: Minimum spectral efficiency per time-slot for $\eta_2 = 0$dB.

TDMA and INTF are not fair approaches in most conditions. For example, the minimum spectral efficiency of TDMA shows a flooring when $\eta_1 > \eta_2$ because the increase in η_1 benefits one user until its spectral efficiency reaches the

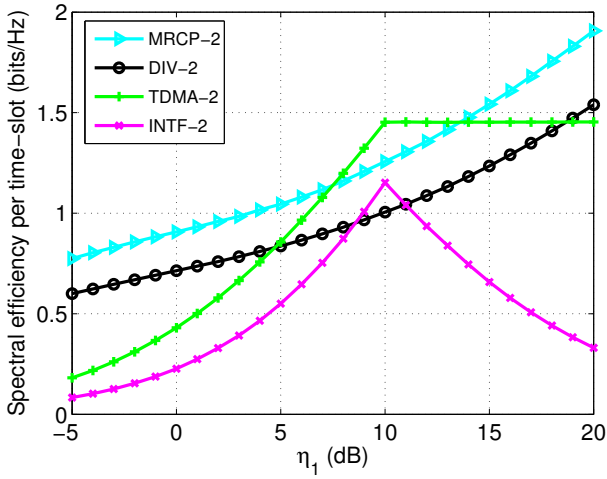

Figure 4.4: Minimum spectral efficiency per time-slot for $\eta_2 = 10$dB.

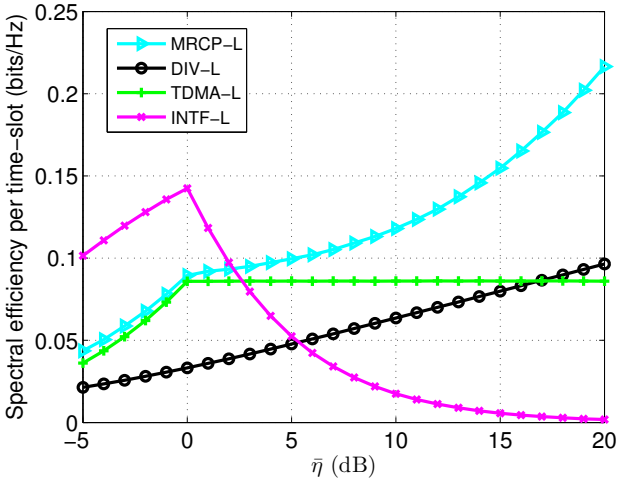

Figure 4.5: Minimum spectral efficiency per time-slot for L = 10. We consider the same η_m from all but one base station, i.e. $\eta_1 = \eta_3 = \cdots = \eta_L = \bar{\eta}$ and $\eta_2 = 0$dB.

spectral efficiency of the other user (see Figs. 4.3 and 4.4). A similar lack of fairness can be seen for $L = 10$ in Fig. 4.5. In the case of INTF, an increase in η_1 or $\bar{\eta}$ only increases the interference level, reducing the spectral efficiency.

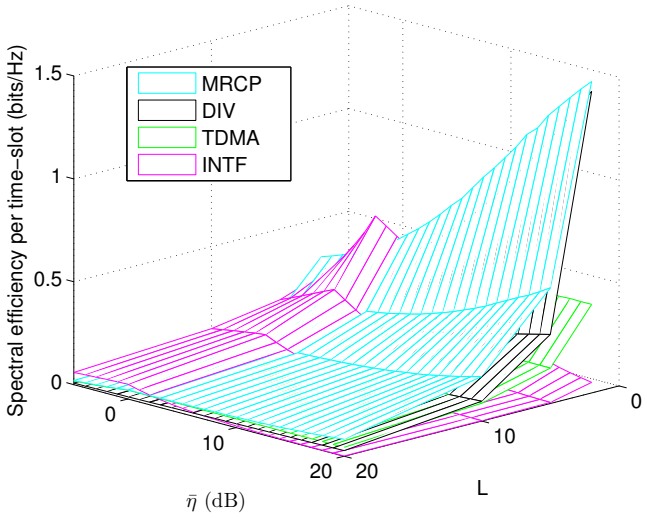

Figure 4.6: Minimum spectral efficiency of the studied approaches. We consider the same η_m from all but one base station, i.e. $\eta_1 = \eta_3 = \cdots = \eta_L = \bar{\eta}$ and $\eta_2 = 0$dB.

4.4.3 BER Evaluation

Let us first consider symmetric conditions with equal η_m from *all* the base stations (i.e. $\eta_1 = \eta_2 = \cdots = \eta_L = \bar{\eta}$), MRCP presents almost the same BER as DIV for $L = 2$, and it degrades smoothly for $L = 5$, 10, and 20 (see Fig. 4.7). In the limit, with a very large value of L, MRCP achieves a similar BER as TDMA since the diversity gain comes only from time-slot $L + 1$. Needless to say, INTF is the approach with the poorest BER since increasing the number of base stations only decreases the diversity gain. Since DIV exploits full diversity, it has the best BER performance compared to the other approaches and its diversity gain increases with L (see Fig. 4.7). This comes at a price of increasing the number of time-slots to L^2.

Dealing with asymmetric conditions, i.e. different values of η_m, is a more realistic scenario for dense networks. In this case, the performance of MRCP and DIV are both the highest compared to the other approaches due to the exploited spatial diversity, with a marginal difference between them (see Fig. 4.8). Also, as the value of η_2 increases from 0 to 10dB, the performance gap between MRCP and DIV remains the same, while the performance gap between them and TDMA and INTF increases.

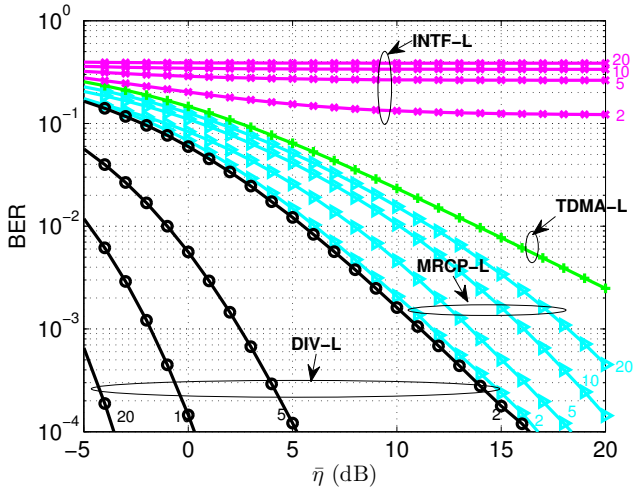

Figure 4.7: BER for BPSK for $L = 2, 5, 10, 20$ (small numbers). For simplicity we consider the same η_m from all the base stations $\eta_1 = \eta_2 = \cdots = \eta_L = \bar{\eta}$.

Note that the BER of TDMA is the same for all values of L due to the lack of diversity (see Fig. 4.7). Also, the BER of TDMA for $L = 2$ is the same for η_2 =0dB and η_2 =10dB as this is the BER of U1, which experiences no interference from U2 (see Fig. 4.8).

4.4.4 Final remarks

From the previous analysis of JFI, minimum spectral efficiency, and BER, we can conclude INTF and TDMA are both unfair approaches. On the other hand, DIV, closely followed by MRCP, can achieve the highest JFI fairness by exploiting the spatial diversity from the transmission of different base stations. However, the JFI fairness achieved by DIV comes at the cost of increasing the number of time-slots quadratically, while MRCP achieves the highest max-min fairness with less time-slots. This highlights the ability of MRCP to find a balance between spatial diversity and transmission time. Regarding the BER, DIV and MRCP are able to achieve the highest diversity gains with asymmetric transmissions.

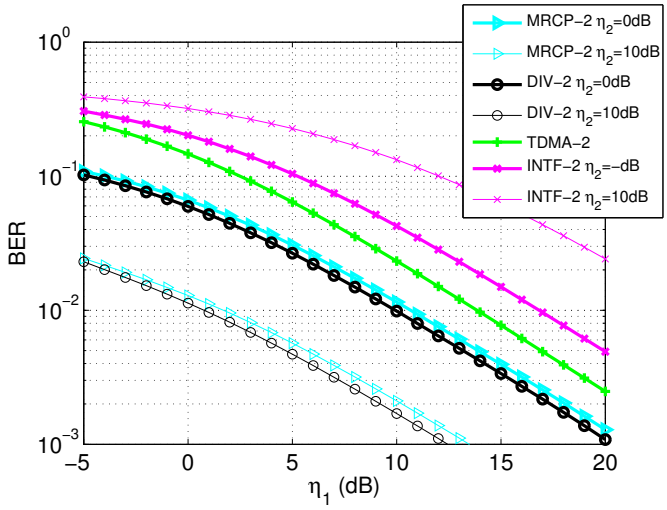

Figure 4.8: BER for BPSK for $L = 2$ and $\eta_2 = 0$dB, 10dB.

4.5 Conclusions

In this chapter we have proposed MRCP, a multiple-relay communication protocol for achieving fairness in dense networks. The proposed approach exploits spatial diversity without requiring a backhaul connection or additional infrastructure as it uses currently-deployed base stations as relays. In this way, the proposed approach is able to find an efficient balance between spatial diversity and transmission time. Also, different from other relaying-PNC schemes, MRCP is applicable to any number of base stations and users, while keeping a small transmission time.

We have shown that MRCP reaches almost maximum JFI fairness and the highest max-min fairness when compared to other communication schemes. This comes with a BER that reaches almost full diversity with asymmetric transmissions, typical of dense networks.

Chapter 5

Topology-Aware Space-Time Network Coding

Abstract

Space-Time Network Coding (STNC) is a time-division multiple access (TDMA)-based scheme that combines network coding and space-time coding by allowing relay nodes to combine the information received from different source nodes during the transmission phase and to forward the combined signal to a destination node in the relaying phase. However, STNC schemes require all the relay nodes to overhear the signals transmitted from all the source nodes in the network. They also require a large number of time-slots to achieve full diversity in a multipoint-to-multipoint transmission. Both conditions are particularly challenging for large cellular networks where, assuming a downlink transmission, base stations (BSs) and users only overhear a subset of all the BSs. In this chapter, we exploit basic knowledge of the network topology in order to reduce the number of time-slots by allowing simultaneous transmissions from those BSs that do not overhear each other. Our results show that these topology-aware schemes are able to increase the spectral efficiency per time-slot and BER with unequal transmit power and channel conditions.[1]

[1]This chapter is cited from Torrea-Duran, R., Plata-Chaves, J., Morales-Céspedes, M., Vandendorpe, L., Moonen, M., "Topology-Aware Space-Time Network Coding in Cellular Networks". Submitted to IEEE Access, 2017.

5.1 Introduction

Cooperative communication has emerged as a promising solution to satisfy the ever-increasing demand in wireless connectivity. Cooperative protocols exploit the broadcast nature of the wireless channel by allowing relay nodes to retransmit the overheard information to the destination nodes. This is usually done in two phases. In the first phase, the source nodes broadcast the information, which is received by the destination nodes and the relays. In the second phase, the relays forward this information to the destination nodes, which combine it with the information received from the source nodes in the first phase.

The cooperation between spatially distributed nodes requires perfect timing and frequency synchronization of the received signals. This is in practice a challenging task, for instance timing synchronization requires signals from different source nodes to arrive simultaneously at a destination node. Imperfect frequency synchronization results from the difference in the local oscillator frequency of every node. These imperfections results in intersymbol interference, which can bring a severe degradation of the system performance [48, 97]. The most commonly-used technique to completely avoid the imperfect synchronization issue in multi-node systems is time-division multiple access (TDMA), in which each transmitting node (source or relay) takes a dedicated time-slot to transmit information.

Space-Time Network Coding (STNC) [56] has been proposed as a TDMA-based technique to achieve cooperation among the nodes in a network while avoiding the synchronization issues. It combines network coding and space-time coding by allowing signals coming from different source nodes during the transmission phase to be combined at the relays and then forwarded to destination nodes in dedicated time-slots during the relaying phase. Considering a system with L source nodes, M relays and 1 destination node, STNC is able to achieve full diversity order of $M+1$ with $L+M$ time-slots. This multipoint-to-point (M2P) transmission can be translated into a point-to-multipoint (P2M) transmission by instead considering a single source node transmitting to multiple destination nodes. A step towards increasing the capacity of the previous scheme was taken in [91] and in [99], where the authors propose that each relay decodes the transmission not only from the source nodes but also from the previously-transmitting relays. Furthermore, the source nodes can also be used as relays (as assumed in this chapter), avoiding in this way the deployment of additional relays, as proposed in clustering-based STNC [42] and optimal node selection-based STNC schemes [12]. Although all the previous schemes focus on the P2M or M2P scenario, a multipoint-to-multipoint (M2M) transmission can be derived as a combination of the previous schemes [56].

A main disadvantage of the previous schemes is that they require that all the M relays (or the L source nodes acting as relays) overhear the signals transmitted by the L source nodes in order to forward the overheard information to the destination nodes. In a cellular downlink transmission for instance, relays (or base stations acting as relays) and users typically overhear only a subset of all the base stations (BSs), i.e. the closest BSs, and treat the other transmissions as noise [37]. Therefore, relay retransmissions are only useful to the closest users. Furthermore, the previous schemes require dedicated time-slots for each transmission in order to achieve full diversity order. These conditions render these schemes impractical in particular for large networks.

In this chapter we exploit basic knowledge of the network topology, i.e. the knowledge of the different subsets of BSs that can be overheard by other BSs and users. In this way, we are able to reduce the number of time-slots and hence make our schemes practical for large networks. This can be done in two ways: firstly by allowing simultaneous transmissions from the BSs that do not overhear each other, which can be done both during the transmission and during the relaying phase. Secondly, by allowing all the BSs to transmit the overheard information in a single time-slot during the relaying phase instead of using dedicated time-slots. This last scheme comes with an imperfect synchronization during the single time-slot of the relaying phase. However, recent advances in delay-tolerant codes [26] or joint frequency and timing synchronization [97] show that this issue can be mitigated.

We analyze in this chapter both proposed schemes in terms of spectral efficiency and bit error rate (BER). Our analytical and numerical results show that the topology-aware schemes are able to reduce drastically the number of time-slots and increase the spectral efficiency compared to traditional STNC, with a marginal decrease in the spatial diversity. Furthermore, we are able to compute closed-form expressions for the spectral efficiency and BER for any number of nodes, which allows us to analyze and predict the achievable gains for any network size and to compare it with other TDMA-based schemes.

This chapter is organized as follows. In Section 5.2 the system model is presented. Section 5.3 provides a brief overview of the baseline schemes used for benchmarking. In Section 5.4 the proposed topology-aware schemes are presented. Section 5.5 provides some simulation results where the performance of the proposed schemes is compared with the baseline schemes. Finally, Section 5.6 provides concluding remarks.

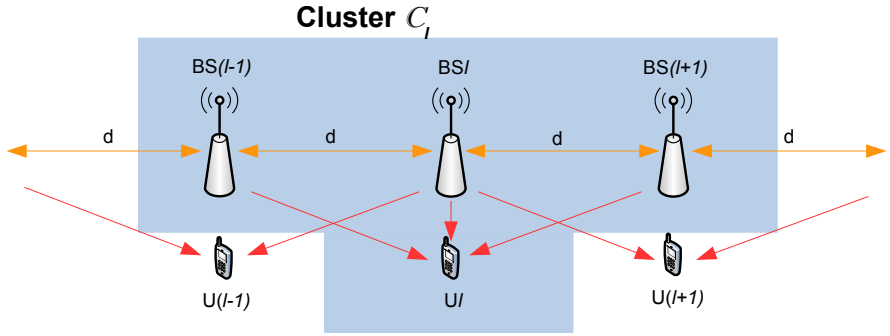

Figure 5.1: Wyner model for a cellular network. The cluster considers the $2K$ closest BSs, i.e. $\mathcal{C}_l = \text{BS}\{l-1, l, l+1\}$ for $K = 1$, with a distance d between BSs.

5.2 System Model

We consider a downlink cellular network with L single-antenna BSs, each of which has data intended for a specific user. To avoid the deployment of relays it is assumed that each BS can also act as a relay. It is assumed that the BSs and the users are half-duplex, i.e., they cannot transmit and receive simultaneously. The available network topology knowledge is limited to the knowledge of the different subsets of BSs that can be overheard by other BSs and users. We assume that there is no backhaul link between BSs (or that it is only used for transmitting control information), which excludes the use of transmission schemes that require data sharing among the BSs. Since we consider single-antenna BSs, notice that this condition excludes the use of space-time block codes, e.g., Alamouti codes. It is assumed that the intracell interference is avoided through orthogonal multiple access techniques, e.g., orthogonal frequency division multiple access (OFDMA), so that only the intercell interference is considered. In this context, the user connected to the l-th BS, which is referred to as Ul, is only subject to intercell interference from other BSs. Specifically, we consider a topological scheme where Ul receives all the signals from the cluster $\mathcal{C}_l$ composed by BSl and the neighboring $2K$ BSs. BSl can also overhear the transmission from the other BSs inside cluster $\mathcal{C}_l$. The transmissions from the BSs outside the cluster is then treated as noise.

For the sake of simplicity, we focus on the widely-used linear Wyner model [92] to formulate the considered system, as shown in Fig. 5.1. We assume a symmetric scenario where the BSs of $\mathcal{C}_l$ correspond to the K BSs on the left (numbered

BS($l-K$), ..., BS($l-1$)) and the K BSs on the right (numbered BS($l+1$), ..., BS($l+K$)) of BSl. We use shorthand notation with BS numbers to define clusters, e.g. $\mathcal{C}_l = \{l-K, ..., l-1, l, l+1, ..., l+K\}$. The BSs of cluster $\mathcal{C}_l$ that transmit in time-slot (TS) t are comprised in $\mathcal{C}_l^{(t)}$. Thus, assuming BS$l \in \mathcal{C}_l^{(t)}$, the signal received by Ul in TSt in the transmission phase can be written as

$$y_l^{(t)} = \sqrt{P_l} h_{l,l} s_l + \sum_{k \in \mathcal{C}_l^{(t)} \setminus l} i_{k,l}^{(t)} + n_l^{(t)}, \tag{5.1}$$

where $h_{k,l}$ is the channel between BSk and user Ul, which follows a Rayleigh distribution with zero mean and unit variance. Furthermore, P_l is the transmit power of BSl, s_l is the symbol transmitted by BSl intended for Ul, and $n_l^{(t)}$ is the additive white Gaussian noise (AWGN) with zero mean and variance σ_{n}^2, which is assumed to be equal for all the users. The parameter $i_{k,l}^{(t)}$ denotes the interference received by Ul from BSk in TSt. Therefore, $\sum_{k \in \mathcal{C}_l^{(t)} \setminus l} i_{k,l}^{(t)}$ corresponds to the intercell interference within cluster $\mathcal{C}_l$. We also define $\gamma_{k,l} = \sqrt{P_k} h_{k,l}$, $\xi_{m,n} = \sqrt{P_m} g_{m,n}$, where $g_{m,n}$ is the channel between BSm and BSn, and $\sigma_{\mathrm{s}}^2 = \mathbb{E}\{|s_l|^2\}$ $\forall l$. Finally, we assume that the channel coherence time is larger than the transmission round of each scheme, i.e. that the channel gains do not change within one transmission round.

5.3 Baseline Schemes

This section presents the baseline schemes that will be used to benchmark the performance of the proposed topology-aware schemes.

5.3.1 Simultaneous Transmissions Scheme (INTF)

The simplest baseline scheme consists in all the BSs transmitting simultaneously regardless of the interference that they cause to the users. This means that the transmission phase has one time-slot ($t = 1$) and that there is no relaying phase. We refer to this scheme as INTF. The signal received by Ul in TSt ($t = 1$) is given by (5.1) with $\mathcal{C}_l^{(t)} = \mathcal{C}_l$.

Since each BSl transmits to its corresponding user Ul in every time-slot, the spectral efficiency per time-slot for Ul can be directly computed as

$$S_l^{\mathrm{INTF}} = \mathbb{E}\left\{\log_2\left(1 + \frac{|\gamma_{l,l}|^2\sigma_{\mathrm{s}}^2}{\sigma_{\mathrm{n}}^2 + \sum\limits_{\substack{k=l-K \\ k\neq l}}^{l+K} |\gamma_{k,l}|^2\sigma_{\mathrm{s}}^2}\right)\right\}. \tag{5.2}$$

Notice that the use of every available time-slot by every BS typically leads to a considerable degradation in equivalent signal-to-interference-and-noise ratio (SINR) since the received signal is polluted by the interference from the surrounding BSs.

Using a minimum mean square error (MMSE) receiver with BPSK modulation over a Rayleigh fading channel (assumptions holding throughout this chapter), the BER can be computed in terms of the Q function as

$$\mathrm{BER}_l^{\mathrm{INTF}} = \mathbb{E}\left\{Q\left(\sqrt{2\gamma_{\mathrm{INTF}}}\right)\right\}, \tag{5.3}$$

where $\gamma_{\mathrm{INTF}} = |\gamma_{l,l}|^2\sigma_{\mathrm{s}}^2 / \left(\sigma_{\mathrm{n}}^2 + \sum_{\substack{k=l-K \\ k\neq l}}^{l+K} |\gamma_{k,l}|^2\sigma_{\mathrm{s}}^2\right)$.

5.3.2 Orthogonal Transmissions Scheme (TDMA)

For an orthogonal scheme such as TDMA, the communication is done in turns. Since two BSs separated by $K+1$ BSs do not overhear each other, they can transmit simultaneously. For instance, in TS1, BS$(l-K)$ and BS$(l+1)$ can transmit s_{l-K}, and s_{l+1} simultaneously to their corresponding user, while the other BSs of $\mathcal{C}_l$ are inactive. Then in TS2, BS$(l-K+1)$ and BS$(l+2)$ can transmit s_{l-K+1}, and s_{l+2} simultaneously to their corresponding user, while the other BSs of $\mathcal{C}_l$ are inactive. The process continues until in TS$(K+1)$ BSl transmits s_l to Ul. This allows a similar strategy in the rest of the network and hence the interference from neighboring BSs can be completely avoided. The transmission strategy of this topology-aware TDMA for a cluster of 3 BSs $(K=1)$ is summarized in Table 5.1 (the shaded part corresponds to $\mathcal{C}_l$).

For this TDMA scheme, the signal received by user Ul from BSl in TSt, i.e. in the time-slot in which the user is served, can be written as

$$y_l^{(t)} = \sqrt{P_l}h_{l,l}s_l + n_l^{(t)}. \tag{5.4}$$

Table 5.1: TDMA transmission strategy

Time-slot	BS($l-3$)	BS($l-2$)	BS($l-1$)	BSl	BS($l+1$)	BS($l+2$)	BS($l+3$)
TS1	s_{l-3}		s_{l-1}		s_{l+1}		s_{l+3}
TS2		s_{l-2}		s_l		s_{l+2}	

Since $K+1$ time-slots are required to complete the transmission to all the users, the spectral efficiency per time-slot of TDMA for Ul can be directly computed as

$$S_l^{\mathrm{TDMA}} = \frac{1}{K+1}\mathbb{E}\left\{\log_2\left(1+\frac{|\gamma_{l,l}|^2\sigma_{\mathrm{s}}^2}{\sigma_{\mathrm{n}}^2}\right)\right\}. \tag{5.5}$$

Notice the pre-log factor of $\frac{1}{K+1}$, which can be interpreted as the multiplexing gain.

The BER of Ul can be computed as [78]

$$\begin{aligned}\mathrm{BER}_l^{\mathrm{TDMA}} &= \mathbb{E}\left\{Q\left(\sqrt{\frac{2|\gamma_{l,l}|^2\sigma_{\mathrm{s}}^2}{\sigma_{\mathrm{n}}^2}}\right)\right\} \\ &= \frac{1}{\pi}\int_0^{\pi/2}\left(\frac{1}{1+\frac{\bar{\gamma_{l,l}}}{\sin^2\phi}}\right)d\phi \approx \frac{1}{\bar{\gamma_{l,l}}},\end{aligned} \tag{5.6}$$

where $\bar{\gamma_{k,l}} = \mathbb{E}\{|\gamma_{k,l}|^2\}\frac{\sigma_{\mathrm{s}}^2}{\sigma_{\mathrm{n}}^2} = \frac{P_k\mathbb{E}\{|h_{k,l}|^2\}\sigma_{\mathrm{s}}^2}{\sigma_{\mathrm{n}}^2}$ and the approximation holds in the high SNR regime [40]. From the last approximation of equation (5.6), it can be seen that the BER is independent of K and hence no diversity gain is achieved.

5.3.3 Modified STNC (mSTNC)

In order to achieve full diversity in a scenario where BSs and users overhear the BSs inside their cluster, we require the use of dedicated time-slots per transmission. Hence, here we redefine the M2M transmission scheme using STNC presented in [56] for this scenario. We refer to this scheme as mSTNC, which can be explained as follows.

In a first (transmission) phase each BS of the considered cluster $\mathcal{C}_l$ transmits the symbol intended for its corresponding user in a dedicated time-slot while all the other BSs in $\mathcal{C}_l$ (as well as in the cluster of the transmitting BSs) remain silent. In a second (relaying) phase, each BS of cluster $\mathcal{C}_l$ transmits one of the symbols overheard in the first phase in a dedicated time-slot. In a third (relaying) phase, each BS of cluster $\mathcal{C}_l$ transmits another of the symbols overheard in the first phase in a dedicated time-slot. This process continues until in phase $2K+1$

Table 5.2: mSTNC transmission strategy ($K = 1$)

Time-slot	BS($l-3$)	BS($l-2$)	BS($l-1$)	BSl	BS($l+1$)	BS($l+2$)	BS($l+3$)
TS1			s_{l-1}			s_{l+2}	
TS2	s_{l-3}			s_l			s_{l+3}
TS3		s_{l-2}			s_{l+1}		
TS4			s_l			s_{l+3}	
TS5	s_{l-2}			s_{l+1}			s_{l+4}
TS6		s_{l-1}			s_{l+2}		
TS7			s_{l-2}			s_{l+1}	
TS8	s_{l-4}			s_{l-1}			s_{l+2}
TS9		s_{l-3}			s_l		

each BS of cluster $\mathcal{C}_l$ transmits the last of the symbols overheard in the first phase in a dedicated time-slot. Hence this scheme requires $(2K+1)^2$ time-slots for one transmission round.

The transmission strategy of mSTNC for $K = 1$ is summarized in Table 5.2 (the shaded part corresponds to $\mathcal{C}_l$). Focusing on the l-th user, the symbol s_l is received in three time-slots (TS2, TS4, and TS9) corresponding to the transmission from BSs $\{l, l-1, l+1\}$. Specifically, the received signal can then be expressed as

$$\begin{aligned} y_l^{(2)} &= \sqrt{P_l} h_{l,l} s_l + n_l^{(2)} \\ y_l^{(4)} &= \sqrt{P_{l-1}} h_{l-1,l} z_{l,l-1}^{(2)} + n_l^{(4)} \\ y_l^{(9)} &= \sqrt{P_{l+1}} h_{l+1,l} z_{l,l+1}^{(2)} + n_l^{(9)} \end{aligned} \tag{5.7}$$

where the relayed symbol $z_{m,n}^{(t)}$ is defined as

$$z_{m,n}^{(t)} = s_m + \frac{n_{\mathrm{BS}n}^{(t)}}{\sqrt{P_m} g_{m,n}}, \tag{5.8}$$

where $n_{\mathrm{BS}n}^{(t)}$ is the AWGN noise received by BSn in TSt with zero mean and variance also assumed to be equal to σ_{n}^2. Notice that the interference from the BSs inside cluster $\mathcal{C}_l$ is completely avoided.

The spectral efficiency per time-slot of mSTNC for Ul (calculated as described in Section 5.4) can be directly computed as

$$S_l^{\mathrm{mSTNC}} = \frac{1}{(2K+1)^2} \mathbb{E}\left\{\log_2\left(1 + \gamma_{\mathrm{mSTNC}}\right)\right\}, \tag{5.9}$$

where

$$\gamma_{\mathrm{mSTNC}} = \frac{|\gamma_{l,l}|^2 \sigma_{\mathrm{s}}^2}{\sigma_{\mathrm{n}}^2} + \sum_{\substack{k=l-K \\ k \neq l}}^{l+K} \frac{|\gamma_{k,l}|^2 \sigma_{\mathrm{s}}^2}{\frac{|\gamma_{k,l}|^2 \sigma_{\mathrm{n}}^2}{|\xi_{l,k}|^2} + \sigma_{\mathrm{n}}^2} \tag{5.10}$$

Notice that mSTNC ensures that each user receives its symbol from the $2K+1$ BSs of the cluster in dedicated time-slots.

The BER of Ul can be computed as

$$\mathrm{BER}_l^{\mathrm{mSTNC}} = \mathbb{E}\left\{Q\left(\sqrt{2\gamma_{\mathrm{mSTNC}}}\right)\right\}. \tag{5.11}$$

Since γ_{mSTNC} is not affected by any interference from other BSs within cluster $\mathcal{C}_l$, mSTNC can achieve full diversity gain of $2K+1$.

5.4 Topology-Aware STNC (TAS)

While INTF provides full multiplexing gain, it comes with a large interference from the neighboring BSs. On the other hand, mSTNC provides full diversity gain with a large number of time-slots. Exploiting the topology of the network can provide a trade-off between diversity and multiplexing gain. We propose two schemes to achieve this. The first scheme consists in allowing simultaneous transmissions from the BSs that do not overhear each other both during the transmission phase and during the relaying phase. We refer to it as TAS1. A second scheme consists in allowing simultaneous transmissions as in TAS1 during the transmission phase, while during the relaying phase all the BSs transmit the overheard information in a single time-slot. We refer to it as TAS2 and it shares the same rationale as the MRCP approach described in Chapter 4. These schemes are described in the next two sections.

5.4.1 Simple Case with $K = 1$

In this scenario each user receives the transmissions from the closest 3 BSs. Similarly, each BS overhears the transmissions from the closest 2 BSs (one to the right and one to the left). Therefore, all the even-numbered BSs will not cause interference to any particular user when transmitting simultaneously, and neither will the odd-numbered BSs when transmitting simultaneously. Based on this, the proposed schemes work as follows.

In TS1, BS$(l-1)$ and BS$(l+1)$ transmit simultaneously the symbol intended for their corresponding user, i.e. s_{l-1} and s_{l+1}, respectively, as shown in Fig. 5.2. Hence, U$(l-1)$ and U$(l+1)$ receive their desired symbol without interference from other BSs. BSl and Ul also overhear a combination of symbols s_{l-1} and s_{l+1}. In TS2 BSl transmits s_l avoiding the interference from the BSs in cluster $\mathcal{C}_l$ as shown in Fig. 5.3. This means that Ul receives s_l without interference

from other BSs. Due to the overhearing capabilities of the network, BS$(l-1)$ and BS$(l+1)$ (and also U$(l-1)$ and U$(l+1)$) receive a combination of symbols including s_l. The transmission phase thus corresponds to TDMA (Table 5.1). The relaying phase is different between TAS1 and TAS2. For TAS1, in TS3 BS$(l-1)$ and BS$(l+1)$ transmit simultaneously the combination of overheard symbols from TS2 as shown in Fig. 5.4. Finally in TS4, BSl transmits the combination of the overheard symbols s_{l-1} and s_{l+1} from TS1 as shown in Fig. 5.5. For TAS2, in TS3 each BS transmits simultaneously the combination of overheard symbols from TS1 or TS2 as shown in Fig. 5.6. As a result, in both schemes Ul receives its desired symbol s_l from all the BSs in cluster $\mathcal{C}_l$ in one transmission round. The transmission strategy of the proposed schemes for $K = 1$ is summarized in Table 5.3 for TAS1 and Table 5.4 for TAS2. Note that the BSs outside the cluster have a similar transmission scheme.

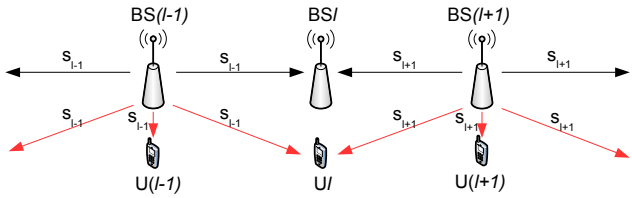

Figure 5.2: Transmission phase TAS1 and TAS2. BS$(l-1) \rightarrow s_{l-1}$ and BS$(l+1)$ $\rightarrow s_{l+1}$.

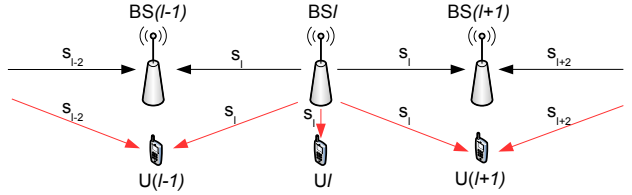

Figure 5.3: Transmission phase TAS1 and TAS2. BS$l \rightarrow s_l$.

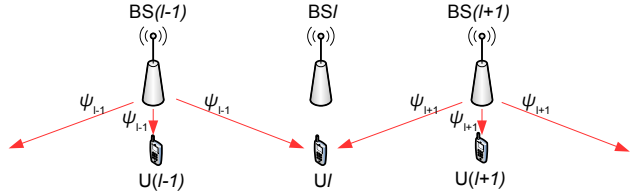

Figure 5.4: Relaying phase TAS1. BS$(l-1) \rightarrow s_{l-2}+s_l$ and BS$(l+1) \rightarrow s_l+s_{l+2}$.

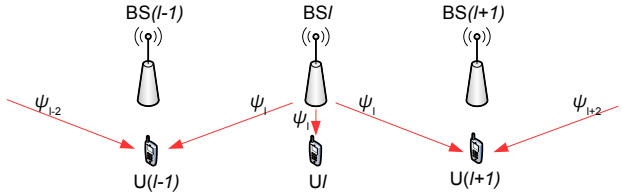

Figure 5.5: Relaying phase TAS1. BS$l \to s_{l-1} + s_{l+1}$.

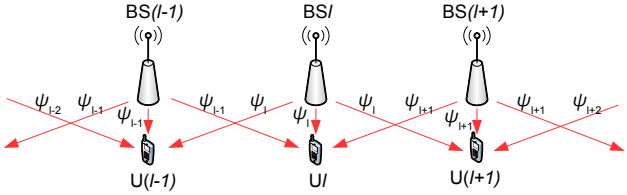

Figure 5.6: Relaying phase TAS2. BS$(l-1) \to s_{l-2} + s_l$, BS$l \to s_{l-1} + s_{l+1}$, and BS$(l+1) \to s_l + s_{l+2}$.

For TAS1, the received signals for Ul can be expressed as

$$\begin{aligned} y_l^{(1)} &= \sqrt{P_{l-1}} h_{l-1,l} s_{l-1} + \sqrt{P_{l+1}} h_{l+1,l} s_{l+1} + n_l^{(1)} \\ y_l^{(2)} &= \sqrt{P_l} h_{l,l} s_l + n_l^{(2)} \\ y_l^{(3)} &= \sqrt{P_{l-1}} h_{l-1,l} \psi_{l-1} + \sqrt{P_{l+1}} h_{l+1,l} \psi_{l+1} + n_l^{(3)} \\ y_l^{(4)} &= \sqrt{P_l} h_{l,l} \psi_l + n_l^{(4)}, \end{aligned} \tag{5.12}$$

where the relayed symbols are normalized by the total received power to avoid exceeding the maximum transmit power:

$$\psi_k = \frac{\sqrt{P_{k-1}} g_{k-1,k} s_{k-1} + \sqrt{P_{k+1}} g_{k+1,k} s_{k+1} + n_{\mathrm{BS}k}^{(\tau)}}{\tilde{P}_{k-1,k}} \tag{5.13}$$

where τ is the time-slot in which BSk receives the transmission from BS$(k-1)$ and BS$(k+1)$ and $\tilde{P}_{m,k} = P_m |g_{m,k}|^2 + P_{m+K+1} |g_{m+K+1,k}|^2 + \frac{\sigma_{\mathrm{n}}^2}{\sigma_{\mathrm{s}}^2}$, corresponding to the power received by BSk from BSm and from BS$(m+K+1)$. For $K=1$, $m = k-1$ and $m+K+1 = k+1$. Notice that the normalization is such that the transmission power in the relaying phase is equal to the transmission power in the transmission phase.

Table 5.3: TAS1 transmission strategy ($K = 1$)

Time-slot	BS$(l-3)$	BS$(l-2)$	BS$(l-1)$	BSl	BS$(l+1)$	BS$(l+2)$	BS$(l+3)$
TS1	s_{l-3}		s_{l-1}		s_{l+1}		s_{l+3}
TS2		s_{l-2}		s_l		s_{l+2}	
TS3	$s_{l-4}+$ s_{l-2}		$s_{l-2}+$ s_l		s_l+ s_{l+2}		$s_{l+2}+$ s_{l+4}
TS4		$s_{l-3}+$ s_{l-1}		$s_{l-1}+$ s_{l+1}		$s_{l+1}+$ s_{l+3}	

Table 5.4: TAS2 transmission strategy ($K = 1$)

Time-slot	BS$(l-3)$	BS$(l-2)$	BS$(l-1)$	BSl	BS$(l+1)$	BS$(l+2)$	BS$(l+3)$
TS1	s_{l-3}		s_{l-1}		s_{l+1}		s_{l+3}
TS2		s_{l-2}		s_l		s_{l+2}	
TS3	$s_{l-4}+$ s_{l-2}	$s_{l-3}+$ s_{l-1}	$s_{l-2}+$ s_l	$s_{l-1}+$ s_{l+1}	s_l+ s_{l+2}	$s_{l+1}+$ s_{l+3}	$s_{l+2}+$ s_{l+4}

For TAS2, the received signals for Ul can be expressed as

$$\begin{aligned} y_l^{(1)} &= \sqrt{P_{l-1}} h_{l-1,l} s_{l-1} + \sqrt{P_{l+1}} h_{l+1,l} s_{l+1} + n_l^{(1)} \\ y_l^{(2)} &= \sqrt{P_l} h_{l,l} s_l + n_l^{(2)} \\ y_l^{(3)} &= \sqrt{P_l} h_{l,l} \psi_l^{(1)} + \sum_{\substack{k=l-1 \\ k \neq l}}^{l+1} \sqrt{P_k} h_{k,l} \psi_k^{(2)} + n_l^{(3)}. \end{aligned} \tag{5.14}$$

Notice that the desired symbol s_l for Ul is received from three signal paths. Specifically, from its corresponding BSl in a dedicated time-slot during the transmission phase and from BS$(l-1)$ and BS$(l+1)$ during the relaying phase.

To represent the normalized channels effectively used to relay the overheard symbols during the relaying phase let us define

$$\eta_{m,l}^{v,w} = \frac{\gamma_{m,l} \xi_{v,m}}{\tilde{P}_{w,m}}, \tag{5.15}$$

corresponding to the relaying of s_v from BSm to Ul, normalized by the power received by BSm resulting from the transmission from BSw and from BS$(w + K + 1)$ (one of which is also BSv).

Equation (5.12) can then be expressed in a matrix form as (5.16) and equation (5.14) as (5.17).

$$\mathbf{y}_l = \underbrace{\begin{bmatrix} 0 & \gamma_{l-1,l} & 0 & \gamma_{l+1,l} & 0 \\ 0 & 0 & \gamma_{l,l} & 0 & 0 \\ \eta_{l-1,l}^{l-2,l-2} & 0 & \eta_{l-1,l}^{l,l-2} + \eta_{l+1,l}^{l,l} & 0 & \eta_{l+1,l}^{l+2,l} \\ 0 & \eta_{l,l}^{l-1,l-1} & 0 & \eta_{l,l}^{l+1,l-1} & 0 \end{bmatrix}}_{\mathbf{C}} \begin{bmatrix} s_{l-2} \\ s_{l-1} \\ s_l \\ s_{l+1} \\ s_{l+2} \end{bmatrix} + \begin{bmatrix} n_l^{(1)} \\ n_l^{(2)} \\ n_l^{(3)} + \frac{\gamma_{l-1,l} n_{\mathrm{BS}(l-1)}^{(2)}}{\tilde{P}_{l-2,l-1}} + \frac{\gamma_{l+1,l} n_{\mathrm{BS}(l+1)}^{(2)}}{\tilde{P}_{l,l+1}} \\ n_l^{(4)} + \frac{\gamma_{l,l} n_{\mathrm{BS}l}^{(1)}}{\tilde{P}_{l-1,l}} \end{bmatrix} \tag{5.16}$$

$$\mathbf{y}_l = \underbrace{\begin{bmatrix} 0 & \gamma_{l-1,l} & 0 & \gamma_{l+1,l} & 0 \\ 0 & 0 & \gamma_{l,l} & 0 & 0 \\ \eta_{l-1,l}^{l-2,l-2} & \eta_{l,l}^{l-1,l-1} & \eta_{l-1,l}^{l,l-2} + \eta_{l+1,l}^{l,l} & \eta_{l,l}^{l+1,l-1} & \eta_{l+1,l}^{l+2,l} \end{bmatrix}}_{\mathbf{B}} \begin{bmatrix} s_{l-2} \\ s_{l-1} \\ s_l \\ s_{l+1} \\ s_{l+2} \end{bmatrix} + \begin{bmatrix} n_l^{(1)} \\ n_l^{(2)} \\ n_l^{(3)} + \frac{\gamma_{l,l} n_{\mathrm{BS}l}^{(1)}}{\tilde{P}_{l-1,l}} + \frac{\gamma_{l-1,l} n_{\mathrm{BS}(l-1)}^{(2)}}{\tilde{P}_{l-2,l-1}} + \frac{\gamma_{l+1,l} n_{\mathrm{BS}(l+1)}^{(2)}}{\tilde{P}_{l,l+1}} \end{bmatrix} \tag{5.17}$$

In the next section, we derive the general expressions of the received signal for a general $K \geq 1$ and then compute the achieved spectral efficiency.

5.4.2 General Case with $K \geq 1$

In TS1 of the transmission phase a first pair of BSs within cluster $\mathcal{C}_l$ *that do not overhear each other* (nor do they overhear the transmitting BSs in other clusters), i.e. BS$(l-K)$ and BS$(l+1)$, transmit simultaneously the symbol intended for their corresponding user, i.e. s_{l-K} and s_{l+1}, respectively. In TS2 the next pair of BSs, i.e. BS$(l-K+1)$ and BS$(l+2)$, transmit s_{l-K+1} and s_{l+2}, respectively. This continues until finally, in TS$(K+1)$ the middle BS of cluster $\mathcal{C}_l$, i.e. BSl, transmits s_l. Meanwhile, the BSs outside cluster $\mathcal{C}_l$ can use a similar transmission strategy. The transmission phase thus corresponds to TDMA. Once the transmission phase ($K+1$ time-slots) concludes, each

BS has overheard the combination of the symbols from its $2K$ neighboring BSs. For TAS1, in the relaying phase ($K+1$ time-slots) the same pairs of BSs transmit the combination of overheard symbols in dedicated time-slots. For TAS2 in the relaying phase (1 time-slot), all the BSs transmit simultaneously the combination of overheard symbols.

For TAS1, the received signals for Ul can be expressed as

$$\begin{aligned}
y_l^{(1)} &= \sqrt{P_{l-K}}h_{l-K,l}s_{l-K} + \sqrt{P_{l+1}}h_{l+1,l}s_{l+1} + n_l^{(1)} \\
y_l^{(2)} &= \sqrt{P_{l-K+1}}h_{l-K+1,l}s_{l-K+1} + \sqrt{P_{l+2}}h_{l+2,l}s_{l+2} + n_l^{(2)} \\
&\vdots \\
y_l^{(K+1)} &= \sqrt{P_l}h_{l,l}s_l + n_l^{(K+1)} \\
y_l^{(K+2)} &= \sqrt{P_{l-K}}h_{l-K,l}\Psi_{l-K} + \sqrt{P_{l+1}}h_{l+1,l}\Psi_{l+1} + n_l^{(K+2)} \\
y_l^{(K+3)} &= \sqrt{P_{l-K+1}}h_{l-K+1,l}\Psi_{l-K+1} + \sqrt{P_{l+2}}h_{l+2,l}\Psi_{l+2} + n_l^{(K+3)} \\
&\vdots \\
y_l^{(2K+2)} &= \sqrt{P_l}h_{l,l}\Psi_l + n_l^{(2K+2)},
\end{aligned} \tag{5.18}$$

where

$$\Psi_k = \frac{1}{K}\sum_{m=1}^{K} \frac{\begin{pmatrix}\sqrt{P_{k-K+m-1}}g_{k-K+m-1,k}s_{k-K+m-1}+ \\ \sqrt{P_{k+m}}g_{k+m,k}s_{k+m} + n_{\mathrm{BS}k}^{(\tau)}\end{pmatrix}}{\tilde{P}_{k-K+m-1,k}}. \tag{5.19}$$

Note that τ depends on m and k as it is is the time-slot in which BSk receives the transmissions from BS$(k-K+m-1)$ and BS$(k+m)$. Also note that each of the K terms of (5.19) is normalized independently, which requires a $1/K$ factor to have the same transmission power in the relaying phase and the transmission phase. The normalization is done independently for each term so that large differences in transmission power and/or average channel gains only affect the symbols relayed in a given time-slot.

For TAS2, the received signals for Ul can be expressed as

$$\begin{aligned} y_l^{(1)} &= \sqrt{P_{l-K}} h_{l-K,l} s_{l-K} + \sqrt{P_{l+1}} h_{l+1,l} s_{l+1} + n_l^{(1)} \\ y_l^{(2)} &= \sqrt{P_{l-K+1}} h_{l-K+1,l} s_{l-K+1} + \sqrt{P_{l+2}} h_{l+2,l} s_{l+2} + n_l^{(2)} \\ &\vdots \\ y_l^{(K+1)} &= \sqrt{P_l} h_{l,l} s_l + n_l^{(K+1)} \\ y_l^{(K+2)} &= \sqrt{P_l} h_{l,l} \Psi_l + \sum_{\substack{m=l-K \\ m \neq l}}^{l+K} \sqrt{P_m} h_{m,l} \Psi_m + n_l^{(K+2)} \end{aligned} \tag{5.20}$$

Following this scheme, the signal received by user Ul, $\mathbf{y}_l \in \mathbb{C}^{2(K+1)\times 1}$ for TAS1 and $\mathbf{y}_l \in \mathbb{C}^{(K+2)\times 1}$ for TAS2, can be written as equation (5.21)

$$\mathbf{y}_l = \mathbf{n}_l + \underbrace{\begin{bmatrix} \mathbf{0}_{K,K} & \operatorname{diag}\left(\{\gamma_{l',l}\}_{l'=l-K}^{l-1}\right) & \mathbf{0}_{K,1} & \operatorname{diag}\left(\{\gamma_{l',l}\}_{l'=l+1}^{l+K}\right) & \mathbf{0}_{K,K} \\ \mathbf{0}_{1,K} & \mathbf{0}_{1,K} & \gamma_{l,l} & \mathbf{0}_{1,K} & \mathbf{0}_{1,K} \\ \mathbf{H}_{\text{left}}^{\text{TAS}n} & & \mathbf{H}_{\text{cluster}_1}^{\text{TAS}n} + \mathbf{H}_{\text{cluster}_2}^{\text{TAS}n} & & \mathbf{H}_{\text{right}}^{\text{TAS}n} \end{bmatrix}}_{\mathbf{A}} \begin{bmatrix} \mathbf{s}_{\text{left}} \\ \mathbf{s}_{\text{cluster}} \\ \mathbf{s}_{\text{right}} \end{bmatrix} \tag{5.21}$$

where diag($\mathbf{a}$) denotes the diagonal matrix with the vector $\mathbf{a}$ as the main diagonal, $\mathbf{s}_{\text{cluster}} = \operatorname{col}\{s_{l'}\}_{l'=l-K}^{l+K}$ are the symbols intended for the users within cluster $\mathcal{C}_l$ and $\mathbf{s}_{\text{left}} = \operatorname{col}\{s_{l'}\}_{l'=l-2K}^{l-K-1}$ and $\mathbf{s}_{\text{right}} = \operatorname{col}\{s_{l'}\}_{l'=l+K+1}^{l+2K}$ are the symbols intended for the users outside the cluster to the left- and right-hand side, respectively. The first two rows of matrix $\mathbf{A}$ in equation (5.21) correspond to the transmission phase, which is equal for TAS1 and TAS2. However, the last row corresponds to the relaying phase, which is different for TAS1 and TAS2.

$$\mathbf{H}^{\mathrm{TAS1}}_{\mathrm{cluster}_1} =$$

$$\begin{bmatrix} 0 & \eta^{l-K+1,l-2K}_{l-K,l} & \cdots & \eta^{l-1,l-2-K}_{l-K,l} & \eta^{l,l-1-K}_{l-K,l} & 0 & 0 & \cdots & 0 \\ \eta^{l-K,l-K}_{l-K+1,l} & 0 & \cdots & \eta^{l-1,l-2-K}_{l-K+1,l} & \eta^{l,l-1-K}_{l-K+1,l} & \eta^{l+1,l-K}_{l-K+1,l} & 0 & \cdots & 0 \\ \vdots & \vdots & \ddots & \vdots & \vdots & \vdots & \vdots & \ddots & \vdots \\ \eta^{l-K,l-K}_{l-1,l} & \eta^{l-K+1,l-K+1}_{l-1,l} & \cdots & 0 & \eta^{l,l-1-K}_{l-1,l} & \eta^{l+1,l-K}_{l-1,l} & \eta^{l+2,l+1-K}_{l-1,l} & \cdots & 0 \\ \eta^{l-K,l-K}_{l,l} & \eta^{l-K+1,l-K+1}_{l,l} & \cdots & \eta^{l-1,l-1}_{l,l} & 0 & \eta^{l+1,l-K}_{l,l} & \eta^{l+2,l+1-K}_{l,l} & \cdots & \eta^{l+K,l-1}_{l,l} \end{bmatrix}$$

$$\in \mathbb{C}^{K+1\times 2K+1} \tag{5.22}$$

$$\mathbf{H}^{\mathrm{TAS1}}_{\mathrm{cluster}_2} =$$

$$\begin{bmatrix} 0 & \eta^{l-K+1,l-K+1}_{l+1,l} & \cdots & \eta^{l-1,l-1}_{l+1,l} & \eta^{l,l}_{l+1,l} & 0 & \eta^{l+2,l+1-K}_{l+1,l} & \cdots & \eta^{l+K,l-1}_{l+1,l} \\ 0 & 0 & \cdots & \eta^{l-1,l-1}_{l+2,l} & \eta^{l,l}_{l+2,l} & \eta^{l+1,l+1}_{l+2,l} & 0 & \cdots & \eta^{l+K,l-1}_{l+2,l} \\ \vdots & \vdots & \ddots & \vdots & \vdots & \vdots & \vdots & \ddots & \vdots \\ 0 & 0 & \cdots & 0 & \eta^{l,l}_{l+K,l} & \eta^{l+1,l+1}_{l+K,l} & \eta^{l+2,l+2}_{l+K,l} & \cdots & 0 \\ 0 & 0 & \cdots & 0 & 0 & 0 & 0 & \cdots & 0 \end{bmatrix}$$

$$\in \mathbb{C}^{K+1\times 2K+1} \tag{5.23}$$

Recall that TAS1 uses a relaying phase of equal duration as the transmission phase. Moreover, during the relaying phase the combination of overheard symbols is transmitted by each BS in dedicated time-slots. Referring to the last block row in matrix $\mathbf{A}$ of (5.21), this results in matrices (5.22) and (5.23) that contain the channel entries for the symbols $\mathbf{s}_{\mathrm{cluster}}$ corresponding to $\mathcal{C}_l$: $\mathbf{H}^{\mathrm{TAS1}}_{\mathrm{cluster}_1}$ contains the channel entries for the symbols relayed from the BSs of $\mathcal{C}_l$ to the left of BSl (including BSl) and $\mathbf{H}^{\mathrm{TAS1}}_{\mathrm{cluster}_2}$ contains the channel entries for the symbols relayed from the BSs of $\mathcal{C}_l$ to the right of BSl. Similarly,

$$\mathbf{H}^{\mathrm{TAS1}}_{\mathrm{left}} = \begin{bmatrix} \eta^{l-2K,l-2K}_{l-K,l} & \eta^{l-2K+1,l-2K+1}_{l-K,l} & \cdots & \eta^{l-K-1,l-K-1}_{l-K,l} \\ 0 & \eta^{l-2K+1,l-2K+1}_{l-K+1,l} & \cdots & \eta^{l-K-1,l-K-1}_{l-K+1,l} \\ \vdots & \vdots & \ddots & \vdots \\ 0 & 0 & \cdots & \eta^{l-K-1,l-K-1}_{l-1,l} \\ 0 & 0 & \cdots & 0 \end{bmatrix} \tag{5.24}$$

$$\in \mathbb{C}^{K+1\times K}$$

and

$$\mathbf{H}_{\text{right}}^{\text{TAS1}} = \begin{bmatrix} \eta_{l+1,l}^{l+K+1,l} & 0 & \cdots & 0 \\ \eta_{l+2,l}^{l+K+1,l} & \eta_{l+2,l}^{l+K+2,l+1} & \cdots & 0 \\ \vdots & \vdots & \ddots & \vdots \\ \eta_{l+K,l}^{l+K+1,l} & \eta_{l+K,l}^{l+K+2,l+1} & \cdots & \eta_{l+K,l}^{l+2K,l+K-1} \\ 0 & 0 & \cdots & 0 \end{bmatrix} \in \mathbb{C}^{K+1\times K} \tag{5.25}$$

contain the channel entries for the symbols $\mathbf{s}_{\text{left}}$ and $\mathbf{s}_{\text{right}}$, respectively. Note that BSl transmits without interference from the other BSs in cluster $\mathcal{C}_l$ in the last time-slot of both phases. Specifically in the relaying phase, this transmission includes all the symbols of $\mathcal{C}_l$ except s_l.

Since TAS2 uses a relaying phase consisting of a single time-slot where the combination of overheard symbols is transmitted by all the BSs simultaneously, then the channel matrices are a row vector formed by the *summation* of the rows of $\mathbf{H}_{\text{cluster}_1}^{\text{TAS1}}$, $\mathbf{H}_{\text{cluster}_2}^{\text{TAS1}}$, $\mathbf{H}_{\text{left}}^{\text{TAS1}}$, and $\mathbf{H}_{\text{right}}^{\text{TAS1}}$, i.e.

$$\mathbf{H}_{\text{cluster}_1}^{\text{TAS2}} = \begin{bmatrix} \sum_{m=1}^{K+1} \mathbf{h}_{\text{cluster}_1}^{\text{TAS1},1}(m) & \sum_{m=1}^{K+1} \mathbf{h}_{\text{cluster}_1}^{\text{TAS1},2}(m) & \cdots & \sum_{m=1}^{K+1} \mathbf{h}_{\text{cluster}_1}^{\text{TAS1},2K+1}(m) \end{bmatrix} \tag{5.26}$$

$\in \mathbb{C}^{1\times 2K+1}$

$$\mathbf{H}_{\text{cluster}_2}^{\text{TAS2}} = \begin{bmatrix} \sum_{m=1}^{K+1} \mathbf{h}_{\text{cluster}_2}^{\text{TAS1},1}(m) & \sum_{m=1}^{K+1} \mathbf{h}_{\text{cluster}_2}^{\text{TAS1},2}(m) & \cdots & \sum_{m=1}^{K+1} \mathbf{h}_{\text{cluster}_2}^{\text{TAS1},2K+1}(m) \end{bmatrix} \tag{5.27}$$

$\in \mathbb{C}^{1\times 2K+1}$

$$\mathbf{H}_{\text{left}}^{\text{TAS2}} = \begin{bmatrix} \sum_{m=1}^{K+1} \mathbf{h}_{\text{left}}^{\text{TAS1},1}(m) & \sum_{m=1}^{K+1} \mathbf{h}_{\text{left}}^{\text{TAS1},2}(m) & \cdots & \sum_{m=1}^{K+1} \mathbf{h}_{\text{left}}^{\text{TAS1},K}(m) \end{bmatrix} \tag{5.28}$$

$\in \mathbb{C}^{1\times K}$

$$\mathbf{H}_{\text{right}}^{\text{TAS2}} =$$

$$\left[\sum_{m=1}^{K+1}\mathbf{h}_{\text{right}}^{\text{TAS1},1}(m) \quad \sum_{m=1}^{K+1}\mathbf{h}_{\text{right}}^{\text{TAS1},2}(m) \quad \cdots \quad \sum_{m=1}^{K+1}\mathbf{h}_{\text{right}}^{\text{TAS1},K}(m)\right] \tag{5.29}$$

$$\in \mathbb{C}^{1\times K}$$

where $\mathbf{h}_{\text{text}}^{\text{TAS}n,k}(m)$ is the m-th element of the k-th column of matrix $\mathbf{H}_{\text{text}}^{\text{TAS}n}$. In this way, it can be seen that for $K = 1$ equation (5.21) reduces to (5.16) for TAS1 and to (5.17) for TAS2.

The noise vector $\mathbf{n}_l$ of equation (5.21) is defined for TAS1 as

$$\begin{aligned}
&\mathbf{n}_l = \\
&\left[n_l^{(1)} \quad \cdots \quad n_l^{(K+1)}\right. \\
&\left(n_l^{(K+2)} + \tfrac{1}{K}\sum_{m=1}^{K}\frac{\gamma_{l-K,l}n_{\text{BS}(l-K)}^{(\tau)}}{\tilde{P}_{l-2K+m-1,l-K}} + \frac{1}{K}\sum_{m=1}^{K}\frac{\gamma_{l+1,l}n_{\text{BS}(l+1)}^{(\tau)}}{\tilde{P}_{l-K+m,l+1}}\right) \\
&\left(n_l^{(K+3)} + \tfrac{1}{K}\sum_{m=1}^{K}\frac{\gamma_{l-K+1,l}n_{\text{BS}(l-K+1)}^{(\tau)}}{\tilde{P}_{l-2K+m,l-K+1}} + \frac{1}{K}\sum_{m=1}^{K}\frac{\gamma_{l+2,l}n_{\text{BS}(l+2)}^{(\tau)}}{\tilde{P}_{l+1-K+m,l+2}}\right) \\
&\cdots \\
&\left.\left(n_l^{(2K+2)} + \tfrac{1}{K}\sum_{m=1}^{K}\frac{\gamma_{l,l}n_{\text{BS}l}^{(\tau)}}{\tilde{P}_{l-K+m-1,l}}\right)\right]^T \\
&\in \mathbb{C}^{1\times 2K+2}
\end{aligned} \tag{5.30}$$

and for TAS2 as

$$\begin{aligned}
\mathbf{n}_l = \Bigg[&n_l^{(1)} \quad \cdots \quad n_l^{(K+1)} \\
&\left(n_l^{(K+2)} + \frac{1}{K}\sum_{k=l-K}^{l+K}\gamma_{k,l}\sum_{m=1}^{K}\frac{n_{\text{BS}k}^{(\tau)}}{\tilde{P}_{k-K+m-1,k}}\right)\Bigg]^T \\
&\in \mathbb{C}^{1\times K+2}
\end{aligned} \tag{5.31}$$

5.4.3 Performance Analysis

Formula (5.21) can also be written as

$$\mathbf{y}_l = \sum_{k=l-2K}^{l+2K} \mathbf{a}_k s_k + \mathbf{n}_l = \mathbf{a}_l s_l + \mathbf{w}_l, \tag{5.32}$$

where $\mathbf{a}_l$ is the column of matrix $\mathbf{A}$ in (5.21) corresponding to s_l and $\mathbf{w}_l$ is the vector of interference plus noise $\mathbf{w}_l = \sum_{\substack{k=l-2K \\ k\neq l}}^{l+2K} \mathbf{a}_k s_k + \mathbf{n}_l$.

Using the well-known expression for the entropy of a multivariate complex Gaussian distribution [25] the capacity of the system is computed as

$$\begin{aligned} \log_2 \frac{|\mathbf{R}_{\mathbf{y}_l}|}{|\mathbf{R}_{\mathbf{w}_l}|} &= \log_2 \left(1 + \mathbf{a}_l^H \mathbf{R}_{\mathbf{w}_l}^{-1} \mathbf{a}_l \sigma_{\mathrm{s}}^2\right) \\ &= \log_2 \left(1 + \mathrm{SNR}_l^{\mathrm{TAS}n}\right), \end{aligned} \tag{5.33}$$

where $\mathrm{SNR}_l^{\mathrm{TAS}n}$ is the signal-to-noise ratio (SNR) of Ul using TASn and $|x|$ is the determinant of x. The covariance matrix of the received signal $\mathbf{R}_{\mathbf{y}_l}$ is given as

$$\mathbf{R}_{\mathbf{y}_l} = \mathbf{a}_l \mathbf{a}_l^H \sigma_{\mathrm{s}}^2 + \mathbf{R}_{\mathbf{w}_l} \tag{5.34}$$

and the covariance matrix of the interference plus noise $\mathbf{R}_{\mathbf{w}_l}$ is given as

$$\begin{aligned} \mathbf{R}_{w_l} &= \mathbb{E}\left\{ \left(\sum_{\substack{k=l-2K \\ k\neq l}}^{l+2K} \mathbf{a}_k s_k + \mathbf{n}_l \right) \left(\sum_{\substack{k=l-2K \\ k\neq l}}^{l+2K} \mathbf{a}_k s_k + \mathbf{n}_l \right)^H \right\} \\ &= \sum_{\substack{k=l-2K \\ k\neq l}}^{l+2K} \mathbf{a}_k \mathbf{a}_k^H \sigma_{\mathrm{s}}^2 + \mathbf{N}_l \end{aligned} \tag{5.35}$$

where $\mathbf{N}_l = \mathbb{E}\left\{\mathbf{n}_l \mathbf{n}_l^H\right\}$ and N_l is the l-th element in the main diagonal of the matrix

$$\begin{aligned}
\mathbf{N}_l = \operatorname{diag}\Bigg[& \sigma_{\mathrm{n}}^2 \quad \cdots \quad \sigma_{\mathrm{n}}^2 \\
& \left(\sigma_{\mathrm{n}}^2 + \frac{1}{K}\sum_{m=1}^{K} \frac{|\gamma_{l-K,l}|^2 \sigma_{\mathrm{n}}^2}{\left(\tilde{P}_{l-2K+m-1,l-K}\right)^2} + \frac{1}{K}\sum_{m=1}^{K} \frac{|\gamma_{l+1,l}|^2 \sigma_{\mathrm{n}}^2}{\left(\tilde{P}_{l-K+m,l+1}\right)^2}\right) \\
& \left(\sigma_{\mathrm{n}}^2 + \frac{1}{K}\sum_{m=1}^{K} \frac{|\gamma_{l-K+1,l}|^2 \sigma_{\mathrm{n}}^2}{\left(\tilde{P}_{l-2K+m,l-K+1}\right)^2} + \frac{1}{K}\sum_{m=1}^{K} \frac{|\gamma_{l+2,l}|^2 \sigma_{\mathrm{n}}^2}{\left(\tilde{P}_{l+1-K+m,l+2}\right)^2}\right) \\
& \cdots \\
& \left(\sigma_{\mathrm{n}}^2 + \frac{1}{K}\sum_{m=1}^{K} \frac{|\gamma_{l,l}|^2 \sigma_{\mathrm{n}}^2}{\left(\tilde{P}_{l-K+m-1,l}\right)^2}\right)\Bigg]^T \\
& \in \mathbb{R}^{1\times 2K+2}
\end{aligned} \tag{5.36}$$

for TAS1 and

$$\begin{aligned}
\mathbf{N}_l = \operatorname{diag}\Bigg[& \sigma_{\mathrm{n}}^2 \quad \cdots \quad \sigma_{\mathrm{n}}^2 \\
& \left(\sigma_{\mathrm{n}}^2 + \frac{1}{K}\sum_{k=l-K}^{l+K} |\gamma_{k,l}|^2 \sum_{m=1}^{K} \frac{\sigma_{\mathrm{n}}^2}{\left(\tilde{P}_{k-K+m-1,k}\right)^2}\right)\Bigg]^T \\
& \in \mathbb{R}^{1\times K+2}
\end{aligned} \tag{5.37}$$

for TAS2.

In the case of TAS2 and $K = 1$, substituting $\mathbf{R}_{y_l}$ and $\mathbf{R}_{w_l}$ results in (5.38), where $\mathbf{b}^k(m)$ is the m-th element of the k-th column in matrix $\mathbf{B}$ in (5.17).

$$\frac{|\mathbf{R}_{y_l}|}{|\mathbf{R}_{w_l}|} =$$

$$\frac{\begin{vmatrix} \left[(\mathbf{b}^2(1))^2 + (\mathbf{b}^4(1))^2\right]\sigma_s^2 + N_1 & 0 & \left[\mathbf{b}^2(1)\mathbf{b}^2(3) + \mathbf{b}^4(1)\mathbf{b}^4(3)\right]\sigma_s^2 \\ 0 & (\mathbf{b}^3(2))^2\sigma_s^2 + N_2 & \mathbf{b}^3(2)\mathbf{b}^3(3)\sigma_s^2 \\ \left[\mathbf{b}^2(1)\mathbf{b}^2(3) + \mathbf{b}^4(1)\mathbf{b}^4(3)\right]\sigma_s^2 & \mathbf{b}^3(2)\mathbf{b}^3(3)\sigma_s^2 & \begin{matrix}[(\mathbf{b}^1(3))^2 + (\mathbf{b}^2(3))^2 + (\mathbf{b}^3(3))^2 \\ +(\mathbf{b}^4(3))^2 + (\mathbf{b}^5(3))^2]\sigma_s^2 + N_3\end{matrix} \end{vmatrix}}{\begin{vmatrix} \left((\mathbf{b}^2(1))^2 + (\mathbf{b}^4(1))^2\right)\sigma_s^2 + N_1 & 0 & \left[\mathbf{b}^2(1)\mathbf{b}^2(3) + \mathbf{b}^4(1)\mathbf{b}^4(3)\right]\sigma_s^2 \\ 0 & N_2 & 0 \\ \left[\mathbf{b}^2(1)\mathbf{b}^2(3) + \mathbf{b}^4(1)\mathbf{b}^4(3)\right]\sigma_s^2 & 0 & \begin{matrix}[(\mathbf{b}^1(3))^2 + (\mathbf{b}^2(3))^2 + (\mathbf{b}^4(3))^2 + \\ (\mathbf{b}^5(3))^2]\sigma_s^2 + N_3\end{matrix} \end{vmatrix}} \tag{5.38}$$

By solving the determinants, (5.39) is obtained.

$$\mathrm{SNR}_l^{\mathrm{TAS2}} = \frac{|\gamma_{l,l}|^2\sigma_s^2}{N_2} + \frac{\left(\eta_{l-1,l}^{l,l-2} + \eta_{l+1,l}^{l,l}\right)^2\sigma_s^2}{\left(N_3 + \left[\left(\eta_{l-1,l}^{l-2,l-2}\right)^2 + \left(\eta_{l+1,l}^{l+2,l}\right)^2\right]\sigma_s^2 + \frac{(\gamma_{l-1,l}\eta_{l,l}^{l+1,l-1} - \gamma_{l+1,l}\eta_{l,l}^{l-1,l-1})^2\sigma_s^4 + N_1\left[\left(\eta_{l,l}^{l-1,l-1}\right)^2 + \left(\eta_{l,l}^{l+1,l-1}\right)^2\right]\sigma_s^2}{(|\gamma_{l-1,l}|^2 + |\gamma_{l+1,l}|^2)\sigma_s^2 + N_1}\right)} \tag{5.39}$$

Similarly, by computing $\frac{|\mathbf{R}_{\mathbf{y}_l}|}{|\mathbf{R}_{\mathbf{w}_l}|}$ for TAS2 $K > 1$, it can be generalized that that $\mathrm{SNR}_l^{\mathrm{TAS2}}$ results in

$$\mathrm{SNR}_l^{\mathrm{TAS2}} = \frac{|\gamma_{l,l}|^2\sigma_{\mathrm{s}}^2}{N_{K+1}} + \frac{\left(\mathbf{h}_{\mathrm{cluster}_1}^{\mathrm{TAS2},K+1}(1) + \mathbf{h}_{\mathrm{cluster}_2}^{\mathrm{TAS2},K+1}(1)\right)^2\sigma_{\mathrm{s}}^2}{N_{K+2} + Y_l^{\mathrm{TAS2}}\sigma_{\mathrm{s}}^2 + \sum_{k=l-K}^{l-1}\Upsilon_{k,l}^{\mathrm{TAS2}}} \tag{5.40}$$

where

$$Y_l^{\mathrm{TAS}n} = \sum_{k=1}^{K}\left(\sum_{m=1}^{K+1}\mathbf{h}_{\mathrm{left}}^{\mathrm{TAS}n,k}(m)\right)^2 + \sum_{k=1}^{K}\left(\sum_{m=1}^{K+1}\mathbf{h}_{\mathrm{right}}^{\mathrm{TAS}n,k}(m)\right)^2 \tag{5.41}$$

and $\Upsilon_{k,l}^{\mathrm{TAS2}}$ is defined in equation (5.42)

$$\Upsilon_{k,l}^{\mathrm{TAS2}} = \frac{\left(\begin{array}{c}\left(\gamma_{k,l}\mathbf{h}_{\mathrm{cluster}_+}^{\mathrm{TAS2},k+K+1}(1) - \gamma_{k+K+1,l}\mathbf{h}_{\mathrm{cluster}_+}^{\mathrm{TAS2},k}(1)\right)^2 \sigma_{\mathrm{s}}^4 + \\ N_t\left[\left(\mathbf{h}_{\mathrm{cluster}_+}^{\mathrm{TAS2},k}(1)\right)^2 + \left(\mathbf{h}_{\mathrm{cluster}_+}^{\mathrm{TAS2},k+K+1}(1)\right)^2\right]\sigma_{\mathrm{s}}^2\end{array}\right)}{\left(|\gamma_{k,l}|^2 + |\gamma_{k+K+1,l}|^2\right)\sigma_{\mathrm{s}}^2 + N_t} \tag{5.42}$$

where $\mathbf{h}_{\mathrm{cluster}_+}^{\mathrm{TAS}n,k}(m) = \mathbf{h}_{\mathrm{cluster}_1}^{\mathrm{TAS}n,k}(m) + \mathbf{h}_{\mathrm{cluster}_2}^{\mathrm{TAS}n,k}(m)$ and t is the time-slot corresponding to the transmission of BSk. Note that for TAS2, there is only one element in $\mathbf{h}_{\mathrm{text}}^{\mathrm{TAS2},k}(m)$, while for TAS1 there are $K+1$ elements in $\mathbf{h}_{\mathrm{text}}^{\mathrm{TAS1},k}(m)$.

It can be seen that the term $\frac{|\gamma_{l,l}|^2\sigma_{\mathrm{s}}^2}{N_{K+1}}$ in equation (5.40) corresponds to the SNR received from BSl during the transmission phase. On the other hand the second term corresponds to the contribution of the other BSs in cluster $\mathcal{C}_l$. Specifically, the numerator is the received signal power from all the BSs inside $\mathcal{C}_l$ except BSl and it is divided by the noise power in the last time-slot N_{K+2}, by the received power from the relayed symbols coming from the BSs outside the cluster $Y_l^{\mathrm{TAS2}}\sigma_{\mathrm{s}}^2$, and by $\sum_{k=l-K}^{l-1}\Upsilon_{k,l}^{\mathrm{TAS2}}$, which represents a penalty from the simultaneous transmissions from K BSs inside the cluster during the relaying phase. Note that (5.40) reduces to (5.39) for $K=1$.

In the case of TAS1 and $K = 1$, substituting $\mathbf{R}_{y_l}$ and $\mathbf{R}_{w_l}$ results in (5.43), where $\mathbf{c}^k(m)$ is the m-th element of the k-th column in matrix $\mathbf{C}$ in (5.16).

$$\frac{|\mathbf{R}_{y_l}|}{|\mathbf{R}_{w_l}|} = \frac{\begin{vmatrix} [(\mathbf{c}^2(1))^2+ (\mathbf{c}^4(1))^2]\sigma_s^2 + N_1 & 0 & 0 & [\mathbf{c}^2(1)\mathbf{c}^2(4) +\mathbf{c}^4(1)\mathbf{c}^4(4)]\sigma_s^2 \\ 0 & (\mathbf{c}^3(2))^2\sigma_s^2 + N_2 & \mathbf{c}^3(2)\mathbf{c}^3(3)\sigma_s^2 & 0 \\ 0 & \mathbf{c}^3(2)\mathbf{c}^3(3)\sigma_s^2 & [\left(\mathbf{c}^1(3)\right)^2 + (\mathbf{c}^3(3))^2+ (\mathbf{c}^5(3))^2]\sigma_s^2 + N_3 & 0 \\ [\mathbf{c}^2(1)\mathbf{c}^2(4)+ \mathbf{c}^4(1)\mathbf{c}^4(4)]\sigma_s^2 & 0 & 0 & [(\mathbf{c}^2(4))^2+ (\mathbf{c}^4(4))^2]\sigma_s^2 + N_4 \end{vmatrix}}{\begin{vmatrix} [(\mathbf{c}^2(1))^2+ (\mathbf{c}^4(1))^2]\sigma_s^2 + N_1 & 0 & 0 & [\mathbf{c}^2(1)\mathbf{c}^2(4)+ \mathbf{c}^4(1)\mathbf{c}^4(4)]\sigma_s^2 \\ 0 & N_2 & 0 & 0 \\ 0 & 0 & [(\mathbf{c}^1(3))^2+ (\mathbf{c}^5(3))^2]\sigma_s^2 + N_3 & 0 \\ [\mathbf{c}^2(1)\mathbf{c}^2(4)+ \mathbf{c}^4(1)\mathbf{c}^4(4)]\sigma_s^2 & 0 & 0 & [(\mathbf{c}^2(4))^2+ (\mathbf{c}^4(4))^2]\sigma_s^2 + N_4 \end{vmatrix}} \tag{5.43}$$

Solving the determinants results in

$$\mathrm{SNR}_l^{\mathrm{TAS1}} = \frac{|\gamma_{l,l}|^2\sigma_s^2}{N_2} + \frac{\left(\eta_{l-1,l}^{l,l-2} + \eta_{l+1,l}^{l,l}\right)^2 \sigma_s^2}{N_3 + \left[\left(\eta_{l-1,l}^{l-2,l-2}\right)^2 + \left(\eta_{l+1,l}^{l+2,l}\right)^2\right]\sigma_s^2} \tag{5.44}$$

Computing $\frac{|\mathbf{R}_{\mathbf{y}_l}|}{|\mathbf{R}_{\mathbf{w}_l}|}$ for TAS1 with $K > 1$ does not result in a simple closed-form equation. Comparing equations (5.39) and (5.44), the difference is in the penalty from the simultaneous transmissions in TAS2, which is not present for TAS1. This makes sense as there are fewer simultaneous transmissions for TAS1 during the relaying phase. Therefore, we propose an expression analogous to (5.40) as an approximation:

$$\mathrm{SNR}_l^{\mathrm{TAS1}} = \frac{|\gamma_{l,l}|^2\sigma_{\mathrm{s}}^2}{N_{K+1}} + \frac{\left(\sum_{m=1}^{K+1} \mathbf{h}_{\mathrm{cluster}_1}^{\mathrm{TAS1},K+1}(m) + \sum_{m=1}^{K+1} \mathbf{h}_{\mathrm{cluster}_2}^{\mathrm{TAS1},K+1}(m)\right)^2 \sigma_{\mathrm{s}}^2}{N_{K+2} + Y_l^{\mathrm{TAS1}}\sigma_{\mathrm{s}}^2}. \tag{5.45}$$

As seen in Section 5.5, this approximation turns out to be quite accurate.

The spectral efficiency per time-slot of Ul for TAS1 and TAS2 is then calculated as

$$\begin{aligned} S_l^{\mathrm{TAS1}} &= \frac{1}{2(K+1)}\mathbb{E}\left\{\log_2\left(1+\mathrm{SNR}_l^{\mathrm{TAS1}}\right)\right\} \\ S_l^{\mathrm{TAS2}} &= \frac{1}{K+2}\mathbb{E}\left\{\log_2\left(1+\mathrm{SNR}_l^{\mathrm{TAS2}}\right)\right\} \end{aligned} \tag{5.46}$$

The $\frac{1}{2(K+1)}$ and $\frac{1}{K+2}$ scaling factors correspond to the multiplexing gain due to the number of time-slots used for each transmission round. It can be seen that TAS1 and TAS2 can reduce the number of time-slots compared to mSTNC while still achieving diversity from multiple BSs.

The BER of Ul for both schemes is given as

$$\mathrm{BER}_l^{\mathrm{TAS}n} = \mathbb{E}\left\{Q\left(\sqrt{2\left(\mathrm{SNR}_l^{\mathrm{TAS}n}\right)}\right)\right\}. \tag{5.47}$$

5.5 Performance Evaluation

In this section we compare the performance of TAS1 and TAS2 with the baseline schemes described in Section 5.3. As cellular model, we consider the Wyner model of Fig. 5.1 with $K = \{1, 2, 4\}$. Our evaluations consider a Rayleigh fading channel model with $\sigma_s^2 = \sigma_{\mathrm{n}}^2 = 1$ and BPSK modulation.

5.5.1 Evaluation with Equal Transmit Power and Channel Conditions

In this section we evaluate the performance of the studied schemes with equal transmit power from all the BSs, i.e. $P_1 = P_2 = P_3 = \cdots = P_l$, and equal average channel gains, i.e. $\mathbb{E}\{|h_{m,l}|^2\} = \mathbb{E}\{|g_{m,n}|^2\} = 1\ \forall m, l, n$.

The spectral efficiency per time-slot as a function of the transmit power is depicted in Figs. 5.7, 5.8, and 5.9 for $K = \{1, 2, 4\}$, respectively. It can be seen that TDMA has the highest performance followed by TAS2 and TAS1. This is mainly due to the multiplexing gain achieved by reducing the number of time-slots per transmission round. With equal transmit power and equal average channel conditions, the SNR received by Ul from BSl is similar to that received by other BSs inside the cluster, hence TDMA turns out to be the

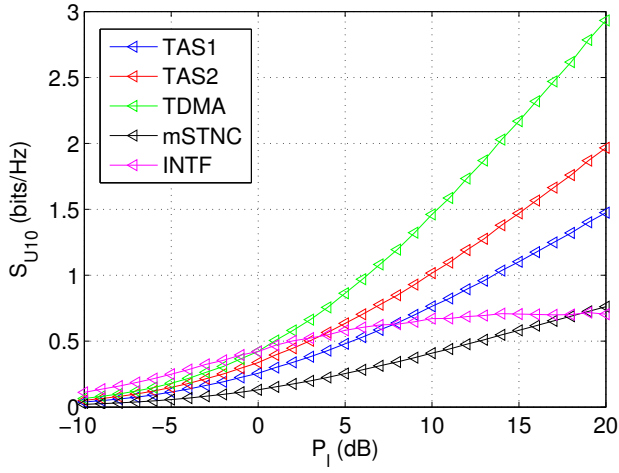

Figure 5.7: Spectral efficiency per time-slot of the different schemes with $K = 1$ and equal transmit power and channel conditions.

best strategy. However, the difference with respect to TAS2 decreases as K increases. Notice also the large penalty in the spectral efficiency for mSTNC due to the large number of time-slots required to achieve full diversity and the low performance of INTF that floors at 0dB because of the increasing interference.

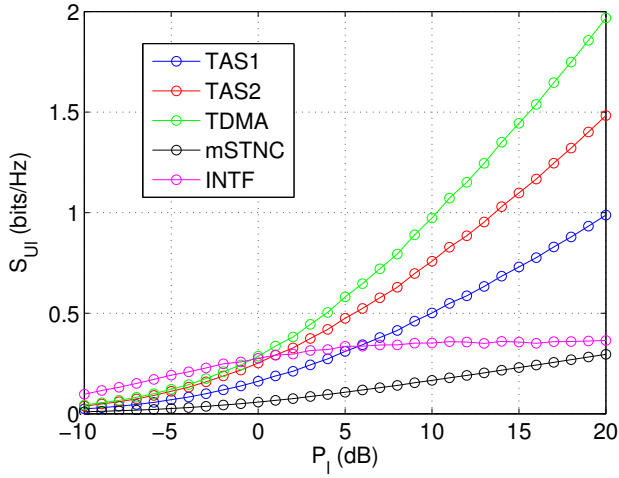

Figure 5.8: Spectral efficiency per time-slot of the different schemes with $K = 2$ and equal transmit power and channel conditions.

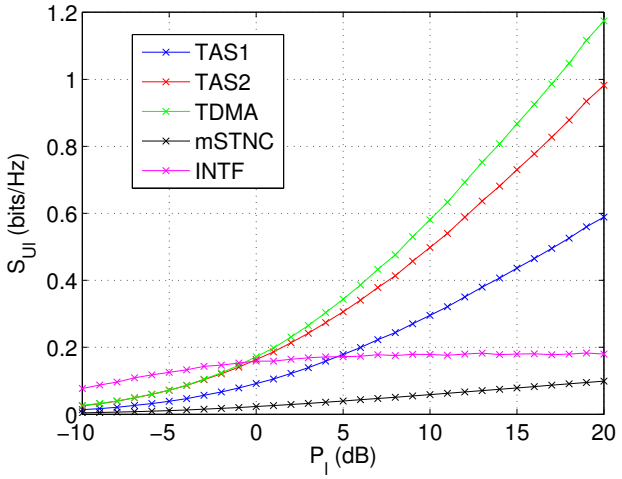

Figure 5.9: Spectral efficiency per time-slot of the different schemes with $K = 4$ and equal transmit power and channel conditions.

The BER performance of the different schemes is depicted in Fig. 5.10. It can be seen that INTF and mSTNC correspond to the upper and lower bounds of the BER, respectively. At this point it is interesting to recall that mSTNC achieves a low BER and full diversity gain at the cost of a large number of time-slots. However, TAS1 and TAS2 achieve a BER lower than INTF and TDMA. Therefore, by taking advantage of the network topology, TAS1 and TAS2 provide a trade-off between multiplexing gain and diversity.

It is worth to note the small difference in BER of TAS1 and TAS2 for different values of K. As K increases, more BSs are able to retransmit a given symbol providing a higher spatial diversity. At the same time, each BS retransmits *more* symbols that interfere with the decoding of the desired symbol. These two opposing effects prevent the BER from decreasing with K.

We also show the spectral efficiency of the approximation for TAS1 compared to its exact value in Fig. 5.11. It can be seen that the approximation is exact for $K = 1$ and very accurate for $K > 1$. The advantage of this approximation for TAS1 is that it corresponds to a closed-form expression that allows us to analyze and predict the achievable gains for any cluster size and to compare it with other schemes.

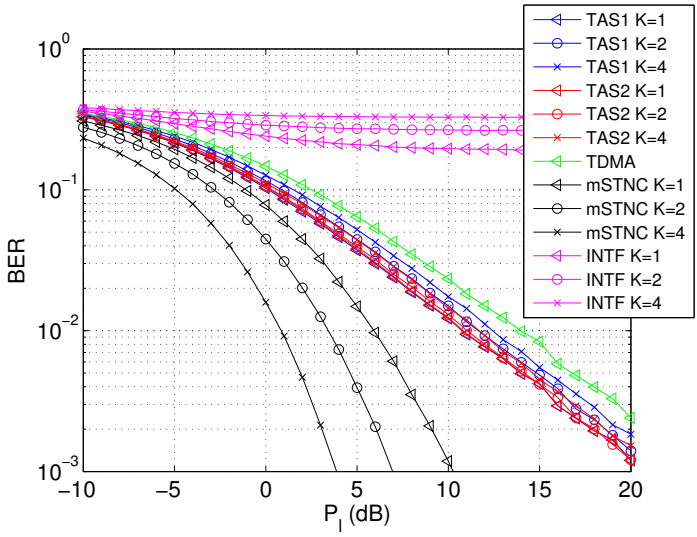

Figure 5.10: BER of the different schemes with equal transmit power and channel conditions..

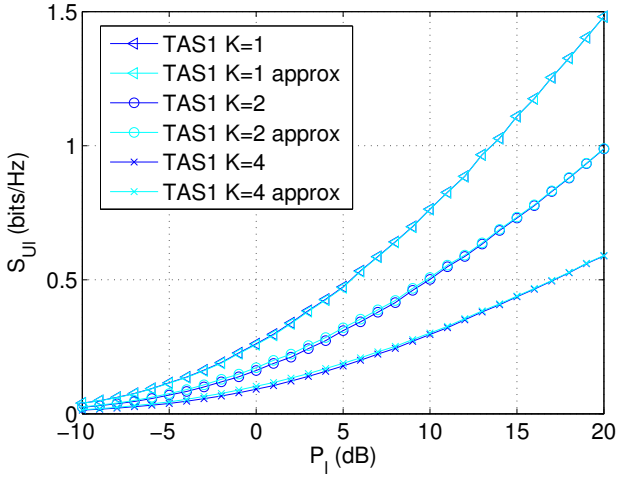

Figure 5.11: Spectral efficiency per time-slot of TAS1.

5.5.2 Evaluation with Unequal Transmit Power and Channel Conditions

In this section we evaluate the performance of the studied schemes with unequal transmit power and unequal average channel conditions. For simplicity we only present the case of $K = 2$.

First we analyze the case where BSl has a transmit power 10dB lower than the rest of the BSs, but with equal average channel gains such that $\mathbb{E}\{|h_{m,l}|^2\} = \mathbb{E}\{|g_{m,n}|^2\} = 1\ \forall m, l, n$. The spectral efficiency per time-slot and BER in this case is depicted in Figs. 5.12 and 5.13, respectively. Then we analyze the case where the average channel gain of Ul, i.e. $\mathbb{E}\{|h_{l,l}|^2\}$, is 10dB lower than the average channel gain of the rest of the links (and equal transmit power from all the BSs). The spectral efficiency per time-slot and BER in this case is depicted in Figs. 5.14 and 5.15, respectively. Finally, we analyze the case where the average channel gain of Ul, i.e. $\mathbb{E}\{|h_{l,l}|^2\}$, and the average channel gain between all the BSs, i.e. $\mathbb{E}\{|g_{m,n}|^2\}\ \forall m, n$, are 10dB lower than the average channel gain of the rest of the links (and equal transmit power from all the BSs). The spectral efficiency per time-slot and BER in this case is depicted in Figs. 5.16 and 5.17, respectively.

In the the first case, TAS2 presents a similar spectral efficiency as TDMA followed by TAS1 as seen in Fig. 5.12. In the second case, the performance difference between TAS2 and TDMA is larger as seen in Fig. 5.14. This is because, in the first case, the lower transmit power affects the received SNR of Ul, but it also affects the SNR received by the other BSs of the cluster. Hence the gain provided by relaying is limited. In the second case, the lower channel gain only affects Ul and therefore, TAS1 and TAS2 are able to exploit the diversity from the neighboring BSs to provide a higher received SNR to Ul. In terms of BER the differences between mSTNC, TAS1, TAS2, and TDMA increase when comparing unequal transmit power and unequal channel gains as seen in Fig. 5.13 and Fig. 5.15.

Finally, in the third case, when the average channel gain of Ul and the average channel gain between BSs are lower than the rest of the links, we can see that mSTNC has the largest performance penalty in spectral efficiency (Fig. 5.16) and BER (Fig. 5.17). In this case, TAS2 has the best performance in spectral efficiency and TAS1 has slightly the best performance in BER followed by TAS2.

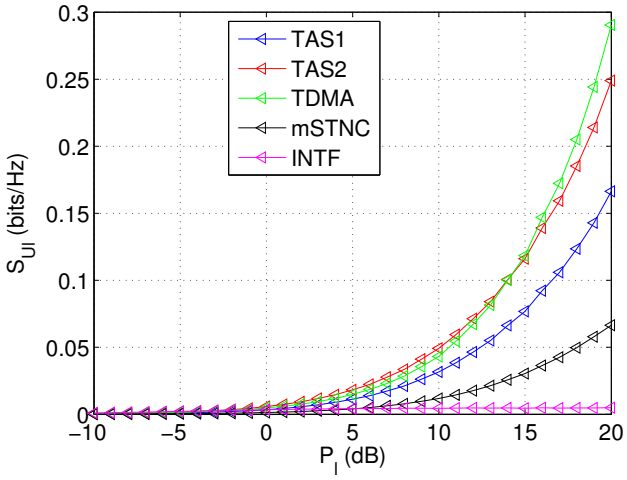

Figure 5.12: Spectral efficiency per time-slot of the different schemes for $K = 2$ with unequal transmit power and equal average channel gains, i.e. $\mathbb{E}\{|h_{m,l}|^2\} = \mathbb{E}\{|g_{m,n}|^2\} = 1\ \forall m, l, n$.

5.6 Conclusions

In this chapter we have proposed two topology-aware STNC schemes that exploit basic knowledge of the network topology, i.e. the knowledge of the subset of BSs that can be overheard by each BS and user, in particular using the Wyner cellular model. This is achieved by allowing simultaneous transmissions from the BSs that do not overhear each other during the transmission phase. In the relaying phase, each BS transmits the information overheard during the transmission phase in two ways. With TAS1, BSs that do not overhear each other transmit simultaneously. With TAS2, all the BSs transmit in one single time-slot. Our results show that TAS1 and TAS2 can improve the spectral efficiency per time-slot and BER with unequal transmit power and unequal channel conditions compared to traditional STNC and other baseline schemes.

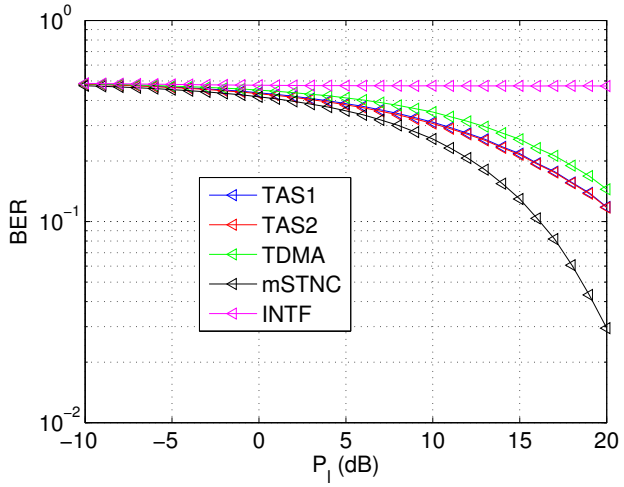

Figure 5.13: BER of the different schemes for $K = 2$ with unequal transmit power and equal average channel gains, i.e. $\mathbb{E}\{|h_{m,l}|^2\} = \mathbb{E}\{|g_{m,n}|^2\} = 1$ $\forall m, l, n$.

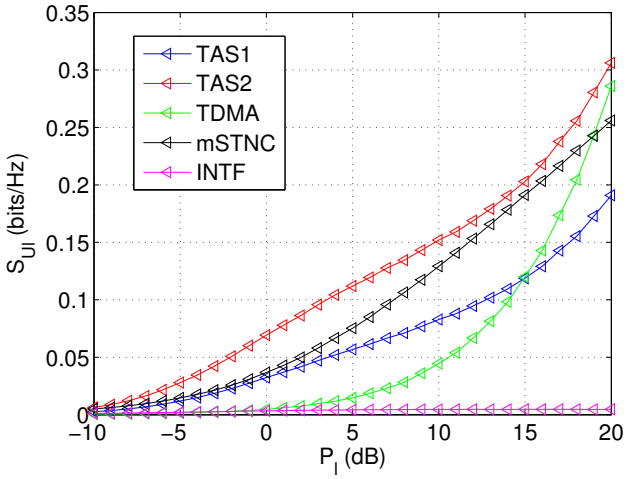

Figure 5.14: Spectral efficiency per time-slot of the different schemes for $K = 2$ with equal transmit power and unequal channel conditions, i.e. $\mathbb{E}\{|h_{l,l}|^2\}$ is 10dB lower than the average channel gain of the rest of the links.

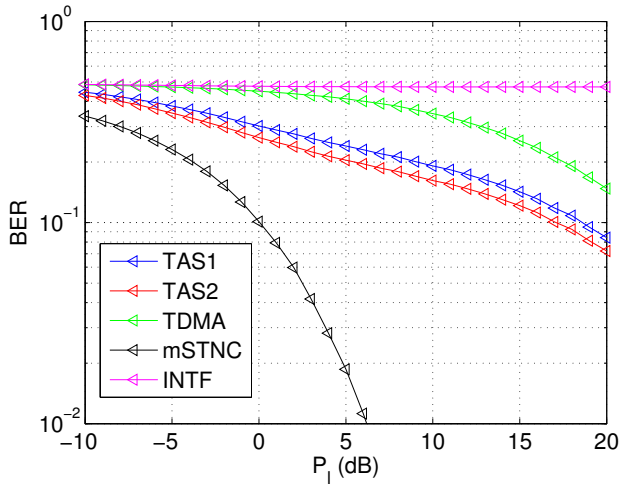

Figure 5.15: BER of the different schemes for $K = 2$ with equal transmit power and unequal channel conditions, i.e. $\mathbb{E}\{|h_{l,l}|^2\}$ is 10dB lower than the average channel gain of the rest of the links.

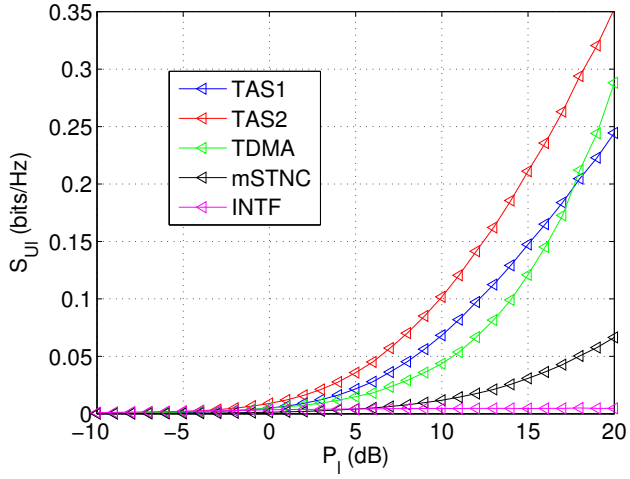

Figure 5.16: Spectral efficiency per time-slot of the different schemes for $K = 2$ with equal transmit power and unequal channel conditions, i.e. $\mathbb{E}\{|h_{l,l}|^2\}$ and $\mathbb{E}\{|g_{m,n}|^2\}$ $\forall m, n$ are 10dB lower than the average channel gain of the rest of the links

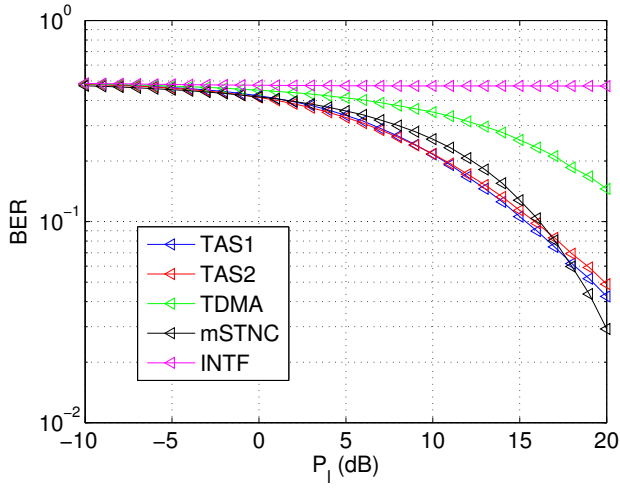

Figure 5.17: BER of the different schemes for $K = 2$ with equal transmit power and unequal channel conditions, i.e. $\mathbb{E}\{|h_{l,l}|^2\}$ and $\mathbb{E}\{|g_{m,n}|^2\}$ $\forall m, n$ are 10dB lower than the average channel gain of the rest of the links

Chapter 6

Are Overhearing Strategies Energy Efficient?

Abstract

The 1000-fold capacity increase envisioned by dense 5G networks results also in a tremendous increase in the energy consumption of the whole network. Utilizing relays in combination with physical-layer network coding (PNC) has been proposed as an energy-efficient solution to this problem by creating several short-distance low-power transmissions and by reducing the transmission time. However, deploying relay nodes can be very costly for dense networks. On the other hand, the proximity of transmitting nodes in dense networks allows the transmitting nodes to serve as relays and retransmit the signals overheard from other transmitting nodes using PNC. This approach has been shown to increase the spectral efficiency, but the impact on energy efficiency has not been studied yet. Therefore, in this chapter we analyse two approaches that exploit the overhearing capabilities of the transmitting nodes in terms of spectral efficiency, energy efficiency, and success rate. We then provide a low-complexity power control strategy that achieves a performance close to the optimal for each approach. We show that when at least one indirect link is stronger than the direct links, exploiting the overhearing capabilities of the transmitting nodes provides the highest performance in both the transmit power dominated and circuit power dominated regimes. [1]

[1]This chapter is cited from Torrea-Duran, R., Rosas, F. Pollin, S., Vandendorpe, L., Moonen, M., "Exploiting the Overhearing Capabilities of Transmitting Nodes to Increase the

6.1 Introduction

5G wireless networks aim for a 1000-fold increase of the system capacity compared to current state-of-the-art technology [88]. To achieve this, a tremendous increase in the number of base stations and connected devices is expected in the coming years, increasing not only the density of the network [17, 51], but also its energy consumption. Therefore, finding ways to increase the energy efficiency while maintaining a high spectral efficiency is one of the main challenges in wireless networks for a sustainable growth, both economically and environmentally [96].

Relays have been proposed to deal with these challenges by dividing long-distance transmissions into several short-distance low-power transmissions [76, 83]. However, relay nodes require certain coordination with the rest of the network nodes in order to manage transmissions efficiently. Cooperative protocols have thus gained much attention by using relays to retransmit the overheard information to an intended receiver.

One of these protocols combines relays with physical-layer network coding (PNC) [60, 64]. Most works that study the energy efficiency of relaying schemes using PNC are limited to the TWRC case. For instance, the authors in [31] propose an optimal power allocation strategy for a TWRC using PNC with per-node power constraints, while the authors in [100] use end-to-end rate constraints. In [82], the authors show that TWRC transmissions are more energy efficient in the high spectral efficiency and large path loss attenuation region compared to direct transmissions and one-way relay transmissions. In [83] the authors show that TWRC transmissions are more energy-efficient in symmetric systems where the circuit power consumption and the transmitted bits in both directions are equal. Finally, in [90], the energy-efficient resource allocation for OFDMA-based two-way relay is studied by maximizing the aggregate energy efficiency while providing proportional fairness in energy efficiency.

A main disadvantage of these approaches is that by considering a TWRC, received signals only from the relay node, hence disregarding potentially useful signals originating directly from the transmitting node. Furthermore, all the previous approaches require the deployment of relays, which can be costly or even prohibitive for dense networks.

A similar effect can be achieved if, instead of deploying relay nodes, the overhearing capabilities of the transmitting nodes are exploited by allowing these to retransmit the signals overheard from other transmitting nodes. In

Energy Efficiency in Dense Networks". EURASIP Journal on Wireless Communications and Networking, 2017.

this way, the transmit power from all the transmitting nodes is utilized, while the deployment of relays is avoided. A main challenge in this case is that the resources need to be split for serving the intended user and other users. Taking this into account, it has been shown that cooperation among transmitting nodes can actually improve the users' energy efficiency [59, 70].

Future networks foresee the proliferation of additional base stations (microcells, picocells, femtocells) underlaid in the traditional (macro) cellular network in order to increase the area spectral efficiency [38]. Similar to relays, these base stations can also help to increase the energy efficiency, especially for a high area throughput and a high user density [18]. These low-power base stations often do not count with a backhaul link for data transmission, while the backhaul operating costs are substantial [20]. Hence the potential increase in spectral and energy efficiency of dense networks serves as incentive for the base stations to act as relays. Furthermore, in dense networks the proximity of the nodes results in a high probability of finding transmitting nodes with a strong link between them as seen in Fig. 6.1. For instance, neighboring base stations in a dense network can retransmit the overheard signals from the other base stations in order to increase both the downlink data rate and the energy efficiency. Similarly, energy-limited devices in close proximity can retransmit the overheard signals from other devices through a D2D link to increase the total uplink data rate.

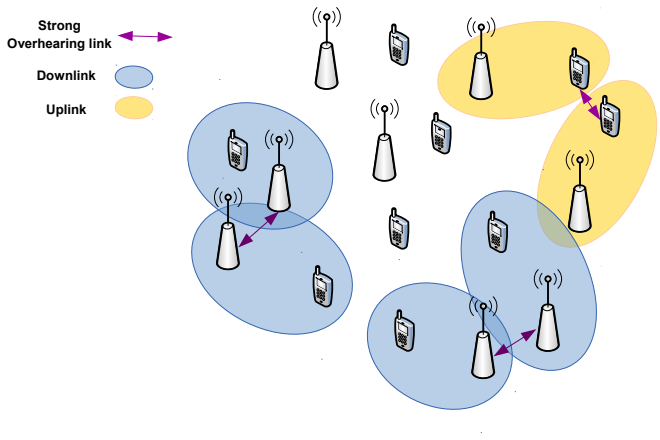

Figure 6.1: Exploiting the strong overhearing link in dense networks for downlink and uplink communication.

A way of exploiting the overhearing capabilities of transmitting nodes using

PNC principles is through space-time network coding (STNC) [56]. For a network with L transmitting nodes, M relay nodes and one destination, STNC can achieve a diversity order of $M + 1$ with $L + M$ time-slots.

An alternative that also exploits the overhearing capabilities of transmitting nodes with fewer time-slots is proposed in Chapter 4. Similar to [56, 91, 99], each of the L transmitting nodes transmits its own signal in a dedicated time-slot during the transmission phase. Then, during the relaying phase all the transmitting nodes retransmit a combination of the previously overheard signals simultaneously, hence requiring only $L + 1$ time-slots. Combining transmissions from different transmitting nodes in one time-slot can drastically reduce the number of time-slots required per transmission round, but it can also increase the interference during the relaying phase.

In terms of data rate, it is clear that when the (direct) link between a transmitter and its intended receiver is strong, relaying might not be necessary. However, when the interference is strong, exploiting alternative (indirect) links proves beneficial, either using a single or dedicated time-slots during the relaying phase. However, the energy efficiency analysis is not straightforward since relaying might have a larger delay and energy cost compared to the data rate benefit. Furthermore, the energy efficiency might be very different when the transmit power is the largest energy contributor compared to when the circuit power is the largest contributor. To the best of our knowledge, an energy efficiency analysis of this type of approaches that exploit the overhearing capabilities of the transmitting nodes has not been reported in literature.

The first contribution of this chapter consists in the analysis of two approaches (the first one based on [56] and the second one based on [85]) that exploit the overhearing capabilities of transmitting nodes in terms of spectral efficiency, energy efficiency, and success rate. The first approach (referred to as DIV) is a variation of the traditional space-time network coding (STNC) approach that uses no relays but the same transmitting nodes to relay overheard information. The second approach (referred to as MRCP) also exploits the overhearing capabilities of transmitting nodes but uses fewer time-slots. The motivation behind this energy efficiency analysis is that both approaches aim to utilize the power transmitted by *other* nodes. Although we limit the analysis to the case of two transmitting nodes and two receiving nodes, the ideas presented here can also be used in a larger scenario. The second contribution consists in a low-complexity power control strategy that achieves a similar energy efficiency as the optimal strategy for each approach (DIV and MRCP). The proposed strategy requires only a comparison of the channel conditions between direct and indirect links. This results in a closed-form formula for each case. We are then able to show that when at least one indirect link is stronger than the direct links, exploiting the overhearing capabilities of the transmitting nodes provides

the highest performance. This is particularly beneficial for dense networks since there is a high probability of finding strong indirect links.

The rest of the chapter is organized as follows. Section 6.2 describes the system model. Section 6.3 presents the two baseline approaches not exploiting overhearing capabilities. Section 6.4 presents the energy efficiency optimization of two approaches that exploit overhearing capabilities. Section 6.5 presents the complexity analysis. Section 6.6 shows the performance evaluation. Finally, Section 6.7 draws some conclusions.

6.2 System Model

Consider a system composed by a pair of transmitting nodes (TXs), each of which has data to be delivered to a specific receiving node (RX). We assume that all the nodes are half-duplex (i.e. they cannot transmit and receive simultaneously) and that no backhaul link exists between the TXs. This last condition excludes the use of transmission schemes that require coordinated transmitters or antennas, e.g. space-time block codes such as Alamouti codes. We also assume that each TX can overhear the transmission of the other TXs in a reliable way, i.e. that the links between TXs (overhearing links) are stronger than the links between TXs and RXs (direct/indirect links).

We consider a standard power model including transmit power and circuit power. While the transmit power is radiated by the TXs for data transmission, the circuit power represents the average energy consumption of electronic components, typically modeled as a constant, independent of the transmission rate [59]. A regime in which the transmit power dominates over the circuit power is typical for cellular networks, where TXs need to compensate for the large path loss of communication over long distances. On the other hand, a regime in which the circuit power dominates over the transmit power corresponds to short-range communication scenarios [10]. In this chapter we focus on the case where both TXs operate either in the transmit power regime or in the circuit power regime.

Let us denote s_l as the symbol from the l-th TX to be delivered to the l-th RX. Symbols are assumed to be uncorrelated. Let us define $P_l^{(t)}$ as the transmit power of TX l in time-slot t and $p_l^{(t)}$ as the circuit power of TX l in time-slot t. We also define $\gamma_{lm}^{(t)} = \frac{\sigma_s^2}{\sigma_n^2} P_l^{(t)} |h_{lm}|^2$ and $\xi_{lm}^{(t)} = \frac{\sigma_s^2}{\sigma_n^2} P_l^{(t)} |g_{lm}|^2$, where h_{lm} is the link from TX l to RX m and g_{lm} is the link from TX l to TX m (overhearing link). If $l = m$ we call h_{lm} a direct link, else we call h_{lm} an indirect link. Given the likelihood of finding strong overhearing links in dense networks, in

this chapter we focus on the case where the overhearing links are stronger than the other communication links, i.e. $\xi_{lm}^{(t)} \gg \gamma_{mn}^{(t)}$, $\forall l, m, n$. The parameter $\sigma_{\mathrm{s}}^2 = \mathbb{E}\{|s_1|^2\} = \mathbb{E}\{|s_2|^2\}$, and σ_{n}^2 is the received noise power, assumed to be equal for all nodes. Without loss of generality, we assume $\sigma_{\mathrm{s}}^2 = \sigma_{\mathrm{n}}^2 = 1$.

We define the energy efficiency ϵ as the number of bits received by a RX in units of bits per unit of bandwidth per unit of energy. The energy efficiency can then be expressed as a function of the spectral efficiency (bits per unit of bandwidth per unit of time) and the power (energy per unit of time) as [58, 66]

$$\epsilon = \frac{S_1}{\Phi_1} + \frac{S_2}{\Phi_2}, \tag{6.1}$$

where S_l is the spectral efficiency of RX l and Φ_l is the average power to transmit symbol s_l to RX l defined as

$$\begin{aligned} \Phi_l &= \frac{\left(p_1^{(t_{l,1})} + P_1^{(t_{l,1})}\right) T + \left(p_2^{(t_{l,2})} + P_2^{(t_{l,2})}\right) T}{NT} \\ &= \frac{\left(p_1^{(t_{l,1})} + P_1^{(t_{l,1})}\right) + \left(p_2^{(t_{l,2})} + P_2^{(t_{l,2})}\right)}{N} \end{aligned} \tag{6.2}$$

where T is the time-slot duration, N is the total number of time-slots per transmission round, and $t_{l,m}$ is the time-slot in which symbol s_l is transmitted by TX m.[2] To avoid a cumbersome notation, we will simply use t without a subscript. With equations (6.1) and (6.2), we can establish a fair comparison among schemes that use a different number of time-slots per transmission round.

Our objective is then to maximize ϵ subject to transmit power and minimum spectral efficiency constraints:

$$\begin{aligned} &\underset{P_1^{(t)}, P_2^{(t)}\ \forall t}{\text{maximize}}\ \epsilon \\ &\qquad \text{s.t. } 0 \le P_1^{(t)} \le P_1^{\max},\ \forall t, \\ &\qquad\qquad 0 \le P_2^{(t)} \le P_2^{\max},\ \forall t, \\ &\qquad\qquad S_1 \ge S_1^{\min}, \\ &\qquad\qquad S_2 \ge S_2^{\min}. \end{aligned} \tag{6.3}$$

[2] Equation (6.2) shows the transmission of one symbol by *both* TXs. However, for some approaches the symbol will only be transmitted by one TX, leaving equation (6.2) with only half of the terms.

6.3 Baseline Approaches That Do Not Exploit the Overhearing Capabilities of TXs

This section presents the analysis of the baseline approaches, which will be used in Section 6.6 to compare the performance of the overhearing approaches presented in Section 6.4.

6.3.1 TDMA

In a basic time division multiple access (TDMA) approach, the communication is done in turns, i.e. first TX 1 transmits s_1 to RX 1 while TX 2 is inactive, and then TX 2 transmits s_2 to RX 2 while TX 1 is inactive, hence requiring two time-slots per transmission round.

The energy efficiency maximization of TDMA is given as

$$\begin{aligned} \underset{P_1^{(1)},P_2^{(2)}}{\text{maximize}}\ \epsilon^{\text{TDMA}} &= \frac{S_1^{\text{TDMA}}}{\frac{1}{2}\left(p_1^{(1)}+P_1^{(1)}\right)} + \frac{S_2^{\text{TDMA}}}{\frac{1}{2}\left(p_2^{(2)}+P_2^{(2)}\right)} \\ \text{s.t. } 0 &\le P_l^{(l)} \le P_l^{\max} \\ S_l^{\text{TDMA}} &\ge S_l^{\min} \end{aligned} \tag{6.4}$$

for $l = \{1, 2\}$ where

$$S_l^{\text{TDMA}} = \frac{1}{2}\log_2\left(1+\gamma_{ll}^{(l)}\right) \tag{6.5}$$

and the $\frac{1}{2}$ pre-log factor comes from the two time-slots required. Since the two transmissions are fully decoupled, the energy efficiency is maximized independently for each term of equation (6.4).

In the transmit power dominated regime $P_1^{(1)} \gg p_1^{(1)}$ and $P_2^{(2)} \gg p_2^{(2)}$ and we can see that equation (6.4) is strictly decreasing with both $P_1^{(1)}$ and $P_2^{(2)}$ (see Appendix A.4 with $a = |h_{ll}|^2$ and $k = b = 0$). In this case, the maximization of the energy efficiency corresponds to using the following transmit powers to satisfy the minimum spectral efficiency constraints

$$P_l^{(l)} = \begin{cases} \frac{2^{2S_l^{\min}}-1}{|h_{ll}|^2}, & \text{if } \frac{2^{2S_l^{\min}}-1}{|h_{ll}|^2} \le P_l^{\max} \\ \text{no solution (no success)}, & \text{otherwise} \end{cases} \tag{6.6}$$

Note the exponent 2 corresponding to the two time-slots required per transmission round. This factor reveals a penalty in the power of schemes that use several time-slots.

In the circuit power dominated regime $p_1^{(1)} \gg P_1^{(1)}$ and $p_2^{(2)} \gg P_2^{(2)}$ and assuming for simplicity $p_1^{(1)} = p_2^{(2)} = p^{(t)}$, the energy efficiency maximization of TDMA is given as

$$\begin{aligned} \underset{P_1^{(1)}, P_2^{(2)}}{\text{maximize}}\ & \epsilon^{\text{TDMA}} \approx \frac{S_1^{\text{TDMA}} + S_2^{\text{TDMA}}}{\frac{1}{2}p^{(t)}}, \\ \text{s.t. } & 0 \leq P_l^{(l)} \leq P_l^{\max} \\ & S_l^{\text{TDMA}} \geq S_l^{\min} \end{aligned} \tag{6.7}$$

where the energy efficiency is maximized independently for each term. In this case, the maximization of the energy efficiency corresponds to both TXs transmitting with maximum power, i.e. $P_1^{(1)} = P_1^{\max}$ and $P_2^{(2)} = P_2^{\max}$, assuming that the minimum spectral efficiency constraints are satisfied (success rate), otherwise there is no solution.

6.3.2 INTF

This approach consists in both TXs transmitting simultaneously regardless of the resulting interference, hence requiring one time-slot per transmission round. We refer to this approach as INTF (interference).

The energy efficiency maximization of INTF is given as

$$\begin{aligned} \underset{P_1^{(1)}, P_2^{(1)}}{\text{maximize}}\ & \epsilon^{\text{INTF}} = \frac{S_1^{\text{INTF}}}{p_1^{(1)} + P_1^{(1)}} + \frac{S_2^{\text{INTF}}}{p_2^{(1)} + P_2^{(1)}} \\ \text{s.t. } & 0 \leq P_l^{(1)} \leq P_l^{\max} \\ & S_l^{\text{INTF}} \geq S_l^{\min} \end{aligned} \tag{6.8}$$

where

$$S_l^{\text{INTF}} = \log_2\left(1 + \frac{\gamma_{ll}^{(1)}}{1 + \gamma_{ml}^{(1)}}\right) \tag{6.9}$$

for $l = \{1, 2\}$, $m = \{2, 1\}$, and $l \neq m$.

From the analysis presented in Appendix A.4 (with $a = \frac{|h_{ll}|^2}{1+\gamma_{ml}^{(1)}}$, $k = b = 0$), in the transmit power dominated regime, i.e. $P_1^{(1)} \gg p_1^{(1)}$ and $P_2^{(1)} \gg p_2^{(1)}$, equation (6.8) is strictly decreasing with both $P_1^{(1)}$ and $P_2^{(1)}$. In this case,

the maximization of the energy efficiency corresponds to using the following transmit powers

$$P_l^{(1)} = \begin{cases} \Delta_{\text{INTF}}, & \text{if} \begin{cases} \Delta_{\text{INTF}} \leq P_l^{\max} \\ |h_{ll}|^2|h_{mm}|^2 > |h_{lm}|^2|h_{ml}|^2(2^{S_1^{\min}}-1)(2^{S_2^{\min}}-1) \end{cases} \\ \text{no solution (no success)}, & \text{otherwise} \end{cases} \tag{6.10}$$

for $l = \{1, 2\}$, $m = \{2, 1\}$, and $l \neq m$ where

$$\Delta_{\text{INTF}} = \frac{(2^{S_l^{\min}}-1)\left(|h_{mm}|^2 + |h_{lm}|^2(2^{S_m^{\min}}-1)\right)}{|h_{ll}|^2|h_{mm}|^2 - |h_{lm}|^2|h_{ml}|^2(2^{S_1^{\min}}-1)(2^{S_2^{\min}}-1)}. \tag{6.11}$$

In the circuit power dominated regime $p_1^{(1)} \gg P_1^{(1)}$ and $p_2^{(1)} \gg P_2^{(1)}$ and assuming $p_1^{(1)} = p_2^{(1)} = p^{(1)}$, equation (6.8) can be expressed as

$$\begin{aligned} \underset{P_1^{(1)}, P_2^{(1)}}{\text{maximize}}\ & \epsilon^{\text{INTF}} = \frac{S_1^{\text{INTF}} + S_2^{\text{INTF}}}{p^{(1)}} \\ \text{s.t. } & 0 \leq P_l^{(1)} \leq P_l^{\max} \\ & S_l^{\text{INTF}} \geq S_l^{\min} \end{aligned} \tag{6.12}$$

which is equivalent to maximizing the sum spectral efficiency in an interference channel. The optimal solution is then binary, i.e. both TXs transmit with maximum power or only one of them with maximum power and the other with zero power depending on the SNR [39].

6.4 Approaches That Exploit the Overhearing Capabilities of TXs

In this section we analyse the energy efficiency of two approaches (based on [56] and [85]) that exploit the overhearing capabilities of TXs. We refer to them as DIV and MRCP.

6.4.1 DIV

One way of exploiting the overhearing capabilities of the TXs consists in sharing the transmitted symbols between TXs in order to have each symbol retransmitted by a different TX. This approach resembles what was proposed in [56] but using the TXs as relays. For instance, TX 1 transmits s_1, which is received by RX 1 and TX 2 in time-slot 1, and TX 2 transmits s_2, which is received by RX 2 and TX 1 in time-slot 2. Then, in time-slot 3 TX 1 transmits s_2 and in time-slot 4 TX 2 transmits s_1. We refer to this approach as DIV (diversity).

Assuming a channel coherence time larger than 4 time-slots, the received signals can be expressed as:

$$\begin{aligned} y_1^{(1)} &= \sqrt{P_1^{(1)}} h_{11} s_1 + n_1^{(1)} \\ y_2^{(2)} &= \sqrt{P_2^{(2)}} h_{21} s_2 + n_1^{(2)} \\ y_2^{(3)} &= \sqrt{P_1^{(3)}} h_{11} z_{12} + n_1^{(3)} \\ y_1^{(4)} &= \sqrt{P_2^{(4)}} h_{21} z_{21} + n_1^{(4)}, \end{aligned} \tag{6.13}$$

where $y_l^{(t)}$ is the signal received by RX l in time-slot t, $n_l^{(t)}$ is the noise received by RX l in time-slot t and

$$z_{lm} = s_m + \frac{n_{l'}^{(m)}}{\sqrt{P_m^{(m)}} g_{ml}}, \tag{6.14}$$

where $n_{l'}^{(t)}$ is the received noise for TX l in time-slot t.

The signal received by RX 1, $\mathbf{y}_1 = \mathbf{a}_1 s_1 + \mathbf{n}_1$, can be expressed in matrix form as

$$\begin{bmatrix} y_1^{(1)} \\ y_1^{(4)} \end{bmatrix} = \underbrace{\begin{bmatrix} \sqrt{P_1^{(1)}} h_{11} \\ \sqrt{P_2^{(4)}} h_{21} \end{bmatrix}}_{\mathbf{a}_1} s_1 + \underbrace{\begin{bmatrix} n_1^{(1)} \\ n_1^{(4)} + \frac{\sqrt{P_2^{(4)}} h_{21}}{\sqrt{P_1^{(1)}} g_{12}} n_{2'}^{(1)} \end{bmatrix}}_{\mathbf{n}_1}. \tag{6.15}$$

A similar expression can be derived for RX 2.

The spectral efficiency of DIV using an MMSE estimator (see Section 6.4.2) is given as

$$S_l^{\mathrm{DIV}} = \frac{1}{4}\log_2\left(1+\gamma_{ll}^{(t_1)}+\frac{\gamma_{ml}^{(t_2)}}{\frac{\gamma_{ml}^{(t_2)}}{\xi_{lm}^{(t_1)}}+1}\right) \tag{6.16}$$

for $l=\{1,2\}$, $m=\{2,1\}$, and $l\neq m$ and where $t_1=1$, $t_2=4$ for $l=1$ and $t_1=2$, $t_2=3$ for $l=2$. Notice that the pre-log factor of $\frac{1}{4}$ is due to the use of four time-slots for transmitting both symbols by both TXs but that there is the corresponding SNR gain inside the logarithm.

The energy efficiency maximization of DIV is given as

$$\begin{aligned}\underset{P_1^{(t)},P_2^{(t)}}{\text{maximize}}\ \epsilon^{\mathrm{DIV}} &= \frac{S_1^{\mathrm{DIV}}}{\frac{1}{4}\left(p_1^{(1)}+p_2^{(4)}+P_1^{(1)}+P_2^{(4)}\right)}+\frac{S_2^{\mathrm{DIV}}}{\frac{1}{4}\left(p_2^{(2)}+p_1^{(3)}+P_2^{(2)}+P_1^{(3)}\right)}\\ \text{s.t. } & 0\leq P_l^{(t)}\leq P_l^{\max}\\ & S_l^{\mathrm{DIV}}\geq S_l^{\min}\end{aligned} \tag{6.17}$$

In the transmit power dominated regime $P_1^{(1)}+P_2^{(4)}\gg p_1^{(1)}+p_2^{(4)}$ and $P_2^{(2)}+P_1^{(3)}\gg p_2^{(2)}+p_1^{(3)}$ and assuming a strong overhearing link $\xi_{lm}^{(t)}\gg\gamma_{ml}^{(t)}$, we can observe that equation (6.17) has a maximum found by solving

$$P_l^{(t)} = \begin{cases}\frac{e^{W\left(|h_{ll}|^2(P_m^{(t)}+P_l^{(t)})\right)}-1-P_m^{(t)}|h_{ml}|^2}{|h_{ll}|^2}, & \text{if } \begin{cases}\frac{e^{W\left(|h_{ll}|^2(P_m^{(t)}+P_l^{(t)})\right)}-1-P_m^{(t)}|h_{ml}|^2}{|h_{ll}|^2}\leq P_l^{\max}\\ e^{W\left(|h_{ll}|^2(P_m^{(t)}+P_l^{(t)})\right)}\geq 1+P_m^{(t)}|h_{ml}|^2\\ P_l^{(t)}|h_{ll}|^2+P_m^{(t)}|h_{ml}|^2\geq 2^{4S_l^{\min}}-1\end{cases}\\ \text{no solution (no success)}, & \text{otherwise},\end{cases} \tag{6.18}$$

for $l=\{1,2\}$, $m=\{2,1\}$, and $l\neq m$, and where $W(x)$ is the Lambert function of x. For a proof see Appendix A.4 with $a=|h_{ll}|^2$, $b=\gamma_{ml}^{(t)}$, and $k=P_m^{(t)}$. Note that since equation (6.18) depends on $P_l^{(t)}$ and given the exponential growth with respect to $P_l^{(t)}$ and $P_m^{(t)}$, both $P_l^{(t)}$ and $P_m^{(t)}$ will tend to be as small as possible. Hence, an approximation consists in selecting whether we use the transmission or the relaying phase to transmit a given symbol with the transmit

power that satisfies the spectral efficiency constraints. Therefore, we propose to use the following transmit powers that satisfy the minimum spectral efficiency constraints.

$$
\begin{aligned}
P_1^{(1)} &= \begin{cases} \frac{2^{4S_1^{\min}}-1}{|h_{11}|^2}, & \text{if} \begin{cases} |h_{11}|^2 \geq |h_{21}|^2 \\ \frac{2^{4S_1^{\min}}-1}{|h_{11}|^2} \leq P_1^{\max} \end{cases} \\ \frac{2^{S_1^{\min}}-1}{|g_{12}|^2}, & \text{if} \begin{cases} |h_{21}|^2 > |h_{11}|^2 \\ \frac{2^{4S_1^{\min}}-1}{|h_{21}|^2} \leq P_2^{\max} \end{cases} \\ \text{no solution (no success)}, & \text{otherwise} \end{cases} \\
P_2^{(2)} &= \begin{cases} \frac{2^{4S_2^{\min}}-1}{|h_{22}|^2}, & \text{if} \begin{cases} |h_{22}|^2 \geq |h_{12}|^2 \\ \frac{2^{4S_2^{\min}}-1}{|h_{22}|^2} \leq P_2^{\max} \end{cases} \\ \frac{2^{S_2^{\min}}-1}{|g_{21}|^2}, & \text{if} \begin{cases} |h_{12}|^2 > |h_{22}|^2 \\ \frac{2^{4S_2^{\min}}-1}{|h_{12}|^2} \leq P_1^{\max} \end{cases} \\ \text{no solution (no success)}, & \text{otherwise} \end{cases} \\
P_1^{(3)} &= \begin{cases} \frac{2^{4S_2^{\min}}-1}{|h_{12}|^2}, & \text{if} \begin{cases} |h_{12}|^2 > |h_{22}|^2 \\ \frac{2^{4S_2^{\min}}-1}{|h_{12}|^2} \leq P_1^{\max} \end{cases} \\ 0, & \text{if} \begin{cases} |h_{22}|^2 \geq |h_{12}|^2 \\ \frac{2^{4S_2^{\min}}-1}{|h_{22}|^2} \leq P_2^{\max} \end{cases} \\ \text{no solution (no success)}, & \text{otherwise} \end{cases} \\
P_2^{(4)} &= \begin{cases} \frac{2^{4S_1^{\min}}-1}{|h_{21}|^2}, & \text{if} \begin{cases} |h_{21}|^2 > |h_{11}|^2 \\ \frac{2^{4S_1^{\min}}-1}{|h_{21}|^2} \leq P_2^{\max} \end{cases} \\ 0, & \text{if} \begin{cases} |h_{11}|^2 \geq |h_{21}|^2 \\ \frac{2^{4S_1^{\min}}-1}{|h_{11}|^2} \leq P_1^{\max} \end{cases} \\ \text{no solution (no success)}, & \text{otherwise} \end{cases}
\end{aligned}
\tag{6.19}
$$

Note that the minimum value in the first two time-slots needs to be sufficiently large to be decoded by the overhearing TX and the exponent 4 corresponding to the 4 time-slots required per transmission round. We will later compare this approximation with the optimal solution obtained through an exhaustive search over all possible transmit power combinations.

In the circuit power dominated regime $P_1^{(1)} + P_2^{(4)} \ll 2p^{(t)}$ and $P_2^{(2)} + P_1^{(3)} \ll 2p^{(t)}$, assuming $p_1^{(t)} = p_2^{(t)} = p^{(t)}$, equation (6.17) can be expressed as

$$\begin{aligned} \underset{P_1^{(t)}, P_2^{(t)}}{\text{maximize}}\ & \epsilon^{\text{DIV}} = \frac{S_1^{\text{DIV}} + S_2^{\text{DIV}}}{\frac{1}{4}\left(2p^{(t)}\right)} \\ \text{s.t. } & 0 \leq P_l^{(t)} \leq P_l^{\max} \\ & S_l^{\text{DIV}} \geq S_l^{\min} \end{aligned} \tag{6.20}$$

where the energy efficiency is maximized independently for each term, which corresponds to both TXs transmitting with maximum power, i.e. $P_1^{(1)} = P_1^{(3)} = P_1^{\max}$ and $P_2^{(2)} = P_2^{(4)} = P_2^{\max}$. If the spectral efficiency constraints are not satisfied, we assume that there is no solution.

6.4.2 MRCP

A different way of exploiting the overhearing capabilities of the TXs without requiring so many time-slots as DIV is proposed in [85]. The MRCP is shown to increase the spectral efficiency by finding a balance between spatial diversity and transmission time. During the transmission phase, each TX transmits a symbol in a dedicated time-slot. Then, during the relaying phase, all the TXs transmit simultaneously the overheard symbol. Specifically, in time-slot 1, TX 1 transmits s_1 to both RXs and to TX 2. In time-slot 2, TX 2 transmits s_2 to both RXs and to TX 1. In time-slot 3, each TX acts as a relay to transmit the overheard symbol (s_2 for TX 1 and s_1 for TX 2) to both RXs.

Assuming a channel coherence time larger than 3 time-slots, the received signals for RX 1 in the three time-slots can be expressed as:

$$\begin{aligned} y_1^{(1)} &= \sqrt{P_1^{(1)}} h_{11} s_1 + n_1^{(1)} \\ y_1^{(2)} &= \sqrt{P_2^{(2)}} h_{21} s_2 + n_1^{(2)} \\ y_1^{(3)} &= \sqrt{P_1^{(3)}} h_{11} z_{12} + \sqrt{P_2^{(3)}} h_{21} z_{21} + n_1^{(3)}. \end{aligned} \tag{6.21}$$

The signal received by RX 1, $\mathbf{y}_1 = \mathbf{a}_1 s_1 + \mathbf{a}_2 s_2 + \mathbf{n}_1 = \mathbf{a}_1 s_1 + \mathbf{w}_1$, can be expressed in matrix form as

$$\begin{bmatrix} y_1^{(1)} \\ y_1^{(2)} \\ y_1^{(3)} \end{bmatrix} = \begin{bmatrix} \sqrt{P_1^{(1)}} h_{11} & 0 \\ 0 & \sqrt{P_2^{(2)}} h_{21} \\ \underbrace{\sqrt{P_2^{(3)}} h_{21}}_{\mathbf{a}_1} & \underbrace{\sqrt{P_1^{(3)}} h_{11}}_{\mathbf{a}_2} \end{bmatrix} \begin{bmatrix} s_1 \\ s_2 \end{bmatrix} + \underbrace{\begin{bmatrix} n_1^{(1)} \\ n_1^{(2)} \\ n_1^{(3)} + \frac{\sqrt{P_1^{(3)}} h_{11}}{\sqrt{P_2^{(2)}} g_{21}} n_{1'}^{(2)} + \frac{\sqrt{P_2^{(3)}} h_{21}}{\sqrt{P_1^{(1)}} g_{12}} n_{2'}^{(1)} \end{bmatrix}}_{\mathbf{n}_1}. \tag{6.22}$$

where $\mathbf{w}_1$ is defined as the interference-plus-noise vector of RX 1. A similar expression can be derived for RX 2.

The MMSE is well known for being an efficient low-complexity linear receiver [86]. The MMSE of RX 1 can be derived in two steps. The first step consists in whitening the colored noise term $\mathbf{w}_1$ with its covariance matrix $\mathbf{R}_{w_1}$. This is achieved by filtering the received signal $\mathbf{y}_1$ with the matrix $\mathbf{R}_{w_1}^{-1/2}$ and then performing maximal ratio combining (MRC) over the remaining signal by taking the inner product of the resulting signal and the vector $\mathbf{R}_{w_1}^{-1/2}\mathbf{a}_1$, resulting in

$$\begin{aligned} \hat{z} = (\mathbf{R}_{w_1}^{-1/2}\mathbf{a}_1)^H \mathbf{R}_{w_1}^{-1/2}\mathbf{y}_1 &= \mathbf{a}_1^H \mathbf{R}_{w_1}^{-1}\mathbf{a}_1 s_1 + \mathbf{a}_1^H \mathbf{R}_{w_1}^{-1}\mathbf{w}_1 \\ &= \hat{z}_{\text{sig}} + \hat{z}_{\text{noise}}. \end{aligned} \tag{6.23}$$

The signal-to-noise ratio (SNR) of RX 1 using the MMSE is found to be

$$\text{SNR}_1^{\text{MRCP}} = \frac{\mathbb{E}\{|\hat{z}_{\text{sig}}|^2\}}{\mathbb{E}\{|\hat{z}_{\text{noise}}|^2\}} = \mathbf{a}_1^H \mathbf{R}_{w_1}^{-1}\mathbf{a}_1 \sigma_{\text{s}}^2, \tag{6.24}$$

which, as shown in Appendix A.5, results in

$$\text{SNR}_l^{\text{MRCP}} = \gamma_{ll}^{(l)} + \frac{\gamma_{ml}^{(3)}}{\frac{\gamma_{ll}^{(3)}}{\gamma_{ml}^{(m)}+1} + \frac{\gamma_{ll}^{(3)}}{\xi_{ml}^{(m)}} + \frac{\gamma_{ml}^{(3)}}{\xi_{lm}^{(l)}} + 1}. \tag{6.25}$$

for $l = \{1, 2\}$, $m = \{2, 1\}$, and $l \neq m$.

The energy efficiency maximization of MRCP is given as

$$\begin{aligned} \underset{P_1^{(t)}, P_2^{(t)}}{\text{maximize}} \; \epsilon^{\text{MRCP}} &= \frac{S_1^{\text{MRCP}}}{\frac{1}{3}\left(p_1^{(1)} + p_2^{(3)} + P_1^{(1)} + P_2^{(3)}\right)} + \frac{S_2^{\text{MRCP}}}{\frac{1}{3}\left(p_2^{(2)} + p_1^{(3)} + P_2^{(2)} + P_1^{(3)}\right)} \\ \text{s.t. } & 0 \leq P_l^{(t)} \leq P_l^{\max} \\ & S_l^{\text{MRCP}} \geq S_l^{\min} \end{aligned} \tag{6.26}$$

where

$$S_l^{\mathrm{MRCP}} = \frac{1}{3}\log_2\left(1 + \mathrm{SNR}_l^{\mathrm{MRCP}}\right). \tag{6.27}$$

Finding the globally optimal solution of (6.26) requires the joint optimization over different time-slots and TXs. For this purpose, we analyze the energy efficiency of MRCP for different cases and propose an approximate solution for each of them. In Section 6.6 we then compare our approximation with the global optimum that is found by an exhaustive search over all possible power combinations. In all cases we assume a stonger link between TXs than between TXs and RXs, i.e. $\xi_{np}^{(t)} \gg \gamma_{lm}^{(t)}\ \forall l, m, n, p, t$.

Transmit Power Dominated Regime

Case with dominant direct links. When the direct links are stronger than the indirect links, i.e. $|h_{11}|^2 > |h_{21}|^2$ and $|h_{22}|^2 > |h_{12}|^2$, we can approximate the spectral efficiency (6.27) as

$$S_l^{\mathrm{MRCP}} \approx \frac{1}{3}\log_2\left(1 + \gamma_{ll}^{(l)}\right). \tag{6.28}$$

With this approximation $P_1^{(3)}$ and $P_2^{(3)}$ only decrease the energy efficiency of the system, so we set them as $P_1^{(3)} = 0$ and $P_2^{(3)} = 0$. Note that the minimum spectral efficiency constraints will be satisfied with the transmission of the first two time-slots, however introducing a penalty by leaving the last time-slot unused.

Similarly to the TDMA case, (6.26) is strictly decreasing with both $P_1^{(1)}$ and $P_2^{(2)}$ (for a proof see Appendix A.4 and use $a = |h_{ll}|^2$ and $k = b = 0$). In this case the energy efficiency maximization corresponds to using the following transmit power that satisfy the minimum spectral efficiency constraints for $l = \{1, 2\}$ and $t = \{1, 2\}$.

$$P_l^{(t)} = \begin{cases} \frac{2^{3S_l^{\min}} - 1}{|h_{ll}|^2}, & \text{if } \frac{2^{3S_l^{\min}} - 1}{|h_{ll}|^2} \leq P_l^{\max} \\ \text{no solution (no success)}, & \text{otherwise} \end{cases} \tag{6.29}$$

Notice the exponent 3 corresponding to the 3 time-slots required per transmission round.

Case with one dominant direct link and one dominant indirect link. If for one RX the direct link is stronger than the indirect link whereas for the other RX the indirect link is stronger than the direct link, specifically either (i) $|h_{11}|^2 > |h_{21}|^2$ and $|h_{12}|^2 > |h_{22}|^2$ or (ii) $|h_{22}|^2 > |h_{12}|^2$ and $|h_{21}|^2 > |h_{11}|^2$, we can approximate the spectral efficiency (6.27) as

$$\begin{aligned} S_1^{\mathrm{MRCP}} &\approx \frac{1}{3}\log_2\left(1+\gamma_{11}^{(1)}\right) \\ S_2^{\mathrm{MRCP}} &\approx \frac{1}{3}\log_2\left(1+\gamma_{12}^{(3)}\right) \end{aligned} \tag{6.30}$$

for case (i). For TX 2, it is clear that its transmission only decreases the energy efficiency of the system. For TX 1, (6.26) is strictly decreasing with $P_1^{(1)}$ and $P_1^{(3)}$. In this case we can set the transmit powers as follows:

$$\begin{aligned} P_1^{(1)} &= \begin{cases} \frac{2^{3S_1^{\min}}-1}{|h_{11}|^2}, & \text{if } \frac{2^{3S_1^{\min}}-1}{|h_{11}|^2} \le P_1^{\max} \\ \text{no solution (no success)}, & \text{otherwise} \end{cases} \\ P_2^{(2)} &= \begin{cases} \frac{2^{S_2^{\min}}-1}{|g_{21}|^2}, & \text{if } \frac{2^{3S_2^{\min}}-1}{|h_{12}|^2} \le P_1^{\max} \\ \text{no solution (no success)}, & \text{otherwise} \end{cases} \\ P_1^{(3)} &= \begin{cases} \frac{2^{3S_2^{\min}}-1}{|h_{12}|^2}, & \text{if } \frac{2^{3S_2^{\min}}-1}{|h_{12}|^2} \le P_1^{\max} \\ \text{no solution (no success)}, & \text{otherwise} \end{cases} \\ P_2^{(3)} &= \begin{cases} 0, & \text{if } \frac{2^{3S_1^{\min}}-1}{|h_{11}|^2} \le P_1^{\max} \\ \text{no solution (no success)}, & \text{otherwise} \end{cases} \end{aligned} \tag{6.31}$$

Note that in this case $P_2^{(2)}$ needs to be sufficiently large to be decoded by the other TX. For case (ii) we can set the transmit powers as follows:

$$
\begin{aligned}
P_1^{(1)} &= \begin{cases} \frac{2^{3S_1^{\min}}-1}{|g_{12}|^2}, & \text{if } \frac{2^{3S_1^{\min}}-1}{|h_{21}|^2} \leq P_2^{\max} \\ \text{no solution (no success)}, & \text{otherwise} \end{cases} \\
P_2^{(2)} &= \begin{cases} \frac{2^{3S_2^{\min}}-1}{|h_{22}|^2}, & \text{if } \frac{2^{3S_2^{\min}}-1}{|h_{22}|^2} \leq P_2^{\max} \\ \text{no solution (no success)}, & \text{otherwise} \end{cases} \\
P_1^{(3)} &= \begin{cases} 0, & \text{if } \frac{2^{3S_2^{\min}}-1}{|h_{22}|^2} \leq P_2^{\max} \\ \text{no solution (no success)}, & \text{otherwise} \end{cases} \\
P_2^{(3)} &= \begin{cases} \frac{2^{3S_1^{\min}}-1}{|h_{21}|^2}, & \text{if } \frac{2^{3S_1^{\min}}-1}{|h_{21}|^2} \leq P_2^{\max} \\ \text{no solution (no success)}, & \text{otherwise} \end{cases}
\end{aligned}
\tag{6.32}
$$

Note that in this case $P_1^{(1)}$ needs to be sufficiently large to be decoded by the other TX.

Case with dominant indirect links. In this case the indirect links are stronger than the direct links, i.e. $|h_{21}|^2 > |h_{11}|^2$ and $|h_{12}|^2 > |h_{22}|^2$. This case occurs, for instance, when users from a HetNet are closer to an interfering base station than to their serving base station[3]. Different from the previous cases where all the symbols are transmitted in dedicated time-slots, here simultaneous transmissions through the indirect channels occur in the third time-slot, generating interference to both RXs. Therefore, we consider two subcases. If one indirect link is stronger than the other by a factor $\beta > 1$, i.e. $|h_{lm}|^2 > \beta |h_{ml}|^2$, we will allow only TX l to use the third time-slot. Otherwise, both TXs use the third time-slot.

For the first subcase, when $|h_{12}|^2 > \beta |h_{21}|^2$, we can approximate the spectral efficiency (6.27) as equation (6.30). Therefore, we can use the transmit powers of equation (6.31). Similarly, when $|h_{21}|^2 > \beta |h_{12}|^2$ we will use the transmit powers of equation (6.32).

[3]This case happens frequently with closed access base stations where users have a strong interference from a base station that they are not allowed to access and it is one of the main scenarios analyzed by the Small Cell Forum [32]. The analysis presented in this chapter can serve as incentive to cooperate with neighboring base stations with the reward of improving the energy efficiency while sharing the same bandwidth.

For the second subcase, we can approximate the spectral efficiency (6.27) as

$$S_l^{\mathrm{MRCP}} \approx \frac{1}{3}\log_2\left(1+\gamma_{ml}^{(3)}\right). \tag{6.33}$$

for $l=\{1,2\}$, $m=\{2,1\}$, and $l\neq m$. In this case we will use the third time-slot for simultaneous transmissions. Since in this case $P_1^{(1)}$ and $P_2^{(2)}$ only decrease the energy efficiency of the system, we need to make sure that they are sufficiently large to be decoded by the other TX:

$$P_l^{(l)} = \begin{cases} \frac{2^{S_l^{\min}}-1}{|g_{lm}|^2}, & \text{if} \begin{cases} \Delta_{\mathrm{MRCP}_l} \leq P_l^{\max} \\ |h_{11}|^2|h_{22}|^2 > |h_{12}|^2|h_{21}|^2(2^{3S_1^{\min}}-1)(2^{3S_2^{\min}}-1) \end{cases} \\ \text{no solution (no success)}, & \text{otherwise} \end{cases} \tag{6.34}$$

where

$$\Delta_{\mathrm{MRCP}_l} = \frac{(2^{3S_l^{\min}}-1)\left(|h_{mm}|^2+|h_{lm}|^2(2^{3S_m^{\min}}-1)\right)}{|h_{ll}|^2|h_{mm}|^2-|h_{lm}|^2|h_{ml}|^2(2^{3S_1^{\min}}-1)(2^{3S_2^{\min}}-1)} \tag{6.35}$$

for $l=\{1,2\}$, $m=\{2,1\}$, and $l\neq m$.

Furthermore, since (6.26) is strictly decreasing with $P_1^{(3)}$ and $P_2^{(3)}$ (as seen in Appendix A.4 with $a=|h_{ml}|^2$ for $m\neq l$ and $k=b=0$), we propose to use the following transmit powers that satisfy the minimum spectral efficiency constraints

$$P_l^{(3)} = \begin{cases} \Delta_{\mathrm{MRCP}_l}, & \text{if} \begin{cases} \Delta_{\mathrm{MRCP}_l} \leq P_l^{\max} \\ |h_{ll}|^2|h_{mm}|^2 > |h_{lm}|^2|h_{ml}|^2(2^{3S_1^{\min}}-1)(2^{3S_2^{\min}}-1) \end{cases} \\ \text{no solution (no success)}, & \text{otherwise} \end{cases} \tag{6.36}$$

for $l=\{1,2\}$, $m=\{2,1\}$, and $l\neq m$. Note that (6.36) is similar to (6.10) for INTF except for the penalty of requiring 3 time-slots per transmission round.

Circuit Power Dominated Regime

In the circuit power dominated regime we can assume that $p_1^{(1)}+p_2^{(3)} \gg P_1^{(1)}+P_2^{(3)}$ and $p_2^{(2)}+p_1^{(3)} \gg P_2^{(2)}+P_1^{(3)}$. For simplicity we assume $p_1^{(1)} =$

$p_2^{(2)} = p_1^{(3)} = p_2^{(3)} = p^{(t)}$ and we can see that (6.26) can be approximated as

$$\begin{aligned} \underset{P_1^{(t)}, P_2^{(t)} \forall t}{\text{maximize}} \; & \epsilon^{\text{MRCP}} \approx \frac{S_1^{\text{MRCP}} + S_2^{\text{MRCP}}}{\frac{1}{3}\left(2p^{(t)}\right)} \\ \text{s.t. } & 0 \leq P_l^{(t)} \leq P_l^{\max} \\ & S_l^{\text{MRCP}} \geq S_l^{\min} \end{aligned} \tag{6.37}$$

where the energy efficiency is maximized independently for each term of equation (6.37).

Case with dominant direct links. When the direct links are stronger than the indirect links, i.e. $|h_{11}|^2 > |h_{21}|^2$ and $|h_{22}|^2 > |h_{12}|^2$, we can approximate the spectral efficiency as equation (6.28).

For the first two time-slots, this corresponds to both TXs using maximum transmit power, i.e. $P_1^{(1)} = P_1^{\max}$ and $P_2^{(2)} = P_2^{\max}$. For the third time-slot, $P_1^{(3)}$ and $P_2^{(3)}$ only decrease the energy efficiency of the system. Therefore, we propose to set $P_1^{(3)} = 0$ and $P_2^{(3)} = 0$. If the spectral efficiency constraints are not satisfied we assume that there is no solution.

Case with one dominant direct link and one dominant indirect link. This is the case where either (i) $|h_{11}|^2 > |h_{21}|^2$ and $|h_{12}|^2 > |h_{22}|^2$ or (ii) $|h_{22}|^2 > |h_{12}|^2$ and $|h_{21}|^2 > |h_{11}|^2$.

For case (i), we can approximate the spectral efficiency as (6.30). With this approximation, the energy efficiency is maximized independently for each term of (6.37), which corresponds to $P_1^{(1)} = P_1^{\max}$, $P_1^{(3)} = P_1^{\max}$, $P_2^{(2)} = \frac{2^{S_2^{\min}}}{|g_{21}|^2}$ and $P_2^{(3)} = 0$. For case (ii), we set $P_2^{(2)} = P_2^{\max}$, $P_2^{(3)} = P_2^{\max}$, $P_1^{(1)} = \frac{2^{S_1^{\min}}}{|g_{12}|^2}$ and $P_1^{(3)} = 0$. For both cases, if the spectral efficiency constraints are not satisfied we assume that there is no solution.

Case with dominant indirect links. This is the case when the indirect links are stronger than the direct links, i.e. $|h_{21}|^2 > |h_{11}|^2$ and $|h_{12}|^2 > |h_{22}|^2$. We consider again two subcases. When $|h_{12}|^2 > \beta|h_{21}|^2$, we can approximate the

spectral efficiency as equation (6.30) and we use the following transmit powers:

$$
\begin{aligned}
P_1^{(1)} &= \begin{cases} P_1^{\max}, & \text{if } \frac{2^{3S_1^{\min}}-1}{|h_{11}|^2} \leq P_1^{\max} \\ \text{no solution (no success)}, & \text{otherwise} \end{cases} \\
P_2^{(2)} &= \begin{cases} \frac{2^{S_1^{\min}}-1}{|g_{21}|^2}, & \text{if } \frac{2^{3S_2^{\min}}-1}{|h_{12}|^2} \leq P_1^{\max} \\ \text{no solution (no success)}, & \text{otherwise} \end{cases} \\
P_1^{(3)} &= \begin{cases} P_1^{\max}, & \text{if } \frac{2^{3S_2^{\min}}-1}{|h_{12}|^2} \leq P_1^{\max} \\ \text{no solution (no success)}, & \text{otherwise} \end{cases} \\
P_2^{(3)} &= \begin{cases} 0, & \text{if } \frac{2^{3S_1^{\min}}-1}{|h_{11}|^2} \leq P_1^{\max} \\ \text{no solution (no success)}, & \text{otherwise} \end{cases}
\end{aligned}
\tag{6.38}
$$

Similarly, if $|h_{21}|^2 > \beta|h_{12}|^2$ we use

$$
\begin{aligned}
P_1^{(1)} &= \begin{cases} \frac{2^{S_2^{\min}}-1}{|g_{12}|^2}, & \text{if } \frac{2^{3S_1^{\min}}-1}{|h_{21}|^2} \leq P_2^{\max} \\ \text{no solution (no success)}, & \text{otherwise} \end{cases} \\
P_2^{(2)} &= \begin{cases} P_2^{\max}, & \text{if } \frac{2^{3S_2^{\min}}-1}{|h_{22}|^2} \leq P_2^{\max} \\ \text{no solution (no success)}, & \text{otherwise} \end{cases} \\
P_1^{(3)} &= \begin{cases} 0, & \text{if } \frac{2^{3S_2^{\min}}-1}{|h_{22}|^2} \leq P_2^{\max} \\ \text{no solution (no success)}, & \text{otherwise} \end{cases} \\
P_2^{(3)} &= \begin{cases} P_2^{\max}, & \text{if } \frac{2^{3S_1^{\min}}-1}{|h_{21}|^2} \leq P_2^{\max} \\ \text{no solution (no success)}, & \text{otherwise} \end{cases}
\end{aligned}
\tag{6.39}
$$

In the second subcase, we can approximate the spectral efficiency as equation (6.33), where $P_1^{(1)}$ and $P_2^{(2)}$ only decrease the energy efficiency of the system. Therefore, we only need to make sure that they are sufficiently large to be decoded by the other TX as in equation (6.34). For the third time-slot, given that these are simultaneous transmissions as in INTF, the optimal solution is binary [39]. Again if the spectral efficiency constraints are not satisfied we assume that there is no solution.

The whole MRCP power control strategy for the different cases can be summarized in algorithm 2.

Algorithm 2 MRCP power control

if Transmit power regime **then**
  if $|h_{11}|^2 > |h_{21}|^2$ and $|h_{22}|^2 > |h_{12}|^2$ **then**
    Use $P_l^{(t)}$ as in (6.29) for $l = t = 1, 2$ and $P_1^{(3)} = P_2^{(3)} = 0$
  else if ($|h_{11}|^2 > |h_{21}|^2$ and $|h_{12}|^2 > |h_{22}|^2$) or ($|h_{22}|^2 > |h_{12}|^2$ and $|h_{21}|^2 > |h_{11}|^2$) **then**
    Use $P_l^{(t)}$ as in (6.31) or use $P_l^{(t)}$ as in (6.32) for $l = 1, 2$ and $t = 1, 2, 3$.
  else if $|h_{12}|^2 > |h_{22}|^2$ and $|h_{21}|^2 > |h_{11}|^2$ **then**
    Use $P_l^{(t)}$ as in (6.31) if $|h_{12}|^2 > \beta|h_{21}|^2$ or use $P_l^{(t)}$ as in (6.32) if $|h_{21}|^2 > \beta|h_{12}|^2$ for $l = 1, 2$ and $t = 1, 2, 3$, otherwise use $P_l^{(t)}$ as in (6.34) for $l = t = 1, 2$ and use $P_l^{(3)}$ as in (6.36) for $l = 1, 2$
  end if
else if Circuit power regime **then**
  if $|h_{11}|^2 > |h_{21}|^2$ and $|h_{22}|^2 > |h_{12}|^2$ **then**
    $P_1^{(1)} = P_1^{\max}$, $P_2^{(2)} = P_2^{\max}$ and $P_1^{(3)} = P_2^{(3)} = 0$.
  else if ($|h_{11}|^2 > |h_{21}|^2$ and $|h_{12}|^2 > |h_{22}|^2$) or ($|h_{22}|^2 > |h_{12}|^2$ and $|h_{21}|^2 > |h_{11}|^2$) **then**
    $P_1^{(1)} = P_1^{(3)} = P_1^{\max}$, $P_2^{(2)} = \frac{2^{S_2^{\min}}}{|g_{21}|^2}$, and $P_2^{(3)} = 0$ or $P_2^{(2)} = P_2^{(3)} = P_2^{\max}$, $P_1^{(1)} = \frac{2^{S_1^{\min}}}{|g_{12}|^2}$, and $P_1^{(3)} = 0$.
  else if $|h_{12}|^2 > |h_{22}|^2$ and $|h_{21}|^2 > |h_{11}|^2$ **then**
    Use $P_l^{(t)}$ as in (6.38) if $|h_{12}|^2 > \beta|h_{21}|^2$ or use $P_l^{(t)}$ as in (6.39) if $|h_{21}|^2 > \beta|h_{12}|^2$ for $l = 1, 2$ and $t = 1, 2, 3$, otherwise use $P_l^{(t)}$ as in (6.34) for $l = t = 1, 2$ and use a binary $P_l^{(3)}$ for $l = 1, 2$
  end if
end if

6.5 Complexity Analysis

As seen in previous sections, knowing the optimal power control strategy for DIV and MRCP requires an exhaustive search over all the possible power values in every time-slot and for every TX. In contrast, with the proposed sub-optimal power control strategy, we divide the problem into two power regimes and classify it according to the dominance of certain links. Based on this, we select the closed-form formula that computes the power for every TX.

For instance, for the system in consideration, with two TXs and two RXs, we are looking for 4 power values for DIV and also 4 power values for MRCP. Assuming that each TX can use one of K possible transmit power values, an exhaustive search that can lead to the optimal power control yields up to K^4

different transmit power combinations for both DIV and MRCP (the higher the K the higher the accuracy).

The proposed sub-optimal power control strategy for both DIV and MRCP classifies the scenario according to the dominance of the transmit power or the circuit power and according to the dominance of certain links (direct or indirect). According to this classification, the proposed power control strategy obtains the corresponding power value for each TX through a closed-form formula. Specifically for DIV, this results in using the formulas of (6.19) when the system works in the transmit power dominated regime and using maximum power for each TX when the system works in the circuit power dominated regime. Specifically for MRCP, the proposed power control strategy obtains the corresponding power value for each TX through Algorithm 2. Hence, instead of performing K^4 operations to obtain the optimal power control, we only need to classify the scenario (regime and links dominance) and then use a closed-form formula to obtain a sub-optimal power control. This complexity reduction comes with a small degradation in spectral efficiency, energy efficiency, and success rate with respect to the optimal power control strategy as can be seen in Section 6.6.

6.6 Performance Evaluation

In this section we compare the approaches analyzed in previous sections in terms of energy efficiency, spectral efficiency, and success rate (probability of reaching a solution that satisfies the constraints). We consider a Rayleigh fading channel model with $\mathbb{E}\{|g_{12}|^2\} = \mathbb{E}\{|g_{21}|^2\} = 100$ and direct links with $\mathbb{E}\{|h_{11}|^2\} = \mathbb{E}\{|h_{22}|^2\} = 1$ (we will only vary the indirect links average gain). We use a fixed circuit power of $p_1^{(t)} = p_2^{(t)} = 0.1W \ \forall t$ with $\sigma_{\mathrm{s}}^2 = \sigma_{\mathrm{n}}^2 = 1$, $\beta = 3$, and $S_1^{\min} = S_2^{\min} = 0.3$bits/Hz.

We consider the two regimes studied in this chapter: transmit power dominated and circuit power dominated. In the first one, the maximum transmit power of both TXs is 10W. In the second one, it is 0.05W. In order to evaluate the performance under different conditions, we first vary the average of both indirect links equally, i.e. $R_1 = \mathbb{E}\{|h_{21}|^2\} = \mathbb{E}\{|h_{12}|^2\}$. As a second example, we vary the average of one indirect link relative to the average of the other indirect link, i.e. $R_2 = \frac{1}{\mathbb{E}\{|h_{21}|^2\}} = \mathbb{E}\{|h_{12}|^2\}$. For the circuit power dominated regime we vary only R_1 (with a gain 10 times larger for all the links). In the case of DIV and MRCP we include the optimal solution obtained with an exhaustive search over all the possible power combinations, named respectively 'DIV optimal' and 'MRCP optimal'. Finally, considering all equal average links, i.e. $\mathbb{E}\{|h_{11}|^2\} =$

$\mathbb{E}\{|h_{12}|^2\} = \mathbb{E}\{|h_{21}|^2\} = \mathbb{E}\{|h_{22}|^2\} = 1$, we analyze the performance of the studied approaches with respect to the spectral efficiency constraints assuming $S_1^{\min} = S_2^{\min}$. If, for a given instance, two links happen to have same exact instantaneous value, we assume for the sake of our approximations that the direct one is larger than the indirect one.

For the transmit power dominated regime, our simulations show that when the difference between indirect and direct channels grows, so does the energy efficiency, as can be seen in Fig. 6.2. It can also be seen that a small value of R_1 has a positive impact for both TDMA and INTF (since both direct channels are larger than both indirect channels). This effect decreases with R_1. In fact, when $\log_2 R_1 = 0$ (all equal links), the energy efficiency of both DIV and MRCP is larger than that of TDMA and INTF and for $\log_2 R_1 = 3$ the increase is more than double. In this context, both DIV and MRCP have a similar energy efficiency with a slightly larger energy efficiency by DIV. The success rate of this scenario also shows that DIV, MRCP, and TDMA have a good performance as seen in Fig. 6.3 although with a decline of MRCP for high values of $\log_2 R_1$. The spectral efficiency results are not shown since optimizing the energy efficiency in the transmit power dominated regime boils down to using the transmit power that satisfies the minimum spectral efficiency constraints.

On the other hand when one indirect channel grows while the other decreases, we can still see that both DIV and MRCP have the best performance for any value of $\log_2 R_2$ as seen in Fig. 6.4. This shows that both DIV and MRCP are able to exploit one or both of the indirect channels to achieve a higher energy efficiency. In terms of success rate, the performance of DIV, MRCP and TDMA is higher than 0.8 as seen in Fig. 6.5. This highlights the result that when at least one indirect link is larger than the direct links, exploiting the overhearing capabilities of the TXs provides the highest performance.

For the circuit power dominated regime, our simulations show a similar trend where the energy efficiency of DIV and MRCP increase with $\log_2 R_1$ as seen in Fig. 6.6. However, only above a value of $\log_2 R_1 = 1.5$ and $\log_2 R_1 = 2.5$ does DIV and MRCP show a higher energy efficiency than INTF and TDMA, respectively. Since here we mainly consider maximum transmit powers, it is interesting to see a similar behavior in the spectral efficiency as seen in Fig. 6.7. However, the spectral efficiency of INTF turns out to be the highest due to the pre-log factor and the low transmit power conditions. This comes at the price of a very low success rate as can be seen in Fig. 6.8.

Finally, it is interesting to notice that the energy efficiency also depends on the spectral efficiency constraints. Considering all equal links, we can see in Fig. 6.9 and Fig. 6.10 for the transmit power dominated regime that DIV and MRCP achieve the highest energy efficiency and success rate when the minimum

spectral efficiencies are small. However, when the minimum spectral efficiencies are large, a large difference between indirect and direct links is necessary to provide a similar performance. Again considering all equal channels gains, we observe in Fig. 6.11 and Fig. 6.12 that TDMA has the largest energy efficiency, but MRCP and DIV have the largest success rate. This shows that strong indirect links are necessary in this regime for the overhearing strategies to achieve a higher energy efficiency.

The choice of whether to use DIV or MRCP depends on the spectral efficiency constraints. In the transmit power dominated regime, DIV has a higher energy efficiency than MRCP when the minimum spectral efficiencies are small, while MRCP has a higher energy efficiency when the minimum spectral efficiencies are large. This is because DIV requires more time-slots per transmission round, and hence a higher transmit power, especially when the spectral efficiency constraint is high. In the circuit power dominated regime, the transmit power used is maximum or binary, hence the number of time-slots are not considered. Therefore, DIV shows a higher energy efficiency for any spectral efficiency constraints. However, in both cases the success rate for DIV drops faster than for MRCP.

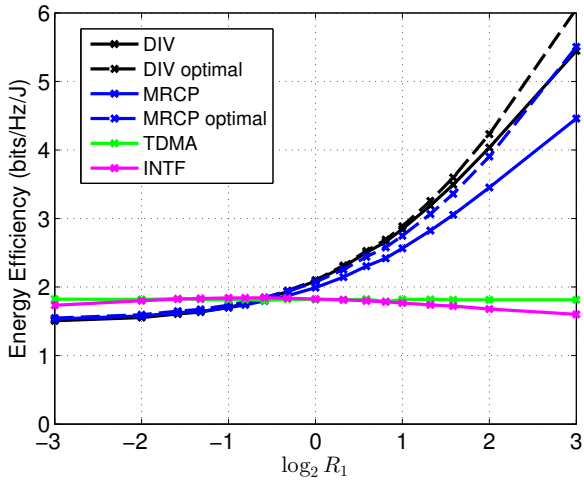

Figure 6.2: Energy efficiency of the studied approaches in the transmit power dominated regime with $S_1^{\min} = S_1^{\min} = 0.3$bits/Hz.

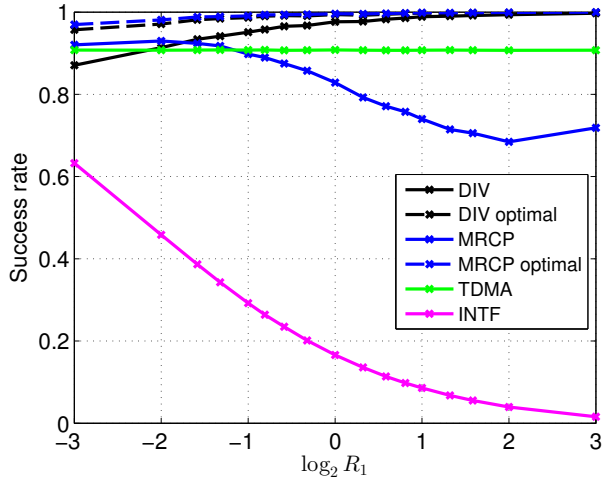

Figure 6.3: Success rate of the studied approaches in the transmit power dominated regime with $S_1^{\min} = S_1^{\min} = 0.3$bits/Hz.

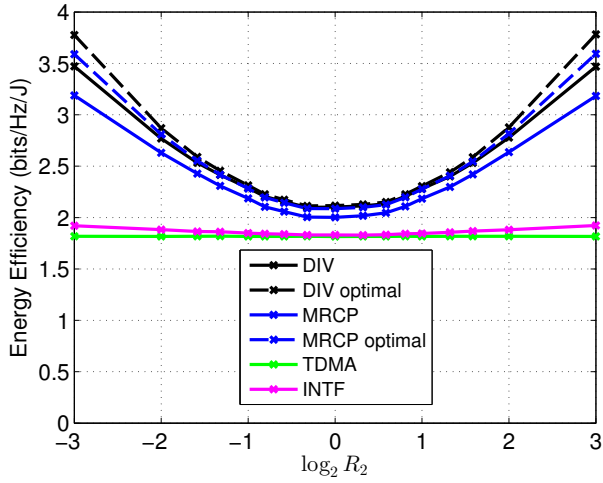

Figure 6.4: Energy efficiency of the studied approaches in the transmit power dominated regime with $S_1^{\min} = S_1^{\min} = 0.3$bits/Hz.

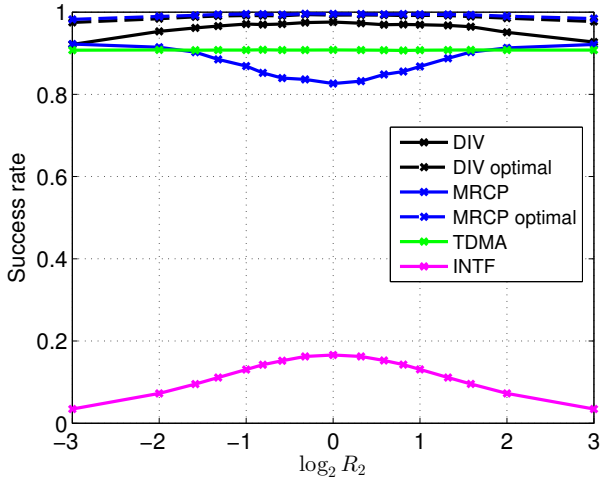

Figure 6.5: Success rate of the studied approaches in the transmit power dominated regime with $S_1^{\min} = S_1^{\min} = 0.3$bits/Hz.

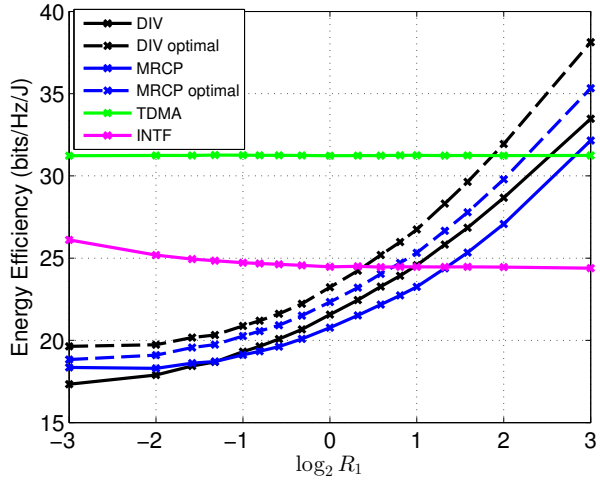

Figure 6.6: Energy efficiency of the studied approaches in the circuit power dominated regime with $S_1^{\min} = S_1^{\min} = 0.3$bits/Hz.

6.7 Conclusions

In this chapter we have analyzed two approaches that exploit the overhearing capabilities of TXs in terms of spectral efficiency, energy efficiency, and success

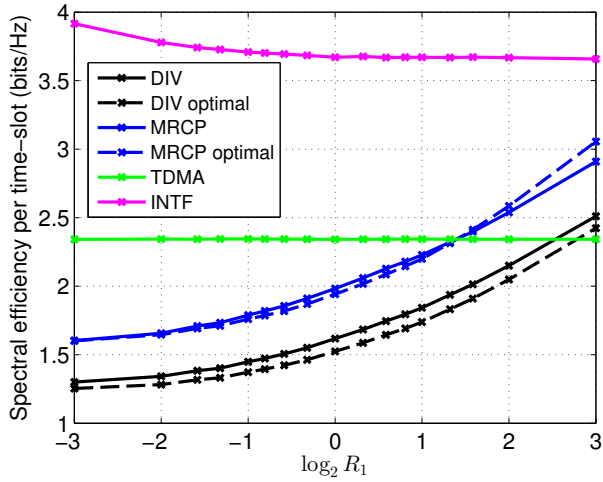

Figure 6.7: Spectral efficiency of the studied approaches in the circuit power dominated regime with $S_1^{\min} = S_1^{\min} = 0.3$bits/Hz.

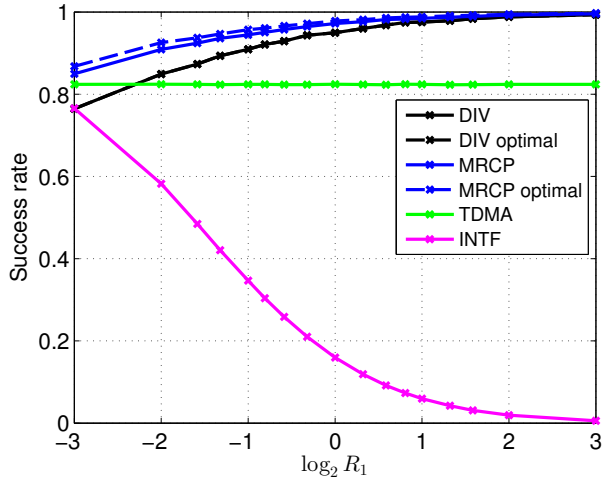

Figure 6.8: Success rate of the studied approaches in the circuit power dominated regime with $S_1^{\min} = S_1^{\min} = 0.3$bits/Hz.

rate, under the assumption of a strong overhearing link typical of dense networks. We have also provided a low-complexity power control strategy that achieves a performance close to the optimal for each of these approaches.

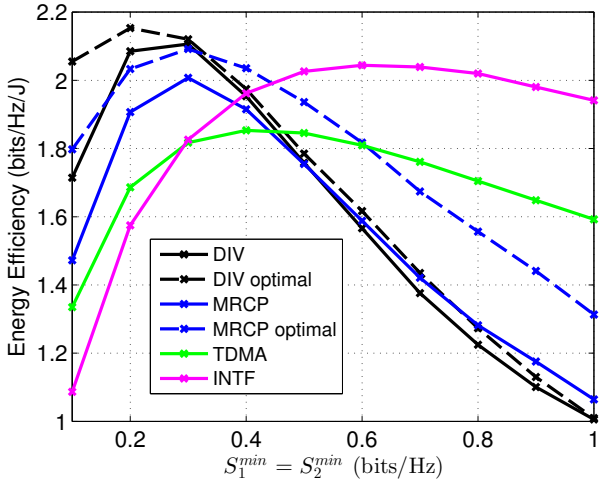

Figure 6.9: Energy efficiency of the studied approaches in the transmit power dominated regime with equal average links.

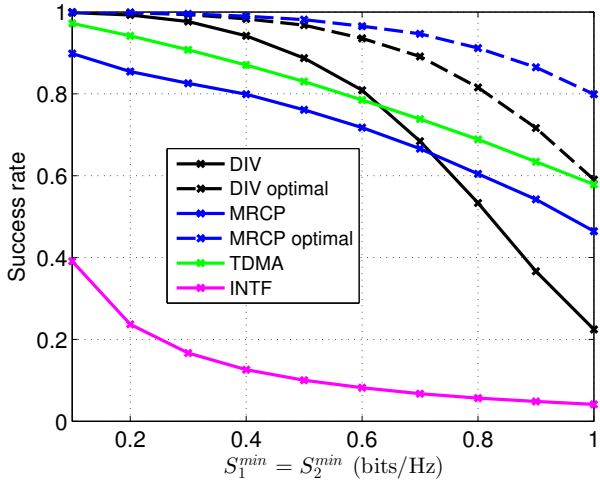

Figure 6.10: Success rate of the studied approaches in the transmit power dominated regime with equal average links.

When comparing the use of overhearing capabilities with other baseline approaches that do not exploit overhearing capabilities, we show that when at least one indirect link is stronger than the direct links, exploiting the overhearing

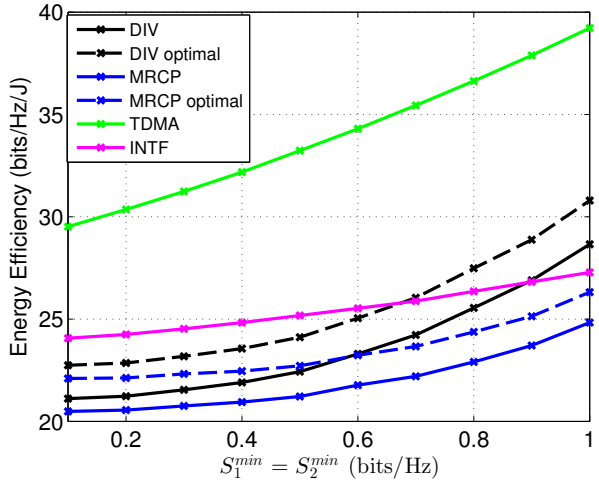

Figure 6.11: Energy efficiency of the studied approaches in the circuit power dominated regime with equal average links.

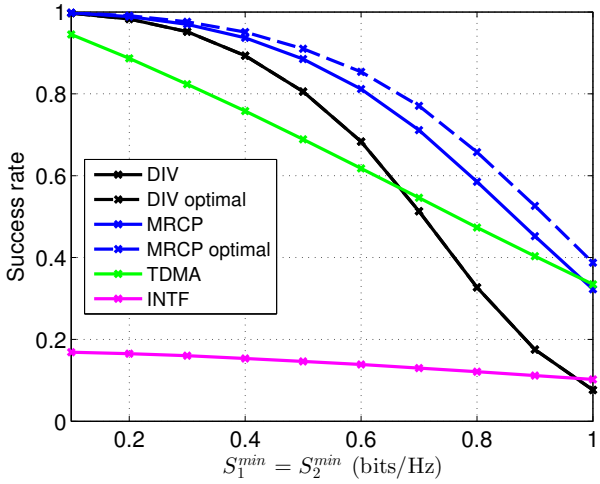

Figure 6.12: Success rate of the studied approaches in the circuit power dominated regime with equal average links.

capabilities of the TXs provides the highest performance. In particular, using the transmit power that satisfies the minimum spectral efficiency constraints and using only the strongest links is shown to achieve the best performance in

the transmit power dominated regime, while using maximum transmit power or a binary power with the strongest links achieves the best performance in the circuit power dominated regime. The choice of using simultaneous transmissions (MRCP) or dedicated time-slots (DIV) during the relaying phase depends on the spectral efficiency constraints. Using dedicated time-slots shows a larger energy efficiency in the circuit power dominated regime and when the minimum spectral efficiencies are small in the transmit power dominated regime, while using simultaneous transmissions shows a larger energy efficiency in the transmit power dominated regime when the minimum spectral efficiencies are large.

Chapter 7

General Conclusions and Future Work

In this thesis we have analyzed different cooperative strategies that reduce the inter-cell interference in dense networks, while reusing the wireless bandwidth and keeping the exchange of CSI among base stations to a minimum. These strategies can be easily applied to dense cellular networks, where there is a high probability of overhearing data and CSI from different nodes. Since some strategies apply to a particular scenario or network topology, a direct comparison between them remains a complex task that requires further investigation. Nevertheless, the results in this thesis show that by exploiting the overhearing capabilities of the network and using the overheard information in an altruistic way, significant performance gains (or performance trade-offs) can be achieved.

First, in Chapter 2, we propose an autonomous power control that can be tuned to increase the data rate of users served by the base station performing the power control strategy, while protecting the data rate of users from neighboring cells. In Chapter 3 we propose the use of D2D communication between cell edge users. This is done by allowing cell edge users to overhear signals from other base stations intended to users located in the proximity. These overheard signals are then retransmitted to the intended users during the time-slots in which they are not receiving their intended signal in order to avoid creating additional inter-cell interference. In Chapter 4 we propose a communication protocol in which the base stations in a dense network retransmit the overheard signals from neighboring BSs in order to provide spatial diversity and fairness to all the users of the network. However, not all the base stations and users can overhear the transmissions from all the other base stations in the

network. Therefore, in Chapter 5 we exploit the network topology by allowing simultaneous transmissions from the base stations that do not overhear each other in a first phase and allowing retransmissions of the overheard signals in a second phase, hence reusing the available bandwidth and increasing the spatial diversity and spectral efficiency. The previous strategies require to split some of the resources for serving the intended user and other users, which has a cost on the consumed energy and resources. The cost is analyzed in Chapter 6 and a sub-optimal power control strategy is proposed.

We now summarize the main conclusions from each chapter.

7.1 Chapter 2

In this chapter we have proposed NF-IWF, a neighbor-friendly autonomous algorithm for power control in wireless heterogeneous networks. NF-IWF protects the data rate of victim users located within a certain distance from the base station. This is done through a factor that penalizes the power allocation in those subcarriers that damage the data rate of victim users.

Our results show that NF-IWF presents higher tunability, robustness, and better data rate performance, especially in high interference conditions compared to greedy algorithms such as IWF, SFR, and EPA with a marginal decrease of the primary users data rate. Furthermore, the rate region of NF-IWF lies close to the upper bound with full knowledge of the interfering channel and the power allocation of the neighboring cell.

7.2 Chapter 3

In this chapter we have exploited the overhearing capabilities of cell edge users by allowing them to relay the signals overheard from other base stations. Our approach based on AFR uses D2D communication among cell edge users during the time-slots in which they are not receiving the intended signal from their serving base station. We have developed this approach for different cellular array configurations and extended it to the scenario with multiple cell edge users.

Our results show that the proposed approach increases the spatial diversity and the spectral efficiency per time-slot without affecting the DoF. This gain is independent of the cellular array configuration and it grows with the number of cell edge users.

7.3 Chapter 4

In this chapter we have proposed MRCP, a multiple-relay communication protocol for achieving fairness in dense networks. The proposed approach is able to find an efficient balance between spatial diversity and transmission time by using currently-deployed base stations as relays. Moreover, MRCP is applicable to any number of base stations and users, while keeping a small transmission time.

Our results show that MRCP reaches almost maximum JFI fairness and the highest max-min fairness when compared to communication schemes like TDMA, INTF, and DIV. This comes with a BER that achieves almost full diversity with asymmetric transmissions, typical of dense networks.

7.4 Chapter 5

Using the Wyner cellular model, in this chapter we have proposed two topology-aware STNC schemes (TAS1 and TAS2) that exploit the knowledge of the $2K$ neighboring base stations by allowing simultaneous transmissions of the base stations that do not overhear each other during the transmission phase. During the relaying phase, each base station transmits the information overheard during the transmission phase in two ways. With TAS1, base stations that do not overhear each other transmit simultaneously. With TAS2, all the base stations transmit in one single time-slot.

Our results show an improvement in the spectral efficiency per time-slot and BER in scenarios with unequal transmit power and unequal channel conditions compared to traditional STNC and other baseline schemes.

7.5 Chapter 6

In this chapter we have analyzed the cost of base stations to relay overheard signals in terms of energy efficiency, spectral efficiency, and success rate. This is done for two approaches that exploit the overhearing capabilities of transmitting nodes under the assumption of a strong overhearing link typical of dense networks.

Our results show that when at least one indirect link is stronger than the direct links, exploiting the overhearing capabilities of the base stations provides the highest performance. This should be combined with the transmit power

that satisfies the minimum spectral efficiency constraints in the transmit power dominated regime and with the maximum or binary transmit power in the circuit power dominated regime.

The choice of using simultaneous transmissions (MRCP) or dedicated time-slots (DIV) during the relaying phase depends on the setting. Using dedicated time-slots shows a larger energy efficiency in the circuit power dominated regime and when the minimum spectral efficiency is small in the transmit power dominated regime. Using simultaneous transmissions shows a larger energy efficiency when the minimum spectral efficiency is large in the transmit power dominated regime. In terms of success rate using simultaneous transmissions is generally slightly better.

7.6 Future Work

The quest for cooperative strategies that can reuse the bandwidth still offers different possibilities worth to explore. For instance, the power control algorithms proposed in Chapter 2 present adaptability in the selection of the operating point within the achievable rate region. This means that the protection from inter-cell interference offered to a victim user can be tuned in favor of protecting a primary user. It was proposed that the selection of this operating point can be done based on the quality of service demanded by the users. However, this selection can be based on other metrics such as the load of each base station, the queue backlog sizes of the users, or the energy efficiency, each of which will result in a different operating point.

Furthermore, the stream of data intended to each user is not an infinite stream of bits with a uniform rate of arrival. It can be a bursty traffic with high data rate peaks, or a more uniform low-latency traffic. Therefore, selecting a certain operating point in the achievable rate region does not mean that such a data rate will be achieved. For this purpose it is important to develop cross-layer algorithms that can jointly optimize the data rate of both the primary and the victim users taking into account this information.

In Chapter 3, it was assumed as cellular model an infinite and uniform array of cells. However, more realistic models show that arrays of cells are not uniform and each cell has a different number of cell edges. It would be interesting to explore transmission strategies such as AFR that work for non-uniform arrays of cells, and which can also offer the potential of exploiting D2D communication among cell edge users. A HetNet is an interesting showcase: the different transmit power of each base station and their irregular deployment results in

each cell having a different number of cell edge users and each cell edge user receiving inter-cell interference from a different number of base stations.

Also, only AF strategy was analyzed in Chapter 3. Extending the proposed approach with DF as forwarding strategy would require a smart selection of relays since the spectral efficiency and BER in this case are limited by the link from the base station to the relaying D2D users. Multiple antennas can also be used in this context to transmit simultaneously to different cell edge users.

Chapters 4, 5, and 6 share the scenario of base stations that relay overheard information to the users. However, in these chapters we assume single antennas for base stations and users due to the typical small-size energy-limited devices found in dense networks. However, multiple antenna techniques have been implemented successfully in many wireless scenarios achieving both transmit diversity (simultaneous transmission of multiple streams) as well as spatial diversity (combining signals from multiple signal paths). Furthermore, recent advances in transceiver design show that mobile devices can achieve multiple antenna gains with only one RF chain. Different overhearing scenarios can be explored with multiple antennas. For instance, the transmission protocol might be adapted to relay simultaneously different streams of symbols, each of them to possibly different users. Beamforming strategies can also be used. Apart from providing additional spatial diversity, the use of multiple antennas can provide increased energy efficiency if antenna selection is used.

Chapter 5 exploits the network topology to allow base stations to relay signals using the Wyner cellular model. Although widely-used, the Wyner cellular model is a linear model with some limitations, especially for large networks. It would be worth to analyze similar overhearing approaches with different cellular models in a two dimensional array, or even assuming heterogeneous networks, where the different transmission powers result in non-uniform cellular models. One way would be through a graph model that connects the base stations to a number of neighboring base stations. Then through a graph coloring approach, for instance, we could determine which base stations should transmit in each time-slot in order to allow base stations and users to receive signals free of inter-cell interference.

Appendix A

Appendix

A.1

For coherent binary signals with BPSK modulation, the average BER of an L-branch MRC receiver with equally-likely transmitted symbols is given by the Gaussian Q-function [78]

$$\text{BER} = \mathbb{E}\{Q(\sqrt{2\gamma_{\text{tot}}})\} = \int_0^\infty Q(\sqrt{2\gamma_{\text{tot}}}) p_{\gamma_{\text{tot}}}(\gamma_{\text{tot}}) d\gamma_{\text{tot}}, \tag{A.1}$$

where $p(\gamma_{\text{tot}})$ is the probability density function (PDF) of γ_{tot}, and γ_{tot} is the total SNR per symbol at the output of receiver l:

$$\gamma_{\text{tot}} = \sum_{m=1}^{L} \gamma_{ml} = \sum_{m=1}^{L} \eta_l |h_{ml}|^2, \tag{A.2}$$

and where the Q-function is defined as (only for $x \geq 0$) [78]

$$Q(x) = \frac{1}{\pi} \int_0^{\pi/2} \exp\left(-\frac{x^2}{2\sin^2\phi}\right) d\phi. \tag{A.3}$$

The BER in (A.1) then results in

$$\mathrm{BER} = \underbrace{\int_0^\infty \cdots \int_0^\infty}_{L} \frac{1}{\pi} \int_0^{\pi/2} \prod_{m=1}^{L} \exp\left(\frac{-\gamma_{ml}}{\sin^2\phi}\right) p(\gamma_{ml}) d\phi d\gamma_{1l} d\gamma_{2l} ... d\gamma_{Ll}, \tag{A.4}$$

where it is assumed that γ_{ml} for $m = 1, ...L$ are statistically independent. By using the definition of the moment generating function (MGF) of γ_{ml} [78]:

$$M_{\gamma_{ml}}\left(\frac{-1}{\sin^2\phi}\right) = \int_0^\infty p(\gamma_{ml}) \exp\left(\frac{-\gamma_{ml}}{\sin^2\phi}\right) d\gamma_{ml}, \tag{A.5}$$

equation (A.4) becomes

$$\begin{aligned} \mathrm{BER} &= \frac{1}{\pi} \int_0^{\pi/2} \prod_{m=1}^{L} M_{\gamma_{ml}}\left(\frac{-1}{\sin^2\phi}\right) d\phi \\ &= \frac{1}{\pi} \int_0^{\pi/2} \prod_{m=1}^{L} \left(\frac{1}{1+\frac{\bar{\gamma_{ml}}}{\sin^2\phi}}\right) d\phi, \end{aligned} \tag{A.6}$$

where the MGF for a Rayleigh channel is defined as $M_{\gamma_{ml}}(s) = (1 - s\bar{\gamma_{ml}})^{-1}$.

An upper bound of the BER in equation (A.6) is obtained by applying the Chernoff bound $Q(x) \leq \exp(-x^2/2)$ [40]. Assuming BPSK and i.i.d. Rayleigh fading, this results in

$$\begin{aligned} &\mathrm{BER} \leq \\ &\int_0^\infty \exp\left(-\sum_{m=1}^{L} \gamma_{ml}\right) p(\gamma_{1l}) p(\gamma_{2l}) \cdots p(\gamma_{Ll}) d\gamma_{1l} d\gamma_{2l} \cdots d\gamma_{Ll} \\ &= \prod_{m=1}^{L} \frac{1}{1+\bar{\gamma_{ml}}} \approx \frac{1}{\prod_{m=1}^{L} \bar{\gamma_{ml}}}. \end{aligned} \tag{A.7}$$

where the approximation holds only for high SNR values.

A.2

In this section, a simpler expression for the SNR of U1 given by

$$\mathrm{SNR}_{\mathrm{U1}} = \mathbf{a}_1^H \mathbf{R}_{w_1}^{-1} \mathbf{a}_1 \sigma_{\mathrm{s}}^2 \tag{A.8}$$

is derived. Using the Sherman-Morrison-Woodbury formula

$$(\mathbf{A} - \mathbf{B}\mathbf{D}^{-1}\mathbf{C})^{-1} = \mathbf{A}^{-1} + \mathbf{A}^{-1}\mathbf{B}(\mathbf{D} - \mathbf{C}\mathbf{A}^{-1}\mathbf{B})^{-1}\mathbf{C}\mathbf{A}^{-1}, \tag{A.9}$$

where $\mathbf{A}$, $\mathbf{B}$, $\mathbf{C}$, and $\mathbf{D}$ are arbitrary matrices, and substituting the following matrices $\mathbf{A} = \mathbf{N}_1$, $\mathbf{B} = \mathbf{a}_2$, $\mathbf{C} = \mathbf{a}_2^H \sigma_{\mathrm{s}}^2$, $\mathbf{D} = -1$, then $\mathbf{R}_{w_1}^{-1}$ from equation (A.23) becomes

$$\mathbf{R}_{w_1}^{-1} = \mathbf{N}_1^{-1} - \sigma_{\mathrm{s}}^2 \mathbf{N}_1^{-1} \left(1 + \sigma_{\mathrm{s}}^2 \mathbf{a}_2^H \mathbf{N}_1^{-1} \mathbf{a}_2\right)^{-1} \mathbf{a}_2 \mathbf{a}_2^H \mathbf{N}_1^{-1}. \tag{A.10}$$

Now, substituting $\mathbf{R}_{w_1}^{-1}$ in equation (A.22) leads to

$$\begin{aligned} \mathrm{SNR}_{\mathrm{U1}} &= \mathbf{a}_1^H \left(\mathbf{N}_1^{-1} - \sigma_{\mathrm{s}}^2 \mathbf{N}_1^{-1} \left(1 + \sigma_{\mathrm{s}}^2 \mathbf{a}_2^H \mathbf{N}_1^{-1} \mathbf{a}_2\right)^{-1} \mathbf{a}_2 \mathbf{a}_2^H \mathbf{N}_1^{-1}\right) \mathbf{a}_1 \sigma_{\mathrm{s}}^2 \\ &= \sigma_{\mathrm{s}}^2 \mathbf{a}_1^H \mathbf{N}_1^{-1} \mathbf{a}_1 - \sigma_{\mathrm{s}}^2 \left(1 + \sigma_{\mathrm{s}}^2 \mathbf{a}_2^H \mathbf{N}_1^{-1} \mathbf{a}_2\right)^{-1} |\mathbf{a}_2^H \mathbf{N}_1^{-1} \mathbf{a}_1|^2 \sigma_{\mathrm{s}}^2. \end{aligned} \tag{A.11}$$

Using the definition of vectors $\mathbf{a}_1$ and $\mathbf{a}_2$ from Section 4.2.2 leads to

$$\begin{aligned} \mathbf{a}_1^H \mathbf{N}_1^{-1} \mathbf{a}_1 &= \frac{P_1 |h_{11}|^2}{\sigma_{\mathrm{n}}^2} + \frac{P_2 |h_{21}|^2}{\sigma_{\mathrm{n}}^2 \left(1 + \frac{\sqrt{P_1} h_{11}}{\sqrt{P_2} g_{21}} + \frac{\sqrt{P_2} h_{21}}{\sqrt{P_1} g_{12}}\right)} \\ |\mathbf{a}_2^H \mathbf{N}_1^{-1} \mathbf{a}_1|^2 &= \frac{P_1 P_2 |h_{11}|^2 |h_{21}|^2}{\sigma_{\mathrm{n}}^4 \left(1 + \frac{\sqrt{P_1} h_{11}}{\sqrt{P_2} g_{21}} + \frac{\sqrt{P_2} h_{21}}{\sqrt{P_1} g_{12}}\right)^2} \\ \mathbf{a}_2^H \mathbf{N}_1^{-1} \mathbf{a}_2 &= \frac{P_2 |h_{21}|^2}{\sigma_{\mathrm{n}}^2} + \frac{P_1 |h_{11}|^2}{\sigma_{\mathrm{n}}^2 \left(1 + \frac{\sqrt{P_1} h_{11}}{\sqrt{P_2} g_{21}} + \frac{\sqrt{P_2} h_{21}}{\sqrt{P_1} g_{12}}\right)}. \end{aligned} \tag{A.12}$$

Substituting equations (A.27) in (A.26) leads to

$$\begin{aligned}
\mathrm{SNR}_{\mathrm{U1}} &= \sigma_{\mathrm{s}}^2 \left(\frac{P_1|h_{11}|^2}{\sigma_{\mathrm{n}}^2} + \frac{P_2|h_{21}|^2}{\sigma_{\mathrm{n}}^2 \left(1 + \frac{\sqrt{P_1}h_{11}}{\sqrt{P_2}g_{21}} + \frac{\sqrt{P_2}h_{21}}{\sqrt{P_1}g_{12}}\right)} \right) - \\
&\left(1 + \sigma_{\mathrm{s}}^2 \left(\frac{P_2|h_{21}|^2}{\sigma_{\mathrm{n}}^2} + \frac{P_1|h_{11}|^2}{\sigma_{\mathrm{n}}^2 \left(1 + \frac{\sqrt{P_1}h_{11}}{\sqrt{P_2}g_{21}} + \frac{\sqrt{P_2}h_{21}}{\sqrt{P_1}g_{12}}\right)} \right) \right)^{-1} \\
&\frac{\sigma_{\mathrm{s}}^4 P_1 P_2 |h_{11}|^2 |h_{21}|^2}{\sigma_{\mathrm{n}}^4 \left(1 + \frac{\sqrt{P_1}h_{11}}{\sqrt{P_2}g_{21}} + \frac{\sqrt{P_2}h_{21}}{\sqrt{P_1}g_{12}}\right)^2} \\
&= \frac{\sigma_{\mathrm{s}}^2}{\sigma_{\mathrm{n}}^2} P_1 |h_{11}|^2 + \frac{\sigma_{\mathrm{s}}^2}{\sigma_{\mathrm{n}}^2} P_2 |h_{21}|^2 \times \\
&\left(\frac{1 + \frac{\sigma_{\mathrm{s}}^2}{\sigma_{\mathrm{n}}^2} P_2 |h_{21}|^2}{\frac{\sigma_{\mathrm{s}}^2}{\sigma_{\mathrm{n}}^2} P_1 |h_{11}|^2 + \left(\frac{\sigma_{\mathrm{s}}^2}{\sigma_{\mathrm{n}}^2} P_2 |h_{21}|^2 + 1 \right) \left(\frac{\sqrt{P_1}h_{11}}{\sqrt{P_2}g_{21}} + \frac{\sqrt{P_2}h_{21}}{\sqrt{P_1}g_{12}} + 1 \right)} \right).
\end{aligned} \tag{A.13}$$

Following an analogous derivation, $\mathrm{SNR}_{\mathrm{U2}}$ is given by

$$\begin{aligned}
\mathrm{SNR}_{\mathrm{U2}} &= \frac{\sigma_{\mathrm{s}}^2}{\sigma_{\mathrm{n}}^2} P_2 |h_{22}|^2 + \frac{\sigma_{\mathrm{s}}^2}{\sigma_{\mathrm{n}}^2} P_1 |h_{12}|^2 \times \\
&\left(\frac{1 + \frac{\sigma_{\mathrm{s}}^2}{\sigma_{\mathrm{n}}^2} P_1 |h_{12}|^2}{\frac{\sigma_{\mathrm{s}}^2}{\sigma_{\mathrm{n}}^2} P_2 |h_{22}|^2 + \left(\frac{\sigma_{\mathrm{s}}^2}{\sigma_{\mathrm{n}}^2} P_1 |h_{12}|^2 + 1 \right) \left(\frac{\sqrt{P_1}h_{12}}{\sqrt{P_2}g_{21}} + \frac{\sqrt{P_2}h_{22}}{\sqrt{P_1}g_{12}} + 1 \right)} \right).
\end{aligned} \tag{A.14}$$

A.3

In order to find a closed form expression for equation (4.48), an expression for the determinants of the matrices $\mathbf{R}_{y_l}$ and $\mathbf{R}_{w_l}$ is needed. Expanding the matrix

$\mathbf{R}_{y_l}$ results in equation (A.15)

$$\mathbf{R}_{y_l} = \mathbf{a}_1\mathbf{a}_1^H\sigma_{\mathrm{s}}^2 + \mathbf{a}_2\mathbf{a}_2^H\sigma_{\mathrm{s}}^2 + \cdots + \mathbf{a}_L\mathbf{a}_L^H\sigma_{\mathrm{s}}^2 + \mathbf{N}_l$$

$$= \begin{bmatrix} 1+\gamma_{1l} & 0 & \cdots & 0 & \sqrt{\gamma_{1l}\Upsilon_1} \\ 0 & 1+\gamma_{2l} & \cdots & 0 & \sqrt{\gamma_{2l}\Upsilon_2} \\ \vdots & \vdots & \ddots & \vdots & \vdots \\ 0 & 0 & \cdots & 1+\gamma_{Ll} & \sqrt{\gamma_{Ll}\Upsilon_L} \\ \sqrt{\gamma_{1l}\Upsilon_1} & \sqrt{\gamma_{2l}\Upsilon_2} & \cdots & \sqrt{\gamma_{Ll}\Upsilon_L} & \Upsilon_1+\Upsilon_2+\cdots+\Upsilon_L+D_1+1 \end{bmatrix} \tag{A.15}$$

and expanding the matrix $\mathbf{R}_{w_l}$ results in $\mathbf{R}_{w_l} = \sum_{\substack{m=1 \\ m\neq l}}^{L} \mathbf{a}_m\mathbf{a}_m^H\sigma_{\mathrm{s}}^2 + \mathbf{N}_l$, presented in equation (A.16) for $l = 1$.

$$\mathbf{R}_{w_1} = \mathbf{a}_2\mathbf{a}_2^H\sigma_{\mathrm{s}}^2 + \cdots + \mathbf{a}_L\mathbf{a}_L^H\sigma_{\mathrm{s}}^2 + \mathbf{N}_l$$

$$= \begin{bmatrix} 1 & 0 & \cdots & 0 & 0 \\ 0 & 1+\gamma_{21} & \cdots & 0 & \sqrt{\gamma_{21}\Upsilon_2} \\ \vdots & \vdots & \ddots & \vdots & \vdots \\ 0 & 0 & \cdots & 1+\gamma_{L1} & \sqrt{\gamma_{L1}\Upsilon_L} \\ 0 & \sqrt{\gamma_{21}\Upsilon_2} & \cdots & \sqrt{\gamma_{L1}\Upsilon_L} & \Upsilon_2+\cdots+\Upsilon_L+D_1+1 \end{bmatrix} \tag{A.16}$$

Finally, by using the Laplace expansion for the determinants $|\mathbf{R}_{y_l}|$ and $|\mathbf{R}_{w_l}|$, equation (A.17) is obtained.

$$\frac{|\mathbf{R}_{y_l}|}{|\mathbf{R}_{w_l}|} = 1 + \gamma_{ll} + \left(\sum_{\substack{m=1\\m\neq l}}^{L} \sqrt{\gamma_{ml}}\right)^2 \frac{\prod_{\substack{m=1\\m\neq l}}^{L} (1+\gamma_{ml})}{\sum_{\substack{m=1\\m\neq l}}^{L} \prod_{\substack{q=1\\q\neq l\\q\neq m}}^{L} (1+\gamma_{ql}) \left(\sum_{\substack{r=1\\r\neq m}}^{L} \sqrt{\gamma_{rl}}\right)^2 + (D_l+1) \prod_{\substack{m=1\\m\neq l}}^{L} (1+\gamma_{ml})}$$

$$= 1 + \gamma_{ll} + \frac{\left(\sum_{\substack{m=1\\m\neq l}}^{L} \sqrt{\gamma_{ml}}\right)^2}{\sum_{\substack{m=1\\m\neq l}}^{L} \frac{\left(\sum_{\substack{r=1\\r\neq m}}^{L} \sqrt{\gamma_{rl}}\right)^2}{1+\gamma_{ml}} + D_l + 1} \tag{A.17}$$

A.4

We consider the maximization of the following function of $P_l^{(t)}$

$$f\left(P_l^{(t)}\right) = \frac{\log\left(1 + aP_l^{(t)} + b\right)}{k + P_l^{(t)}}, \tag{A.18}$$

where $a > 0$ and $P_l^{(t)}, b, k \geq 0$. We begin by defining the derivative

$$\frac{\partial f\left(P_l^{(t)}\right)}{\partial P_l^{(t)}} = \frac{a\left(k + P_l^{(t)}\right) - (1+b)\log\left(1 + aP_l^{(t)} + b\right) - aP_l^{(t)}\log\left(1 + aP_l^{(t)} + b\right)}{\left(1 + aP_l^{(t)} + b\right)\left(k + P_l^{(t)}\right)^2}. \tag{A.19}$$

The derivative of the numerator of (A.19) is

$$\frac{\partial g\left(P_l^{(t)}\right)}{\partial P_l^{(t)}} = -a\log\left(1+aP_l^{(t)}+b\right) < 0 \tag{A.20}$$

If $k = b = 0$, then $g(0) = 0$ and $f\left(P_l^{(t)}\right)$ is strictly decreasing with $P_l^{(t)}$. Otherwise $f\left(P_l^{(t)}\right)$ has a maximum value found by solving

$$P_l^{(t)} = \frac{e^{W\left(ak+aP_l^{(t)}\right)} - 1 - b}{a}, \tag{A.21}$$

where $W(x)$ is the Lambert function of x. For $P_l^{(t)} > 0$ equation (A.21) must satisfy $e^{W\left(ak+aP_l^{(t)}\right)} \geq 1 + b$.

A.5

In this section, we derive a simpler expression for the SNR given by

$$\mathrm{SNR}_1 = \mathbf{a}_1^H \mathbf{R}_{w_1}^{-1} \mathbf{a}_1 \sigma_\mathrm{s}^2, \tag{A.22}$$

where

$$\mathbf{R}_{w_1} = \mathbb{E}\{(\mathbf{a}_2 s_2 + \mathbf{n}_1)(\mathbf{a}_2 s_2 + \mathbf{n}_1)^H\} = \mathbf{a}_2\mathbf{a}_2^H\sigma_\mathrm{s}^2 + \mathbf{N}_1, \tag{A.23}$$

and where $\mathbf{N}_1 = \mathrm{diag}\left[\sigma_\mathrm{n}^2, \sigma_\mathrm{n}^2, \sigma_\mathrm{n}^2\left(1 + \frac{P_1^{(3)}\mathbb{E}\{|h_{11}|^2\}}{P_2^{(2)}\mathbb{E}\{|g_{21}|^2\}} + \frac{P_2^{(3)}\mathbb{E}\{|h_{21}|^2\}}{P_1^{(1)}\mathbb{E}\{|g_{12}|^2\}}\right)\right]$. Using the Sherman-Morrison-Woodbury formula

$$(\mathbf{A} - \mathbf{B}\mathbf{D}^{-1}\mathbf{C})^{-1} = \mathbf{A}^{-1} + \mathbf{A}^{-1}\mathbf{B}(\mathbf{D} - \mathbf{C}\mathbf{A}^{-1}\mathbf{B})^{-1}\mathbf{C}\mathbf{A}^{-1}, \tag{A.24}$$

where $\mathbf{A}$, $\mathbf{B}$, $\mathbf{C}$, and $\mathbf{D}$ are arbitrary matrices, and substituting the following matrices $\mathbf{A} = \mathbf{N}_1$, $\mathbf{B} = \mathbf{a}_2$, $\mathbf{C} = \mathbf{a}_2^H\sigma_\mathrm{s}^2$, $\mathbf{D} = -1$, $\mathbf{R}_{w_1}^{-1}$ results in

$$\mathbf{R}_{w_1}^{-1} = \mathbf{N}_1^{-1} - \sigma_\mathrm{s}^2\mathbf{N}_1^{-1}\left(1 + \sigma_\mathrm{s}^2\mathbf{a}_2^H\mathbf{N}_1^{-1}\mathbf{a}_2\right)^{-1}\mathbf{a}_2\mathbf{a}_2^H\mathbf{N}_1^{-1}. \tag{A.25}$$

Now, substituting $\mathbf{R}_{w_1}^{-1}$ in equation (A.22) leads to

$$\begin{aligned}\mathrm{SNR}_1 &= \mathbf{a}_1^H\left(\mathbf{N}_1^{-1} - \sigma_\mathrm{s}^2\mathbf{N}_1^{-1}\left(1 + \sigma_\mathrm{s}^2\mathbf{a}_2^H\mathbf{N}_1^{-1}\mathbf{a}_2\right)^{-1}\mathbf{a}_2\mathbf{a}_2^H\mathbf{N}_1^{-1}\right)\mathbf{a}_1\sigma_\mathrm{s}^2 \\ &= \sigma_\mathrm{s}^2\mathbf{a}_1^H\mathbf{N}_1^{-1}\mathbf{a}_1 - \sigma_\mathrm{s}^2\left(1 + \sigma_\mathrm{s}^2\mathbf{a}_2^H\mathbf{N}_1^{-1}\mathbf{a}_2\right)^{-1}|\mathbf{a}_2^H\mathbf{N}_1^{-1}\mathbf{a}_1|^2\sigma_\mathrm{s}^2.\end{aligned} \tag{A.26}$$

Using the definition of vectors $\mathbf{a}_1$ and $\mathbf{a}_2$ leads to

$$\mathbf{a}_1^H \mathbf{N}_1^{-1} \mathbf{a}_1 = \frac{P_1^{(1)}|h_{11}|^2}{\sigma_{\mathrm{n}}^2} + \frac{P_2^{(3)}|h_{21}|^2}{\sigma_{\mathrm{n}}^2 \left(1 + \frac{\sqrt{P_1^{(3)}}h_{11}}{\sqrt{P_2^{(2)}}g_{21}} + \frac{\sqrt{P_2^{(3)}}h_{21}}{\sqrt{P_1^{(1)}}g_{12}}\right)}$$

$$|\mathbf{a}_2^H \mathbf{N}_1^{-1} \mathbf{a}_1|^2 = \frac{P_1^{(3)} P_2^{(3)} |h_{11}|^2 |h_{21}|^2}{\sigma_{\mathrm{n}}^4 \left(1 + \frac{\sqrt{P_1^{(3)}}h_{11}}{\sqrt{P_2^{(2)}}g_{21}} + \frac{\sqrt{P_2^{(3)}}h_{21}}{\sqrt{P_1^{(1)}}g_{12}}\right)^2} \tag{A.27}$$

$$\mathbf{a}_2^H \mathbf{N}_1^{-1} \mathbf{a}_2 = \frac{P_2^{(2)}|h_{21}|^2}{\sigma_{\mathrm{n}}^2} + \frac{P_1^{(3)}|h_{11}|^2}{\sigma_{\mathrm{n}}^2 \left(1 + \frac{\sqrt{P_1^{(3)}}h_{11}}{\sqrt{P_2^{(2)}}g_{21}} + \frac{\sqrt{P_2^{(3)}}h_{21}}{\sqrt{P_1^{(1)}}g_{12}}\right)}.$$

Substituting equations (A.27) in (A.26) leads to

$$\begin{aligned}
&\mathrm{SNR}_1 = \sigma_{\mathrm{s}}^2 \left(\frac{P_1^{(1)}|h_{11}|^2}{\sigma_{\mathrm{n}}^2} + \frac{P_2^{(3)}|h_{21}|^2}{\sigma_{\mathrm{n}}^2 \left(1 + \frac{\sqrt{P_1^{(3)}}h_{11}}{\sqrt{P_2^{(2)}}g_{21}} + \frac{\sqrt{P_2^{(3)}}h_{21}}{\sqrt{P_1^{(1)}}g_{12}}\right)} \right) - \\
&\left(1 + \sigma_{\mathrm{s}}^2 \left(\frac{P_2^{(2)}|h_{21}|^2}{\sigma_{\mathrm{n}}^2} + \frac{P_1^{(3)}|h_{11}|^2}{\sigma_{\mathrm{n}}^2 \left(1 + \frac{\sqrt{P_1^{(3)}}h_{11}}{\sqrt{P_2^{(2)}}g_{21}} + \frac{\sqrt{P_2^{(3)}}h_{21}}{\sqrt{P_1^{(1)}}g_{12}}\right)} \right) \right)^{-1} \\
&\frac{\sigma_{\mathrm{s}}^4 P_1^{(3)} P_2^{(3)} |h_{11}|^2 |h_{21}|^2}{\sigma_{\mathrm{n}}^4 \left(1 + \frac{\sqrt{P_1^{(3)}}h_{11}}{\sqrt{P_2^{(2)}}g_{21}} + \frac{\sqrt{P_2^{(3)}}h_{21}}{\sqrt{P_1^{(1)}}g_{12}}\right)^2} \\
&= \frac{\sigma_{\mathrm{s}}^2}{\sigma_{\mathrm{n}}^2} P_1^{(1)} |h_{11}|^2 + \frac{\sigma_{\mathrm{s}}^2}{\sigma_{\mathrm{n}}^2} P_2^{(3)} |h_{21}|^2 \times \\
&\left(\frac{1 + \frac{\sigma_{\mathrm{s}}^2}{\sigma_{\mathrm{n}}^2} P_2^{(2)} |h_{21}|^2}{\frac{\sigma_{\mathrm{s}}^2}{\sigma_{\mathrm{n}}^2} P_1^{(3)} |h_{11}|^2 + \left(\frac{\sigma_{\mathrm{s}}^2}{\sigma_{\mathrm{n}}^2} P_2^{(2)} |h_{21}|^2 + 1 \right) \left(\frac{\sqrt{P_1^{(3)}}h_{11}}{\sqrt{P_2^{(2)}}g_{21}} + \frac{\sqrt{P_2^{(3)}}h_{21}}{\sqrt{P_1^{(1)}}g_{12}} + 1 \right)} \right) \\
&= \gamma_{11}^{(1)} + \frac{\gamma_{21}^{(3)}}{\frac{\gamma_{11}^{(3)}}{\gamma_{21}^{(2)}+1} + \frac{\gamma_{11}^{(3)}}{\xi_{21}^{(2)}} + \frac{\gamma_{21}^{(3)}}{\xi_{12}^{(1)}} + 1}.
\end{aligned} \tag{A.28}$$

Following an analogous derivation, SNR_2 is given by

$$\begin{aligned}\mathrm{SNR}_2 &= \frac{\sigma_{\mathrm{s}}^2}{\sigma_{\mathrm{n}}^2} P_2^{(2)} |h_{22}|^2 + \frac{\sigma_{\mathrm{s}}^2}{\sigma_{\mathrm{n}}^2} P_1^{(3)} |h_{12}|^2 \times \\ &\left(\frac{1 + \frac{\sigma_{\mathrm{s}}^2}{\sigma_{\mathrm{n}}^2} P_1^{(1)} |h_{12}|^2}{\frac{\sigma_{\mathrm{s}}^2}{\sigma_{\mathrm{n}}^2} P_2^{(3)} |h_{22}|^2 + \left(\frac{\sigma_{\mathrm{s}}^2}{\sigma_{\mathrm{n}}^2} P_1^{(1)} |h_{12}|^2 + 1 \right) \left(\frac{\sqrt{P_1^{(3)}} h_{12}}{\sqrt{P_2^{(2)}} g_{21}} + \frac{\sqrt{P_2^{(3)}} h_{22}}{\sqrt{P_1^{(1)}} g_{12}} + 1 \right)} \right) \\ &= \gamma_{22}^{(2)} + \frac{\gamma_{12}^{(3)}}{\frac{\gamma_{22}^{(3)}}{\gamma_{12}^{(1)}+1} + \frac{\gamma_{22}^{(3)}}{\xi_{12}^{(1)}} + \frac{\gamma_{12}^{(3)}}{\xi_{21}^{(2)}} + 1}.\end{aligned} \tag{A.29}$$

Bibliography

[1] 3GPP. Soft frequency reuse scheme for UTRAN LTE. *R1-050507, Athens, Greece* (May 2005).

[2] 3GPP. Soft frequency reuse scheme for utran lte. *R1-050507* (May 2005). Available: ftp://ftp.3gpp.org/tsg_ran/WG1_RL1/TSGR1_41/Docs/R1-050507.zip.

[3] 3GPP. Considerations on interference coordination in heterogeneous networks. *R1-101369, San Francisco, CA* (Feb. 2010).

[4] 3GPP. Summary of the description of candidate eICIC solutions. *R1-104968, Madrid, Spain* (Aug. 2010).

[5] 3GPP. Evolved universal terrestrial radio access (EUTRA); overall description; stage 2 (release 11). *TS 36.300 V11.1.0* (Mar. 2012).

[6] 3GPP. Physical layer procedures. *TS 36.213 V10.2.0* (Mar. 2012).

[7] 3GPP. Small cell forum - new name for 3GPP partner. [Online; accessed 6-March-2013], Available: http://www.3gpp.org/Small-Cell-Forum-new-name-for-3GPP.

[8] 3GPP. Spatial channel model for multiple input multiple output (MIMO) simulations. *TR 25.996, v11.0.0* (Sep. 2012).

[9] Asadi, A., Wang, Q., and Mancuso, V. A survey on device-to-device communication in cellular networks. *IEEE Communication Surveys & Tutorials 16*, 4 (2014), 1801–1819.

[10] Auer, G., Giannini, V., Desset, C., Godor, I., Skillermark, P., Olsson, M., Imran, M. A., Sabella, D., Gonzalez, M. J., Blume, O., and Fehske, A. How much energy is needed to run a wireless network? *IEEE Wireless Communications 18*, 5 (October 2011), 40–49.

[11] Ayach, O. E., Peters, S. W., and Heath, R. W. The practical challenges of interference alignment. *IEEE Wireless Communications 20*, 1 (March 2013), 35–42.

[12] Baidas, M. W., and MacKenzie, A. B. Many-to-many space–time network coding for amplify-and-forward cooperative networks: Node selection and performance analysis. *EURASIP Journal on Wireless Communications and Networking* (Dec. 2014), 1–17.

[13] Baik, I., and Chung, S. Y. Network coding for two-way relay channels using lattices. *IEEE International Conference on Communications (ICC)* (2008).

[14] Bhushan, N., Li, J., Malladi, D., Gilmore, R., Brenner, D., Damnjanovic, A., Sukhavasi, R. T., Patel, C., and Geirhofer, S. Network densification: The dominant theme for wireless evolution into 5G. *IEEE Communications Magazine 52*, 2 (February 2014), 82–89.

[15] Boccardi, F., Jr, R. W. H., Lozano, A., Marzetta, T. L., and Popovski, P. Five disruptive technology directions for 5G. *IEEE Communications Magazine 52*, 2 (February 2014).

[16] Boudreau, G., Panicker, J., Guo, N., Chang, R., Wang, N., and Vrzic, S. Interference coordination and cancellation for 4G networks. *IEEE Communications Magazine 47*, 4 (Apr. 2009), 74–81.

[17] Bushan, N., Li, J., Malladi, D., Gilmore, R., D. Brenner, A. D., Sukhavasi, R. T., Patel, C., and Geirhofer, S. Network densification: The dominant theme for wireless evolution into 5g. *IEEE Communications Magazine 52*, 1 (Feb. 2014), 82–89.

[18] C. Feng, D. S., and Kschischang, F. An algebraic approach to physical-layer network coding. *IEEE Transactions on Information Theory 59*, 11 (November 2013).

[19] Cendrillon, R., Huang, J., Chiang, M., and Moonen, M. Autonomous spectrum balancing for digital subscriber lines. *IEEE Transactions on Signal Processing 55*, 8 (Oct. 2007).

[20] Chandrasekhar, V., Andrews, J. G., and Gatherer, A. Femtocell networks: A survey. *IEEE Communications Magazine 46*, 9 (Sep. 2008).

[21] Chapman, O. Small cell vendors race to fulfill operator demand for LTE. [Online; accessed 11-September-2013], Available: http://www.smallcellforum.org/newsstory-small-cell-vendors-race-to-fulfill-operator-demand-for-lte.

[22] Cisco. Cisco visual networking index: Global mobile data traffic forecast update, 2016–2021 white paper. http://www.cisco.com/c/en/us/solutions/collateral/service-provider/visual-networking-index-vni/mobile-white-paper-c11-520862.html.

[23] Combes, R., Haddad, Z., and Altman, E. Self-optimizing strategies for interference coordination in OFDMA networks. *IEEE international conference on communications workshops (ICC), Kyoto, Japan* (Jun. 2011).

[24] Cooper, M. Cooper's law. http://www.arraycomm.com/technology/coopers-law/.

[25] Cover, T., and Thomas, J. Elements of information theory. *John Wiley and Sons* (1991).

[26] Damen, M., and Hammons, A. Delay-tolerent distributed-tast codes for cooperative diversity. *IEEE Transactions on Information Theory 53*, 10 (October 2007), 2941–2956.

[27] Damnjanovic, A., Montojo, J., Lozano, A., Wei, Y., Ji, T., Luo, T., Vajapeyam, M., Yoo, T., Song, O., and Malladi, D. A survey on 3GPP heterogeneous networks. *IEEE Communications Magazine 18*, 3 (June 2011).

[28] Delgado, O., and Labeau, F. D2d relay selection and fairness on 5g wireless networks. *GLOBECOM Workshops* (2016). Washington, USA.

[29] Deng, J., Dowhuszko, A., Freij, R., and Tirkkonen, O. Relay selection and resource allocation for d2d-relaying under uplink cellular power control. *GLOBECOM Workshops* (2015). San Diego, USA.

[30] Dhillon, H. S., Ganti, R. K., Baccelli, F., and Andrews, J. G. Modeling and analysis of K-tier downlink heterogeneous cellular networks. *IEEE Journal of Selected Areas in Communications 30*, 3 (April 2012), 550–560.

[31] Fang, L., Xu, J., and Qiu, L. Energy efficiency optimization for two-way relay channels. *IEEE International Conference on Communications (ICC)* (Jun. 2013), 425–430. Budapest, Hungary.

[32] Femto Forum. Interference management in umts femtocells. *[Online; accessed 2013], Available: http://www.femtoforum.org/femto/*.

[33] Fodor, G., Koutsimanis, C., Racz, A., Reider, N., Simonsson, A., and Muller, W. Intercell interference coordination in OFDMA networks and in the 3GPP long term evolution system.

[34] Fritzsche, R., Rost, P., and Fettweis, G. P. Robust rate adaptation and proportional fair scheduling with imperfect csi. https://arxiv.org/pdf/1504.03803.pdf.

[35] G, D. G., Garcia-Lozano, M., Boque, S. R., and Lee, D. S. Optimization of soft frequency reuse for irregular LTE macrocellular networks. *IEEE Transactions on Wireless Communications 12*, 5 (May 2013).

[36] Gatherer, A. Death by starvation?: Backhaul and 5g. *IEEE ComSoc Technology News* (September 2015). http://www.comsoc.org/ctn/death-starvation-backhaul-and-5g.

[37] Geng, C., Naderializadeh, N., Avestimehr, A. S., and Jafar, S. A. On the optimality of treating interference as noise. *IEEE Transactions on Information Theory 61*, 4 (Apr. 2015), 1753–1767.

[38] Ghosh, A., Mangalvedhe, N., Ratasuk, R., Mondal, B., Cudak, M., Visotsky, E., Thomas, T. A., Andrews, J. G., Xia, P., Jo, H. S., Dhillon, H. S., , and Novlan, T. D. Heterogeneous cellular networks: From theory to practice. *IEEE Communications Magazine 50*, 6 (June 2012), 54–64.

[39] Gjendemsjo, A., Gesbert, D., Oien, G. E., and Kiani, S. G. Binary power control for sum rate maximization over multiple interfering links. *IEEE Transactions on Wireless Communications 7*, 8 (Aug. 2008), 3164–3173.

[40] Goldsmith, A. Wireless communications. *Cambridge University Press* (2005).

[41] Gou, T., Wang, C., and Jafar, S. A. Aiming perfectly in the dark-blind interference alignment through staggered antenna switching. *IEEE Transactions on Signal Processing 59*, 6 (June 2011), 2734–2744.

[42] Guan, W., and Liu, K. J. R. Clustering based space-time network coding. *IEEE GLOBECOM* (Dec. 2012), 5633—-5638.

[43] Hoadley, J., and Maveddat, P. Enabling small cell deployment with hetnet. *IEEE Wireless Communications 19*, 2 (April 2012), 4–5.

[44] H.Yang, Jung, B., and Chun, J. Zero-forcing based two-phased relaying with multiple mobile stations. *Asilomar* (2008).

[45] H.Yang, Lee, K., and Chun, J. Zero-forcing based two-phased relaying. *IEEE International Conference on Communications (ICC)* (2007).

[46] J. Wan and, Y. Z., Hui, H., and Zhang, N. Qos-aware proportional fair energy-efficient resource allocation with imperfect CSI in downlink OFDMA systems. *IEEE 26th Annual International Symposium on Personal, Indoor and Mobile Radio Communications (PIMRC)* (September 2015), 1116–1120. Hong Kong.

[47] Jafar, S. A. Topological interference management through index coding. *IEEE Transactions on Information Theory 60*, 1 (Jan. 2014), 529–568.

[48] Jagannathan, S., Aghajan, H., and Goldsmith, A. The effect of time synchronization errors on the performance of cooperative miso systems. *IEEE GLOBECOM* (Dec. 2004), 102–107.

[49] Jain, R., Chiu, D., and Hawe, W. A quantitative measure of fairness and discrimination for resource allocation in shared systems. *Digital Equipment Corporation, Technical Report DEC-TR-301* (1984).

[50] Julian, D., Chiang, M., O'Neill, D., and Boyd, S. Qos and fairness constrained convex optimization of resource allocation for wireless cellular and ad hoc networks. *IEEE INFOCOM* (June 2002), 477–486.

[51] Kamel, M., Hamouda, W., and Youssef, A. Ultra-dense networks: A survey. *IEEE Communications Surveys & Tutorials 18*, 4 (May 2016).

[52] Katti, S., Maric, I., Goldsmith, A., Katabi, D., and Medard, M. Joint relaying and network coding in wireless networks. *IEEE International Symposium on Information Theory (ISIT)* (2007). Nice, France.

[53] Kim, J., Jeong, C., Yu, H., and Park, J. Aereal capacity limit on the growth of small cell density in heterogeneous networks. *IEEE Global Communications Conference (GLOBECOM)* (December 2014).

[54] Kosta, C., Hunt, B., Quddus, A. U., and Tafazolli, R. On interference avoidance through inter-cell interference coordination (ICIC) based on OFDMA mobile systems. *IEEE Communications Surveys & Tutorials 2013*, 1–23.

[55] Kwan, R., and Leung, C. A survey of scheduling and interference mitigation in LTE. *Journal of Electrical and Computer Engineering* (2010).

[56] Lai, H. Q., and Liu, K. J. R. Space time network coding. *IEEE Transactions on Signal Processing 59*, 4 (Apr. 2011).

[57] Laneman, J. N., Tse, D. N. C., and Wornell, G. W. Cooperative diversity in wireless networks: efficient protocols and outage behavior. *IEEE Transactions on Information Theory 50*, 12 (December 2004), 3062–3080.

[58] Li, C., Song, S. H., Zhang, J., and Letaief, K. B. Maximizing energy efficiency in wireless networks with a minimum average throughput requiremente. *IEEE Wireless Communications and Networking Conference* (Apr. 2012), 1130–1134. Shanghai.

[59] Li, G. Y., Xu, Z., Xiong, C., Yang, C., Zhang, S., Chen, Y., and Xu, S. Energy-efficient wireless communications: Tutorial, survey, and open issues. *IEEE Wireless Communications 18*, 6 (Dec. 2011).

[60] Li, S.-Y. R., Yeung, R. W., and Cai, N. Linear network coding. *IEEE Transactions on Information Theory 49*, 2 (Feb. 2003).

[61] Liew, S. C., and Zhang, Y. J. Proportional fairness in multi-channel multi-rate wireless networks–part i: The case of deterministic channels with application to ap association problem in large-scale wlan. *IEEE Transactions on Wireless Communications 7*, 9 (September 2008), 3446–3456.

[62] Liu, W., Hu, C., Wei, D., Peng, M., and Wang, W. An overload indicator & high interference indicator hybrid scheme for inter-cell interference coordination in LTE system. *IEEE International Conference on Broadband Network and Multimedia Technology (IC-BNMT), Beijing, China* (Oct. 2010), 514–518.

[63] Lopez-Perez, D., Guvenc, I., de la Roche, G., Kountouris, M., Quek, T. Q. S., and Zhang, J. Enhanced inter-cell interference coordination challenges in heterogeneous networks. *IEEE Wireless Communications 18*, 3 (Jun. 2011), 22–30.

[64] Louie, R., Li, Y., and Vucetic, B. Practical physical layer network coding for two-way relay channels: Performance analysis and comparison. *IEEE Transactions on Wireless Communications 9*, 2 (Feb. 2010).

[65] Ma, R., Chang, Y.-J., Chen, H.-H., and Chiu, C.-Y. On relay selection schemes for relay assisted d2d communications in lte-a systems. *IEEE Transactions on Vehicular Technology* (2017).

[66] Miao, G., Himayat, N., Li, G. Y., Koc, A. T., and Talwar, S. Interference-aware energy-efficient power optimization. *IEEE International Conference on Communications (ICC)* (2009). Dresden.

[67] Minn, H., and Munoz, D. Channel knowledge acquisition in relay and multipoint-to-multipoint transmission systems. *IEEE Transactions on Vehicular Technology 64*, 4 (April 2015), 1416–1434.

[68] Nazer, B., and Gastpar, M. Compute-and-forward: Harnessing interference through structured codes. *IEEE Transactions on Information Theory 57*, 10 (October 2011).

[69] Necker, M. Interference coordination in cellular OFDMA networks. *IEEE Network 22*, 6 (Dec. 2008), 12–19.

[70] Nokleby, M., and Aazhang, B. User cooperation for energy-efficient cellular communications. *IEEE International Conference on Communications* (May 2010).

[71] Oh, S., Kim, H., Ryu, B., and Park, N. Inbound mobility management on LTE-Advanced femtocell topology using X2 interface. *International Conference on Computer Communications and Networks (ICCCN), Maui, Hawaii* (Aug. 2011).

[72] Popovski, P., and Yomo, H. Physical network coding in two-way wireless relay channels. *IEEE International Conference on Communications (ICC)* (June 2007), 707–712.

[73] R. Cendrillon, W. Yu, M. M. J. V., and Bostoen, T. Optimal multiuser spectrum balancing for digital subscriber lines. *IEEE Transactions on Communications 54*, 5 (May 2006).

[74] Rahman, M., Yanikomeroglu, H., and Wong, W. Interference avoidance with dynamic inter-cell coordination for downlink LTE system. *IEEE Wireless Communications and Networking Conference (WCNC), Budapest, Hungary* (Apr. 2009).

[75] Sendonaris, A., Erkip, E., and Aazhang, B. User cooperative diversity - part i: system description. *IEEE Transactions on Communications 51*, 11 (November 2003), 1927–1938.

[76] Sheng, Z., Fan, J., Liu, C. H., Leung, V. C. M., Liu, X., and Leung, K. K. Energy-efficient relay selection for cooperative relaying in wireless multimedia networks. *IEEE Transactions on Vehicular Technology 64*, 3 (Mar. 2015).

[77] Shi, H., Prasad, R. V., Onur, E., and Niemegeers, I. Fairness in wireless networks: Measures, issues, and challenges. *IEEE Communications Surveys & Tutorials 16*, 1 (February 2014), 5–24.

[78] Simon, M. K., and Alouini, M. S. Digital communication over fading channels: A unified approach to performance analysis. *John Wiley and Sons* (2000). New York.

[79] Small Cell Forum. [Online; accessed 6-March-2013], Available: http://www.smallcellforum.org.

[80] Smirani, S., Kamoun, M., Sarkiss, M., Zaidi, A., and Duhamel, P. Achievable rate regions for two-way relay channl using nested latice coding. *IEEE Transactions on Wireless Communications 13*, 10 (Feb. 2014).

[81] Son, K., Lee, S., Yi, Y., and Chong, S. Refim: A practical interference management in heterogeneous wireless access networks. *IEEE Transactions on Selected Areas in Communications 29*, 6 (Aug. 2011).

[82] Sun, C., and Yang, C. Is two-way relay more energy efficient? *IEEE Global Telecommunications Conference (GLOBECOM)* (Dec. 2011), 1–6. Houston, USA.

[83] Sun, C., and Yang, C. Energy-efficient analysis of one-way and two-way relay systems. *EURASIP Journal on Wireless Communications and Networking 2012*, 46 (Feb. 2012).

[84] Tehrani, M. N., Uysal, M., and Yanikomeroglu, H. Device-to-device communication in 5g cellular networks: challenges, solutions, and future directions. *IEEE Communications Magazine 52*, 5 (May 2014), 86–92.

[85] Torrea-Duran, R., Rosas, F., Khan, Z., Pollin, S., Tsiaflakis, P., and Moonen, M. Double relay communication protocol for bandwidth management in cellular systems. *European Signal Processing Conference (EUSIPCO 2015)* (Aug. 2015).

[86] Tse, D., and Viswanath, P. Fundamentals of wireless communications. *Cambridge University Press* (2005).

[87] Tsiaflakis, P., Diehl, M., and Moonen, M. Distributed spectrum management algorithms for multiuser dsl networks. *IEEE Transactions on Signal Processing 56*, 2 (Oct. 2008).

[88] Wang, C., Haider, F., Gao, X., You, X., Yang, Y., Yuan, D., Aggoune, H. M., Haas, H., Fletcher, S., and Hepsaydir, E. Celluar architecture and key technologies for 5g wireless communication networks. *IEEE Communications Magazine 52*, 2 (Feb. 2014), 122–130.

[89] Wang, T., and Vandendorpe, L. Iterative resource allocation for maximizing weighted sum min-rate in downlink cellular OFDMA systems. *IEEE Transactions on Signal Processing 59*, 1 (Jan. 2011), 223–234.

[90] Xiong, C., Lu, L., and Li, G. Y. Energy-efficient ofdma-based two-way relay. *IEEE Transactions on Communications 63*, 9 (Sep. 2015).

[91] Xiong, K., Fan, P., Yang, H. C., and Letaief, K. B. Space time network coding with overhearing relays. *IEEE Transactions on Signal Processing 13*, 7 (Jul. 2014).

[92] Xu, J., Zhang, J., and Andrews, J. G. On the accuracy of the wyner model in cellular networks. *IEEE Transactions on Wireless Communications 10*, 9 (September 2011), 3098–3109.

[93] Yang, T., and Zhang, L. Approaches to enhancing autonomous power control at femto under co-channel deployment of macrocell and femtocell. *IEEE International Symposium on Personal, Indoor, and Mobile Radio Communications* (2011).

[94] Yang, X. Method and system for implementing soft time reuse in wireless communication system. *CN1859054B/US7796567* (Apr. 2005). Huawei, Shenzhen, China.

[95] Yu, W., Ginis, G., and Cioffi, J. Distributed multiuser power control for digital subscriber lines. *IEEE Transactions on Selected Areas in Communications 20*, 5 (Jun. 2002).

[96] Yunas, S. F., Valkama, M., and Niemela, J. Spectral and energy efficiency of ultra-dense networks under different deployment strategies. *IEEE Communications Magazine 53*, 1 (Jan. 2015), 90–100.

[97] Zhang, J., Shen, C., Deng, G., and Wang, Y. Timing and frequency synchronization for cooperative relay networks. *IEEE Vehicular Technology Conference (VTC)* (September 2013).

[98] Zhang, S., Liew, S., and Lam, P. Hot topic: physical layer network coding. *ACM MOBICOM* (2006).

[99] Zhang, Y., Xiong, K., Fan, P., Di, X., and Zhou, X. Outage performance of space time network coding with overhearing af relays. *IEEE Communications Letters 19*, 12 (Dec. 2015).

[100] Zhou, M., Cui, Q., Jantti, R., and Tao, X. Energy-efficient relay selection and power allocation for two-way relay channel with analog network coding. *IEEE Communications Letters 16*, 6 (Jun. 2012), 816–819.

List of Publications

Published journal papers during PhD

1. Torrea-Duran, R., Tsiaflakis, P., Vandendorpe, L., Moonen, M., "Neighbor-Friendly Autonomous Power Control in Wireless Heterogeneous Networks", EURASIP Journal on Wireless Communications and Networking, vol. 175, 2014, pp. 1-17. doi:10.1186/1687-1499-2014-175.

2. Torrea-Duran, R., Rosas, F. Pollin, S., Vandendorpe, L., Moonen, M., "Exploiting the Overhearing Capabilities of Transmitting Nodes to Increase the Energy Efficiency in Dense Networks". EURASIP Journal on Wireless Communications and Networking, 2017.

Submitted journal papers during PhD

1. Torrea-Duran, R., Rosas, F., Pollin, S., Vandendorpe, L., Moonen, M., "Multiple-Relay Communication Protocol for Achieving Fairness in Cellular Systems". Submitted to IEEE Access, 2017.

2. Torrea-Duran, R., Morales, M., Plata-Chaves, J., Vandendorpe, L., Moonen, M., "Exploiting the Topology of Partially Connected Networks using Space Time Network Coding". Submitted to IEEE Access, 2017

3. Torrea-Duran, R., Morales, M., Plata-Chaves, J., Vandendorpe, L., Moonen, M., "Aligned Frequency Reuse with D2D Communication". Submitted to IEEE Transactions on Communications, 2017.

Published journal papers before PhD

1. Cardoso, F. D., Petersson, S., Boldi, M., Mizuta, S., Dietl, G., Torrea Duran, R., Desset, C., Leinonen, J., Correia, L. M., "Energy efficient transmission techniques for LTE". IEEE Communications Magazine 51(10): 182-190 (2013)

2. Simoens, P., Azmat Ali, F., Vankeirsbilck, B., Deboosere, L., De Turck, F., Dhoedt, B., Demeester, P., Torrea Duran, R., Van der Perre, L., Dejonghe, A., "Cross-layer reduction of wireless network card idle time to optimize energy consumption of pull thin client protocols". Journal of Communications and Networks, 114 (1), 75-90. (2012)

3. Desset, C., Torrea-Duran, R., "Reducing the power of wireless terminals by adaptive baseband processing". Annales des Télécommunications. Vol. 67, no. 3, pp. 161-170. April 2012.

4. Simoens, P., Ali, F. A., Vankeirsbilck, B., Deboosere, L., De Turck, F., Dhoedt, B., Demeester, P., and Torrea-Duran, R., "Cross-Layer Optimization of Radio Sleep Intervals to Increase Thin Client Energy Efficiency." IEEE Communications Letters, 2010.

Published conference papers during PhD

1. Torrea-Duran, R., Morales, M., Plata-Chaves, J., Vandendorpe, L., Moonen, M., "Topology-Aware Space-Time Network Coding". in Proc. of the 2017 European Signal Processing Conference (EUSIPCO), Kos, Greece, Sep. 2017.

2. Torrea-Duran, R., Rosas, F., Pollin, S., Orozco, A., Vandendorpe, L., Moonen, M., "Double Relay Communication Protocol with Power Control for Achieving Fairness in Cellular Systems". In Proc. of the 42th International Conference on Acoustics, Speech, and Signal Processing (ICASSP), New Orleans, March 2017.

3. Torrea-Duran, R., Rosas, F., Pollin, S., Vandendorpe, L., Moonen, M., "Energy-Efficient Double Relay Communication Protocol in Cellular Networks", in Proc. of the 17th IEEE International Workshop on Signal Processing Advances in Wireless Communications (SPAWC), Edinburgh, U.K., Jul. 2016.

4. Torrea-Duran, R., Rosas, F., Khan, Z. K. Z., Pollin, S., Tsiaflakis, P., Moonen, M., "Double Relay Communication Protocol

for Bandwidth Management in Cellular Systems", in Proc. of the 2015 European Signal Processing Conference (EUSIPCO), Nice, France, Sep. 2015.

5. Torrea-Duran, R., Tsiaflakis, P., Vandendorpe, L., Moonen, M., "An Algorithm for Cross-layer Subcarrier and Power Allocation in Cellular Networks", in Proc. of the 2015 European Signal Processing Conference (EUSIPCO), Nice, France, Sep. 2015.

6. Torrea-Duran, R., Vandendorpe, L., Moonen, M., "Neighbor-friendly user scheduling algorithm for interference management in LTE-A networks", in Proc. of the Twelfth International Symposium on Wireless Communication Systems (ISWCS), Brussels, Belgium, Aug. 2015.

7. Torrea-Duran, R., Tsiaflakis, P., Vandendorpe, L., Moonen, M., "A Cell Breathing Approach in Green Heterogeneous Networks", in Proc. of the 15th IEEE International Workshop on Signal Processing Advances in Wireless Communications (SPAWC), Toronto, Canada, Jun. 2014.

8. Torrea-Duran, R., Tsiaflakis, P., Vandendorpe, L., Moonen, M., "Neighbor-Friendly Autonomous Algorithm for Power Spectrum Allocation in OFDM Networks", in International Symposium on Wireless Communication Systems (ISWCS), Barcelona, Spain, Aug. 2014.

9. Rubio del Olmo, M., Torrea-Duran R., Orozco-Lugo, A. G., Moonen M., "Energy-efficient user scheduling algorithm for LTE networks", in 5th joint WIC/IEEE SP Symposium on Information Theory and Signal Processing in the Benelux (WIC), Brussels, Belgium, May 2015, pp. 1-8.

10. Chen H.H., Torrea-Duran, R., Tsiaflakis, P., Moonen, M., "Joint precoding vector and modulation and coding scheme recalculation for LTE-A multi-user MIMO", in Proc. of the Werkgemeenschap voor Informatie- en Communicatietheorie (WIC), Leuven, Belgium, May 2013.

Published conference papers before PhD

1. Torrea Duran, R., Desset, C., Pollin, S., Van der Perre, L., "Reduction of HARQ memory in low mobility LTE systems". International Conference on Communications (ICC). June 2013: 5068-5072.

2. Torrea-Duran, R., Li, M., Desset, C., Pollin, S., Van der Perre, L., "Exploiting Frequency Correlation in LTE to reduce HARQ memory." Globecom, 2012.

3. Torrea-Duran, R., Desset, C., Pollin, S., Dejonghe, A., "Adaptive energy efficient scheduling algorithm for LTE pico base stations." Future Network Mobile Summit, 2012.

4. Torrea-Duran, R., Desset, C., Dejonghe, A., "A Cross-Layer Approach to Save Energy in 3GPP-LTE Terminals." Future Network and MobileSummit, 2010.

5. Torrea-Duran, R., Novo, D., Desset, D., Naessens, F., and Van der Perre, L., "Adaptive Early-stopping Threshold for LTE Turbo Decoder." in Proc. of the 2010 European Signal Processing Conference (EUSIPCO), 2010.

6. Torrea Duran, R., Louveaux, J. and Vandendorpe, L., "Goodput optimized bit and power allocation for OFDM transmission with relaying". IEEE International Symposium on Signal Processing and Information Technology (ISSPIT), 2007.

7. Li, M., Amin, A., Torrea Duran, R., Ahmad, U., Appeltans, R., Dejonghe, A., Van der Perre, L., "Processor based 20Mhz 4×4 Cat-5 LTE MIMO receiver with advanced detectors". International Conference on Acoustics, Speech, and Signal Processing (ICASSP), 2013: 2669-267.

8. Diaz, I., Torrea-Duran, R., Pollin, S., Van der Perre, L., and Owall, V., "Selective Channelization on an SDR Platform for LTE-A Carrier Aggregation." ICECS 2012.

9. Freire-Irigoyen, A., Torrea-Duran, R., Pollin, S., Li, M., Lopez, E., Van der Perre, L., "Energy Efficient PRACH Detector Algorithm in SDR for LTE Femtocells." SCVT , 2011.

10. Baddour, R., Chiumento, A., Desset, C., Torrea Duran, R., Pollin, S., Van der Perre, L., Lauwereins, R., "Energy-Throughput Simulation Approach for Heterogeneous LTE scenarios." ISWCS 2011.

11. Li, M., Appeltans, R., Amin, A., Torrea, R., Cappelle, H., Hartmann, M., Yomo, H., Kobayashi, K., Dejonghe, A., Van Der Perre, L., "Overview of a Software Defined Downlink Inner Receiver for Category-E LTE-Advanced UE." International Conference on Communications (ICC), 2011.

12. Li, M., Amin, A., Appeltans, R., Torrea, R., Cappelle, H., Van Der Perre, L., "Instruction Set Support and Algorithm-Architecture for Fully ParallelMulti-Standard Soft-Output Demapping on Baseband Processors." SIPS 2010.

13. Ali, F. A., Simoens, P., Vankeirsbilck, B., Deboosere, L., Dhoedt, B., Demeester, P., Torrea-Duran, R., Desset, C., "Reducing power consumption of mobile thin client devices." Published in proceedings of NEM Summit: Towards Future Media Internet, 2010.

14. Simoens, P., Vankeirsbilck, B., Ali, F. A., Deboosere, L., De Turck, F., Dhoedt, B., Demeester, P., Torrea-Duran, R., Desset, C., "Characterization of power consumption in thin clients due to protocol data transmission over IEEE 802.11." Published in proceedings of the 7th International Symposium on Modeling and Optimization in Mobile, Ad Hoc, and Wireless Networks, WiOPT, 2009.

15. Sneessens, J., Desset, C., Torrea Duran, R., Megret, P., "Modeling 3GPP-LTE performance for optimal XL control." WIC 2008.

16. Louveaux, J., Torrea Duran, R., Vandendorpe, L., "Efficient algorithm for optimal power allocation in OFDM transmission with relaying." International Conference on Acoustics, Speech, and Signal Processing (ICASSP), 2008.

17. Vandendorpe, L., Torrea Duran, R., Louveaux, J., Zaidi, A., "Power Allocation for OFDM Transmission with DF Relaying." International Conference on Communications (ICC), 2008.